Aircraft Trajectory Prediction Errors:
Including a Summary of Error Sources and Data
(Version 0.2)
July, 2006

FAA/Eurocontrol Action Plan 16
Common Trajectory Prediction Capabilities

Prepared for:
Federal Aviation Administration

Prepared by:
Stéphane Mondoloni, Ph.D.

Table of Contents

1 Foreword ..... - 1 -
2 Statement of the Problem ..... - 2 -
3 Approaches to Trajectory Prediction ..... - 4 -
3.1 Six Degree-of-Freedom ..... - 5 -
3.1.1 Point Mass Model ..... - 8 -
3.1.2 Macroscopic Model or Fully Kinematic Model ..... - 9 -
3.1.3 Model Enhancements ..... - 10 -
4 Error sources ..... - 11 -
4.1.1 Typical Errors ..... - 11 -
4.1.2 Impact of Errors ..... - 12 -
5 Evaluation of Errors ..... - 15 -
5.1 Turn Modeling ..... - 15 -
5.1.1 Description of Error ..... - 15 -
5.1.2 Parametric Analysis ..... - 16 -
5.1.3 Application to Scenarios ..... - 30 -
5.2 Vertical Wind Gradient Omission ..... - 40 -
5.2.1 Description of Error ..... - 40 -
5.2.2 Parametric Analysis ..... - 41 -
5.3 Aircraft Weight Error ..... - 63 -
5.3.1 Description of Error ..... - 63 -
5.3.2 Parametric Analysis ..... - 64 -
5.4 Wind Error ..... - 91 -
5.4.1 Description of Error ..... - 91 -
5.4.2 Parametric Analysis ..... - 108 -
5.5 Top-of-Descent Uncertainty ..... - 120 -
5.5.1 Description of Error ..... - 120 -
5.5.2 Parametric Analysis ..... - 121 -
5.6 Crossing Restrictions and Interim Altitudes ..... - 127 -
5.6.1 Description of Error ..... - 127 -
5.6.2 Parametric Analysis ..... - 127 -
5.7 Aircraft Speed Intent ..... - 146 -
5.7.1 Description of the Error ..... - 146 -
5.7.2 Parametric Analysis ..... - 156 -
5.8 Wind Gradient Error ..... - 179 -
5.8.1 Description of Error ..... - 179 -
5.9 Errors in co-ordinate System ..... - 179 -
5.10 Errors in Track Data ..... - 179 -
5.11 Departure Time Error ..... - 179 -
5.12 Flight Technical Error ..... - 179 -
5.13 Time Lags ..... - 179 -
5.14 Aircraft Performance Data Errors ..... - 179 -
5.14.1 Description of Error ..... - 179 -
5.14.2 Parametric Analysis ..... - 181 -
5.15 Pressure and Temperature Error ..... - 183 -
5.16 Unknown Lateral and Speed Changes ..... - 183 -

5.17 Exit Time from Hold Patterns ..... - 183 -
5.18 Pilot Deviations ..... - 183 -
5.19 Special Controller Instructions ..... - 183 -
5.20 Pilot Operating Procedure ..... - 183 -
References ..... - 184 -

List of Figures

Figure 2-1 Aircraft Trajectory Prediction - Example in flight ..... - 3 -
Figure 3-1 Example execution of a turn in a 6 DOF model ..... - 7 -
Figure 3-2 Geometry used for point-mass model ..... - 8 -
Figure 3-3 Turn modeling given a fixed turn rate ..... - 10 -
Figure 4-1 Definition of along-track, cross-track and altitude errors ..... - 13 -
Figure 5-1 Illustration of a fly-over waypoint ..... - 15 -
Figure 5-2 Description of turn model ..... - 16 -
Figure 5-3 Along and cross-track errors as a function of turn parameters ..... - 17 -
Figure 5-4 Along-track error due to a fly-over waypoint 20 nautical miles from the next waypoint ..... - 18 -
Figure 5-5 Along-track error due to a fly-over waypoint 50 nautical miles from the next waypoint ..... - 18 -
Figure 5-6 Model of a turn with constant roll-rate roll-in and roll-out ..... - 19 -
Figure 5-7 Along-track error due to omission of roll-in and roll-out for a flight at 250 knots, with maximum bank angle of 25 degrees ..... - 21 -
Figure 5-8 Turn model in a wind frame, with wind displacement of end point shown - 23 -
Figure 5-9 Conversion from wind-frame to ground-based frame ..... - 23 -
Figure 5-10 Along-track turn-omission error for a tailwind of various speeds ..... - 26 -
Figure 5-11 Along-track turn-omission error for 45 degree wind at various speeds .... - 26 -
Figure 5-12 Along-track turn-omission error for cross-wind (into turn) at various speeds. - 27 -
Figure 5-13 Along-track turn-omission error for 135 degree wind at various speeds .. - 27 -
Figure 5-14 Along-track turn-omission error for headwind at various speeds ..... - 28 -
Figure 5-15 Along-track turn-omission error for wind at 225 degrees and various speeds - 28 -
Figure 5-16 Along-track turn-omission error for cross-wind (away from turn) and various speeds ..... - 29 -
Figure 5-17 Along-track turn-omission error for wind at 315 degrees and various speeds - 29 -
Figure 5-18 Theoretical windless non-dimensional along-track error versus actual non-dimensional along-track error obtained due to turn model omission ..... - 30 -
Figure 5-19 Temporal distribution of turns from start of climb (obtained from flight plan data) ..... - 31 -
Figure 5-20 Temporal distribution of turns from start of cruise (obtained from flight plan data) ..... - 32 -
Figure 5-21 Temporal distribution of turns from top-of-descent (obtained from flight plan data) ..... - 32 -
Figure 5-22 Distribution of duration of cruise segments ..... - 33 -
Figure 5-23 Illustration of turn omission error versus look-ahead time ..... - 34 -
Figure 5-24 Average and standard deviation from turn-omission in climb (flight plan data) ..... - 34 -

Figure 5-25 Average and standard deviation from turn-omission in cruise (flight plan data)..... - 35 -
Figure 5-26 Average and standard deviation from turn-omission in descent (flight plan data)..... - 35 -
Figure 5-27 Average and standard deviation due to turn omission (flight plan data) .. - 36 -
Figure 5-28 Turn distribution by phase of flight (from as-flown, ETMS trajectories). - 37 -
Figure 5-29 Turn distribution as a function of altitude for vectors..... - 37 -
Figure 5-30 Distribution of "turnback" angles as a function of initial turn (in degrees) - 38 -
Figure 5-31 Cumulative distribution of along-track errors from turn omission (jets) .. - 38 -
Figure 5-32 Cumulative distribution of along-track errors from turn omission (props). - 39 -
Figure 5-33 Forces on a climbing flight ..... - 40 -
Figure 5-34 $\frac{T-D}{mg}$ during climb as a function of altitude for various aircraft types, weights and true airspeeds ..... - 43 -
Figure 5-35 (cont'd). $\frac{T-D}{mg}$ during climb as a function of altitude for various aircraft types, weights and true airspeeds. ..... - 44 -
Figure 5-36 $\frac{T-D}{mg}$ during descent as a function of altitude for various aircraft types, weights and airspeeds. ..... - 45 -
Figure 5-37 Non-dimensional speed gradient for constant CAS ..... - 46 -
Figure 5-38 Non-dimensional speed gradient for constant Mach..... - 46 -
Figure 5-39 Wind gradients applied in examples ..... - 47 -
Figure 5-40 Variation of true airspeed during a CAS/Mach climb of 280/0.74 ..... - 48 -
Figure 5-41 Small business jet - Errors due to neglect of wind gradient during climb - 50 -
Figure 5-42 Large Regional Jet - Errors due to neglect of wind gradient during climb. - 51 -
Figure 5-43 Large Jet - Errors due to neglect of climb gradient during climb ..... - 52 -
Figure 5-44 Heavy Jet - Errors due to neglect of wind gradient during climb ..... - 53 -
Figure 5-45 Heavy Jet II - Errors due to neglect of wind gradient during climb ..... - 54 -
Figure 5-46 Turboprop - Errors due to neglect of wind gradient during climb..... - 55 -
Figure 5-47 Effect of neglect of wind gradient term on altitude during descent (assumed gradient of 3 knots tailwind per 1000 feet over entire descent)..... - 56 -
Figure 5-48 Small Business Jet - Errors due to neglect of wind gradient during descent ... - 58 -
Figure 5-49 Large Regional Jet - Errors due to neglect of wind gradient during descent ... - 59 -
Figure 5-50 Large Jet - Errors due to neglect of wind gradient during descent ..... - 60 -
Figure 5-51 Heavy Jet - Errors due to neglect of wind gradient during descent ..... - 61 -
Figure 5-52 Turboprop - Errors due to neglect of wind gradient during descent ..... - 62 -
Figure 5-53 Force balance during a climb ..... - 63 -

Figure 5-54 $\frac{T - qSC_{D_0}}{k(mg)^2} qS$ during descent vs. speed and altitude for various aircraft.... - 66 -
Figure 5-55 Small Business Jet - Errors due to weight estimation uncertainty during descent.....- 67 -
Figure 5-56 Large Regional Jet - Errors due to weight estimation uncertainty during descent.....- 68 -
Figure 5-57 Large Jet - Errors due to weight estimation uncertainty during descent...- 69 -
Figure 5-58 Heavy Jet - Errors due to weight estimation uncertainty during descent..- 70 -
Figure 5-59 Turboprop - Errors due to weight estimation uncertainty during descent - 71 -
Figure 5-60 Explanation of the effect of a weight estimation error during descent .....- 72 -
Figure 5-61 Explanation of the effect of a weight estimation error during climb .....- 74 -
Figure 5-62 Small Business Jet - Errors due to weight estimation uncertainty during climb .....- 75 -
Figure 5-63 Large Regional Jet - Errors due to weight estimation uncertainty during climb .....- 76 -
Figure 5-64 Large Jet - Errors due to weight estimation uncertainty during climb.....- 77 -
Figure 5-65 Heavy Jet - Errors due to weight estimation uncertainty during climb.....- 78 -
Figure 5-66 Turboprop - Errors due to weight estimation uncertainty during climb ...- 79 -
Figure 5-67 Small Business Jet - Errors due to weight estimation uncertainty during climb (ISA+10) .....- 81 -
Figure 5-68 Large Regional Jet - Errors due to weight estimation uncertainty during climb (ISA +10) .....- 82 -
Figure 5-69 Large Jet - Errors due to weight estimation uncertainty during climb (ISA+10) .....- 83 -
Figure 5-70 Heavy Jet - Errors due to weight estimation uncertainty during climb (ISA + 10) .....- 84 -
Figure 5-71 Small Business Jet - Errors due to weight estimation uncertainty during climb (ISA +20) .....- 85 -
Figure 5-72 Large Regional Jet - Errors due to weight estimation uncertainty during climb (ISA +20) .....- 86 -
Figure 5-73 Large Jet - Errors due to weight estimation uncertainty during climb (ISA+20) .....- 87 -
Figure 5-74 Heavy Jet - Errors due to weight estimation uncertainty during climb (ISA+20) .....- 88 -
Figure 5-75 Comparison of Breguet range equation to data from an airline operator manual.....- 89 -
Figure 5-76 Impact of initial weight error on predicted step climb location .....- 90 -
Figure 5-77 Effect of relative weight error on step climb location error for a typical transport aircraft.....- 90 -
Figure 5-78 Intermittent data assimilation cycle (from [30]) .....- 92 -
Figure 5-79 Continuous data assimilation cycle (from [30]).....- 93 -
Figure 5-80 Temporal and spatial scales of select physical phenomena affecting the earth climate system (modified from [30]) .....- 93 -

Figure 5-81 Observed minus background correlation for the 500mb geopotential as a function of distance between stations. The background is a forecast background (from [30]).....- 94 -
Figure 5-82 Verification of RUC forecasts against rawinsonde observation. RMS vector difference between observation and forecast is given for 1, 3, 6,9 and 12 hour forecast. Also shown is the difference between observation and analysis. Data from [32].....- 96 -
Figure 5-83 Cumulative distribution of errors for RUC-1 (from [33]) - Also shown is the fitted lognormal cumulative distribution .....- 97 -
Figure 5-84 RUC-20 forecast vector difference from verifying analysis (forecast minus analysis) for 250 hPa wind forecast valid 1200 UTC 8 Feb 2001; (a) 12-h forecast initialized at 0000 UTC 8 Feb, (b) 9-h forecast initialized at 0300 UTC, (c) 6-h forecast initialized at 0600 UTC, and (d) 3-h forecast initialized at 0900 UTC. Units are in m/s.....- 98 -
Figure 5-85 Variation at 200mB of the <l,l> longitudinal correlation of the error in wind forecast from observation as a function of station separation, from [34], compared to a simple theoretical model.....- 99 -
Figure 5-86 Illustration of longitudinal (l) and transverse (t) components of wind errors, the <l,l> and <t,t> correlations are a function of the distance (r) between the points of interest.....- 99 -
Figure 5-87 Impact of measurement error and errors of representation on the longitudinal correlation function (minimum resolved scale is notional, not to scale).....- 100 -
Figure 5-88 Cumulative probability of wind error for simulated versus RUC and Augmented Winds data (AW and RUC data from[33]).....- 103 -
Figure 5-89 Illustration of along-track wind error encountered by an individual flight according to the proposed model.....- 104 -
Figure 5-90 Effect of pressure altitude on the rms values of each term in the wind uncertainty model.....- 105 -
Figure 5-91 Vertical correlation of wind prediction errors for non-divergent (V-Psi) and divergent (V-Chi) terms.....- 106 -
Figure 5-92 Comparison of modeled to non-divergent correlation at 300mB.....- 106 -
Figure 5-93 Vertical profile of the RMS error in vertical wind shear (in m/s per km) comparing modeled to measured for both the error of representation and the prediction error.....- 107 -
Figure 5-94 Illustration of lag in ground speed response to wind uncertainty during cruise .....- 109 -
Figure 5-95 Integration of previous example ground speed yields along-track error.- 109 -
Figure 5-96 Along-track RMS error assuming known airspeed target (h=30,000').....- 110 -
Figure 5-97 Along-track RMS error assuming known airspeed target (h = 40,000').- 110 -
Figure 5-98 Growth in along-track RMS error due to errors of representation with various RMS values (1, 2.5 and 5 m/s).....- 111 -
Figure 5-99 Growth in along-track RMS error due to errors at modeled scales with various RMS (1, 2.5, 5 m/s).....- 111 -
Figure 5-100 Sample of speed error of representation.....- 112 -
Figure 5-101 Sample of speed errors at modeled scales.....- 112 -
Figure 5-102 Along-track RMS error assuming known: airspeed target, initial airspeed and initial ground speed.....- 113 -

Figure 5-103 Illustration of along-track errors (30,000 feet) assuming known target airspeed and wind forecast ..... - 113 -
Figure 5-104 Illustration of range of wind shear errors encountered by transitioning aircraft ..... - 114 -
Figure 5-105 Effect of wind prediction uncertainty on trajectory prediction error for various weight, speed and aircraft types during descent (legend precedes) ..... - 116 -
Figure 5-106 Effect of wind prediction uncertainty on trajectory prediction error for various weight, speed and aircraft types during climb (legend in preceding Table) ..- 118 -
Figure 5-107 Illustration of climb errors at breakpoints ..... - 119 -
Figure 5-108 Illustration of top-of-descent error under specific procedure and backward integration prediction ..... - 120 -
Figure 5-109 Illustration of early descent ..... - 121 -
Figure 5-110 Simplified model of top-of-descent placement error ..... - 122 -
Figure 5-111 Illustration of along-track and altitude error profiles from TOD placement error ..... - 122 -
Figure 5-112 Impact of 10, 20, 30 and 60 second TOD placement errors on heavy jet along-track and altitude errors ..... - 123 -
Figure 5-113 Impact of 10, 20, 30 and 60 second TOD placement errors on large jet along-track and altitude errors ..... - 124 -
Figure 5-114 Impact of 10, 20, 30 and 60 second TOD placement errors on small business jet along-track and altitude errors ..... - 125 -
Figure 5-115 Impact of 10, 20, 30 and 60 second TOD placement errors on large regional jet along-track and altitude errors ..... - 126 -
Figure 5-116 Simple description of level-off impact in climb ..... - 128 -
Figure 5-117 Description of level-off impact in climb with known interim level..... - 128 -
Figure 5-118 Impact of level-offs at various altitudes (FL180, 240 and 300) and of varying duration (30 to 300 seconds) on altitude and along-track error for a large jet in a slow climb at a light weight ..... - 129 -
Figure 5-119 Impact of level-offs at various altitude (FL180 and 240) and of varying duration (30 to 300 seconds) on altitude and along track for a large jet in a slow climb at maximum weight ..... - 130 -
Figure 5-120 Impact of level-offs at various altitude (FL180, 240 and 300) and of varying duration (30 to 300 seconds) on altitude and along track for a large jet in a fast climb at low weight ..... - 131 -
Figure 5-121 Impact of level-offs at various altitude (FL180 and 240) and of varying duration (30 to 300 seconds) on altitude and along track for a large jet in a fast climb at maximum weight ..... - 132 -
Figure 5-122 Explanation or errors on climb due to level-off ..... - 133 -
Figure 5-123 Explanation of errors on climb due to level-off of longer duration ..... - 134 -
Figure 5-124 Illustration of simple level-off error model in descent ..... - 135 -
Figure 5-125 Errors due to level-offs (30, 60, 120 and 300 seconds) on descent at 18000 feet on a heavy jet ..... - 136 -
Figure 5-126 Errors due to level-offs (30, 60, 120 and 300 seconds) on descent at 24000 feet on a heavy jet ..... - 137 -
Figure 5-127 Errors due to level-offs (30, 60, 120 and 300 seconds) on descent at 18000 feet on a large jet ..... - 138 -

Figure 5-128 Errors due to level-offs (30, 60, 120 and 300 seconds) on descent at 24000 feet on a large jet ..... - 139 -
Figure 5-129 Errors due to level-offs (30, 60, 120 and 300 seconds) on descent at 18000 feet on a small business jet ..... - 140 -
Figure 5-130 Errors due to level-offs (30, 60, 120 and 300 seconds) on descent at 24000 feet on a small business jet ..... - 141 -
Figure 5-131 Errors due to level-offs (30, 60, 120 and 300 seconds) on descent at 18000 feet on a large regional jet ..... - 142 -
Figure 5-132 Errors due to level-offs (30, 60, 120 and 300 seconds) on descent at 24000 feet on a large regional jet ..... - 143 -
Figure 5-133 Illustration of altitude and along-track error due to level-off error ..... - 144 -
Figure 5-134 Level-off altitude histogram and cumulative duration distribution ..... - 145 -
Figure 5-135 Radar accuracy versus distance from radar (reproduced from [38]) ..... - 147 -
Figure 5-136 Illustration of noise in simple speed calculation ..... - 148 -
Figure 5-137 Impact of α-β tracker position estimate in turn (SSA) ..... - 149 -
Figure 5-138 Impact of α-β tracker velocity estimate in turn (SSA) ..... - 150 -
Figure 5-139 Impact of α-β tracker position estimate in turn (LSA) ..... - 150 -
Figure 5-140 Impact of α-β tracker velocity estimate in a turn (LSA) ..... - 150 -
Figure 5-141 Velocity estimate obtained through α-β tracker equations ..... - 151 -
Figure 5-142 Error in airspeed derived from ground and wind errors ..... - 151 -
Figure 5-143 Illustration of dynamical response to fluctuating wind field (target airspeed = 400 kts) ..... - 152 -
Figure 5-144 Sample climb speed variance illustrated for a single flight ..... - 153 -
Figure 5-145 Force balance in climb ..... - 156 -
Figure 5-146 Impact of climb speed (CAS), weight, wind gradient and altitude on $\left(V\frac{d\gamma}{dV}\right)$ for a large jet ..... - 159 -
Figure 5-147 Impact of climb speed (CAS), weight, wind gradient and altitude on $\left(V\frac{d\gamma}{dV}\right)$ for a heavy jet ..... - 160 -
Figure 5-148 Impact of climb speed (Mach), weight, wind gradient and altitude on $\left(V\frac{d\gamma}{dV}\right)$ for a large jet ..... - 161 -
Figure 5-149 Impact of climb speed (Mach), weight, wind gradient and altitude on $\left(V\frac{d\gamma}{dV}\right)$ for a heavy jet ..... - 162 -
Figure 5-150 Impact of descent speed (CAS), weight, wind gradient and altitude on $\left(V\frac{d\gamma}{dV}\right)$ for a large jet ..... - 163 -
Figure 5-151 Impact of descent speed (CAS), weight, wind gradient and altitude on $\left(V\frac{d\gamma}{dV}\right)$ for a heavy jet ..... - 164 -
Figure 5-152 Impact of descent speed (Mach), weight, wind gradient and altitude on $\left(V\frac{d\gamma}{dV}\right)$ for a large jet ..... - 165 -

Figure 5-153 Impact of descent speed (Mach), weight, wind gradient and altitude on $\left(V\frac{d\gamma}{dV}\right)$ for a heavy jet ..... - 166 -
Figure 5-154 Comparison of impact of speed error (expressed as a percentage error) when expressed versus distance or time ..... - 167 -
Figure 5-155 Illustration of impact of speed error in climb ..... - 168 -
Figure 5-156 Small Business Jet & Large regional jet - Impact of climb speed intent errors (+10%, +5%, -5% and -10%) during climb ..... - 170 -
Figure 5-157 Large and heavy Jet - Impact of climb speed intent errors (+10%, +5%, -5% and -10%) during climb ..... - 171 -
Figure 5-158 Turboprop - Impact of climb speed intent errors (+10%, +5%, -5%, -10%) during climb ..... - 172 -
Figure 5-159 Illustration of error due to speed intent on descent ..... - 173 -
Figure 5-160 Small Business Jet - Impact of descent speed intent errors (+10%, +5%, -5%, -10%) during descent ..... - 174 -
Figure 5-161 Large Regional Jet - Impact of descent speed intent errors (+10%, +5%, -5%, -10%) during descent ..... - 175 -
Figure 5-162 Large Jet - Impact of descent speed intent errors (+10%, +5%, -5%, -10%) during descent ..... - 176 -
Figure 5-163 Heavy Jet - Impact of descent speed intent errors (+10%, +5%, -5%, -10%) during descent ..... - 177 -
Figure 5-164 Turboprop - Impact of descent speed intent errors (+10%, +5%, -5%, -10%) during descent ..... - 178 -
Figure 5-165 Illustration of potential drag profile errors ..... - 180 -
Figure 5-166 Example - Errors in vertical speed under averaged operational conditions ... - 181 -
Figure 5-167 Effect of a fixed percentage error in drag coefficient on altitude and along-track error for a large jet ..... - 182 -

1 Foreword

Many documents have been produced summarizing different trajectory prediction methods, errors sources and the quantification of those error sources (e.g., [1] to [15]). This document seeks to provide a reference for researchers to determine the sources and magnitudes of errors in aircraft trajectory prediction. Data is provided for various transport aircraft, and a methodology for deriving the data is presented. The focus of this report is on civilian transport aircraft operating within an air traffic system. The role of this air traffic system includes ensuring an orderly flow of traffic, providing separation assurance and delivering such in an efficient manner. These objectives can best be achieved through high quality and timely aircraft trajectory predictions – the cornerstone of current and future automation systems (see [16] to [20]).

2 Statement of the Problem

The problem of aircraft trajectory prediction refers to the development of an estimate of the future positions of a flight given the aircraft initial conditions, a notional path to be followed by the aircraft, environmental information, and aircraft-specific data (such as an aircraft performance model).

Several different approaches exist for aircraft trajectory prediction with differing levels of fidelity and data requirements. However, in almost all cases the following categories of data are required:

- *Initial condition*. This refers to the aircraft state and time at the start of the trajectory calculation. The aircraft state vector will include a greater number of elements in the case of a higher-order model. For example, a full motion simulator would require instantaneous bank angle, whereas a point-mass model would not.
- *Intent information*. This describes the notional path the aircraft will follow in the future. This may be a sequence of control instructions for the aircraft (full control settings schedule), a flight plan, or a simple projection of the state vector (fixed heading and speed). Intent information can also include the effect of operational procedures (e.g., how a climb is effected by the flight crew, altitude restrictions, etc.)
- *Environmental information*. This refers to external elements that will affect the aircraft behavior, such as winds and temperature.
- *Aircraft-specific information*. This includes the aircraft performance model and flight-specific data such as weight.

Figure 2-1 illustrates an example of the trajectory prediction process as applied to a commercial flight already en route. This example refers to a generic trajectory prediction process; some trajectory predictors would require more, different or less information. Increased sophistication in predictors can also lead to intent inferencing, in-flight parameter estimation or trajectory error monitoring and recalibration.

This trajectory predictor will have access to the flight plan containing the flight number (AAA123), the aircraft type (B-757-200), the filed cruise speed (true airspeed of 457 knots), the desired cruise altitude (31,000 feet), and the route of flight (departure from XXX, now heading to ABC, then DEF, finally to XYZ via the BUC 7 STAR). Furthermore, the trajectory predictor will have an estimate of the initial condition (the present aircraft position, speed and heading). Prior to conducting trajectory prediction, the flight plan route, expressed as named points, will be converted to a series of geographical points (e.g., latitude and longitude). This process is known as ***route conversion***.

Flight Plan: AAA123 B752 0457 310 XXX..ABC..DEF.BUC7.XYZ

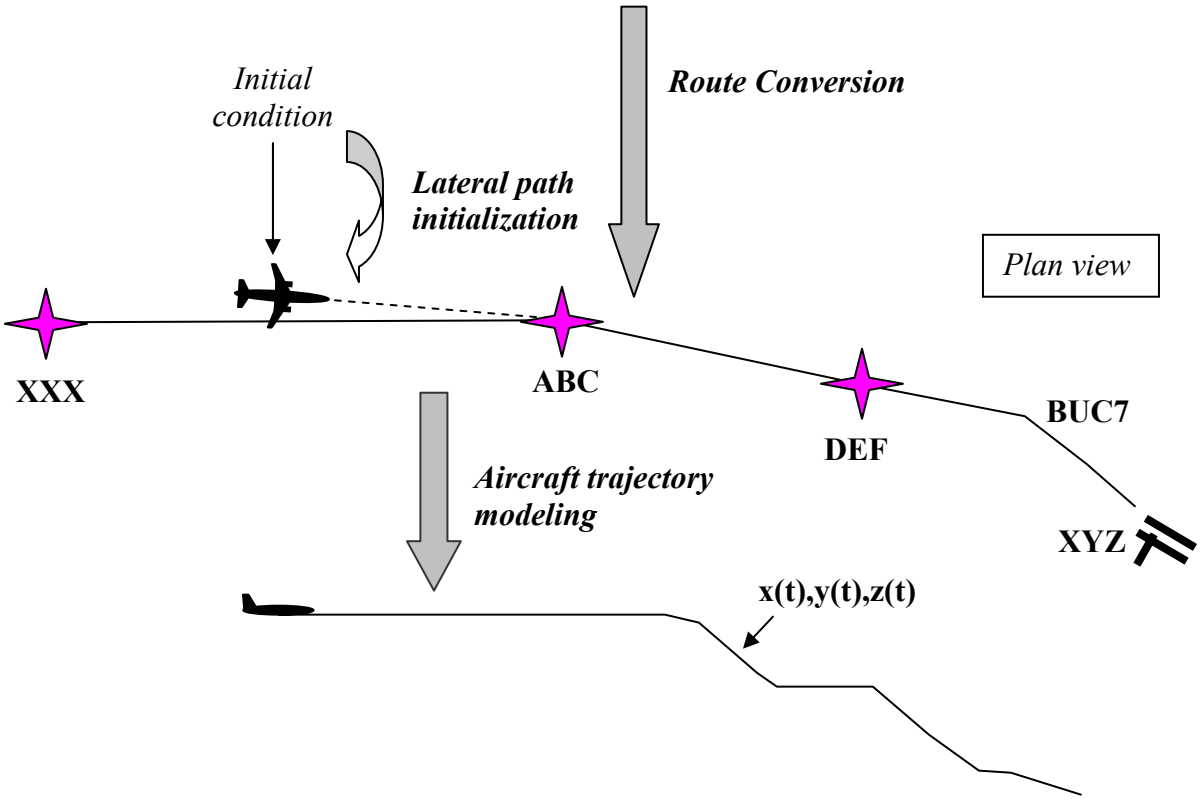

Figure 2-1 Aircraft Trajectory Prediction - Example in flight

Once the route is converted, a mechanism for joining the initial condition to the converted route is required. This process is referred to as ***lateral path initialization***. This process may simply involve the identification of the initial location on the route. More likely, the initial condition will be slightly off-route and some connection from the initial condition to the route will be required.

Once the lateral path is determined, vertical and speed constraints must be considered at different points along the route of flight. For example, speed constraints below 10,000 feet can be applied, as can altitude constraints along a standard terminal arrival route.

The core part of aircraft trajectory prediction follows from the next step. In this part, the speed and vertical path is computed to follow the converted route, meet specified constraints (such as altitude and speed constraints), follow appropriate aircraft dynamics (such as turns, climbs and descents), and consider environmental and aircraft-specific information. The output of this process is that future positions of the aircraft are expressed as a function of time.

Competing approaches for the above trajectory prediction core are described in the next section.

3 Approaches to Trajectory Prediction

Aircraft trajectory prediction can be accomplished using several different approaches. These approaches may require different aircraft-specific and operational data to yield trajectory forecasts at different levels of precision. Generally, the types of trajectory predictors may be broken down as shown below.

- *A full six degree-of-freedom trajectory calculation.* This approach models the forces and moments (loads) affecting the airframe along all axes of motion as a function of the aircraft state and control settings. Accurate functional relationships between the loads and state/control values are typically obtained from the aircraft and engine manufacturers. These relationships are frequently expressed in tabular form as they are derived from empirical measurements. Furthermore, since the aircraft is controlled through operation of control surfaces and engines, this model requires knowledge of the control laws for determining the control settings.
- *A point mass model.* This approach models the aircraft as a point and only requires the modeling of the resulting longitudinal forces affecting this point – Thrust and Drag (it is assumed that the lift compensates the weight). If required, fuel flow can be modeled as a function of Thrust. Thrust, drag and fuel flow data can be expressed in tabular or polynomial form. The reference data required to produce such a model needs to be thrust data (e.g. installed net thrust), drag data (e.g. for high/low speeds and for each a/c configuration) and thrust specific fuel consumption. However as this data is difficult to obtain, profile data (e.g. altitude vs. time) may be used. These data represent the motion of the aircraft as a result of the combination of all the forces affecting it ((thrust-drag)/weight). In order to differentiate individual forces from this set of integrated reference data, a large set of profile data must be used covering the whole flight envelope and the associated operating regime (e.g. climb thrust, idle, etc.).
- *A macroscopic model.* This approach models the macroscopic behavior of the a/c (e.g. rate of climb/descent, rate of acceleration/deceleration) as a function of a set of input parameters affecting that behavior (e.g., altitude, temperature). The reference data required for the modeling process is limited to a/c rates of change and does not require the availability of thrust and drag data.

The above list of model types is ranked in accordance with level of fidelity of the model. However, the reader is cautioned that the trajectory prediction accuracy is a function of both the modeling and the quality of the input data used to drive the model. For example, a macroscopic model considering many operational conditions could produce better results than a 6-dof model using engineering approximations and standard conditions. Thus, data quality is an equally important factor in the ability of trajectory predictors to yield adequate results.

The form of the data used to drive the trajectory prediction models may also vary for each model. For example, aircraft performance data may be expressed as polynomials, look-up tables, analytical expressions or combinations of either. Each type of model may use

data expressed in any of the above forms. Furthermore, the quality of the data is independent of the form of the data.

3.1 Six Degree-of-Freedom

In a six degree-of-freedom model, the forces and moments on an aircraft are modeled and the resulting longitudinal and lateral accelerations are computed. References [21] and [22] have a detailed treatment of this approach, and the equations of motion are duplicated below.

$$X - mg\sin\Theta = m(\dot{U} + QW - RV)$$

$$Y + mg\cos\Theta\sin\Phi = m(\dot{V} + RU - PW)$$

$$Z + mg\cos\Theta\cos\Phi = m(\dot{W} + PV - QU)$$

$$L = \dot{P}I_x - \dot{R}I_{xz} + QR(I_z - I_y) - PQI_{xz}$$

$$M = \dot{Q}I_y + PR(I_z - I_z) + (P^2 - R^2)I_{xz}$$

$$N = \dot{R}I_z - \dot{P}I_{xz} + PQ(I_y - I_x) - QRI_{xz}$$

$$P = \dot{\Phi} - \dot{\Psi}\sin\Theta$$

$$Q = \dot{\Theta}\cos\Phi + \dot{\Psi}\cos\Theta\sin\Phi$$

$$R = \dot{\Psi}\cos\Theta\cos\Phi - \dot{\Theta}\sin\Phi$$

$$\dot{\Theta} = Q\cos\Phi - R\sin\Phi$$

$$\dot{\Phi} = P + Q\sin\Phi\tan\Theta + R\cos\Phi\tan\Theta$$

$$\dot{\Psi} = (Q\sin\Phi + R\cos\Phi)\sec\Theta$$

$$\frac{dx'}{dt} = U\cos\Theta\cos\Psi + V(\sin\Phi\sin\Theta\cos\Psi - \cos\Phi\sin\Psi) + W(\cos\Phi\sin\Theta\cos\Psi + \sin\Phi\sin\Psi)$$

$$\frac{dy'}{dt} = U\cos\Theta\sin\Psi + V(\sin\Phi\sin\Theta\sin\Psi + \cos\Phi\cos\Psi) + W(\cos\Phi\sin\Theta\sin\Psi - \sin\Phi\cos\Psi)$$

$$\frac{dz'}{dt} = -U\sin\Theta + V\sin\Phi\cos\Theta + W\cos\Phi\cos\Theta$$

The above equations are in body-centered co-ordinates and assume a symmetrical and rigid (no aero-elastic effects) aircraft. The forces (X,Y, Z) are in the longitudinal (forward), lateral (right wing) and vertical (down) directions respectively. The rolling (L), pitching (M) and yawing (N) moments are also expressed. The Euler angles (Ψ, Θ, Φ) represent the heading, pitch, and bank angles respectively. Speeds along the longitudinal, lateral and vertical direction are given by U, V and W. Rotational speeds along these same axes are given by P, Q and R. The mass (m) and moments of inertia (I_x, I_y , I_z and I_{xz}) are required for the individual aircraft type. The final three equations allow the translation to an earth-fixed frame of reference from the body-fixed frame.

The above equations allow a relationship to exist between the loads on the aircraft and the associated dynamics. To obtain aircraft trajectories from the above equations, many data elements are required.

- *Initial Conditions* – The initial state of the aircraft is required. This includes the aircraft position (x',y',z') in an Earth-fixed frame, the initial aircraft orientation (Ψ, Θ, Φ), the initial velocity (U,V,W) and angular velocity (P, Q, R).
- *Aircraft Specific Information* – The mass (m) of the aircraft along with the moments of inertia (I_x, I_y, I_z and I_{xz}) are required. In addition the forces (X,Y,Z) and moments (L,M,N) are required. These loads are modeled through the use of an aircraft performance model.
- *Environmental Information* – The ambient temperature and density can be obtained as a function of location (altitude and position). This is used as input into the model of the aircraft forces and moments. Similarly, since the above is a model of the dynamics, all speeds are relative to an inertial frame. Wind enters through an aerodynamical model of the loads.
- *Intent Information* – In this case, intent information is the flight path that a control law would be guiding towards. This implies the need for some control law representing either pilot actions, or actions of an automatic control system (e.g. auto-throttle) in order to track a desired intent. The control law provides the relationship between the intent and the forces and moments required. Prior to obtaining this guidance information, the six degree-of-freedom model will sometimes require the use of a lower-order model. This is required to estimate points at which the guidance will switch (for example, from cruise to descent).

Aircraft loads are modeled as a function of the aircraft state. These can be modeled as look-up tables, polynomials or linear expressions using stability derivatives. Forces are modeled in wind-axes and converted to the body axes as shown below.

$$\begin{pmatrix} X \\ Y \\ Z \end{pmatrix} = \begin{pmatrix} \cos\alpha\cos\beta & -\sin\beta\cos\alpha & -\sin\alpha \\ \sin\beta & \cos\beta & 0 \\ \cos\beta\sin\alpha & -\sin\beta\sin\alpha & \cos\alpha \end{pmatrix} \begin{pmatrix} T-D \\ Sideforce \\ -Lift \end{pmatrix}$$

The above allows the body-axis forces to be expressed in terms of the traditional wind-axis forces of: thrust (T), drag (D), sideforce and lift. The angle of attack (α) and sideslip angle (β) are used to convert between the axes. The traditional aerodynamic loads are approximated as a function of aircraft state and atmospheric conditions. For example lift may be expressed as:

$$Lift = \frac{1}{2}\rho V_T{}^2 S C_L(\alpha, \dot{\alpha}, M, q, \eta)$$

In the above expression, M refers to the Mach number, not the pitching moment. Note that the lift is also a function of the deflection of the elevator control surface (η). Similar equations will apply to other forces and also the moments. These will further introduce the control variables of rudder deflection, elevator deflection and power setting. The

configuration (landing gear, flap deployment) of the aircraft will also impact the loads. An engine model is required to not only obtain the thrust as a function of power setting and state, but also to provide the fuel burn. This ensures that the mass of the aircraft can be decreased as fuel is consumed.

Given a desired intent and a current forecast state, a control law specifies the control values that are required in order to achieve the desired intent. In this case, consider the execution of a simple turn as illustrated in Figure 3-1. At the proper point to intercept the next leg, the pilot or automatic control system will initiate a roll by deflecting the ailerons and co-ordinating the turn using the rudder. Power will be increased, as required, to ensure level flight is maintained. Once a desired turn rate or bank angle has been achieved, the ailerons are deflected back to maintain the bank angle. To exit the turn, the process is reversed.

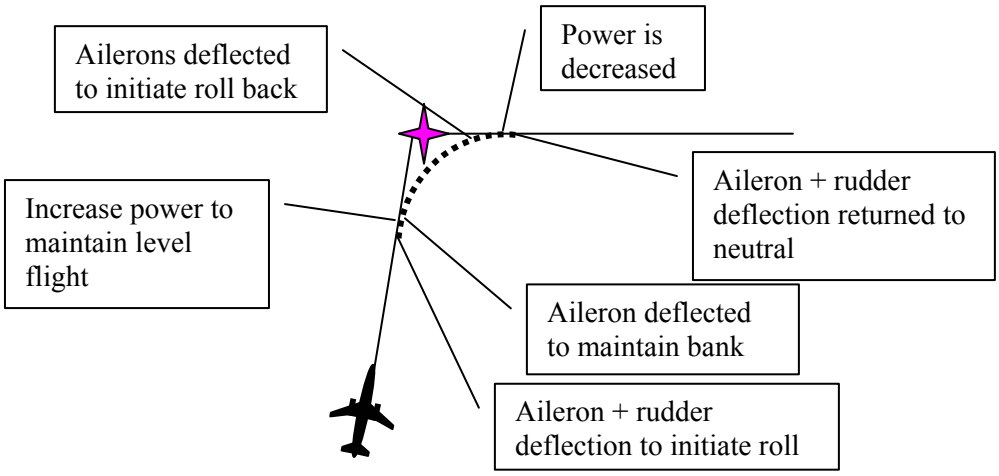

Figure 3-1 Example execution of a turn in a 6 DOF model

The above process illustrates the need for an estimate of the trajectory to exist before the control variables can be set (e.g., the turn must be estimated to know when to initiate the turn). A pilot executing the maneuver may more grossly estimate the turn-initiation time and under/overshoot the turn, or vary the turn rate during the turn. Turns may be fly-by, fly-over, open vectors, or course interception. The details within the turn are dependant upon specific implementation details such as maximum bank angle, and roll-in / roll-out time determined by the magnitude of the aileron deflections. These are also likely to be a function of whether a pilot controls the aircraft, or whether an automatic control system is in control.

The significant quantity of data required for this type of aircraft model is rarely available when modeling trajectories for ground-based air traffic applications. In addition, higher frequency dynamics are modeled in this approach that are not likely to have an impact on air traffic applications. These facts make the six degree-of-freedom model rarely used to calculate trajectories for air traffic applications.

3.1.1 Point Mass Model

In a point mass model of the aircraft, the aircraft is modeled as a point mass. Forces and longitudinal accelerations are modeled, but moments and angular acceleration are not modeled. Typically the aircraft is assumed to be in vertical balance (weight is compensated by lift) and sideforce is not considered (turns are assumed to be coordinated). References [23] to [25] describe a point-mass model for use in air traffic automation applications and the model is described here for reference.

Figure 3-2 describes the geometry of the problem and the equations of motion are simplified (applying small flight-path angles) to:

$$\dot{V}_t = \frac{T(h,M,\kappa) - D(h,V_t,L)}{m} - g\gamma_a - \frac{d}{dt}\left(V_w \cos\theta_{rw}\right)$$

$$\dot{h} = \gamma_a V_t = \gamma_i V_g$$

$$V_g = \sqrt{V_t^2 - \left(V_w \sin\theta_{rw}\right)^2} - V_w \cos\theta_{rw}$$

$$\dot{\psi} = \frac{L\sin\phi}{mV_g}$$

$$L = \frac{mg}{\cos\phi}$$

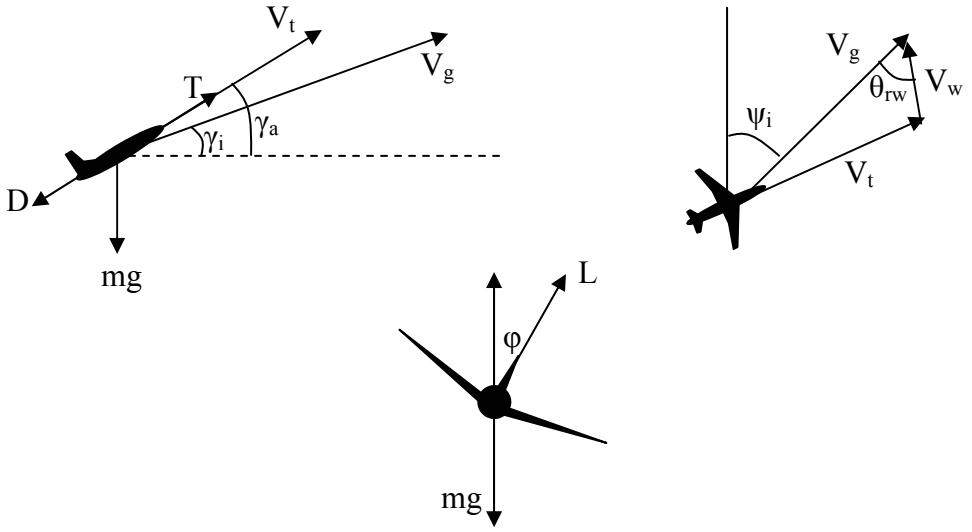

Figure 3-2 Geometry used for point-mass model

Turns are modeled separately assuming coordinated turns. One obtains the heading change by assuming that during the turn, a specified bank angle (φ) has been reached (e.g. 20 degrees en route and 30 degrees in terminal areas). Ground speed is often assumed to be constant during turns. As for the six degree-of-freedom model, the aerodynamic and propulsive forces that are modeled (e.g., thrust and drag) can be modeled to various levels of fidelity using tables, equations, or simplified engineering

approximations. However, the vertical component of the lift is always assumed to balance the weight.

Some information about control variables is required in order to apply the point mass model. In particular, the power setting (κ) is a control variable that can be set by the user during climbing or descending flight. Since additional power can be used to either accelerate the aircraft or climb the aircraft, a desired climb/descent rate or target climb/descent speed is also required to solve the problem. During the modeling of turns, the bank angle is selectable by the user. For these control variables, a schedule of control variables is required.

For commercial aircraft operating in the en route domain, the control variables may be specified as follows:

- During climb, a fixed climb power setting is specified
- A constant CAS (calibrated airspeed) segment is computed during which the climb angle is allowed to vary to maintain the CAS
- A constant Mach segment is computed during which the climb angle is varied to maintain the desired Mach. Transition between the constant CAS and constant Mach occurs when the aircraft first reaches the Mach number.
- During cruise, the power is computed to maintain a target Mach number and the power is left constant. Power may be decreased as fuel is consumed.
- During descent, a fixed descent power is specified, this is only slightly above idle.
- Constant Mach and CAS segments are computed during descent as they were in climb.

Atmospheric effects are modeled with a point-mass model via the following terms:

- Inclusion of the wind term (V_w) and the wind gradient term ($d/dt(V_w \cos\theta_{rw})$)
- The impact of vertical winds are assumed to be negligible
- Impact of altitude (h) on thrust and drag via temperature and density

3.1.2 Macroscopic Model or Fully Kinematic Model

A macroscopic model does not explicitly model the forces and moments on the flight. (However, loads may be used in the derivation of these models.) Climb and descent rates are expressly modeled as a function of conditions. Acceleration and deceleration are also modeled as functions of conditions. The complexity of the model depends on the number of conditions being used to obtain the vertical speeds and accelerations. Reference [26] provides an example of a macroscopic model with a large number of parameters.

One of the simplest cases involves modeling the climb and descent rates as a lookup table based upon aircraft type and altitude. This approximation may be suitable for national-level simulations seeking aggregate behavior, but is not likely sufficient for advanced real-time DST applications [27]. The influence of additional parameters may be added such as temperature, wind, target calibrated airspeed, target Mach number, altitude, and weight. If enough parameters are modeled, the macroscopic model can be identical in

accuracy to the point mass model with the major difference being that the force-balance equations have been solved a priori.

For a macroscopic model, by assuming a turn rate, turn modeling can be incorporated. As an example, the speed could be assumed constant during the turn thereby providing the turn radius. A circular arc turn can be approximated as shown in Figure 3-3. Wind can also be incorporated throughout the turn.

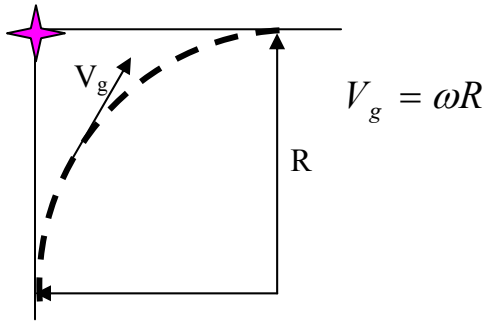

Figure 3-3 Turn modeling given a fixed turn rate

3.1.3 Model Enhancements

For each of the above models, certain enhancements can be made in an effort to improve the solution accuracy when faced with errors in input data, erroneous parameter data or noisy perturbations to the trajectory. In particular, adaptation can be used to improve the aircraft model or parameters in the model. Filtering techniques can be employed to eliminate noisy data. However, one characteristic of these approaches is the time lag required to acquire the information necessary for adaptation or filtering.

As an example, consider the trajectory prediction of an aircraft in climb using a kinetic (point-mass) model. In a perfect world, the following information would be known precisely:

- The aircraft thrust and drag as the aircraft climbs
- The power setting used during the climb
- The target CAS or climb rate being controlled to
- The aircraft weight
- The aircraft initial condition
- Atmospheric data such as wind and temperature profiles

As the aircraft climbs, adaptation requires the observation of the actual flight path of the aircraft and the variation of parameters in order to compensate for erroneous data. However, given the number of parameters that can be varied, to similar effect, the ability of adaptation to achieve meaningful results is a challenging task. For example, a higher than predicted weight would lead to a slower climb, but the same might be obtained if the power setting was lower than expected. If point-mass equations are used as previously described, it is simply not possible to differentiate the impact of one versus the other. However, if the adaptation is properly formulated, the appropriate terms in the equations can be adapted with greater success.

4 Error sources

For each of the types of trajectory models presented, trajectory prediction can never be achieved with perfect accuracy. This comes about due to two major reasons:

- Errors and omissions in the modeling approach. For example, the neglect of turn-dynamics in some macroscopic models, the neglect of higher-order dynamics in point-mass models, or the neglect of aircraft trajectory history in six degree-of-freedom models.
- Errors in the data driving the models. These include errors in all categories of data:
    - Initial conditions
    - Aircraft-specific information
    - Environmental information
    - Intent information

Under certain circumstances, the above categories are not mutually exclusive. For example, a macroscopic model providing a trajectory profile independent of a parameter (e.g. temperature) is an omission in the modeling approach, but can be quantified by observing errors in data.

4.1.1 Typical Errors

An investigation of trajectory predictors currently used for DST applications revealed that the *typical* sources of error falling into each category are as summarized below.

- *Modeling Errors*
    - Omission of turn modeling
    - Omission of impact of vertical wind gradient
    - Errors in co-ordinate system. For example, a flat earth approximation produces positional errors as the flight moves from the point of tangency.
- *Initial Condition Errors*
    - Errors in track data. These include errors in initial position, resulting errors in initial speed, course, acceleration, climb and descent speeds.
    - Errors in departure time. Certain applications computing trajectory prediction prior to departure will be sensitive to departure time errors.
- *Aircraft-specific Errors*
    - Flight technical error. The ability of the aircraft and/or pilot to follow a specified flight path and altitude is dependant on a multitude of factors including the navigational equipment on board and pilot skill.
    - Time lags. The impact of time lags on the execution time of a maneuver will impact the trajectory forecast of the maneuver. These lags may be due to pilot response to instructions, communication lags or controller entry into the automation.
    - Aircraft performance data errors. While the form of the data will be dependant on the type of model being applied, errors in aircraft performance data will propagate as errors in trajectory forecasts.

    - Error in aircraft weight. Errors in the aircraft weight will impact the climb and descent profiles. During cruise, the weight will impact the fuel consumption.
- *Errors in environmental information*
    - Pressure and Temperature errors. Temperature errors will result in errors in aircraft engine performance and in conversion from indicated airspeed to true. Errors in pressure have a direct impact on the error in the actual aircraft height since aircraft fly at pressure altitudes.
    - Wind errors. Errors in the forecast wind will affect the ground speed of the aircraft and hence the positional uncertainty.
    - Wind gradient errors. Errors in the magnitude of the wind gradient will impact the acceleration (deceleration) of an aircraft climbing or descending through this wind field.
- *Intent Errors*
    - Unknown lateral and speed changes. The intended flight path and speed is often altered from the original intent. The trajectory predictor may be lacking this information, thereby leading to additional errors in forecast position and vertical rates.
    - Exit time from hold patterns. Trajectory predictors lacking this information will be subject to errors subsequent to the execution of a hold maneuver.
    - Fly-by or fly-over waypoints. Lack of knowledge of how the flight will execute a maneuver over a waypoint leads to trajectory prediction errors.
    - Pilot deviations. Pilots have some allowance for deviations from horizontal path (e.g., due to weather). In addition, pilots may blunder off-path.
    - Top-of-descent uncertainty. Lack of knowledge of the top-of-descent location leads to errors in forecasting the entire descent.
    - Crossing restrictions and interim altitudes. Lack of this information leads to errors in vertical and speed profiles.
    - Special controller instructions. Certain controller requests (e.g., for expedited climbs and descents) may alter standard operating procedures for flights.
    - Pilot operating procedure. The details of how a pilot executes a maneuver (e.g., FL CH, V/S, VNAV) will impact how the aircraft is controlled, and result in trajectory prediction errors if this information is not known precisely. This is distinct from the uncertainty associated with the control (flight technical error).
    - Aircraft speed intent. Trajectory predictors only have the speed of the aircraft to a low level of precision during cruise. During climb or descent, the speed intent is often not known.

4.1.2 Impact of Errors

Errors in trajectory prediction can be decomposed into three orthogonal directions [28] as illustrated in Figure 4-1: lateral/cross-track, longitudinal/along-track and vertical. While

the errors are orthogonal, coupling may occur between errors. For example, vertical errors during a constant calibrated airspeed segment will lead to errors in true airspeed, thereby producing along-track errors. Cross-track errors lead to errors in flight distance calculations and therefore contribute to along-track errors as well. Table 4-1 illustrates the error dimension affected by each of the error factors presented in the prior section.

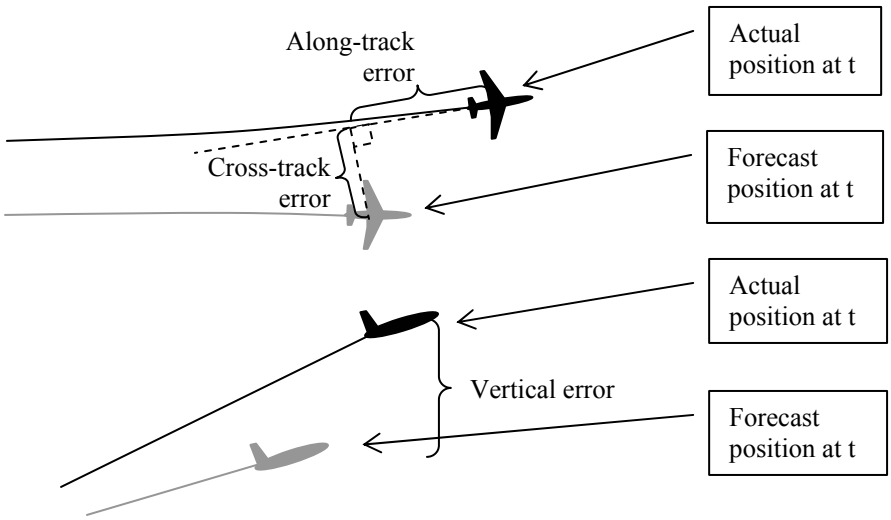

Figure 4-1 Definition of along-track, cross-track and altitude errors

Table 4-1 Errors affected by each error factor

Factor	Cross-track	Along-track	Vertical
Turn model omission	✓	✓	
Vertical wind gradient omission		✓	✓
Errors in co-ordinate system	✓	✓	
Errors in track data	✓	✓	✓
Departure time error		✓	
Flight technical error	✓	✓	✓
Time lags	✓	✓	✓
Aircraft performance data errors		✓	✓
Aircraft weight error		✓	✓
Pressure and temperature errors		✓	✓
Wind error		✓	✓
Wind gradient error		✓	✓
Unknown lateral and speed changes	✓	✓	✓
Exit time from hold patterns	✓	✓	
Fly-by or fly-over waypoints	✓	✓	
Pilot deviations	✓	✓	✓
Top-of-descent uncertainty		✓	✓
Crossing restrictions and interim altitudes		✓	✓
Special controller instructions		✓	✓
Pilot operating procedure		✓	✓
Aircraft speed intent		✓	✓

Note from the prior table that the along-track error is affected by all factors. This is due to the coupling between the along-track error and both the vertical and cross-track terms.

5 Evaluation of Errors

This section provides information on the major errors in several important categories identified before. The sections provide a detailed description of the error together with a parametric evaluation of the contribution to the error under various scenarios of impact to the outcome. The reader may typically use the data presented to obtain an estimate of the prediction error that is likely under certain situations.

5.1 Turn Modeling

5.1.1 Description of Error

Turn model omission errors occur whenever instantaneous turns are assumed on the part of the trajectory modeler. There are two types of turns that are typically referred to: fly-by and fly-over waypoints. The most common type of turn is a fly-by turn. Fly-by turns are the default turn, if not specified, since these turns result in a shorter flight path and are therefore more economical.

When executing a fly-by turn, there are several components in the execution of the turn (see Figure 3-1):

- Roll-in to the turn, during this time, a turn will be initiated. The aircraft bank angle will gradually increase, and the turn rate will increase as a function of the bank angle.
- Constant bank turn, during this time, the aircraft executes a constant-radius turn (in an air-fixed frame of reference) and experiences a constant turn rate.
- Roll-out of the turn, the bank angle is gradually reduced as the new heading is captured. The turn rate gradually decreases with the bank angle.

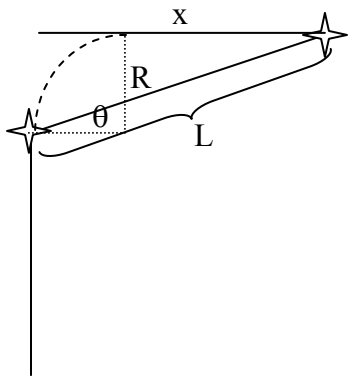

Figure 5-1 Illustration of a fly-over waypoint

For a fly-over turn, the distance to the next waypoint will impact the additional distance flown[29]. Figure 5-1 illustrates the turn for a fly-over waypoint. The components of the turn are identical to the fly-by turn (i.e., roll-in, constant-bank, roll-out).

5.1.2 Parametric Analysis

Simple turn model – Fly-by waypoint

We estimate the impact of this error by comparing trajectories with a *simple* turn model to trajectories assuming a discrete heading change at a waypoint. Here we assume a fly-by waypoint. Note that the error represents the error of exclusion of the turn model and does not attempt to represent errors introduced in the execution of the turn by a pilot. Our parametric analysis assumed a turn model in which the airspeed is held constant, a maximum bank angle of 25 degrees is assumed, no winds are incorporated and the bank angle is achieved instantaneously.

Figure 5-2 shows the turn model employed. The along-track error and maximum cross-track errors are respectively given by:

$$2R\tan(\frac{\Delta\psi}{2}) - R\Delta\psi$$

$$R\left(\frac{1}{\cos(\Delta\psi/2)} - 1\right)$$

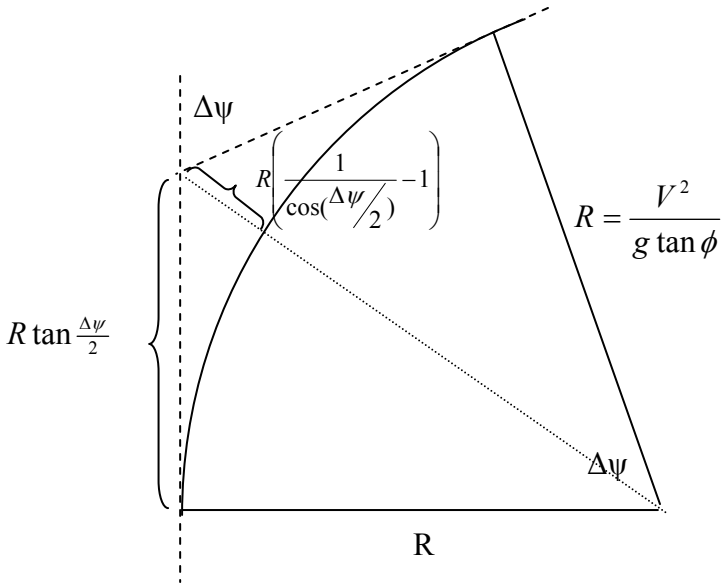

Figure 5-2 Description of turn model

Figure 5-3 illustrates the effect of airspeed and heading change on the maximum cross-track and along track error in a turn. The figure also illustrates the relationship between the turn radius and the assumed bank angle (ϕ). In the figure, airspeed is varied from 250 to 500 knots and heading change is varied from 0 to 90 degrees. Both errors increase as the speed and heading change are increased. A maximum error of 20356 feet along track and 19645 feet across track can be experienced by a flight at 500 knots encountering a

90-degree heading change. These results are consistent with those published in reference [29].

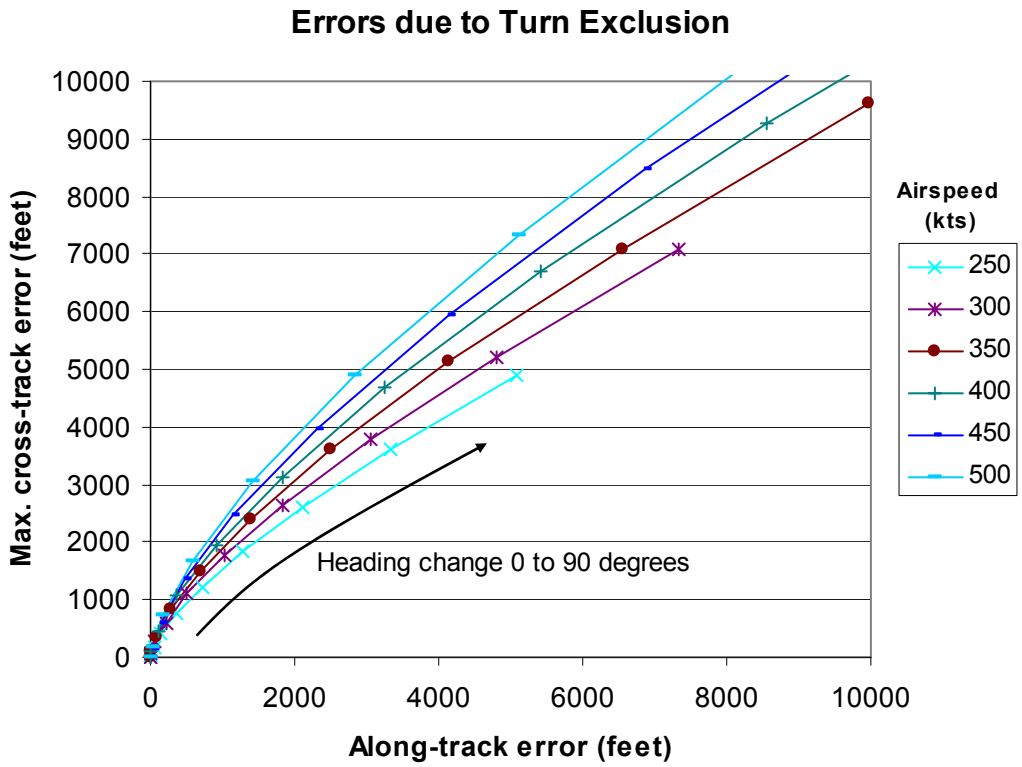

Figure 5-3 Along and cross-track errors as a function of turn parameters

Simple Turn Model – Fly over waypoint

Using the turn model in Figure 5-2, a turn specified with a given turn radius (R), a specified distance to the next waypoint (L) and a heading change ($\Delta\psi$) is computed to have the following distance from roll-out to the next fix:

$$x = -R\sin\Delta\psi + \sqrt{R^2\sin^2\Delta\psi + L^2 - 4R^2\sin^2\frac{\Delta\psi}{2}}$$

Here we also assume instantaneous roll-in and roll-out of turns. The excess lateral path traveled is therefore given by:

$$x + R\Delta\psi - L$$

Where:

$$R = \frac{V^2}{g\tan\phi}$$

Figure 5-4 and Figure 5-5 illustrate the error in along-track position due to calculation using an instantaneous turn compared to a fly-over waypoint as speed and turn angle are varied. We compare the error for a waypoint that is 20 nautical miles away, and one that is 50 nautical miles away. Again, a bank angle of 25 degrees is assumed. ***Note that for a fly-over waypoint, an instantaneous turn model will lead the actual trajectory, whereas for a fly-by waypoint, the instantaneous turn will lag the actual trajectory.***

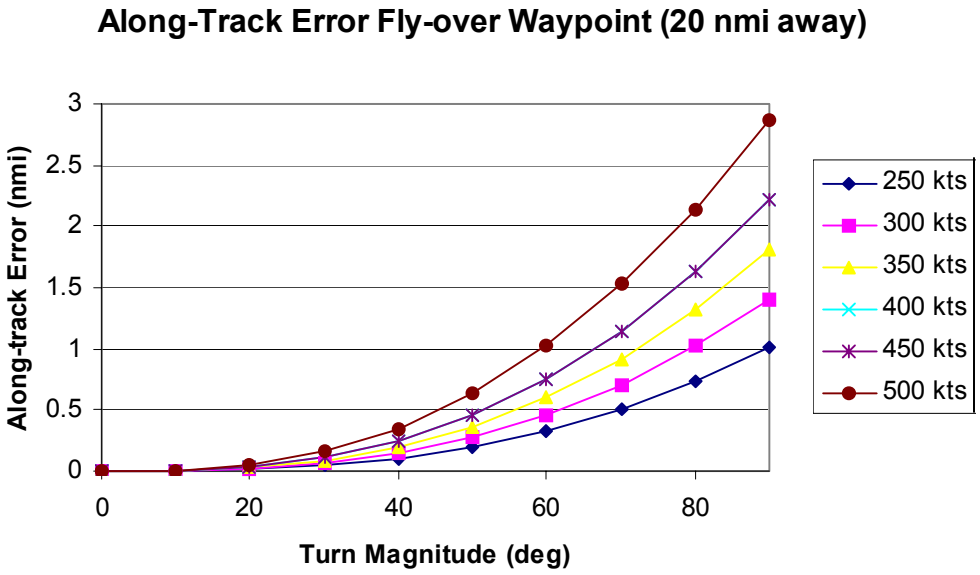

Figure 5-4 Along-track error due to a fly-over waypoint 20 nautical miles from the next waypoint

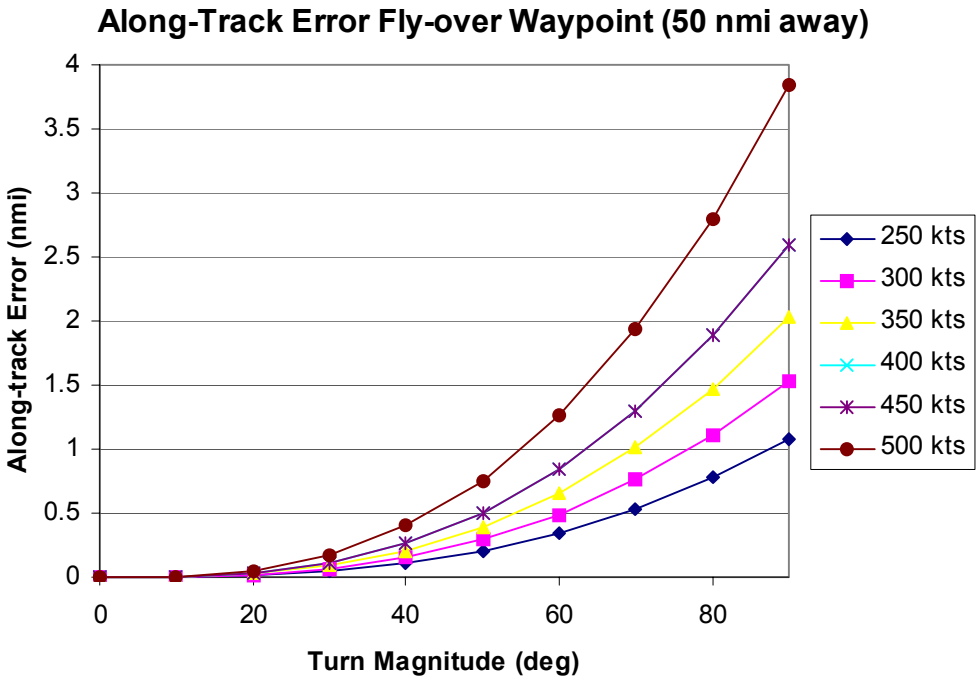

Figure 5-5 Along-track error due to a fly-over waypoint 50 nautical miles from the next waypoint

Impact of roll-in and roll-out

We also assessed the impact of rolling into a turn, and rolling out of a turn on the along-track error imparted. Commercial aircraft roll rates during a turn are within a 10-15 degree per second range depending on configuration (e.g. clean), aircraft type and how the aircraft is being commanded. Note that these roll rates can be significantly smaller if the aircraft is in LNAV trying to offset a cross-track error.

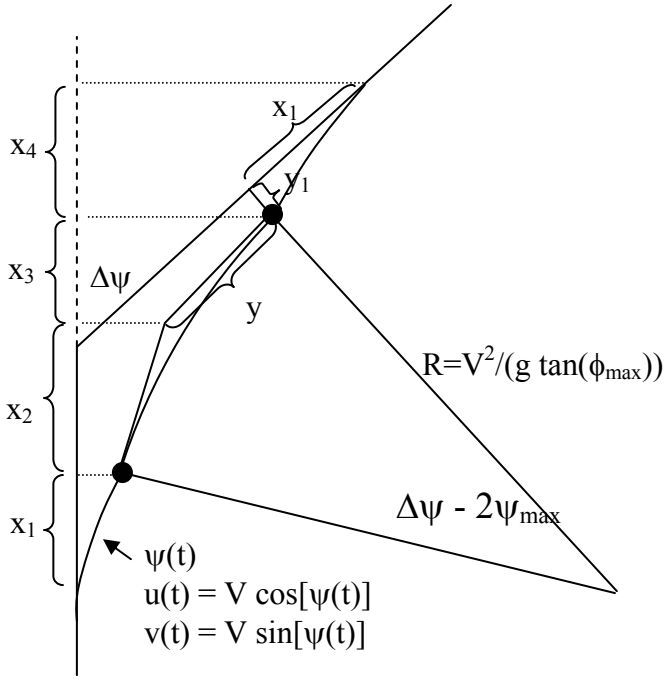

Figure 5-6 Model of a turn with constant roll-rate roll-in and roll-out

Figure 5-6 illustrates the turn being computed. To estimate the impact of the roll-in and roll-out, a constant roll rate is assumed to a maximum bank angle. The turn must be initiated earlier than a constant radius turn, and will terminate later. An along-track error can be computed since the original turn will travel further than the modified turn. During the rolling part of the turn, with a roll-rate (p), the instantaneous heading can be expressed as:

$$\psi(t) = \int_0^t \frac{g\tan(pt)}{V}\,dt$$

$$= -\tfrac{g}{pV}\ln(\cos(pt))$$

Since the roll is limited to a maximum bank angle (ϕ_{max}), the above equation will apply until time (ϕ_{max}/p). This provides the heading at which the rolling-in maneuver will join a circular turn:

$$\psi_{\max} = -\frac{g}{pV}\ln(\cos(\phi_{\max}))$$

A circular turn can then be constructed to the rolling-out portion by reducing the total heading change by twice the above expression.

The difference between the above turn and a circular turn was modeled using expressions shown in Figure 5-6.

The total distance flown during the turn can be obtained from:

$$total_dist = 2Vt_{\max} + R\left[\Delta\psi - 2\psi_{\max}\right]$$

Compared to the instantaneous-turn distance computed as follows:

$$2\frac{x_1 + x_2 + x_3 + x_4}{1 + \cos\Delta\psi}$$

In Figure 5-6, the following distances can be obtained:

$$x_1 = \int_0^{\phi_{\max}/p} V\cos\left(-\tfrac{g}{pV}\ln\left[\cos(pt)\right]\right)dt$$

$$x_2 = \frac{V^2}{g\tan(\phi_{\max})}\left[\tan(\tfrac{\Delta\psi}{2} - \psi_{\max})\right]\cos(\psi_{\max})$$

$$x_3 = \frac{V^2}{g\tan(\phi_{\max})}\left[\tan(\tfrac{\Delta\psi}{2} - \psi_{\max})\right]\cos(\Delta\psi - \psi_{\max})$$

$$x_4 = \cos(\Delta\psi)\int_0^{\phi_{\max}/p} V\cos\left(-\tfrac{g}{pV}\ln\left[\cos(pt)\right]\right)dt + \sin(\Delta\psi)\int_0^{\phi_{\max}/p} V\sin\left(-\tfrac{g}{pV}\ln\left[\cos(pt)\right]\right)dt$$

We compare the additional distance flown using this turn model to the additional distance flown using a circular arc with instantaneous bank angle. Using numerical integration to obtain the above integrals, we obtain *very small errors* for a maximum bank angle of 25 degrees and a roll rate of 15 degrees per second. These errors are less than 5 feet for all turns within 90 degrees and speeds from 250 knots to 500 knots. Thus, within the en route portion of flight, one would expect these errors to be small.

As the roll-rate is reduced, the along-track error will increase, but will still be small. Figure 5-7 illustrates the additional error due to exclusion of the roll-in, roll-out for an aircraft operating at 250 knots with a maximum bank angle of 25 degrees. At smaller roll rates and small heading changes, the aircraft may never reach the maximum bank angle.

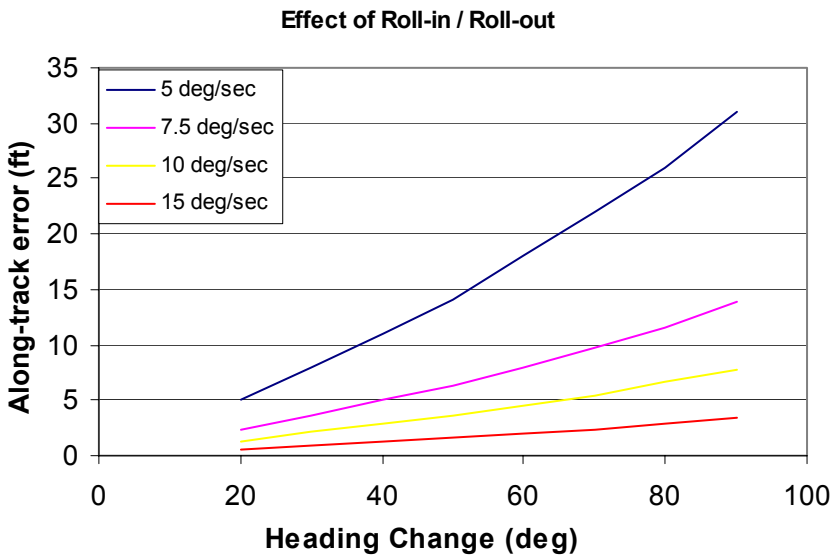

Figure 5-7 Along-track error due to omission of roll-in and roll-out for a flight at 250 knots, with maximum bank angle of 25 degrees

The reader is cautioned that the above results are obtained by taking the difference between two numbers that are large relative to the error obtained. Duplication of the above results using numerical methods requires attention to detail.

Impact of wind in a turn

Inclusion of turn dynamics, as described in the prior section do not account for the effects of wind in the turn. The first-order impact of the wind can be estimated by assuming that the wind will be of constant heading and magnitude during the turn. In an air-fixed frame of reference, all of the prior calculations will apply. However, in a ground-based frame of reference, the aircraft will translate with the wind field.

We assume we know the following parameters:

- ψ_{rw} = angle of wind relative to original track
- V = original airspeed
- $\Delta\psi$ = change of the ground track during the turn
- w = magnitude of the wind

At the start of the turn, we have the following:

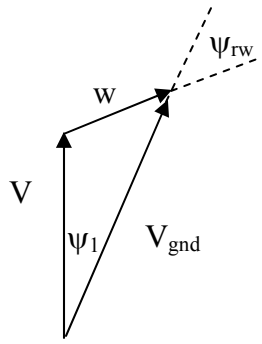

This gives the following relationship:

$$\psi_1 = \sin^{-1}\left(\frac{w\sin(\psi_{rw})}{V}\right)$$

At the end of the turn, we have a similar situation:

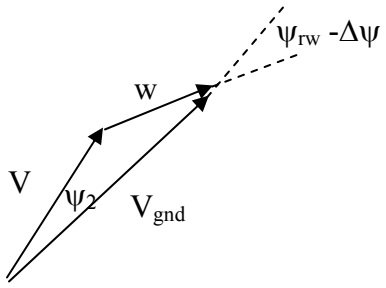

This leads to the following relationship:

$$\psi_2 = \sin^{-1}\left(\frac{w\sin(\psi_{rw} - \Delta\psi)}{V}\right)$$

The change in the air heading is therefore given by:

$$\begin{aligned}\Delta\psi_{air} &= \psi_1 + \Delta\psi - \psi_2 \\ &= \sin^{-1}\left(\frac{w\sin(\psi_{rw})}{V}\right) + \Delta\psi - \sin^{-1}\left(\frac{w\sin(\psi_{rw} - \Delta\psi)}{V}\right)\end{aligned}$$

In a wind-based frame of reference, Figure 5-2 would still apply. The aircraft is performing a coordinated circular turn in the wind frame of reference. In a ground frame of reference, the entire wind frame is moving with the wind velocity. The entire turn takes the following time:

$$t = \frac{R\Delta\psi_{air}}{V}$$

Thus, one can consider the end point of the turn as displaced by the wind vector multiplied by the above time. This produces the situation shown in Figure 5-8.

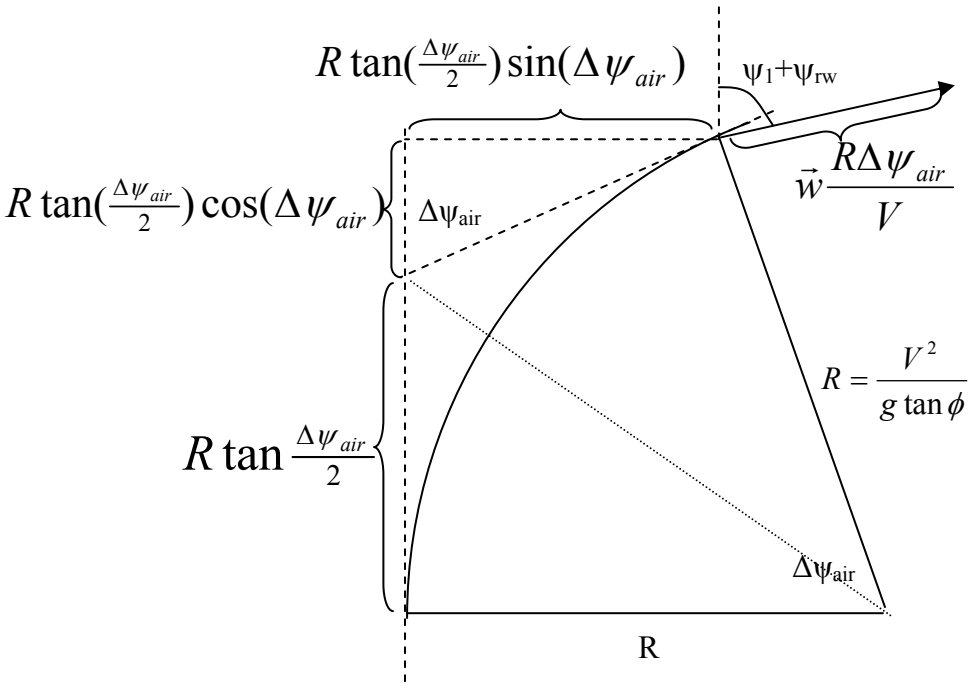

Figure 5-8 Turn model in a wind frame, with wind displacement of end point shown

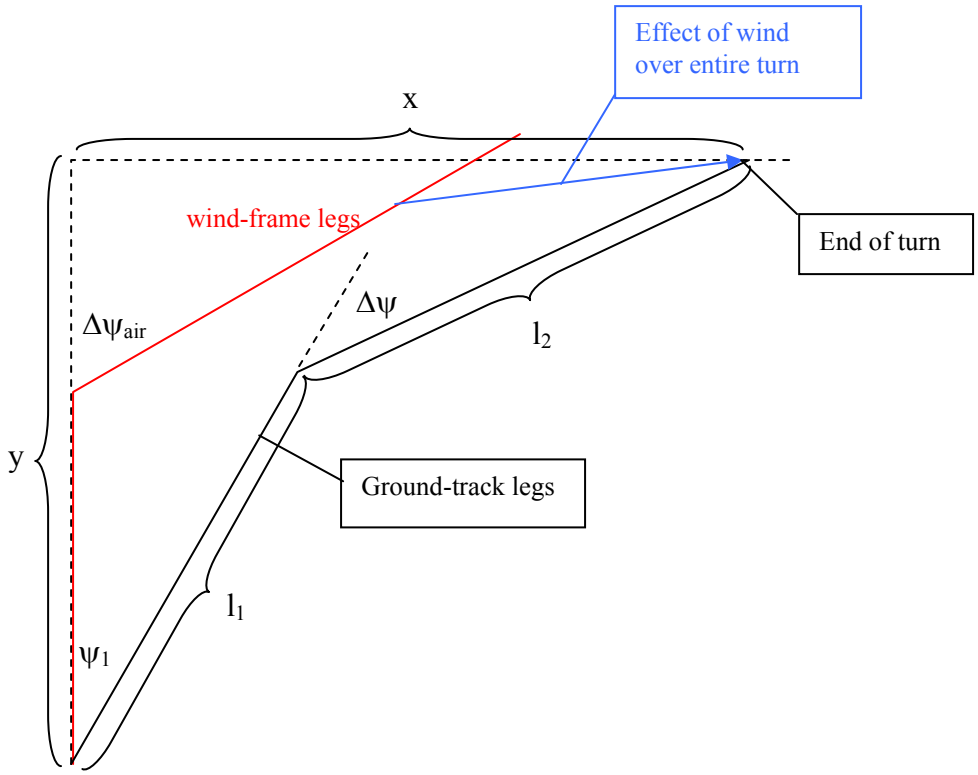

Figure 5-9 Conversion from wind-frame to ground-based frame

Figure 5-9 shows the initial and final legs in the ground-based frame of reference, compared to the legs in the wind frame. The orthogonal distances traveled can be computes as:

$$y = R\tan\left(\frac{\Delta\psi_{air}}{2}\right)\left(1+\cos\Delta\psi_{air}\right)+\frac{wR\Delta\psi_{air}}{V}\cos\left(\psi_1+\psi_{rw}\right)$$

$$x = R\tan\left(\frac{\Delta\psi_{air}}{2}\right)\left(\sin\Delta\psi_{air}\right)+\frac{wR\Delta\psi_{air}}{V}\sin\left(\psi_1+\psi_{rw}\right)$$

This provides the distance traveled along the ground-track legs as follows:

$$l_1 = x\sin\psi_1 + y\cos\psi_1 - \left(\frac{x\cos\psi_1 - y\sin\psi_1}{\tan\Delta\psi}\right)$$

$$l_2 = \left(\frac{x\cos\psi_1 - y\sin\psi_1}{\sin\Delta\psi}\right)$$

To obtain the error, we compute the flight time for an instantaneous turn following the ground track. This includes the impact of the wind on the ground speed. The first leg (l_1) will have a ground speed given by:

$$V_{g1} = \sqrt{V^2 + w^2 + 2Vw\cos\left(\psi_{rw}+\psi_1\right)}$$

The second leg (l_2) will have a ground speed of:

$$V_{g2} = \sqrt{V^2 + w^2 + 2Vw\cos\left(\psi_2+\psi_{rw}-\Delta\psi\right)}$$

Thus, the time error at the end point of the turn is given by:

$$t_{err} = \frac{l_1}{V_{g1}} + \frac{l_2}{V_{g2}} - \frac{R\Delta\psi_{air}}{V}$$

We note that the above can be non-dimensionalized using the airspeed (V) for speed and the turn radius (R) for distance. This leads to the following normalized along-track error:

$$\frac{x_{err}}{R} = \left(\frac{V_{g2}}{V}\right)\left[\frac{l_1/R}{V_{g1}/V} + \frac{l_2/R}{V_{g2}/V} + \Delta\psi_{air}\right]$$

This normalization allows us to express the normalized along-track error as a function of three parameters:

- ψ_{rw} = angle of wind relative to original track
- w/V = the ratio of the wind to the airspeed
- $\Delta\psi$ = change of the ground track during the turn

The results of the above calculation are illustrated in a series of charts from Figure 5-10 to Figure 5-17. Recall that the along-track error is computed as a function of the turn radius. For various speeds, the turn radius is shown in Table 5-1. Combining the information in these figures with Table 5-1, one can obtain along-track errors for a variety of turns and wind conditions.

Table 5-1 Turn radius at various speeds with a 25° maximum bank angle

Airspeed (kts)	Turn Radius (nmi)
250	1.95
300	2.81
350	3.82
400	5.00
450	6.32
500	7.81

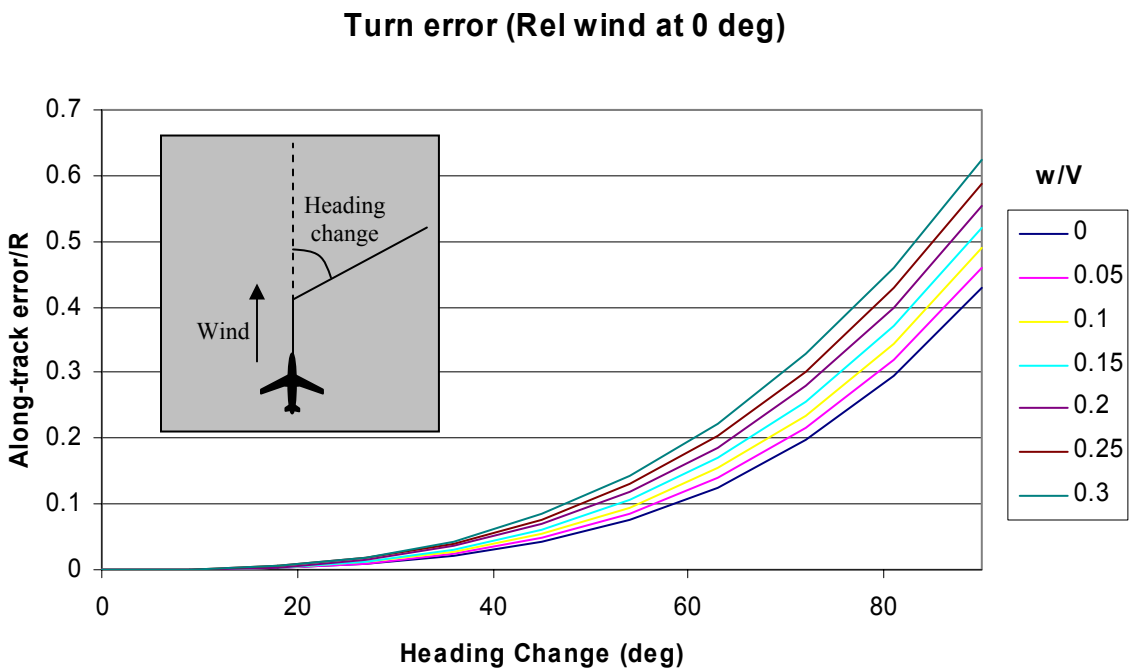

Figure 5-10 Along-track turn-omission error for a tailwind of various speeds

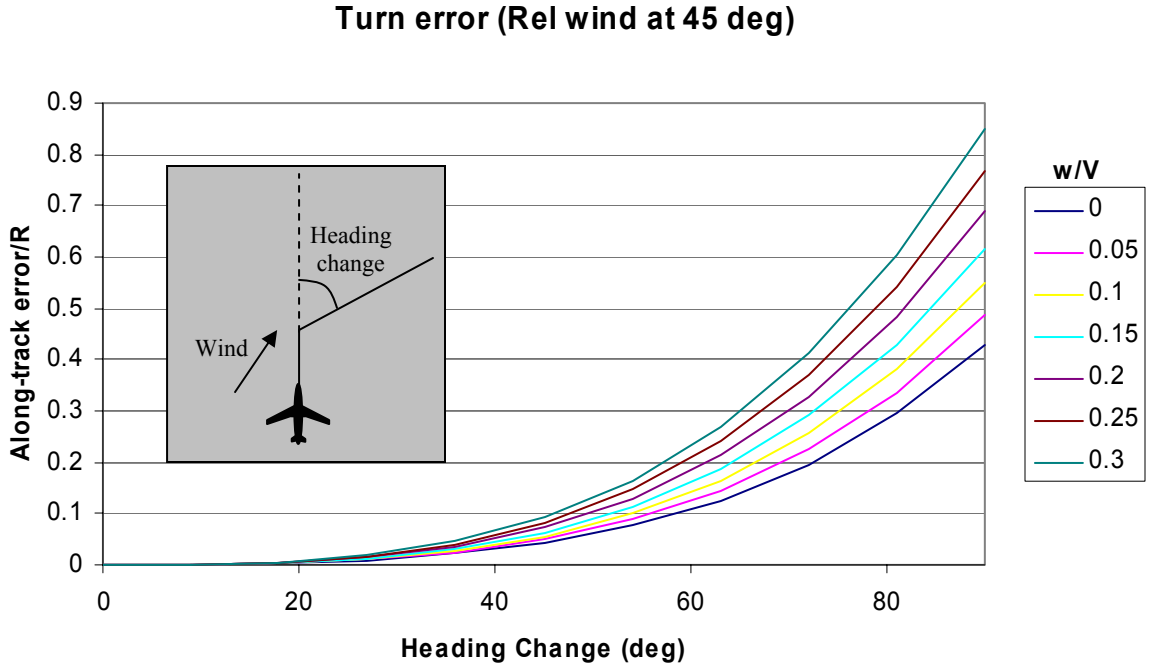

Figure 5-11 Along-track turn-omission error for 45 degree wind at various speeds

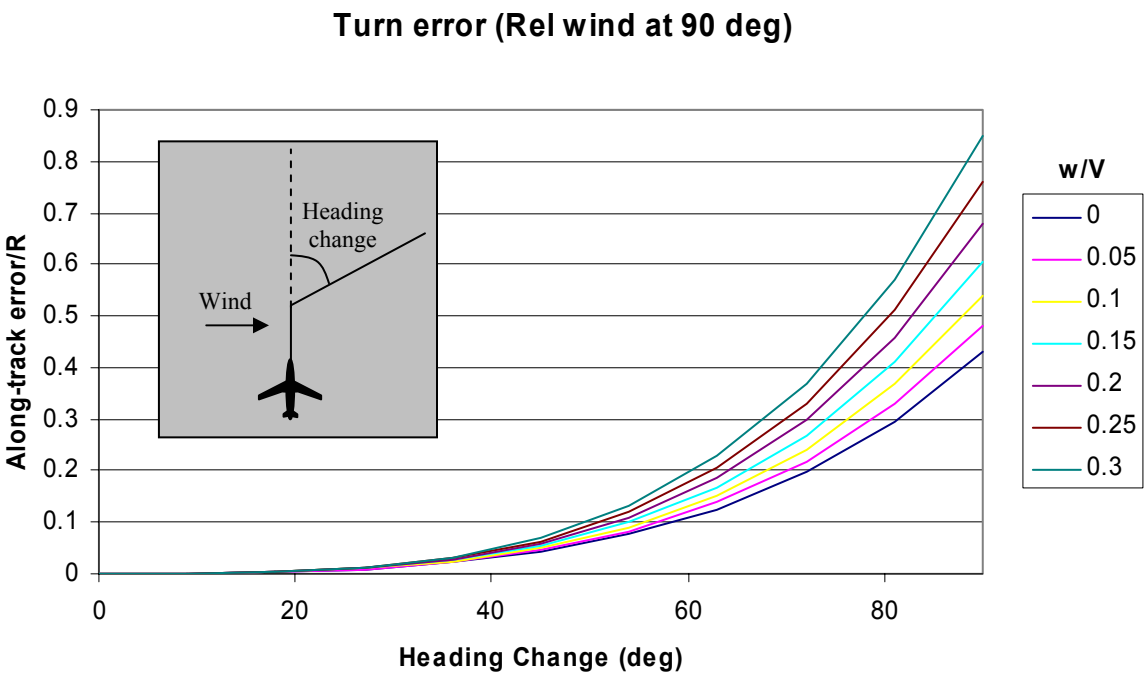

Figure 5-12 Along-track turn-omission error for cross-wind (into turn) at various speeds

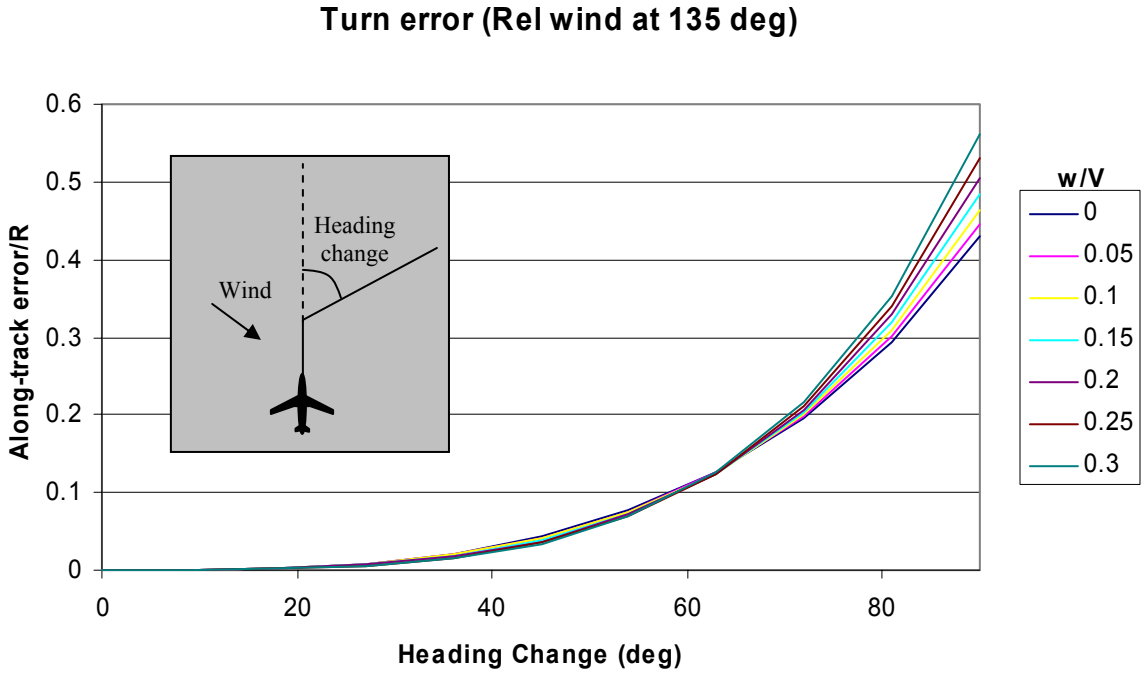

Figure 5-13 Along-track turn-omission error for 135 degree wind at various speeds

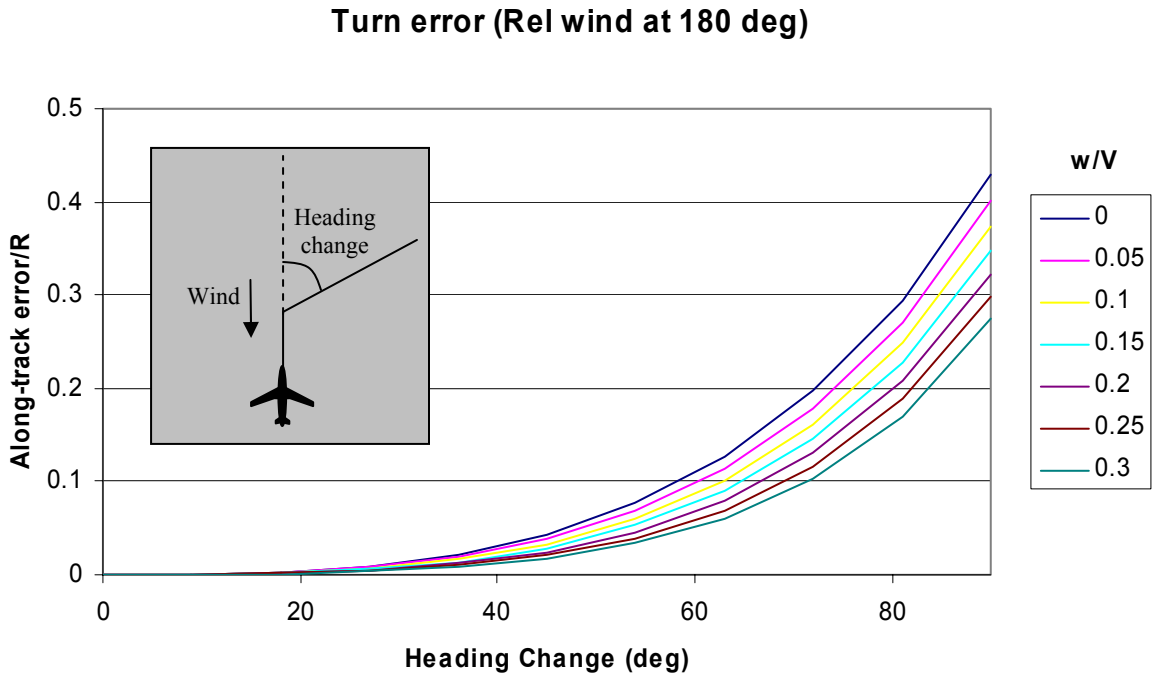

Figure 5-14 Along-track turn-omission error for headwind at various speeds

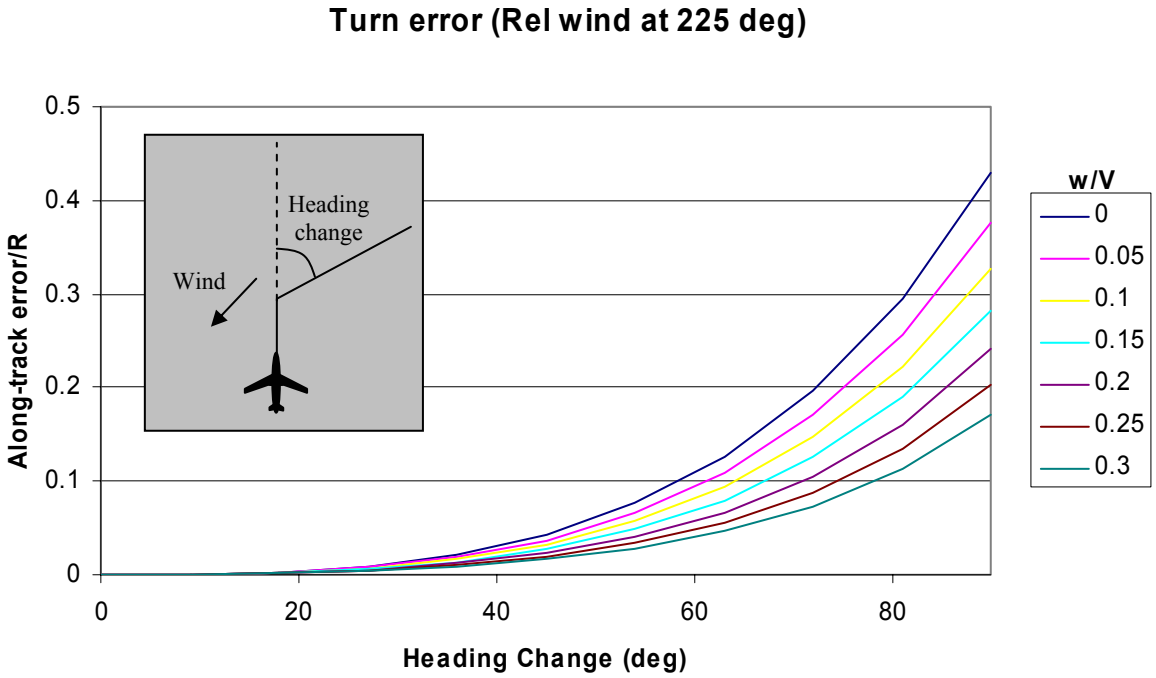

Figure 5-15 Along-track turn-omission error for wind at 225 degrees and various speeds

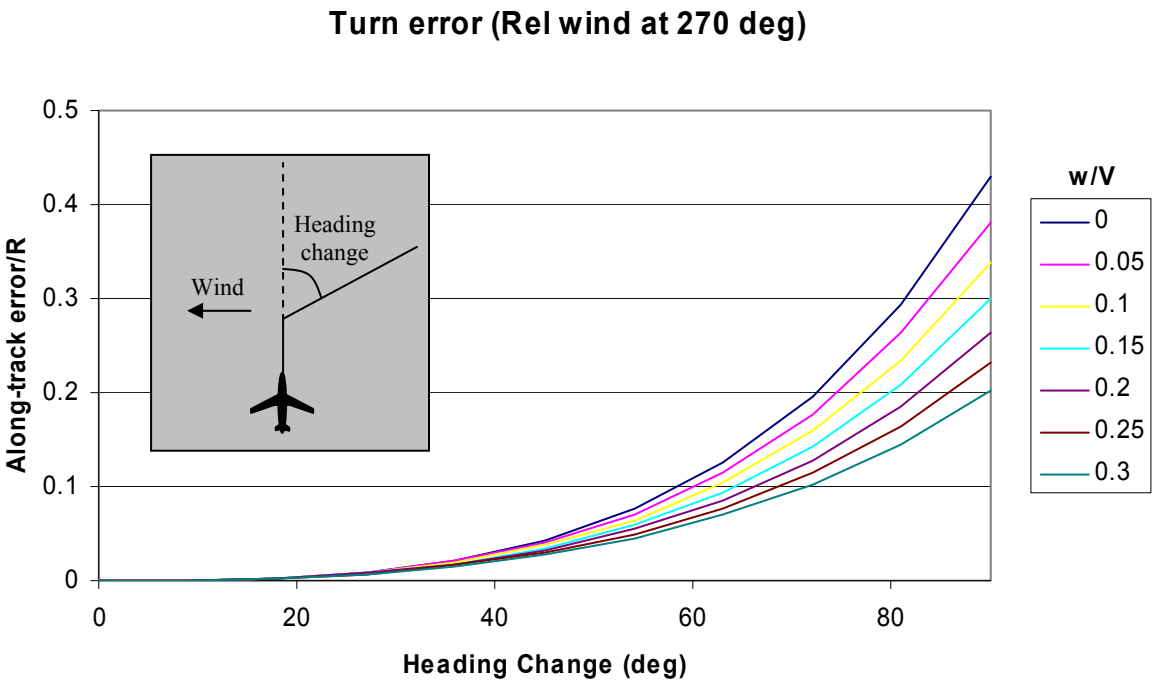

Figure 5-16 Along-track turn-omission error for cross-wind (away from turn) and various speeds

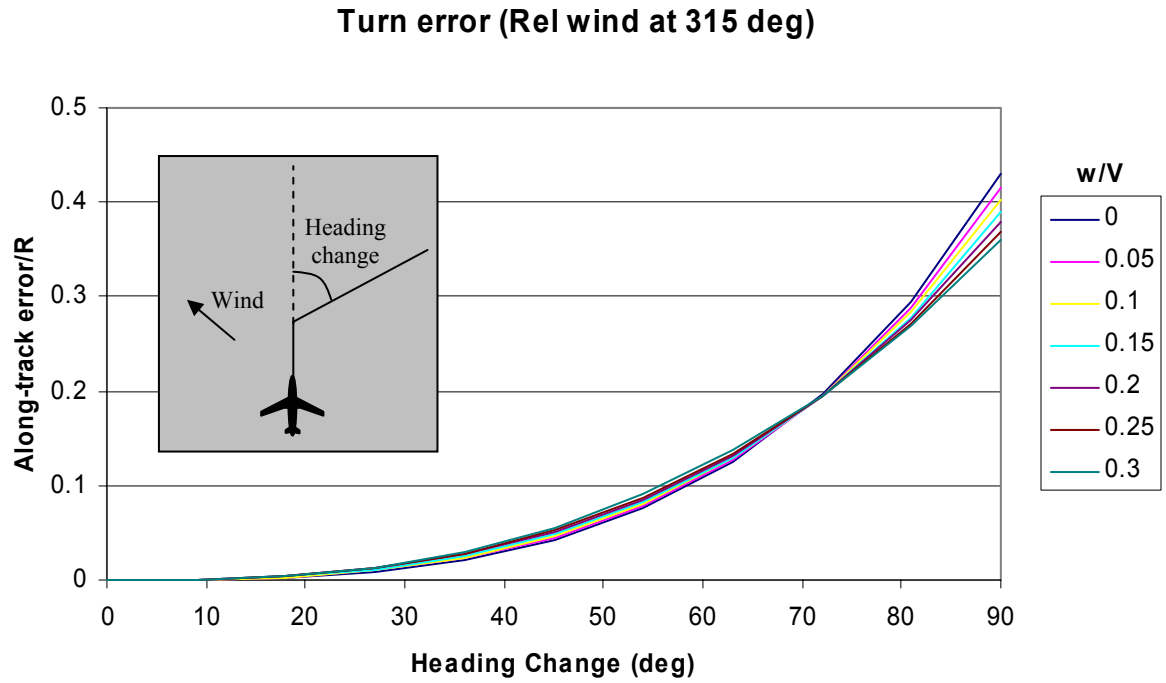

Figure 5-17 Along-track turn-omission error for wind at 315 degrees and various speeds

5.1.3 Application to Scenarios

Comprehensive models of the errors attributable to turn-model omission have been presented. In order to verify the validity of the models presented, Figure 5-18 compares the theoretical error with the actual error obtained by assuming instantaneous turns to estimate the future position of radar tracks. However, to reduce the effect of unknown speed intent, the speed during the turn was assumed to be the measured average speed during the turn. The theoretical error was obtained using the no wind simple turn model for a fly-by waypoint. The along-track error was non-dimensionalized using the theoretical turn radius (R), obtained using a standard rate turn (ω=3 degrees per second) and the measured average speed ($V=\omega R$). Note that radar data was obtained prior to the data being filtered by the tracker, since the filtering algorithm of the tracker introduces lags into the turns. The spread of the measured data is consistent with that occurring due to the neglect of wind and radar measurement accuracy.

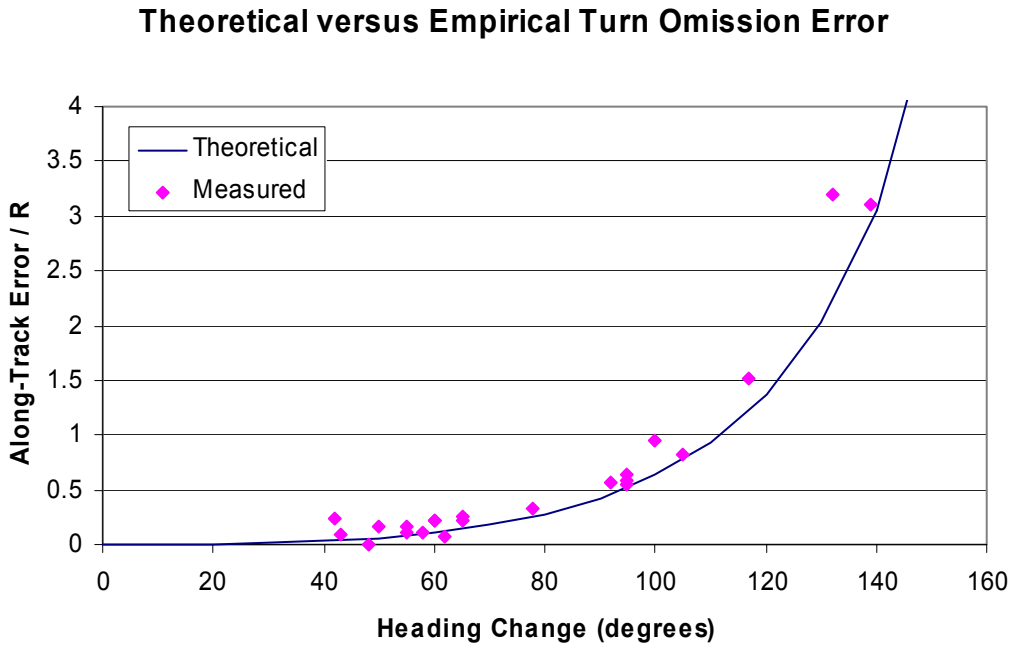

Figure 5-18 Theoretical windless non-dimensional along-track error versus actual non-dimensional along-track error obtained due to turn model omission

Using the above model, we can determine the magnitude of the error due to neglecting turns under specific circumstances. This section presents an assessment of the impact of the turn-model omission error under typical conditions encountered by aircraft in the NAS.

Distribution of Turns – Flight Plans

Using a random selection of flight plans filed for the NAS, we collected statistics on the distribution of turns occurring in the filed flight plans. Note that flight plans do not contain turn information associated with vectors; however, it is useful to understand the relative magnitude of ignoring turn dynamics for the flight plans as well. Prior to collecting these statistics, an altitude profile was assigned to all flights for which flight plans were obtained. The flight was assumed to climb using a nominal profile for the aircraft type, cruise at the filed flight level and descend using a nominal descent profile for the aircraft type. This allowed us to aggregate turn data according to the approximate phase of flight. Since this investigation only focused on the en route portion of flight, we only considered that portion of flight above 10,000 feet. Turns were detected in the flight plan by obtaining those waypoints for which the heading change exceeded 5 degrees.

Figure 5-19 to Figure 5-21 illustrate the temporal distribution of turns from the beginning of the en-route climb phase, from the beginning of the cruise phase (top-of-climb) and to the end of the descent phase (10,000' cut-off). The data show an average of 3.3 turns per flight, with 0.9 turns in the climb phase, 1.7 in the cruise phase and 0.7 turns in descent. During the cruise phase, the distribution of turns is determined by the distribution of flight times (Figure 5-22).

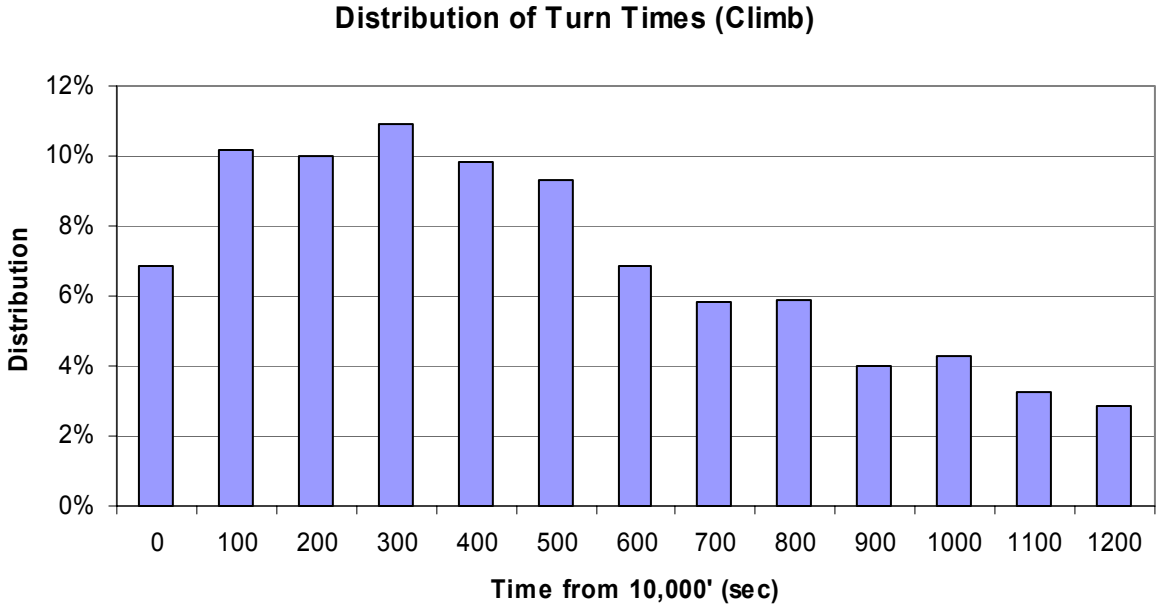

Figure 5-19 Temporal distribution of turns from start of climb (obtained from flight plan data)

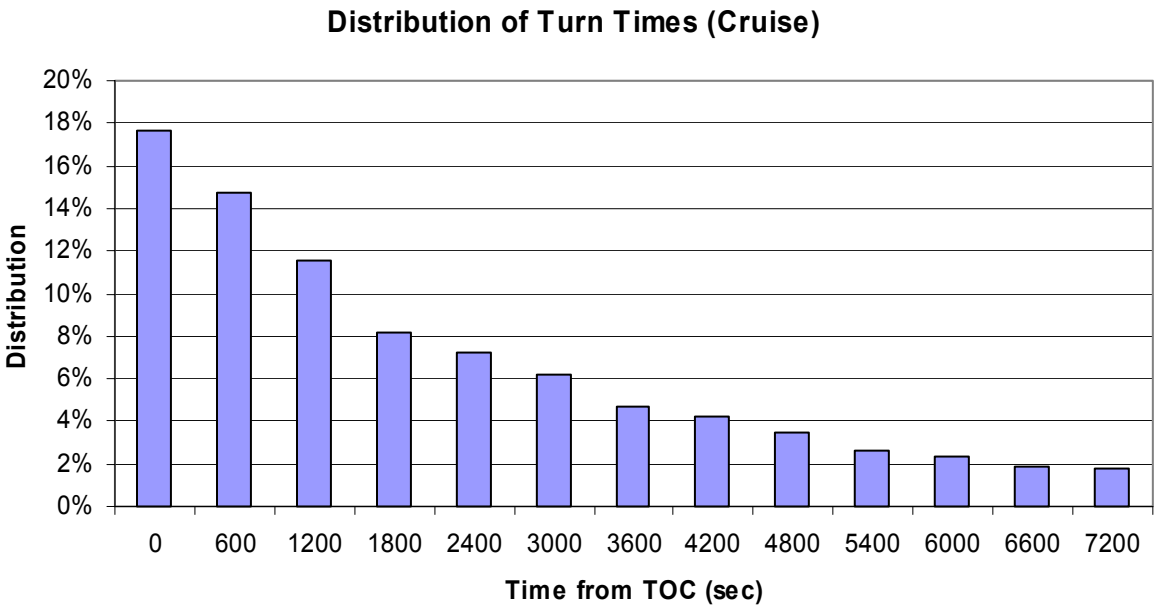

Figure 5-20 Temporal distribution of turns from start of cruise (obtained from flight plan data)

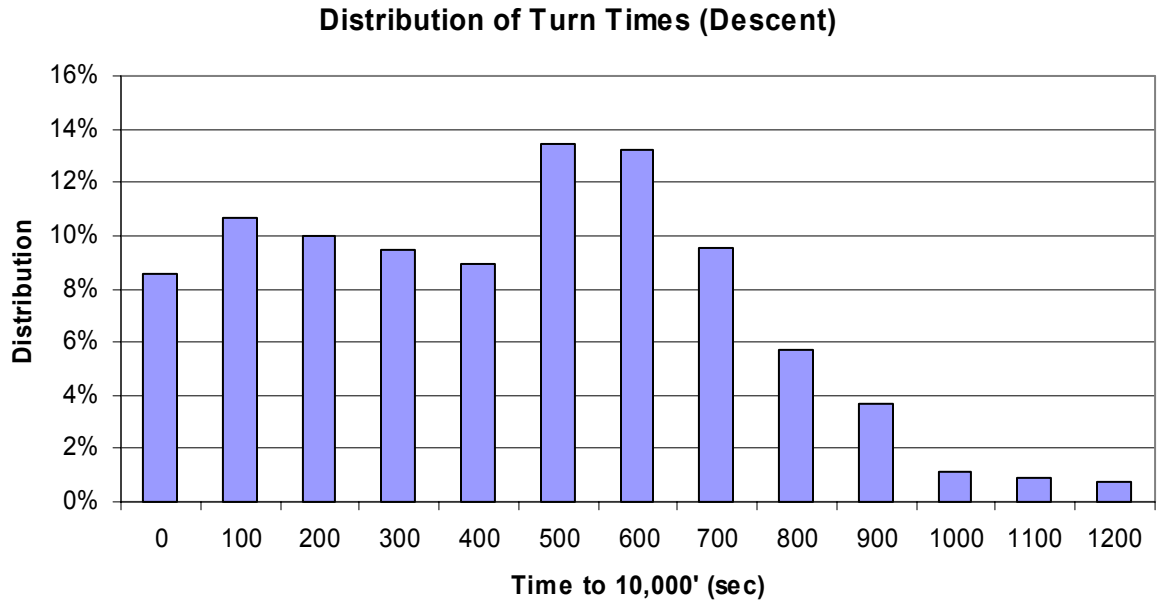

Figure 5-21 Temporal distribution of turns from top-of-descent (obtained from flight plan data)

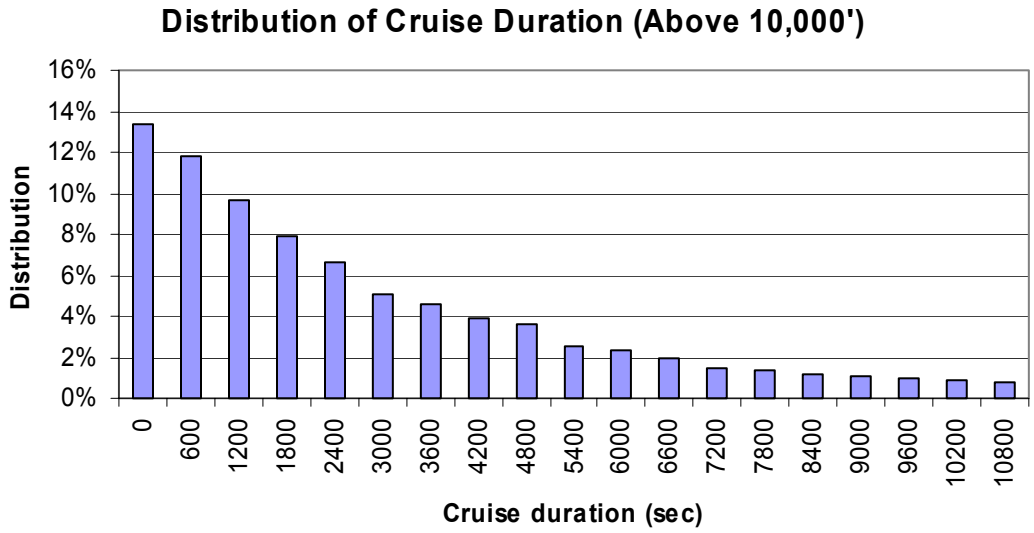

Figure 5-22 Distribution of duration of cruise segments

Turn Omission Errors – Flight Plans

Calculations of the errors attributable to turn model omission were obtained for the above flight plan scenario assuming fly-by waypoints incorporating the effects of forecast winds at the turns. We considered the along-track error as a function of look-ahead time for each flight, at different points along the flight. Figure 5-23 illustrates the process. A flight experiencing a turn at, say 10 minutes, will experience a change in along-track error at the turn. As the flight progresses, the turn moves closer to the present time. When the turn is completed, the along-track error due to the sequenced turn can be "zeroed-out" assuming trajectory prediction will use the current state as an initial condition. We collected statistics on these curves for all flights and time-points along the flight. When a phase of flight ended, the error was assumed to continue until the end of the phase of flight. The mean and standard deviations were obtained as a function of look-ahead times. Figure 5-24 through Figure 5-27 illustrate the mean and mean plus one standard deviation (σ) for various phases of flight and for the flight as a whole. Note that *the averaged statistics will have a much smaller impact than the impact on a specific flight experiencing a turn*. The description of the error as shown in the figures below is useful to compare the impact of neglecting turn modeling for those instances not necessarily associated with turns. However, certain applications require precise trajectory prediction under circumstances with large turns. For these applications, one must consider the errors described previously given the magnitude of the expected turns.

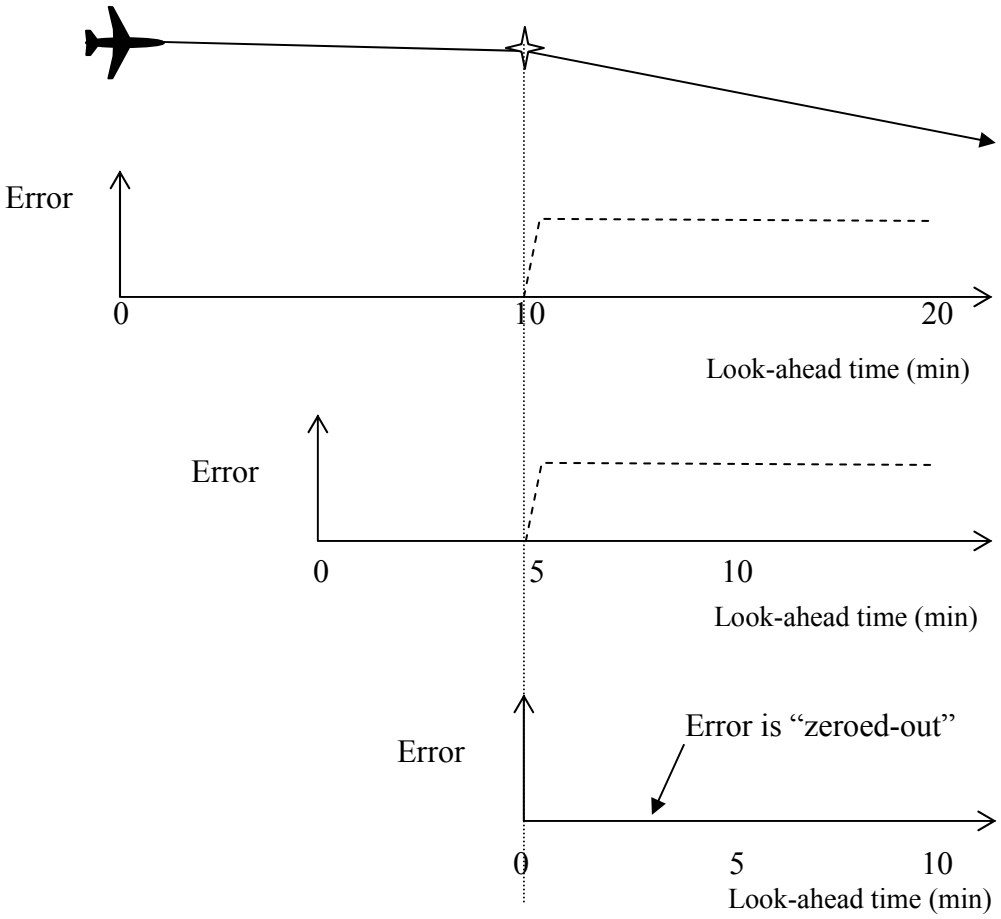

Figure 5-23 Illustration of turn omission error versus look-ahead time

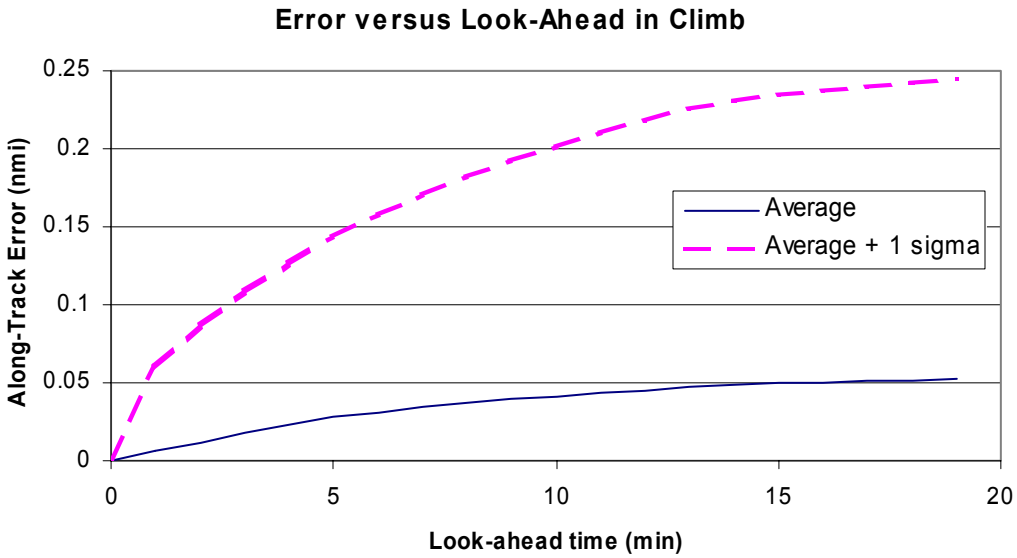

Figure 5-24 Average and standard deviation from turn-omission in climb (flight plan data)

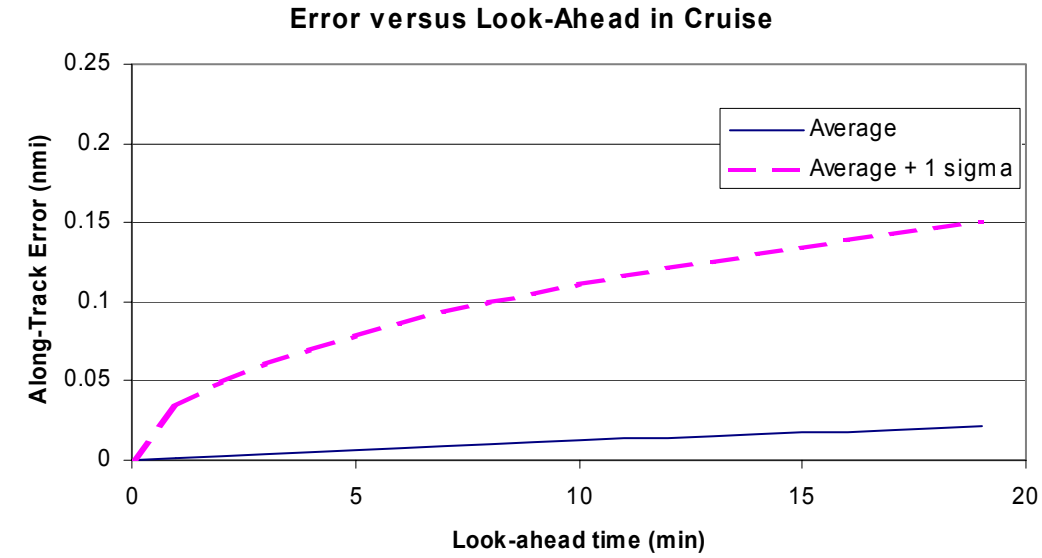

Figure 5-25 Average and standard deviation from turn-omission in cruise (flight plan data)

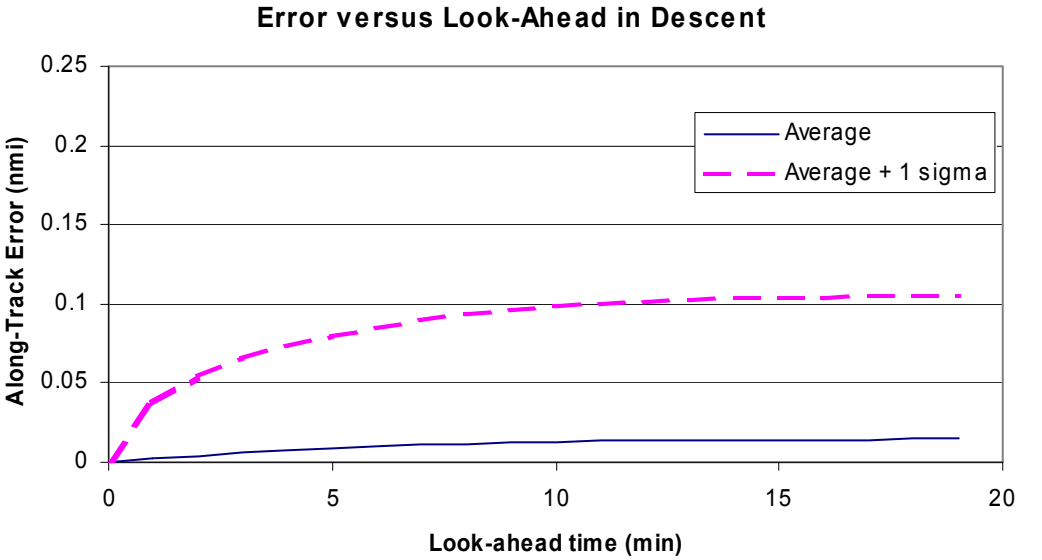

Figure 5-26 Average and standard deviation from turn-omission in descent (flight plan data)

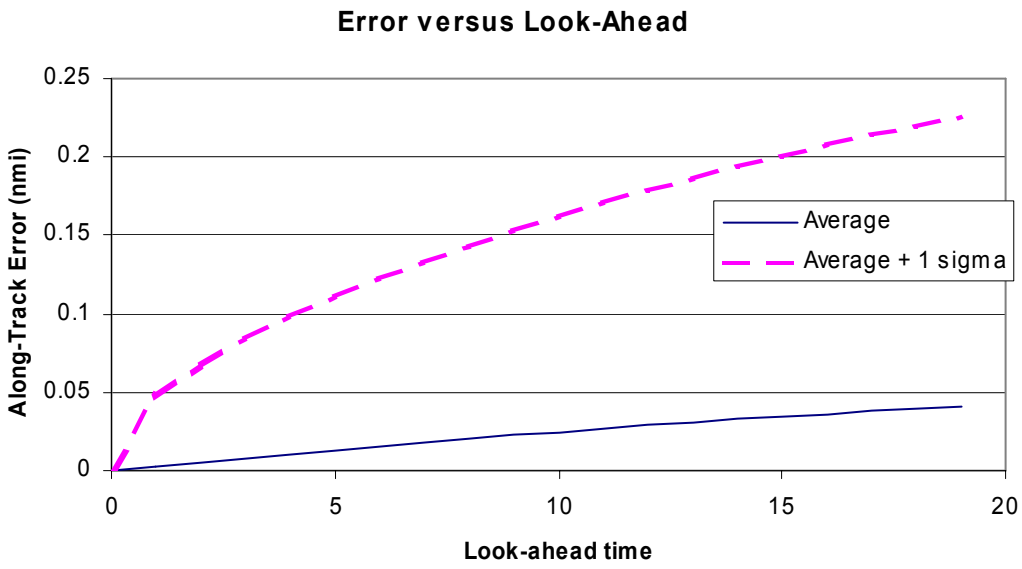

Figure 5-27 Average and standard deviation due to turn omission (flight plan data)

Distribution of Turns – Actual Flights

A random selection of flights was obtained from actual observed ETMS data to approximate the number of turns encountered by flights rather than planned for in the flight plan. Since the data is based upon a low frequency update rate, turns for shorter vectors could easily be missed by this approach to obtaining the data. Again, only turns above 10,000 feet were considered and only those turns with a heading change exceeding 5 degrees were considered. Flight phases were approximated by identifying the top of climb as that point resulting in either the maximum altitude, or a level flight in excess of 5 minutes. The top of descent point was considered that point at which the flight began descending from the maximum altitude to account for stepped descents.

Figure 5-28 shows the turn distribution by phase of flight. Note the higher proportion of small turns in the cruise phase relative to the climb and descent phase. This is expected, as merging functions will require the assignment of larger deviations for climbing and descending flights. We observed an average of 1.6 turns per flight in the climb phase, 3 turns per flight in the cruise phase, and 1.6 turns per flight in the descent phase. However, this data should be viewed with caution as the turns were extracted from ETMS data which is sampled at one-minute intervals, and which is subject to noise in the calculated heading. We filtered for noise by ensuring that turns were larger than 5 degrees and were sustained heading changes.

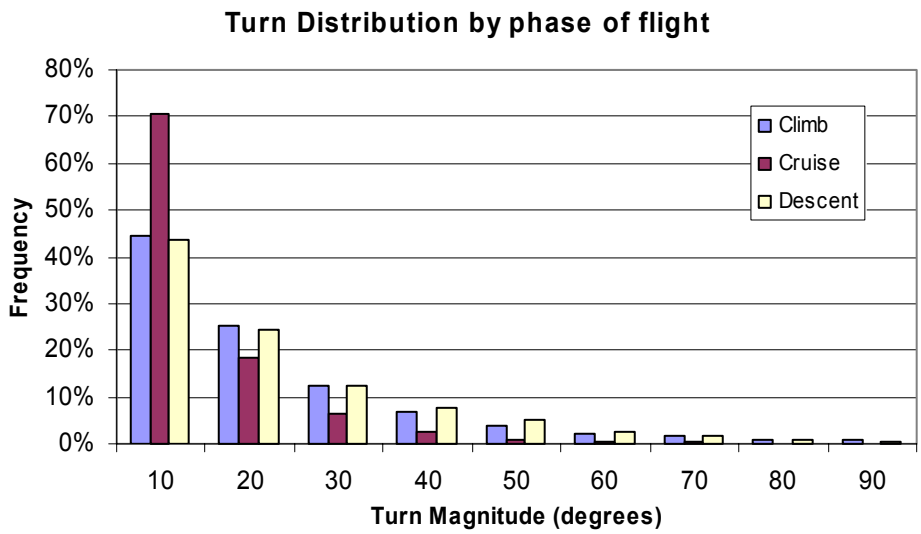

Figure 5-28 Turn distribution by phase of flight (from as-flown, ETMS trajectories)

Using higher-fidelity radar data, statistics were accumulated for turns that appeared to be due to a vector instruction. As this was based upon radar data, only vectors with a "turnback" were identified. Figure 5-29 illustrates the cumulative distribution function of the turn magnitudes as a function of altitude band. These distributions were obtained empirically and fitted to a gamma distribution. Note that most en route flight levels experience a similar distribution of turns with the exception of the highest flight level band which tends to experience smaller vectors.

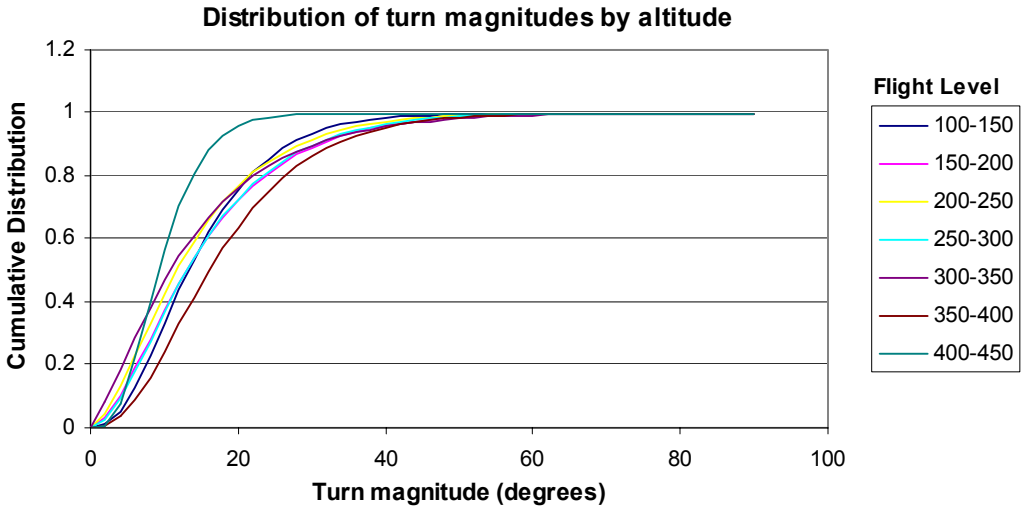

Figure 5-29 Turn distribution as a function of altitude for vectors

The magnitude of the turnback vector is a strong function of the original vector angle, Figure 5-30 illustrates the distribution of the magnitude of this second turn as a function of the original turn angle.

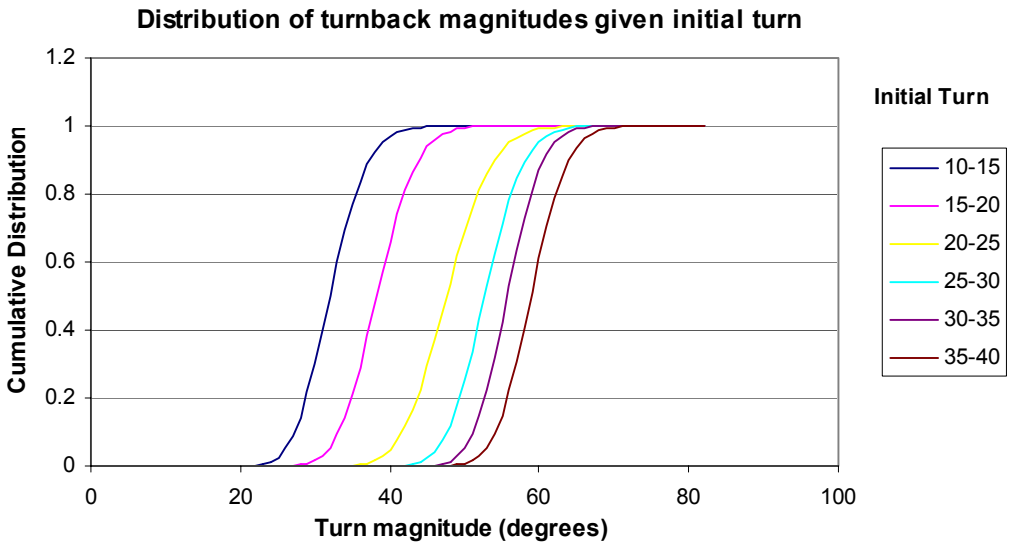

Figure 5-30 Distribution of "turnback" angles as a function of initial turn (in degrees)

Using the distribution of turn magnitudes as a function of altitude, the distribution of along-track errors due to neglecting turn-dynamics (for fly-by waypoints) can be obtained. This required the distribution of speeds for jets and turboprops given an altitude band, which was obtained for the same data sample. Figure 5-31 and Figure 5-32 illustrate the cumulative distribution of along-track errors for jets and props as a result of the initial turn. This information is useful if one is interested in the along-track error that is to be expected for a given turn. Note that the figures describe the error for the initial turn, not the turn-back (which would be greater, and conditioned on the first turn).

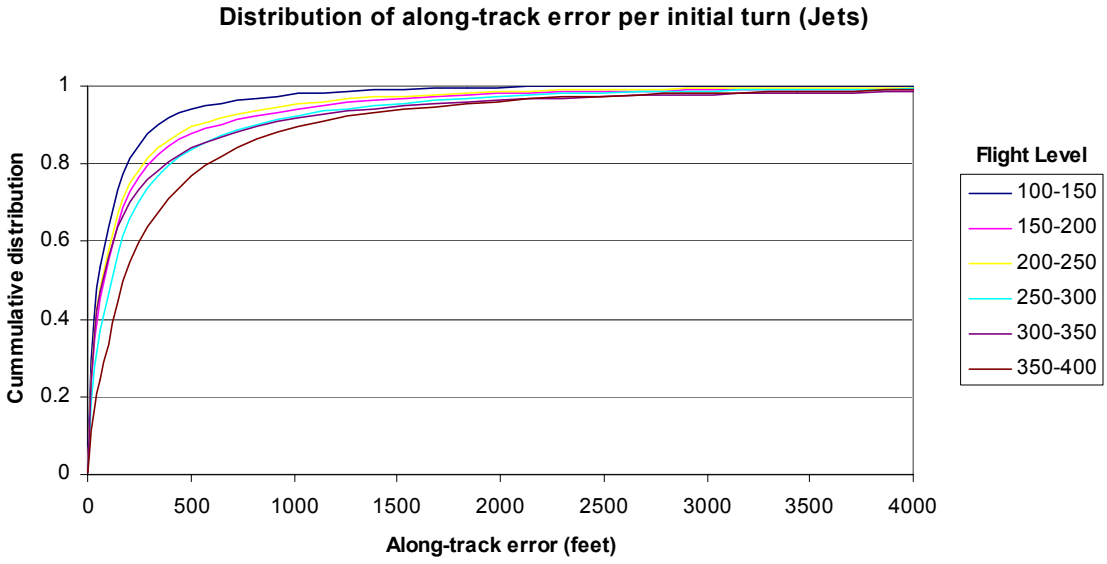

Figure 5-31 Cumulative distribution of along-track errors from turn omission (jets)

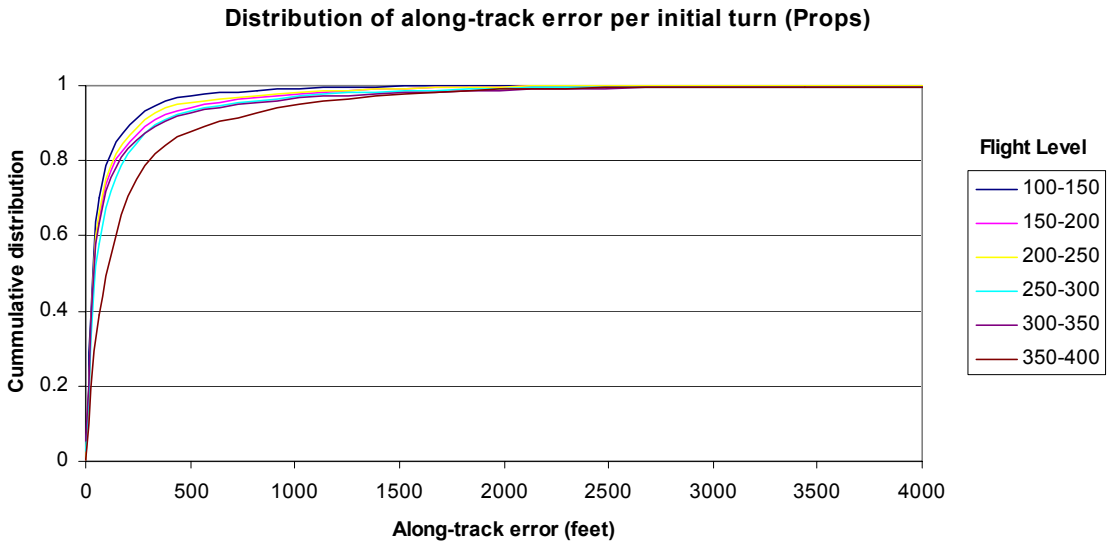

Figure 5-32 Cumulative distribution of along-track errors from turn omission (props)

5.2 Vertical Wind Gradient Omission

5.2.1 Description of Error

Trajectory predictors will often include the effect of winds on climb and descent, but neglect the effect of the wind gradient term. As the aircraft climbs or descends through a vertical gradient in the wind field, the aircraft is subject to an acceleration or deceleration term that must be properly accounted for in the equations of motion. Certain commonly-used quasi-static methods for obtaining vertical profiles neglect this term and are subject to a trajectory prediction error.

This term is best illustrated by an example. Consider a climbing flight as shown in the Figure below. A force balance along the horizontal provides the acceleration in an inertial frame as follows:

$$\left[T-(D+mg\sin(\gamma))\right]\cos(\gamma)=m\frac{dV_g}{dt}$$

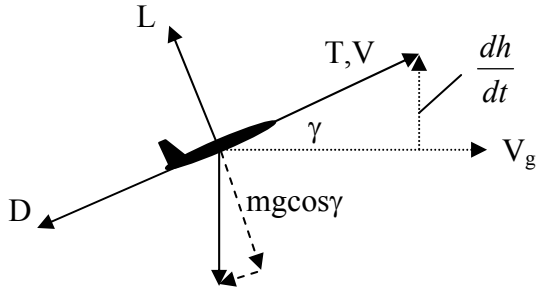

Figure 5-33 Forces on a climbing flight

The horizontal ground speed can be separated into airspeed (V) and wind speed (w) components, assuming a negligible vertical wind component.

$$V_g = V\cos(\gamma)+w$$

Substituting into the force balance equation, and applying the chain rule:

$$\frac{T-D}{m}-g\sin(\gamma)=\left(\frac{dV}{dh}+\frac{1}{\cos(\gamma)}\frac{dw}{dh}\right)\frac{dh}{dt}$$
$$=\left(\frac{dV}{dh}+\frac{1}{\cos(\gamma)}\frac{dw}{dh}\right)V\sin(\gamma)$$

Re-arranging, and assuming a small climb angle, we obtain the following expression for the climb angle:

$$\gamma = \left(\frac{T-D}{m}\right)\left[\left(\frac{dV}{dh}+\frac{dw}{dh}\right)V + g\right]^{-1}$$

An increase in the wind gradient (dw/dh) will result in a decrease in the climb rate.

5.2.2 Parametric Analysis

The expression for the climb gradient can be expressed in terms of three non-dimensional parameters: a force term, an airspeed gradient term and a wind gradient term. Respectively, these are:

$$\frac{T-D}{mg} \quad \frac{V}{g}\frac{dV}{dh} \quad \frac{V}{g}\frac{dw}{dh}$$

The climb gradient can be normalized and expressed as a function of a non-dimensional speed gradient term and a non-dimensional wind gradient term:

$$\frac{\gamma}{\left(\frac{T-D}{mg}\right)} = \left[\frac{V}{g}\frac{dV}{dh}+\frac{V}{g}\frac{dw}{dh}+1\right]^{-1}$$

During the en route portion of flight, four situations are considered herein for jet aircraft. These are:

- Constant Mach climb segment. Power is fixed, the flight climbs at a constant Mach number and the climb rate is an output.
- Constant CAS climb segment. Power is fixed, the flight climbs at a constant CAS and the climb rate is an outcome.
- Constant Mach descent segment. Power is set to idle, the flight descends at a constant Mach number. The descent rate is an outcome.
- Constant CAS descent segment. Power is set to idle, the flight descends at a constant CAS. The descent rate is an outcome.

While these segments are described explicitly in this report, other transition modes would also be subject to errors from omission of the wind gradient term.

For typical jet aircraft in the en route portion of flight (10,000' and above), the following ranges of parameters are typical for the above non-dimensional parameters:

$$\left.\frac{T-D}{mg}\right|_{Cl} \in (0,0.25)$$

$$\left.\frac{T-D}{mg}\right|_{Des} \in (-.04,-.25)$$

$$\left.\frac{V}{g}\frac{dV}{dh}\right|_{CAS} \in (0,0.4)$$

$$\left.\frac{V}{g}\frac{dV}{dh}\right|_{Mach} \in (-0.1,0.)$$

$$\frac{V}{g}\frac{dw}{dh} \in (-0.15,0.15)$$

The first term ($\frac{T-D}{mg}$) has one range for the climb portion of flight and one for the descent portion of flight. The speed gradient term can be obtained for a flight climbing or descending at a constant calibrated airspeed or at a constant Mach number. The wind gradient term will depend on whether the gradient is a headwind (negative) or a tailwind (positive).

The figures below illustrate the behavior of the $\frac{T-D}{mg}$ term and the speed gradient term for a selection of aircraft models in both climb and descent assuming an ICAO standard atmosphere. A variety of aircraft models were investigated across weight categories (from heavy to regional jets). We also investigated models from differing manufacturers and different generations. The range of the above parameters was consistent across all classifications of aircraft. However, in generating the figures below, the flight envelopes were not applied as hard limits on the curves. The reader is cautioned that some speed-altitude combinations may not be applicable even though they are shown as producing a parameter value.

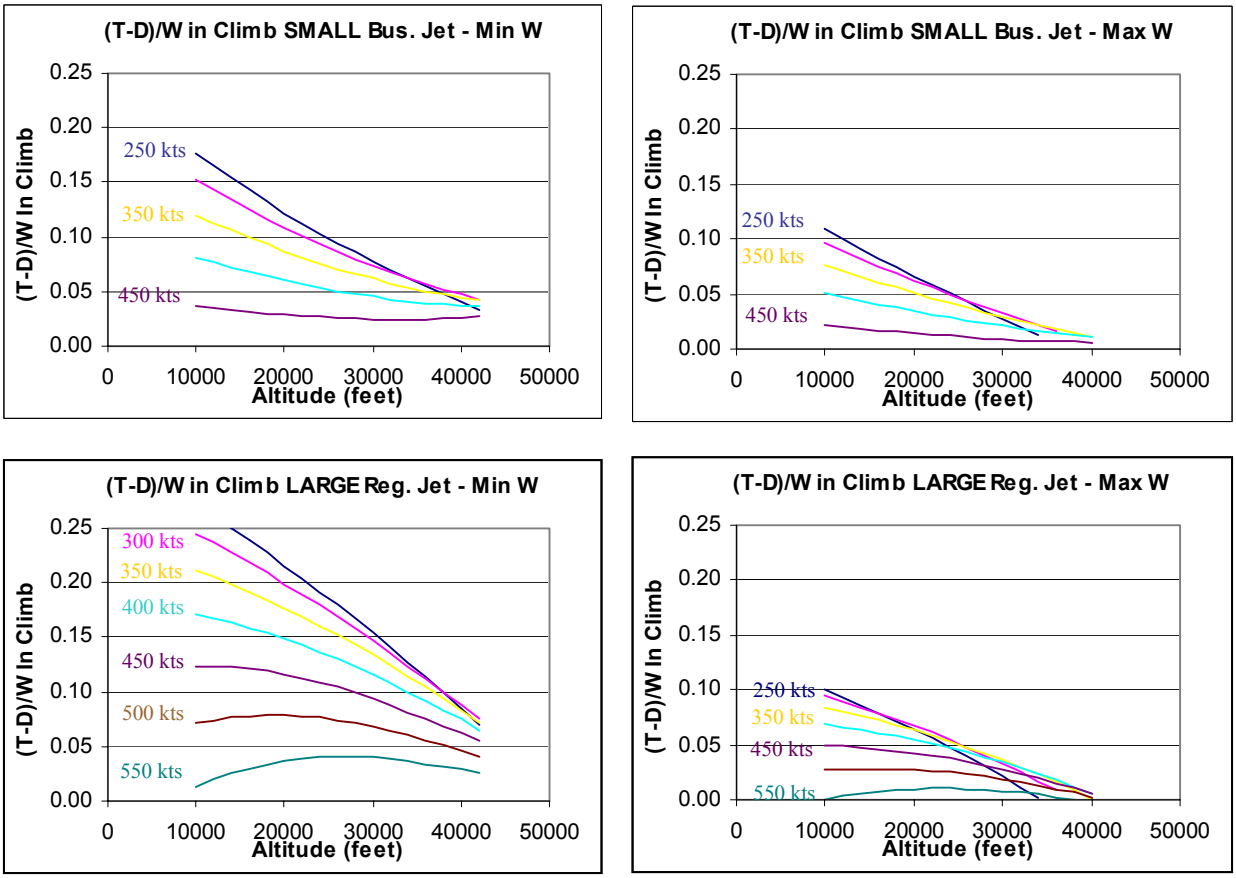

Figure 5-34 $\frac{T-D}{mg}$ during climb as a function of altitude for various aircraft types, weights and true airspeeds

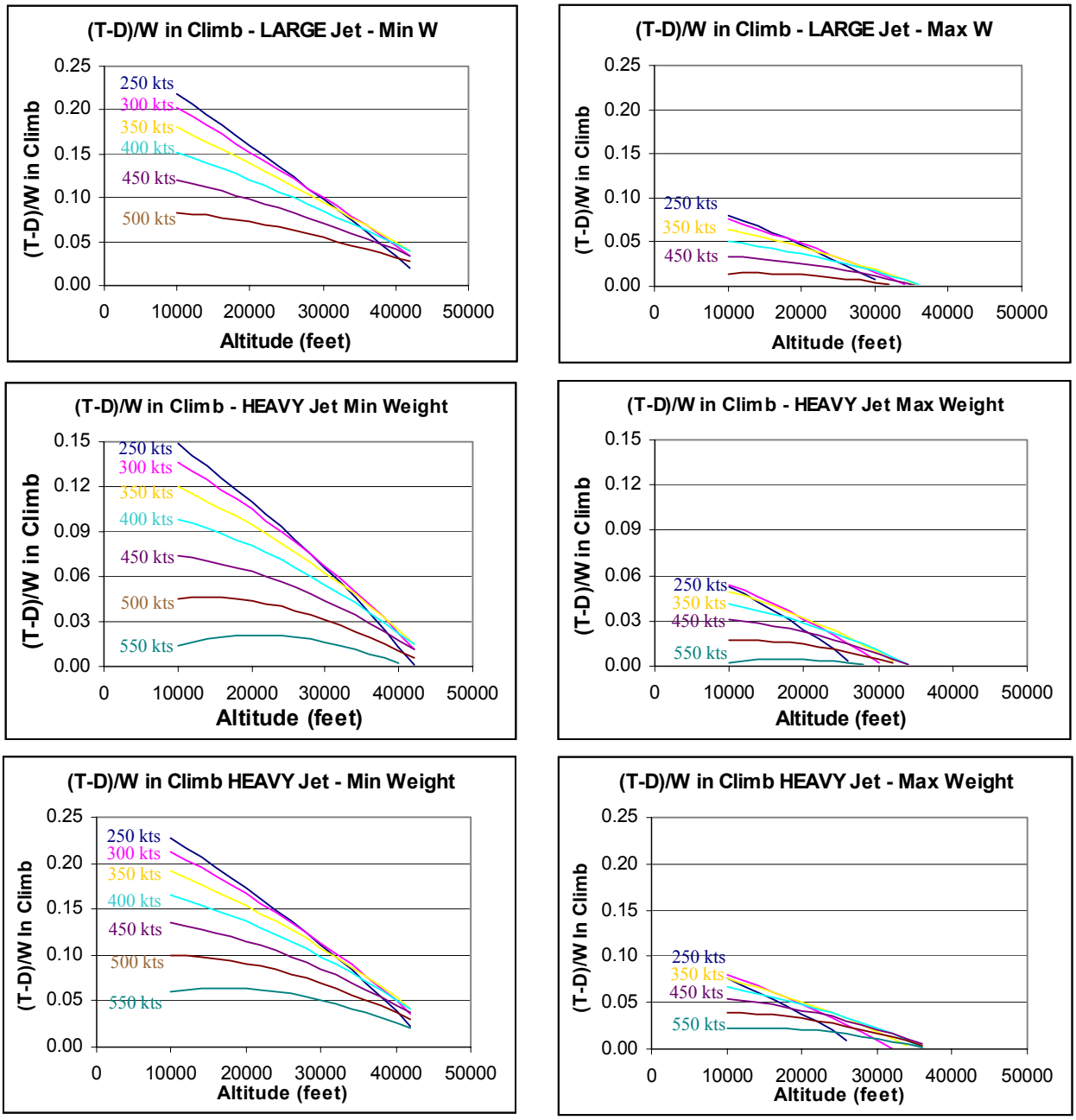

Figure 5-35 (cont'd). $\frac{T-D}{mg}$ **during climb as a function of altitude for various aircraft types, weights and true airspeeds.**

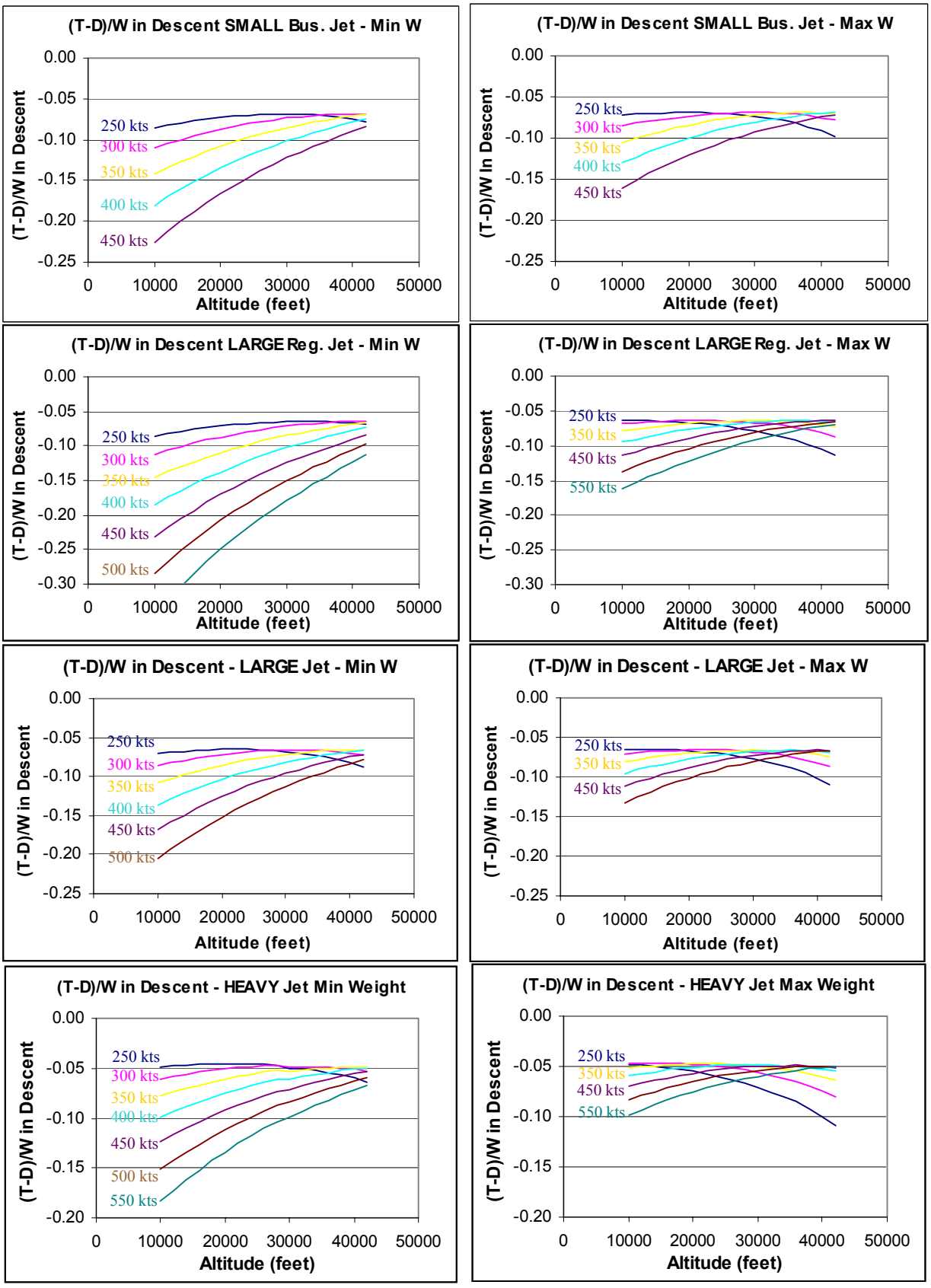

Figure 5-36 $\frac{T-D}{mg}$ **during descent as a function of altitude for various aircraft types, weights and airspeeds.**

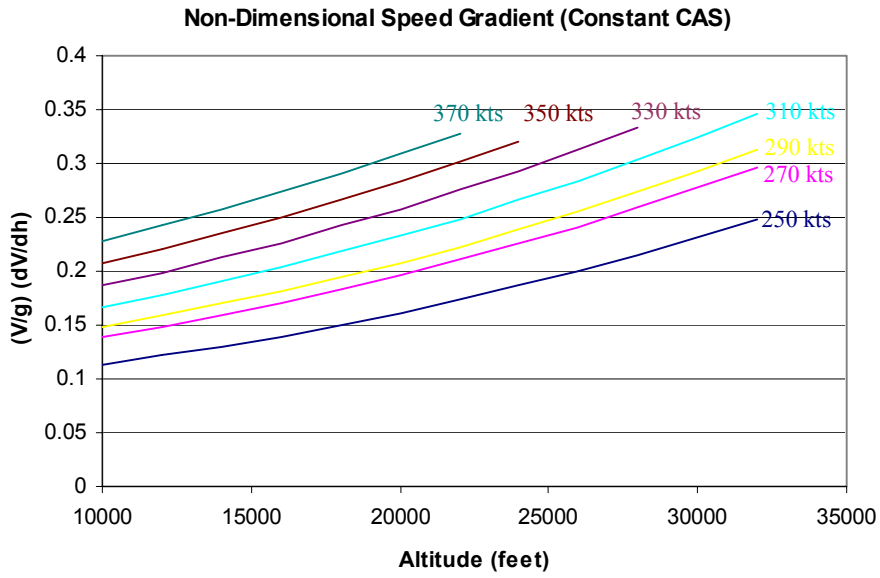

Figure 5-37 Non-dimensional speed gradient for constant CAS

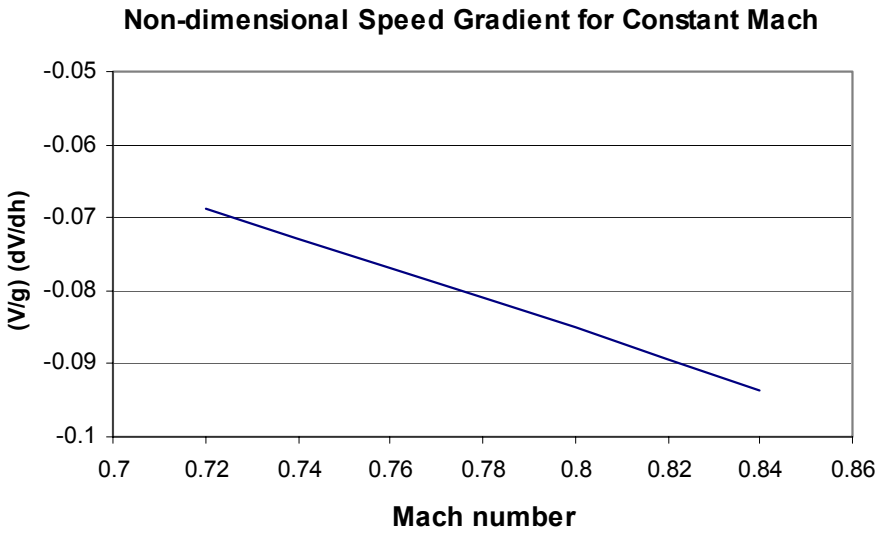

Figure 5-38 Non-dimensional speed gradient for constant Mach

The previous figures may be applied to estimate the climb gradient error associated with a neglect of the wind gradient term. For example, a flight climbing at a calibrated airspeed of 320 knots would encounter a non-dimensional speed gradient ($\frac{V}{g}\frac{dV}{dh}$) of approximately 0.24 at 20000 feet. For a heavy jet at lowest weight, we also have $\frac{T-D}{mg} = 0.064$. If one neglects the wind gradient effect by setting the ($\frac{dw}{dh}$) term to zero, a climb gradient (γ) of 0.0516 (2.95°) is obtained through substitution into the following expression:

$$\frac{\gamma}{\left(\frac{T-D}{mg}\right)} = \left[\frac{V}{g}\frac{dV}{dh} + \frac{V}{g}\frac{dw}{dh} + 1\right]^{-1}$$

However, if one includes in the calculation a constant wind gradient of 2.54 fps per 1000 feet, a gradient of 0.049 (2.82°) is obtained at the 425 knot true airspeed. This yields an instantaneous climb rate error of 95 feet per minute on a climb rate of 2120 feet per minute.

As the flight progresses, these errors can integrate into larger altitude errors. Altitude errors also lead to errors in speed resulting in along-track positional errors. An example of these errors is shown below by comparing the altitude and along-track positions at specific times. A collection of different aircraft types operating at different weights and climb speed profiles illustrates the range of vertical and longitudinal errors that can be obtained. The initial altitude of the flight was assumed to be 10,000 feet operating at a speed consistent with the climb speed. The impact of neglecting four different wind gradients is also illustrated. The wind gradients selected are shown below and correspond to a linear gradient from 0 knots at sea level to a speed of: -100, -50, 50 or 100 knots at 33,000 feet.

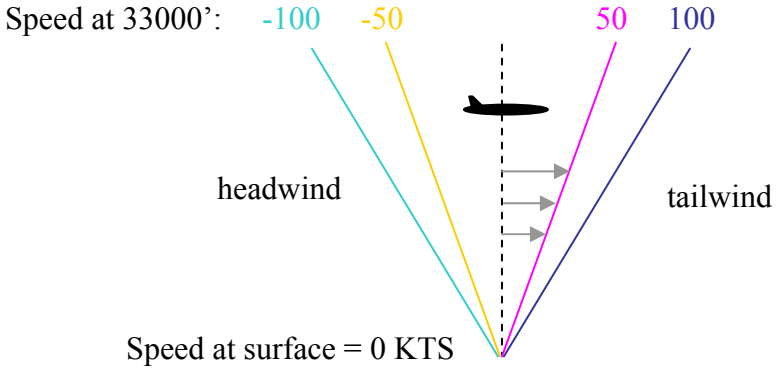

Figure 5-39 Wind gradients applied in examples

The altitude error is easily understood by considering the prior expression for the climb gradient:

$$\frac{\gamma}{\left(\frac{T-D}{mg}\right)} = \left[\frac{V}{g}\frac{dV}{dh} + \frac{V}{g}\frac{dw}{dh} + 1\right]^{-1}$$

Neglecting the $\frac{dw}{dh}$ term gives us too large a climb rate when subject to an increasing tailwind. With an increasing tailwind (positive $\frac{dw}{dh}$ term), neglect of the term provides a path above the actual flight path. Conversely, when subject to an increasing headwind, the climb rate is underestimated. In this case, the erroneous flight path will be below the actual. Assuming the cruise altitude is known precisely, the altitude error will eventually be zero.

The along-track error is a direct consequence of the altitude error. Since the actual flight and the forecast flight are not operating at the same altitude at any time, there is a speed difference between the two. This speed difference will change sign depending on which regime the flights are in. This explains why the along-track error can grow, then decay, then grow again. Consider a flight with a 280/0.74 climb schedule. The speed as a function of altitude is shown below in Figure 5-40. During the constant CAS portion of the schedule, speed increases with altitude. Below the Tropopause, at constant Mach, airspeed decreases with altitude. Above the Tropopause, at constant Mach, airspeed is constant with altitude.

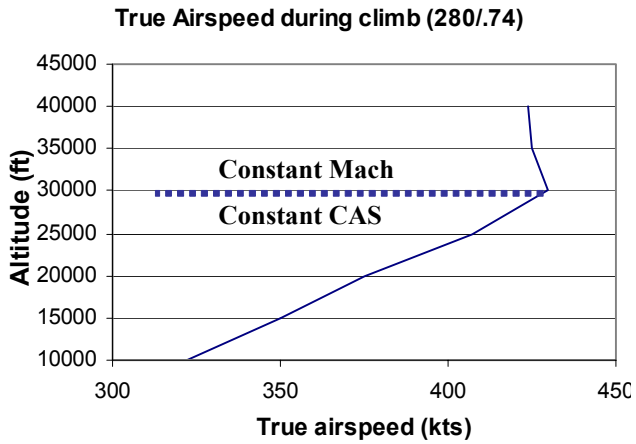

Figure 5-40 Variation of true airspeed during a CAS/Mach climb of 280/0.74

An additional factor to consider is the wind gradient occurring at the altitudes being compared since it is the difference in ground speeds between actual and forecast altitudes that results in an along-track error. The wind gradient explains the lack of symmetry between the headwind and tailwind cases in the figures that follow. For example, headwinds will reduce the altitude effects during the constant CAS segment thereby leading to initially smaller along-track errors with a headwind. For strong headwinds, the wind effect can offset the combined airspeed effects above.

To determine typical wind gradients, statistics on 12 months of forecast wind were obtained over 8 US cities. A principle component analysis (PCA) approach was used to obtain the typical winds as a function of altitude, and the variation around that. Typical wind speeds tended to increase linearly from surface to 35-40,000 feet (depending on location) with gradients as shown in Table 5-2 below. The typical case corresponds to about a 50 knot wind at 33000 feet in the example cases. However, variance in the data indicates that doubling of this gradient is required to capture over half the variance. Thus, gradients twice as large are therefore obtained with some frequency. Furthermore, individual flights may be subject to significantly larger wind gradients over portions of the flight, thus contributing to substantial local climb gradient errors. If the gradients are sustained over a large altitude band, they could integrate into large positional errors.

Table 5-2 Typical wind gradients as a function of location

Location	Wind Gradient (kts/1000')
ATL	1.3
DEN	1.2
DFW	1.2
JFK	1.7
MIA	0.95
ORD	1.5
SEA	1.3
LAX	0.9

The above table represents the *typical* wind gradients that exist in the forecasted winds from surface to cruise altitude. The charts that follow considered the larger gradients as shown in Figure 5-39 and curves are represented with the corresponding colors. For locally larger gradients, the reader is referred to the preceding approach to estimating the error in the climb gradient.

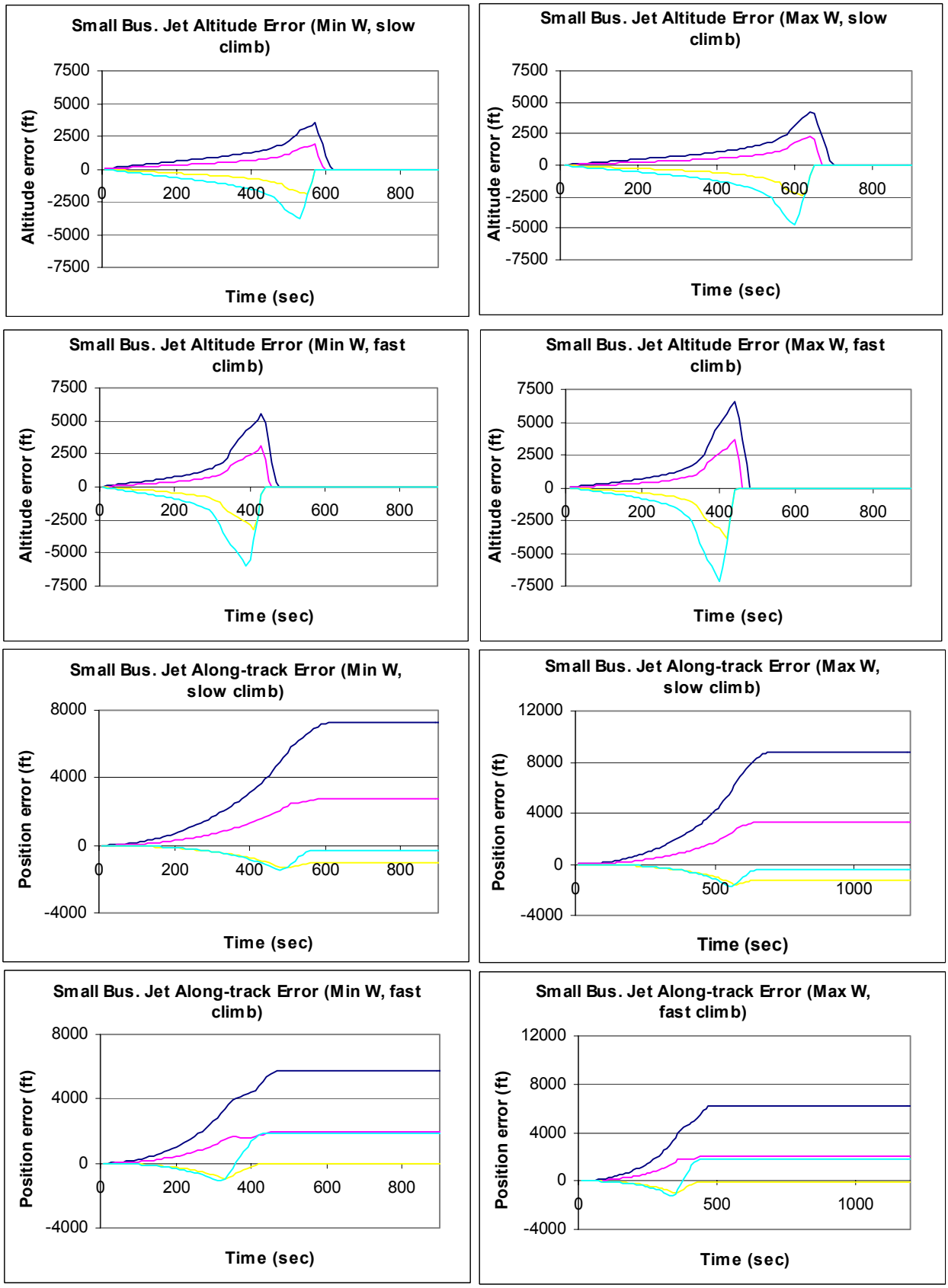

Figure 5-41 Small business jet - Errors due to neglect of wind gradient during climb

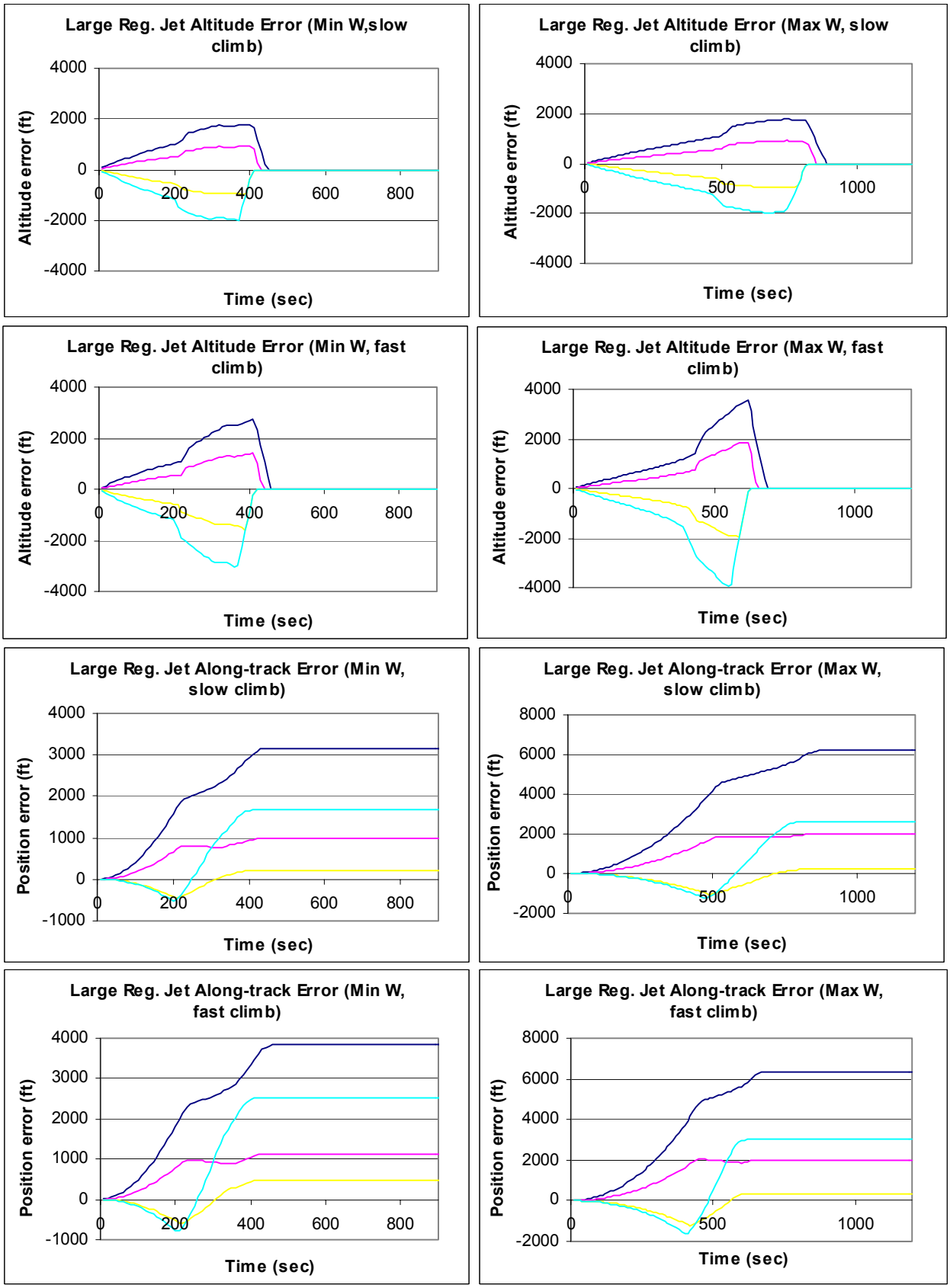

Figure 5-42 Large Regional Jet - Errors due to neglect of wind gradient during climb

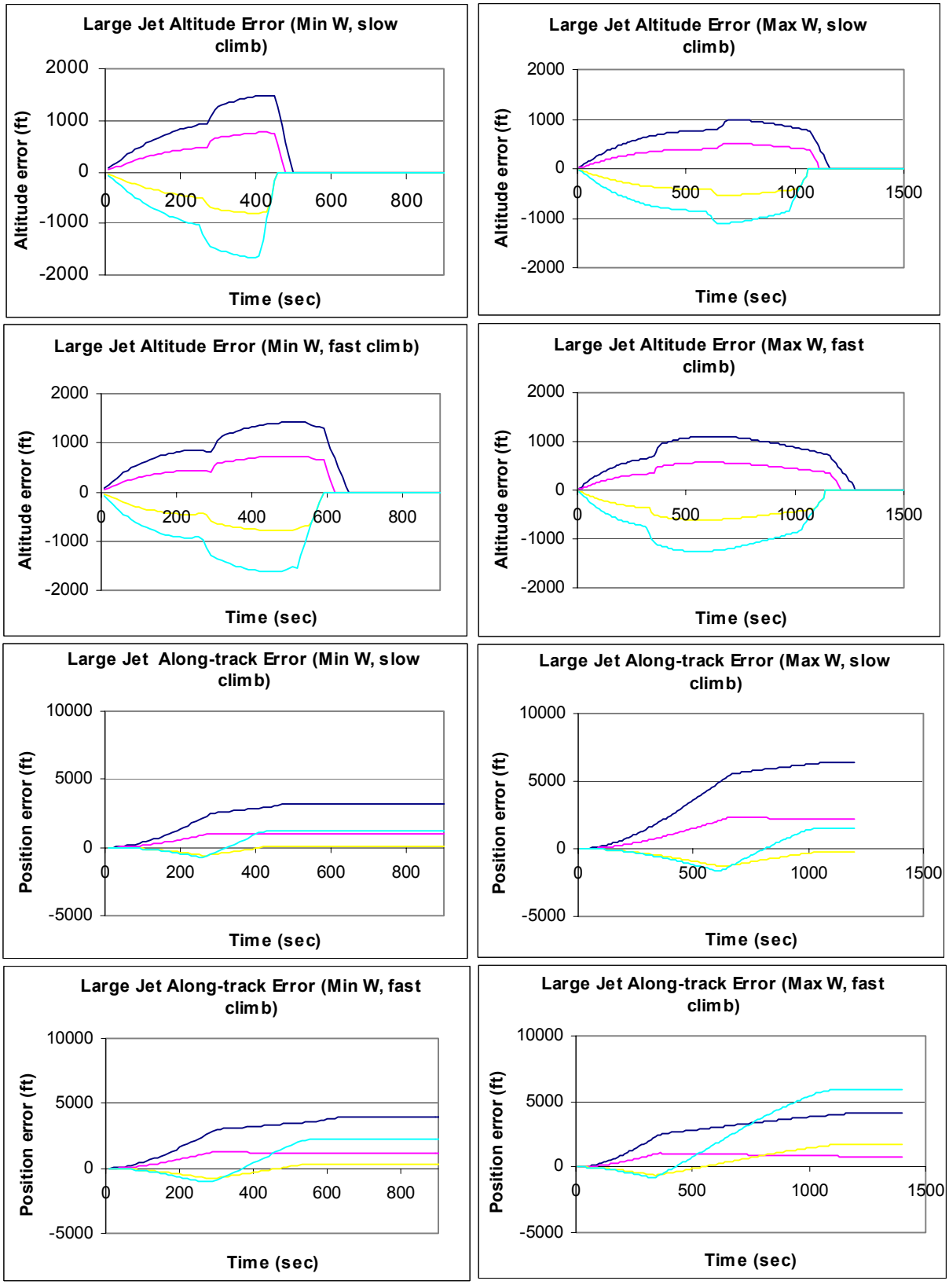

Figure 5-43 Large Jet - Errors due to neglect of climb gradient during climb

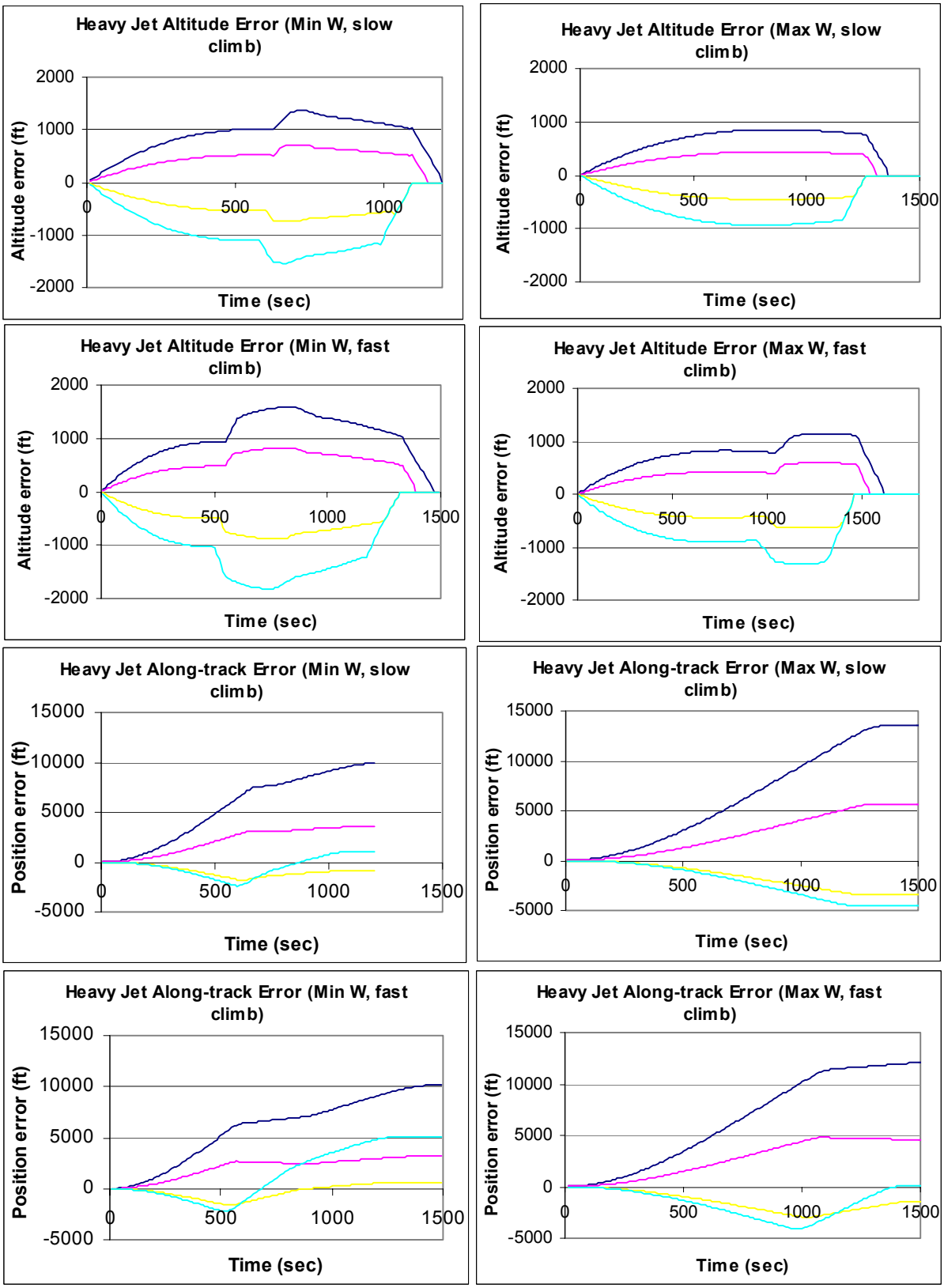

Figure 5-44 Heavy Jet - Errors due to neglect of wind gradient during climb

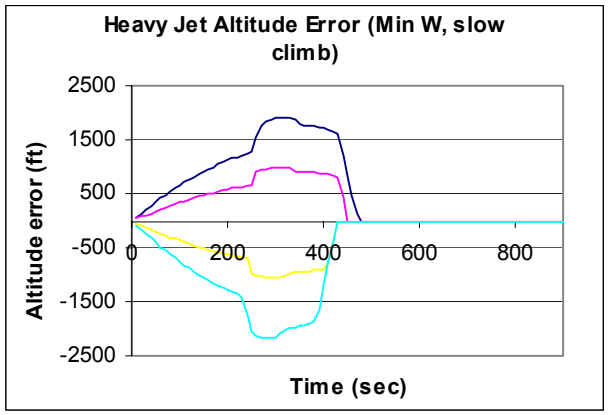

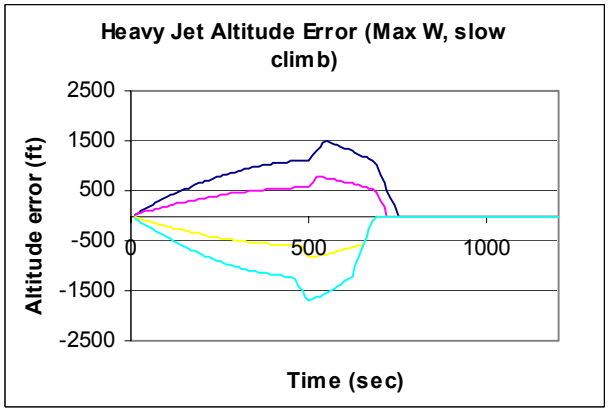

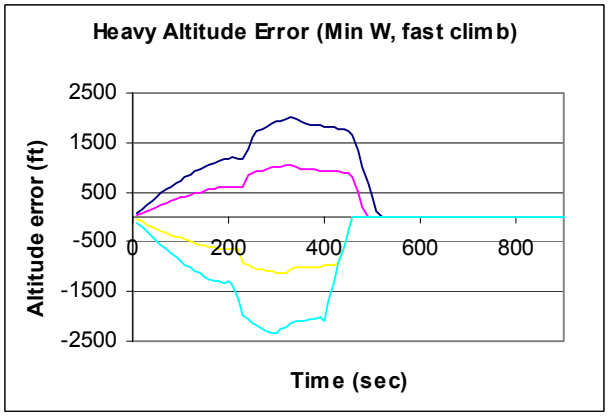

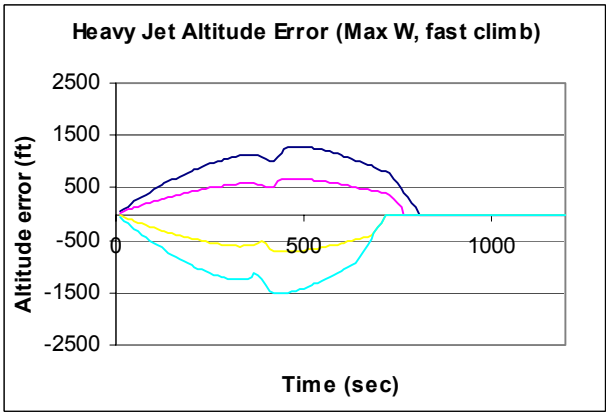

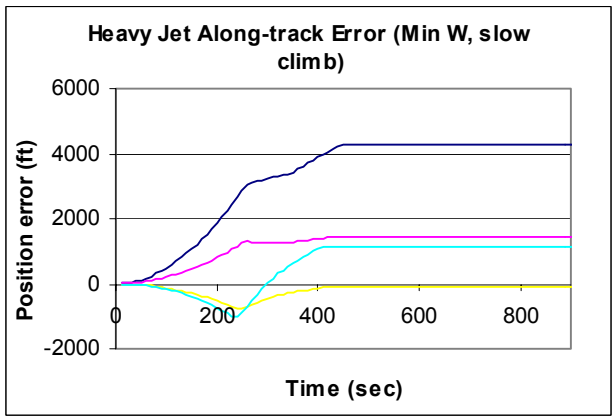

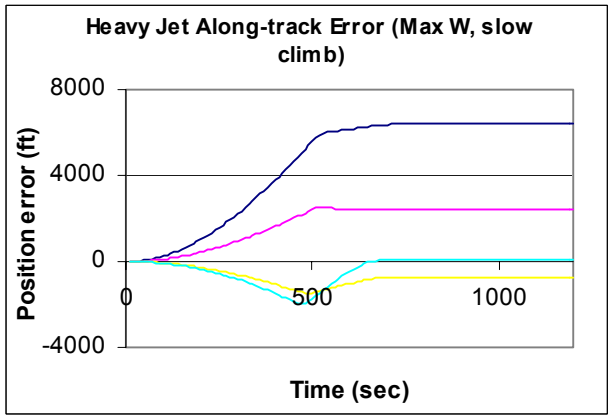

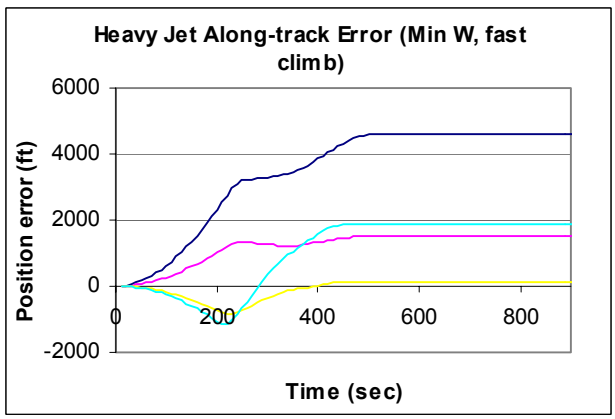

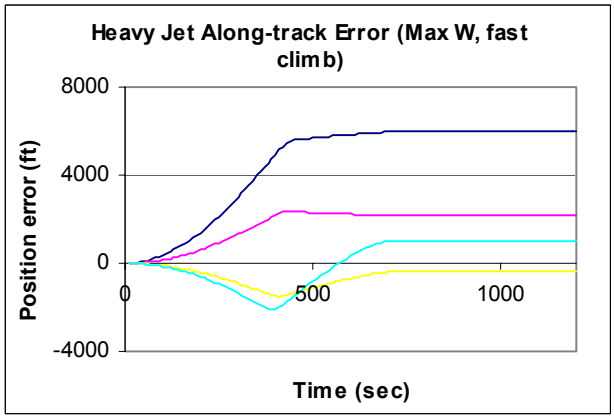

Figure 5-45 Heavy Jet II - Errors due to neglect of wind gradient during climb

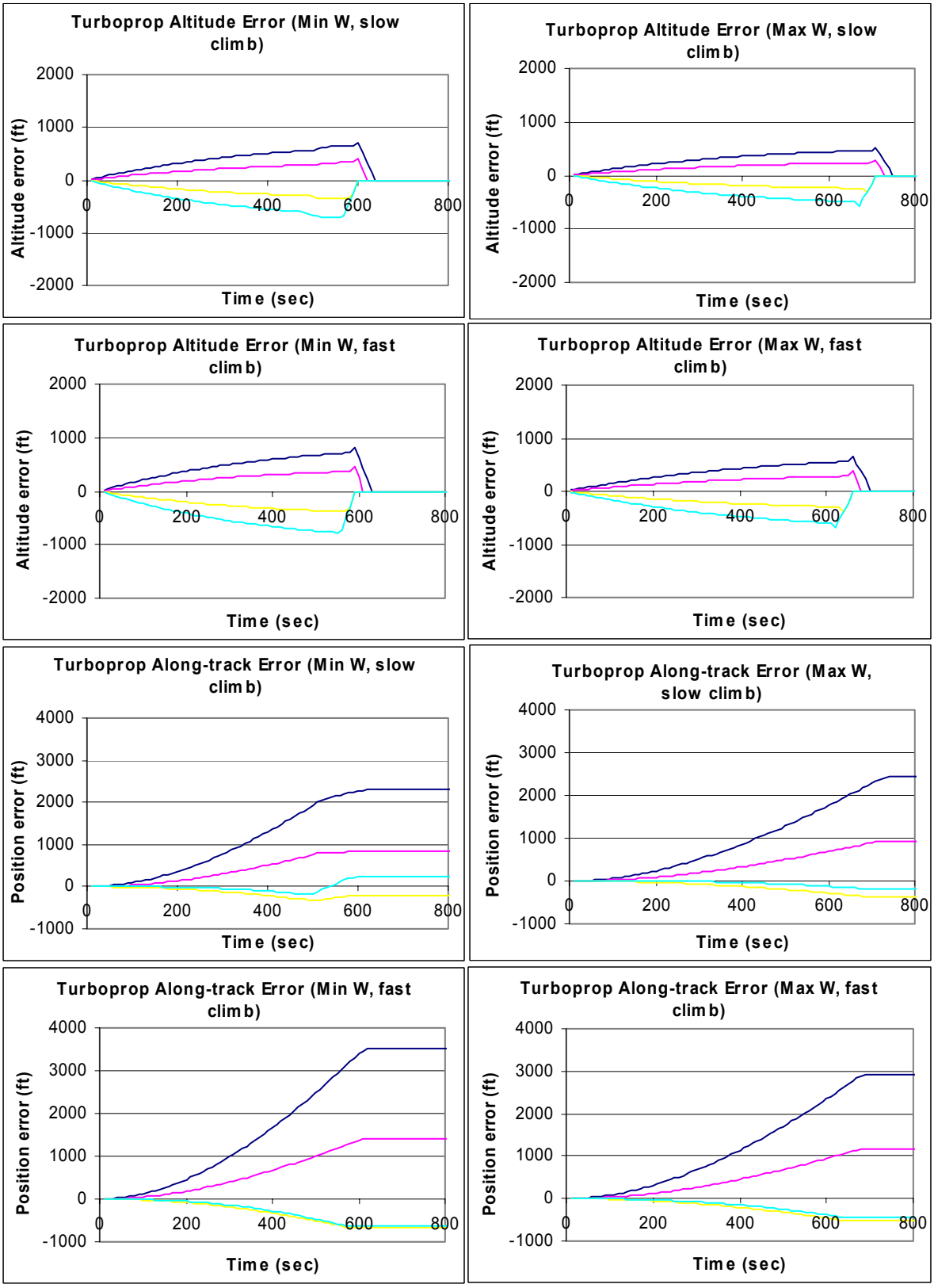

Figure 5-46 Turboprop - Errors due to neglect of wind gradient during climb

During a descent, each flight will encounter three distinct segments. The initial segment will be a constant Mach segment above the tropopause. During this segment, due to the assumed constant temperature, the airspeed will be constant as the flight descends. Changes in ground speed will result due to the assumed wind gradient. Below the tropopause, the flight will experience an increase in airspeed as it descends due to the corresponding increase in temperature and speed of sound. In order to obtain this additional increase in airspeed, the flight will descend more rapidly below the tropopause than above during a constant Mach segment. The third segment is a constant CAS segment during which the airspeed will decrease as the altitude decreases. This results in a shallower flight path angle compared to the constant Mach segment.

When a properly modeled flight is compared to a flight neglecting the wind gradient term, a discrepancy in the altitude profile occurs between the flights as shown below. The difference between these profiles results in a curve with interesting behavior. Since the flights enter each of the previously described segments (constant Mach above/below tropopause and constant CAS) at different times, the difference between the profiles is sometimes the difference between different segment types.

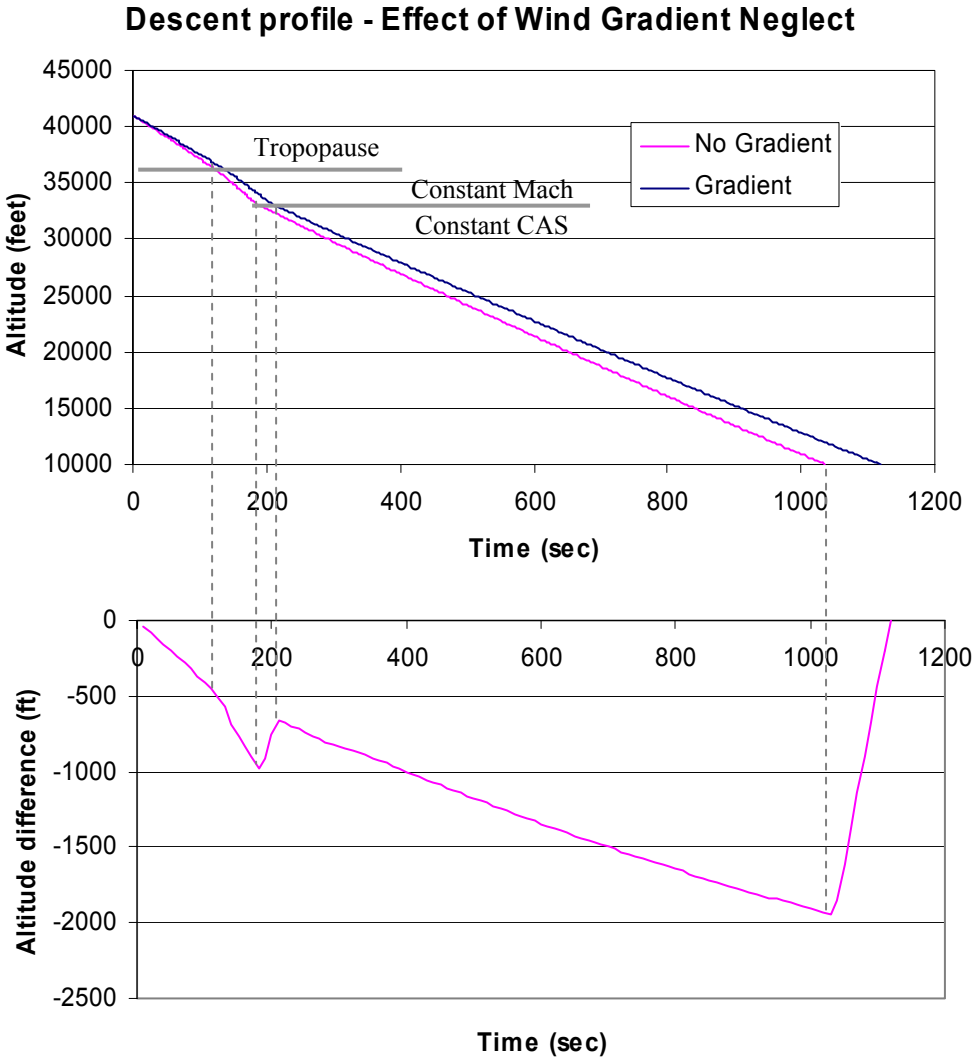

Figure 5-47 Effect of neglect of wind gradient term on altitude during descent (assumed gradient of 3 knots tailwind per 1000 feet over entire descent)

The along-track error is a consequence of the altitude error combined with the speed regimes of the notional flights being compared. As for the case in climb, a flight that is above forecast may experience a higher speed if both the forecast and the actual flight are in a constant CAS regime. However, in the constant Mach regime, the opposite will occur below the tropopause.

Figure 5-48 to Figure 5-52 represent the errors in descent encountered by the same aircraft as modeled in the climb phase. Descents were modeled from cruise altitude to an altitude of 10 000 feet and were assumed to operate at idle thrust during the entire descent from cruise. A range of weights and speeds were used to determine the range of errors that can be encountered due to neglect of the wind gradient term. Each chart shows four curves corresponding to the same wind gradients that were applied for the climb charts (see Figure 5-39 for color description).

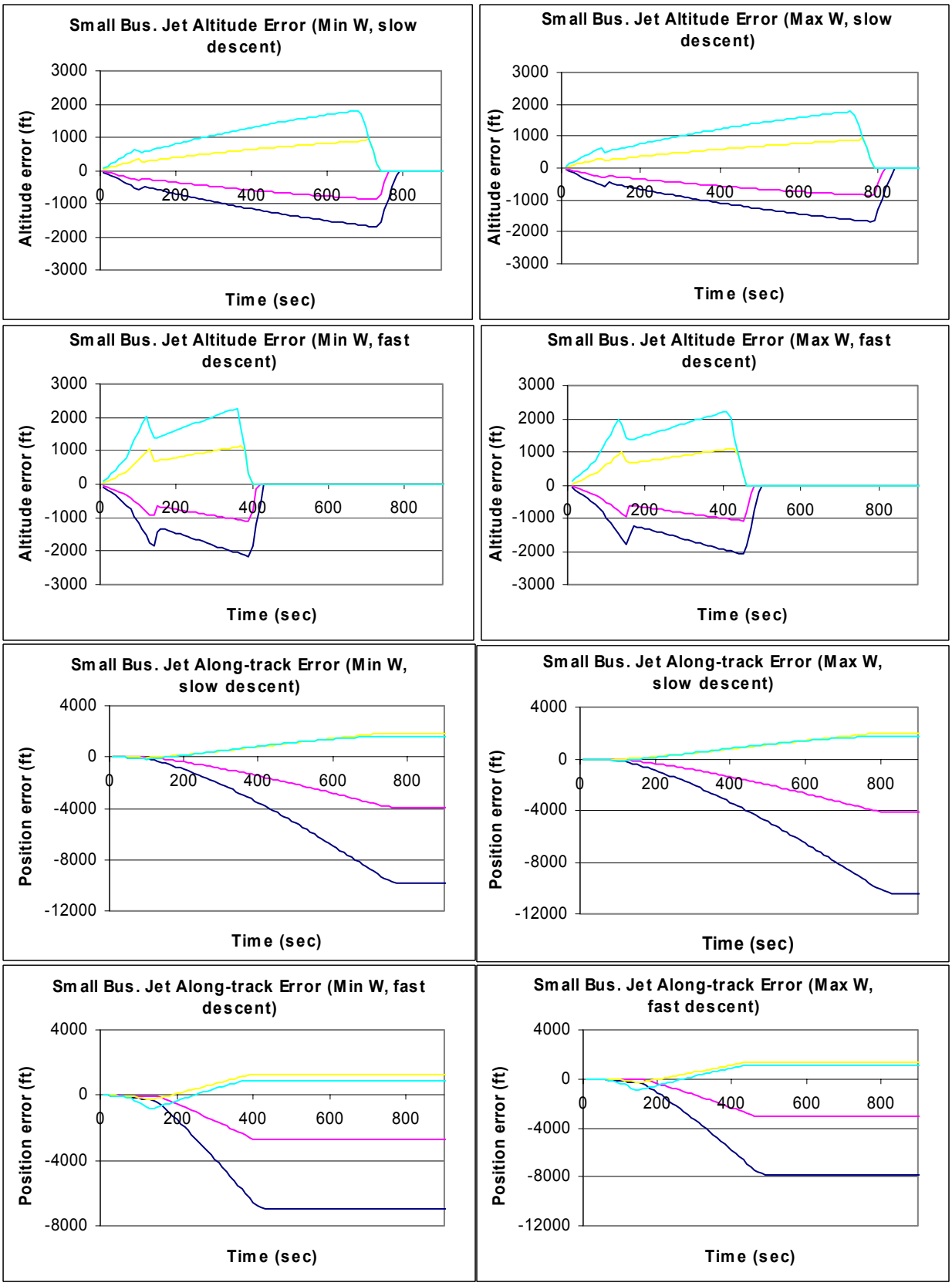

Figure 5-48 Small Business Jet - Errors due to neglect of wind gradient during descent

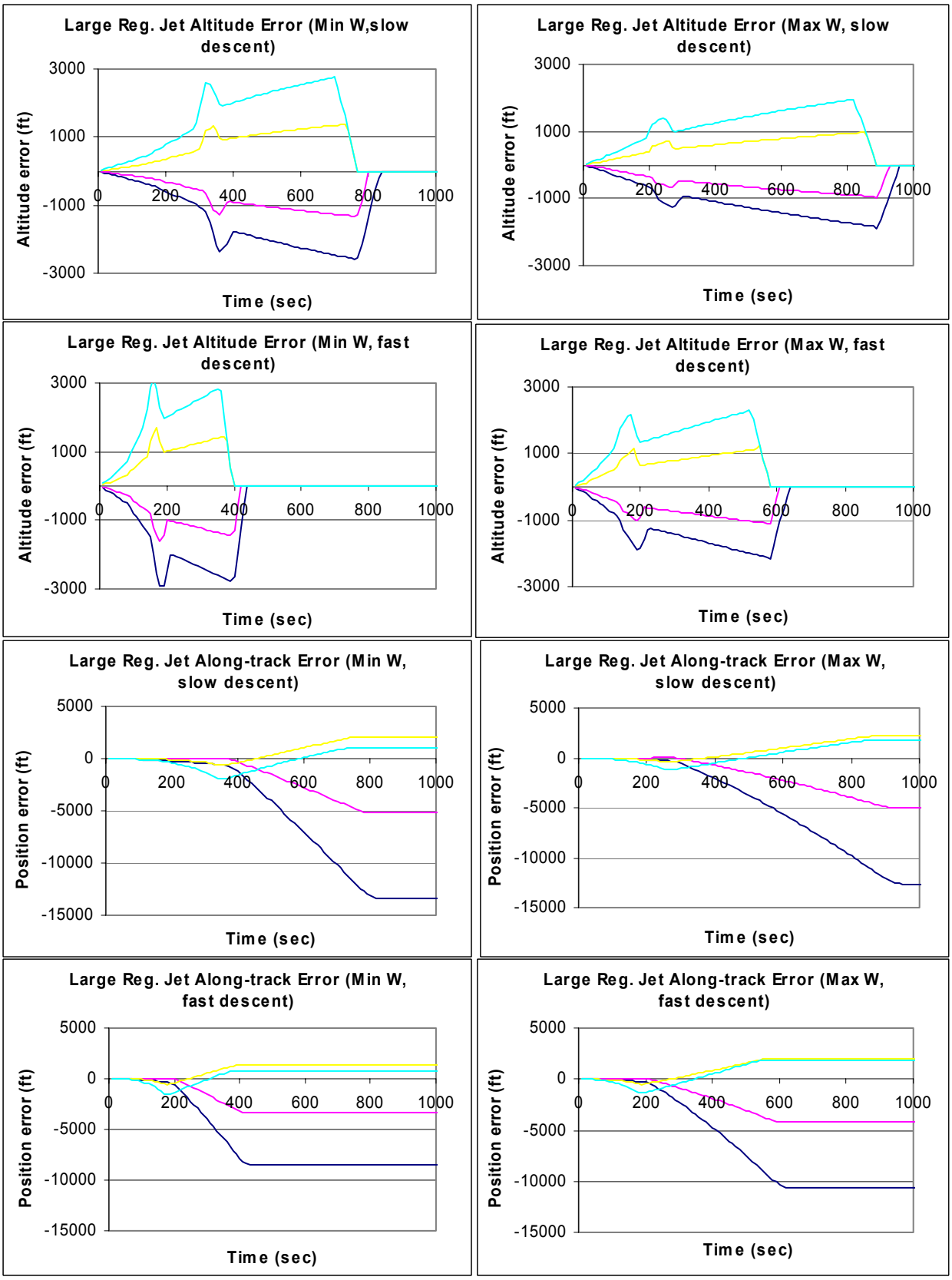

Figure 5-49 Large Regional Jet - Errors due to neglect of wind gradient during descent

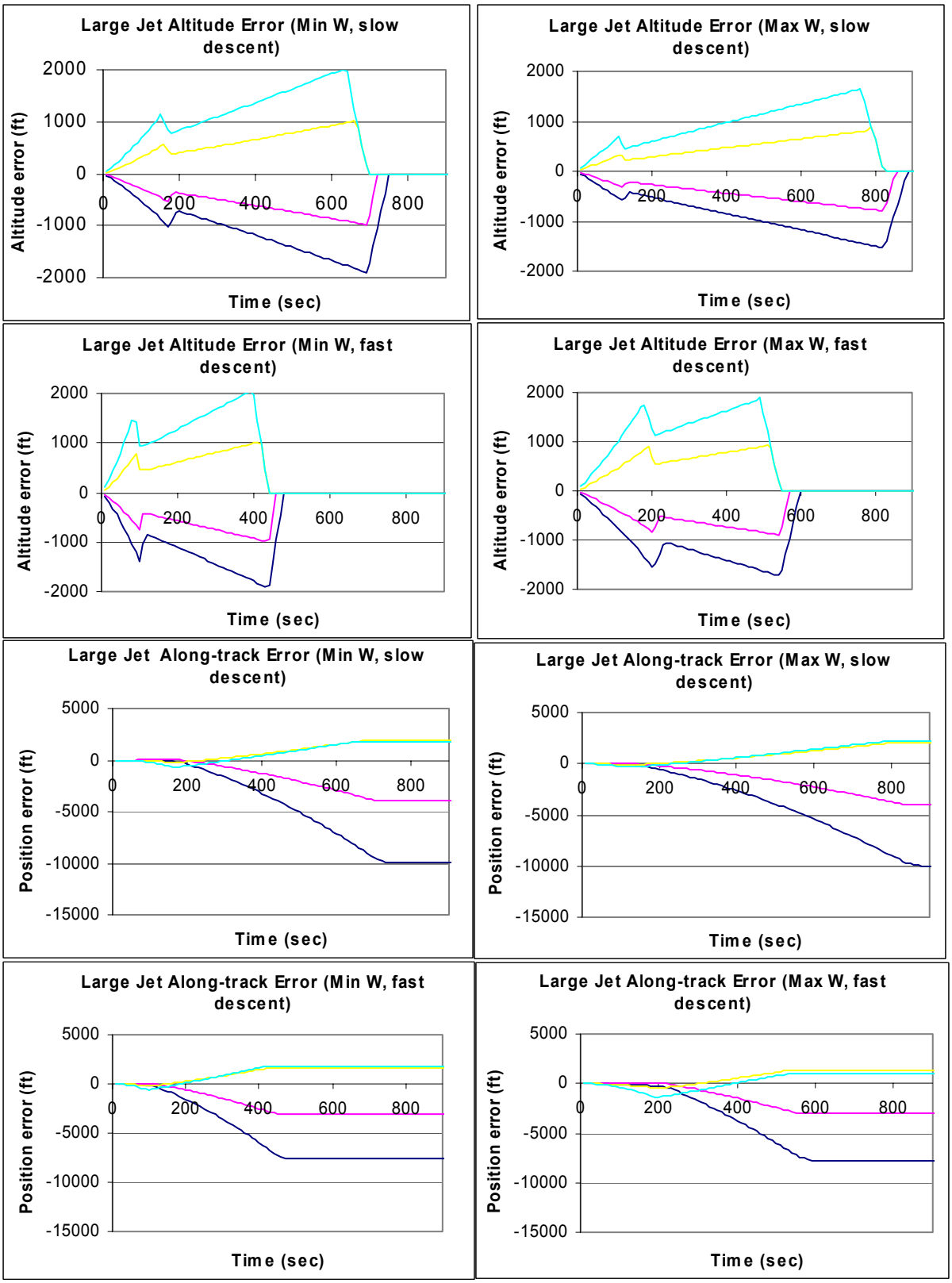

Figure 5-50 Large Jet - Errors due to neglect of wind gradient during descent

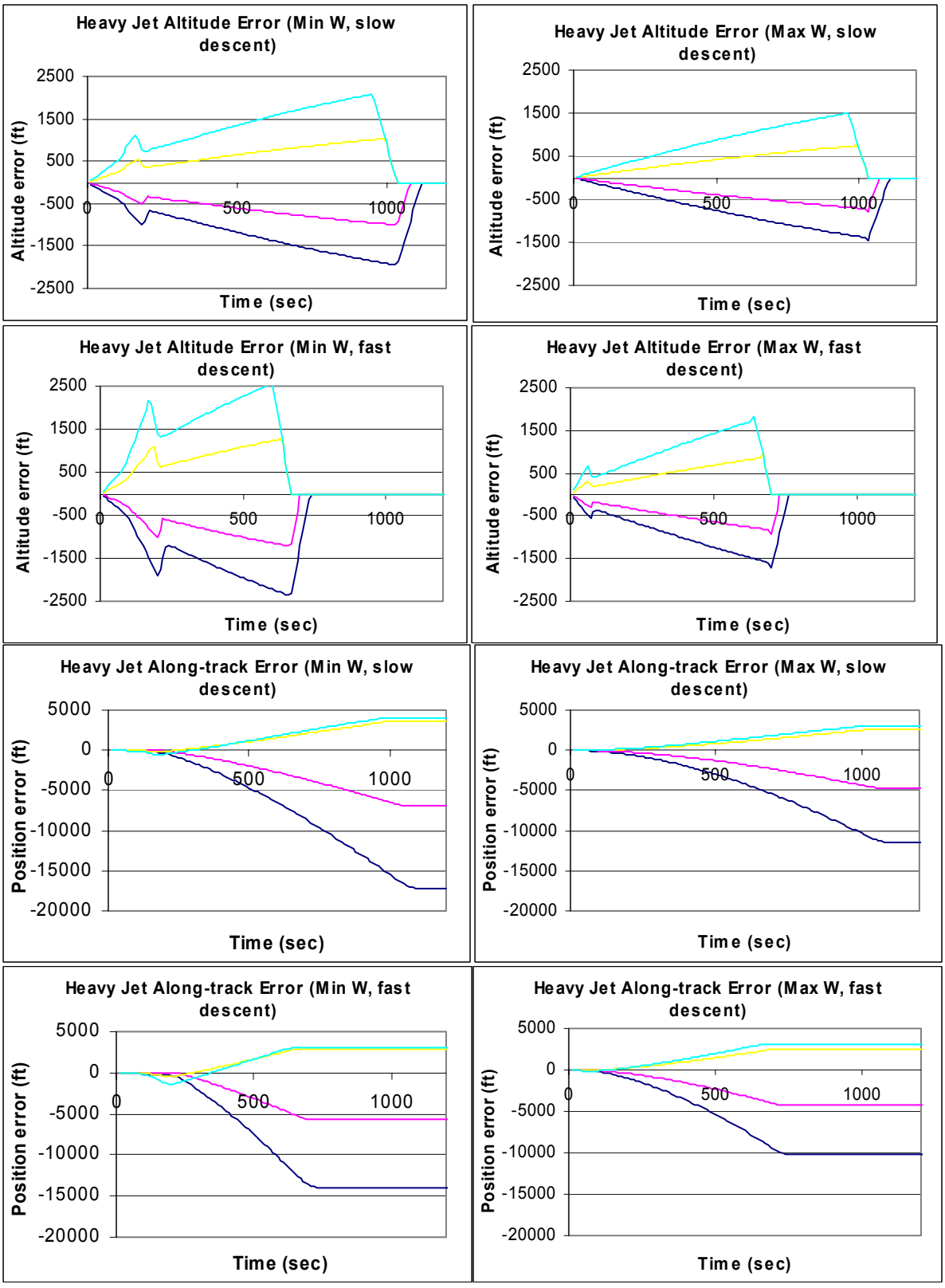

Figure 5-51 Heavy Jet - Errors due to neglect of wind gradient during descent

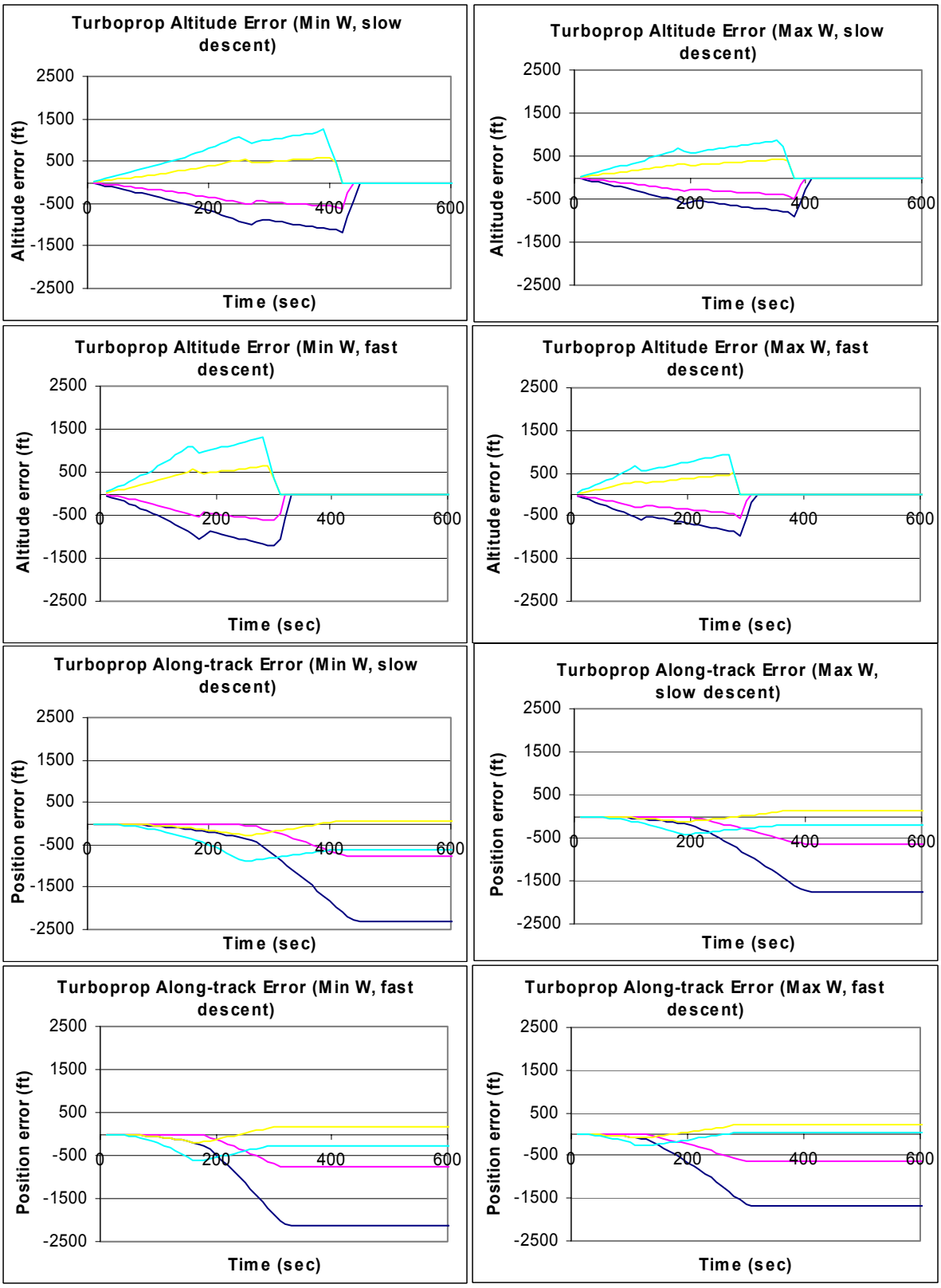

Figure 5-52 Turboprop - Errors due to neglect of wind gradient during descent

5.3 Aircraft Weight Error

5.3.1 Description of Error

During climb and descent, the weight of the aircraft has an impact on the climb and descent rate of a flight. At any given power setting, overestimation of the weight will typically lead to an underestimation of climb rates and an overestimation of descent rates. During all phases of flight, including cruise, the aircraft weight will impact the fuel consumption rate. Since heavier flights consume more fuel, this will lead to a decrease in the absolute weight error as the flight progresses. Trajectory predictors providing estimates of optimal step climb locations will also be affected by weight errors, as the optimal step climb point will be determined in part by the weight of the aircraft.

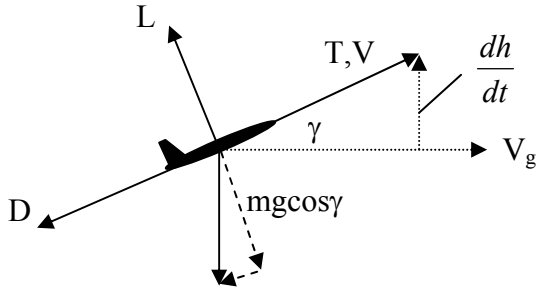

Figure 5-53 Force balance during a climb

Returning to the above force balance figure, recall that we can approximate the climb gradient as the following expression.

$$\gamma = \left(\frac{T - D}{mg} \right) \left[\frac{V}{g} \frac{dV}{dh} + \frac{V}{g} \frac{dw}{dh} + 1 \right]^{-1}$$

While the above expression implies a simple relationship between weight and climb gradient, the reader must note that the drag term (D) is a function of the weight. Thus any error in weight will also be reflected as an error in the drag through the induced drag term. We can rewrite the above expression for zero wind (w=0) using a simple quadratic drag polar expression. We also set lift equal to weight.

$$\gamma = \left(\frac{T - qS\left[C_{D_0} + kC_L^2 \right]}{mg} \right) \left[\frac{V}{g} \frac{dV}{dh} + 1 \right]^{-1}$$

$$= \left(\frac{T - qS\left[C_{D_0} + k\left(\frac{mg}{qS} \right)^2 \right]}{mg} \right) \left[\frac{V}{g} \frac{dV}{dh} + 1 \right]^{-1}$$

Rewriting the above expression in terms of non-dimensional groupings, we obtain the following expression:

$$\gamma = \left(\frac{T/qS - C_{D_0}}{mg/qS} - k\, mg/qS \right) \left[\frac{V}{g}\frac{dV}{dh} + 1 \right]^{-1}$$

The impact of the weight on the climb (or descent) gradient can be determined by the following non-dimensional parameters:

- Thrust coefficient: $C_T = (T/qS)$
- Zero-lift drag coefficient: C_{Do}
- Induced drag coefficient: k
- Ratio of weight to dynamic pressure forces: (mg/qS)
- Speed gradient term: (V/g)(dV/dh)

As one can see from the expression of the gradient, the impact of a weight error on the climb or descent gradient will depend on the ratio of terms. This will be covered in more detail in the parametric analysis.

5.3.2 Parametric Analysis

The impact of errors in weight on the climb and descent gradient can be approximated by observing the derivative of the gradient with respect to the weight:

$$\frac{\partial \gamma}{\partial (mg)} = \left(-\frac{T/qS - C_{D_0}}{(mg)^2/qS} - k/qS \right) \left[\frac{V}{g}\frac{dV}{dh} + 1 \right]^{-1}$$

An increase in weight will lead to an increase in the gradient, under the following circumstance:

$$\left(-\frac{T/qS - C_{D_0}}{(mg)^2/qS} - k/qS \right) > 0$$

Which can be re-arranged:

$$\frac{T - qSC_{D_0}}{k(mg)^2} qS < -1$$

When the above ratio is less than –1, an increase in weight causes an increase in the gradient. When greater than –1, an increase in weight causes a decrease in the gradient.

During the climb phase, the thrust exceeds both components of the drag. As a result, the above ratio is positive leading to an underestimation in the climb rate when the weight is overestimated.

During descent, thrust is smaller than the total drag term leading to a negative gradient term. When the induced drag term dominates (e.g., the ratio is greater than –1), overestimating the weight leads to a *decrease* in the gradient. Since the gradient is negative, the estimated descent will be steeper than the actual. Similarly when the induced drag term is small (ratio is less than –1), overestimating the weight will lead to an estimated descent that is shallower than the actual.

Figure 5-54 shows the behavior of the above ratio for various aircraft types, altitudes and speeds given data obtained from BADA 3.5. While the data depends on aircraft-specific data such as the relative magnitudes of induced drag to zero-lift drag and the magnitude of idle thrust, certain trend data can be observed as follows:

- At any given altitude, increasing the air speed will make the ratio more negative. Thus, overestimating the weight will lead to a more shallow descent at higher airspeeds.
- The ratio becomes more negative at lower altitudes. Thus, overestimating the weight will lead to a more shallow descent at a lower altitude.
- At higher weights, the magnitude of the ratio is decreased. Overestimating the weight will lead to a more shallow descent when the initial weight is lower.
- At higher weights, lower airspeeds and higher altitudes, it is possible for the ratio to become greater than –1. When this occurs, overestimating the weight will result in an estimated trajectory that has a steeper descent than observed.

The above parametric analysis explains the initial error in climb or descent gradient due to weight errors. This is merely the starting point for the accumulation of errors in transition. As a trajectory profile is integrated, different gradients indicate that transition points will generally be reached at different spatial and temporal locations. These transition points refer to the Mach/CAS transition point, or the location of the tropopause. At these locations, the gradient may change dramatically. Since the predicted and actual paths do not reach these transition points at the same time, altitude errors will result from the differences in the gradients. This is identical to the situation explained in the section on wind gradient omission and is illustrated in this case in Figure 5-60.

Descent Errors

Figure 5-55 to Figure 5-59 show the altitude and along-track errors for various aircraft types during descent. As predicted, greater sensitivity in the initial gradient error is observed when the weight is higher and the airspeed is higher. The along-track error is a consequence of the errors in altitude. Whether the flight is flying a constant Mach or constant CAS segment, an altitude error will result in an error in airspeed.

Note that some of the aircraft, at maximum weight and low airspeed, will experience a reversal in the altitude error trend, consistent with the parametric analysis described above.

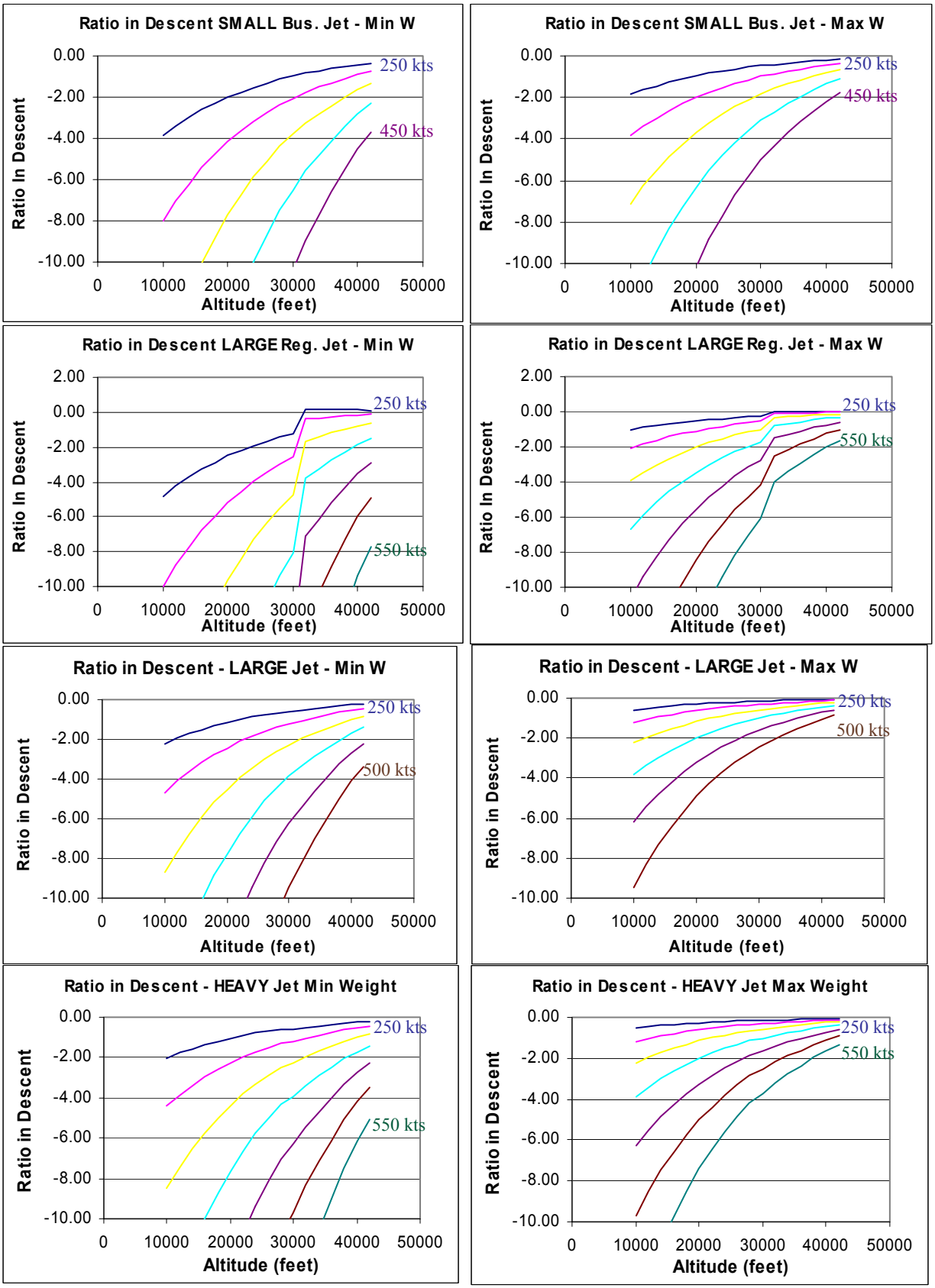

Figure 5-54 $\dfrac{T - qSC_{D_0}}{k(mg)^2} qS$ **during descent vs. speed and altitude for various aircraft**

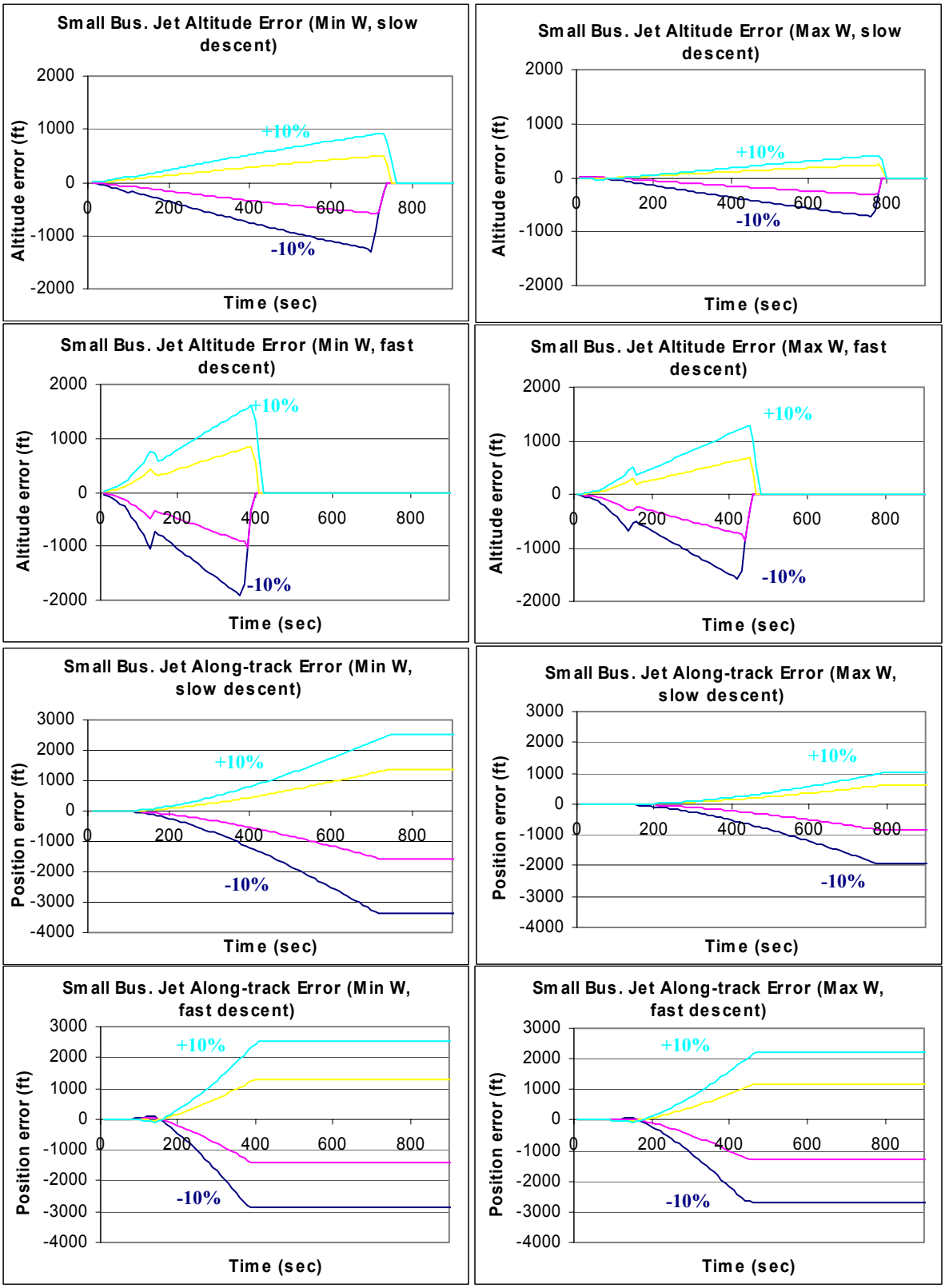

Figure 5-55 Small Business Jet - Errors due to weight estimation uncertainty during descent

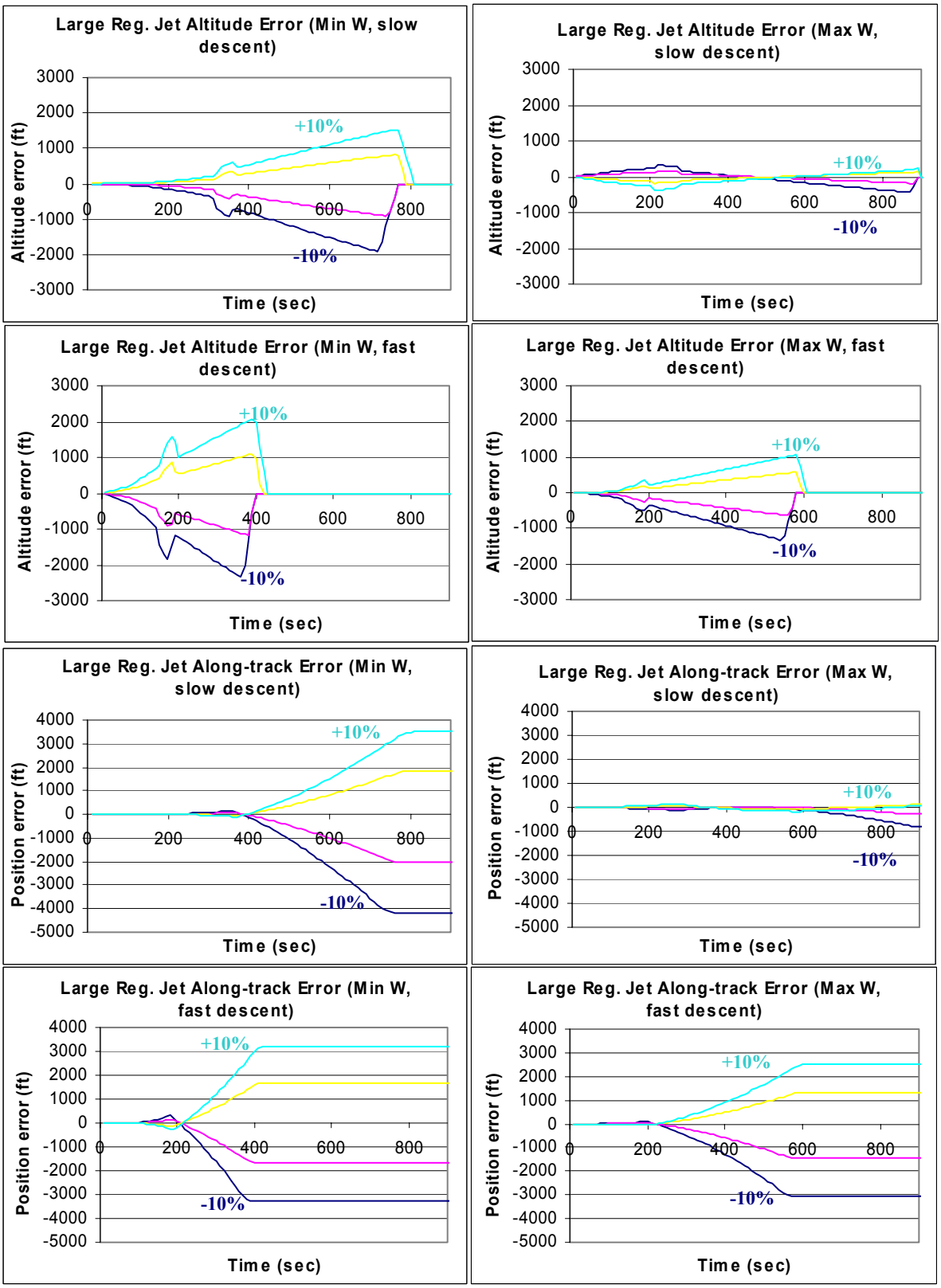

Figure 5-56 Large Regional Jet - Errors due to weight estimation uncertainty during descent

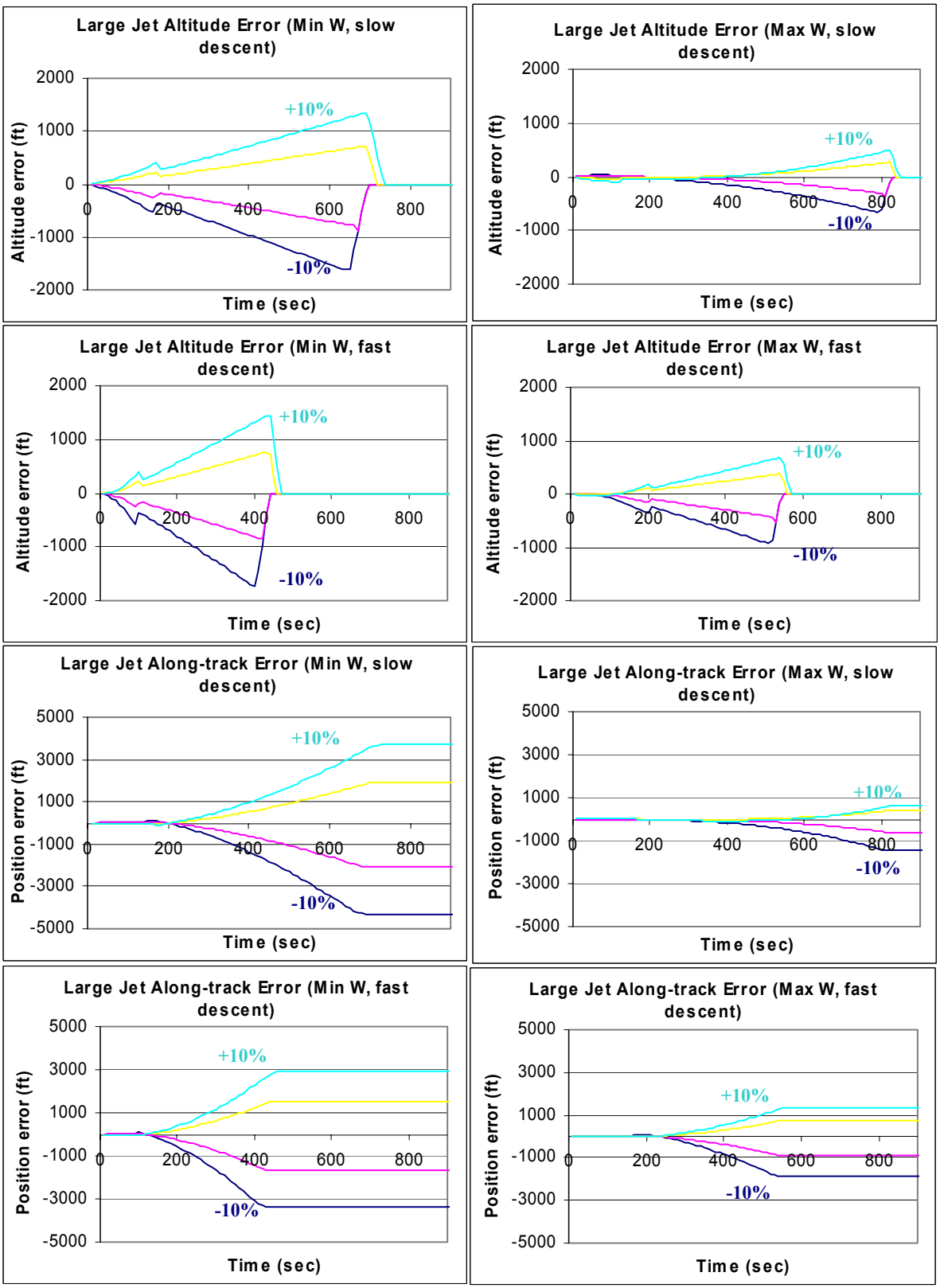

Figure 5-57 Large Jet - Errors due to weight estimation uncertainty during descent

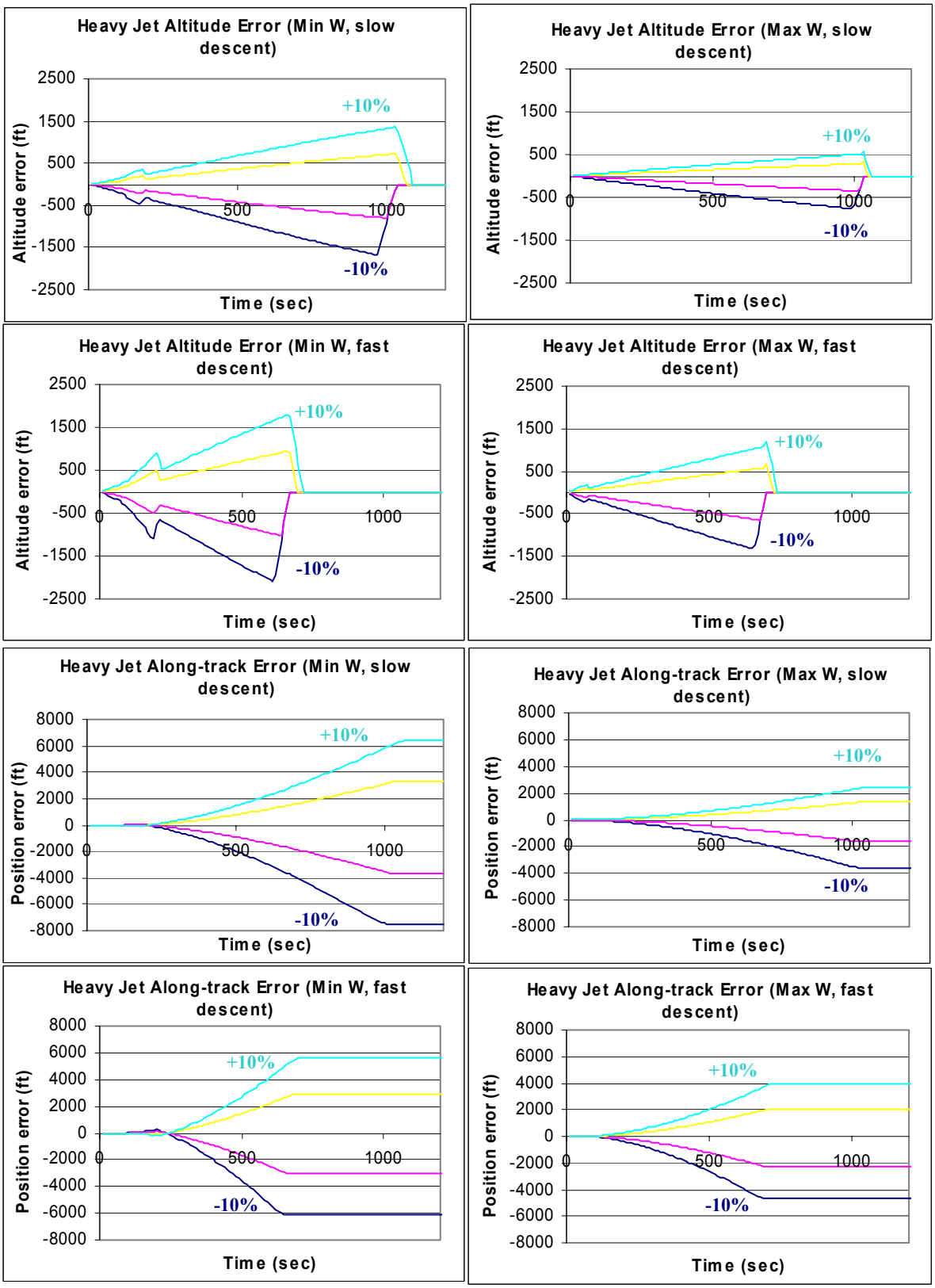

Figure 5-58 Heavy Jet - Errors due to weight estimation uncertainty during descent

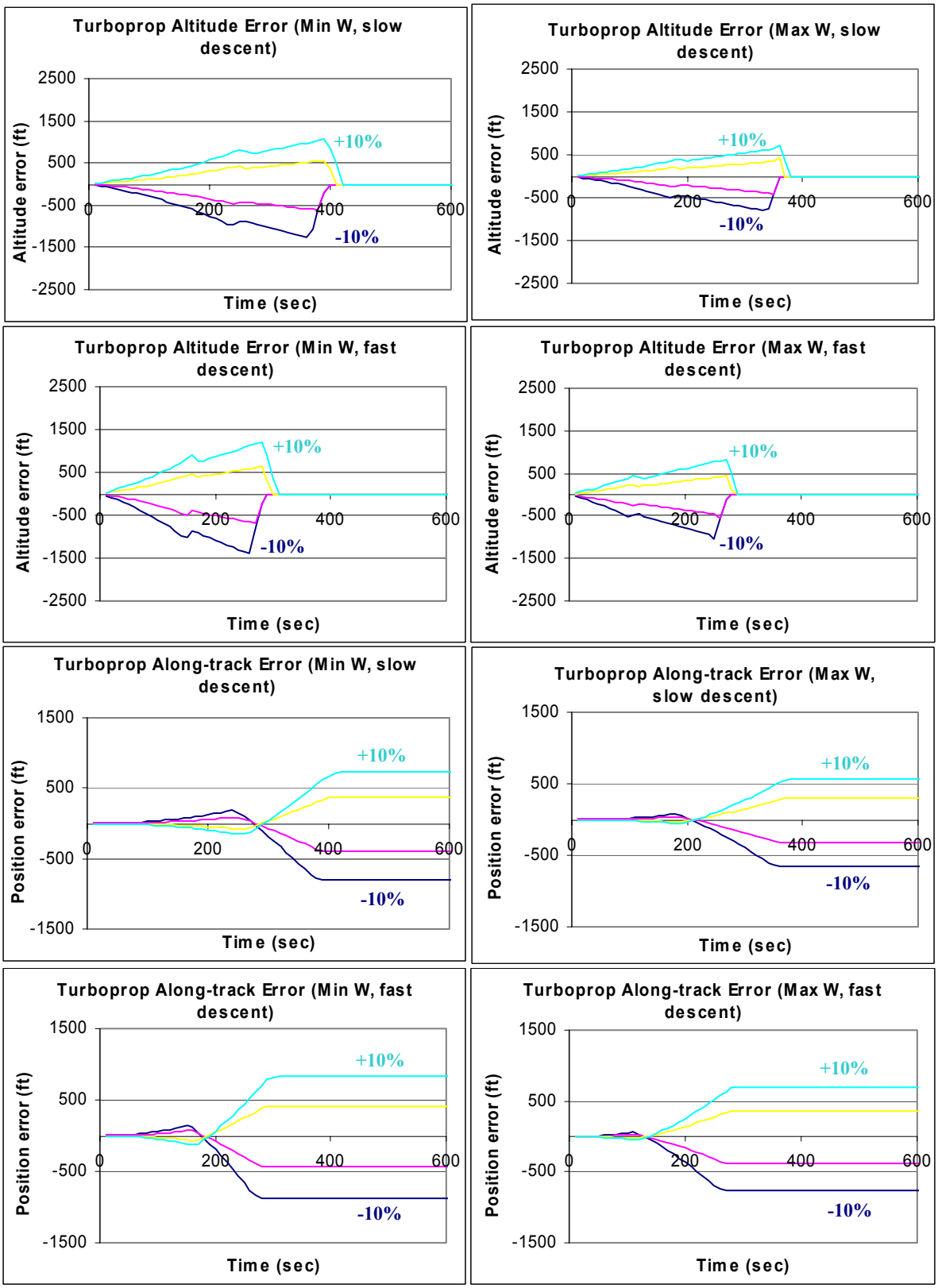

Figure 5-59 Turboprop - Errors due to weight estimation uncertainty during descent

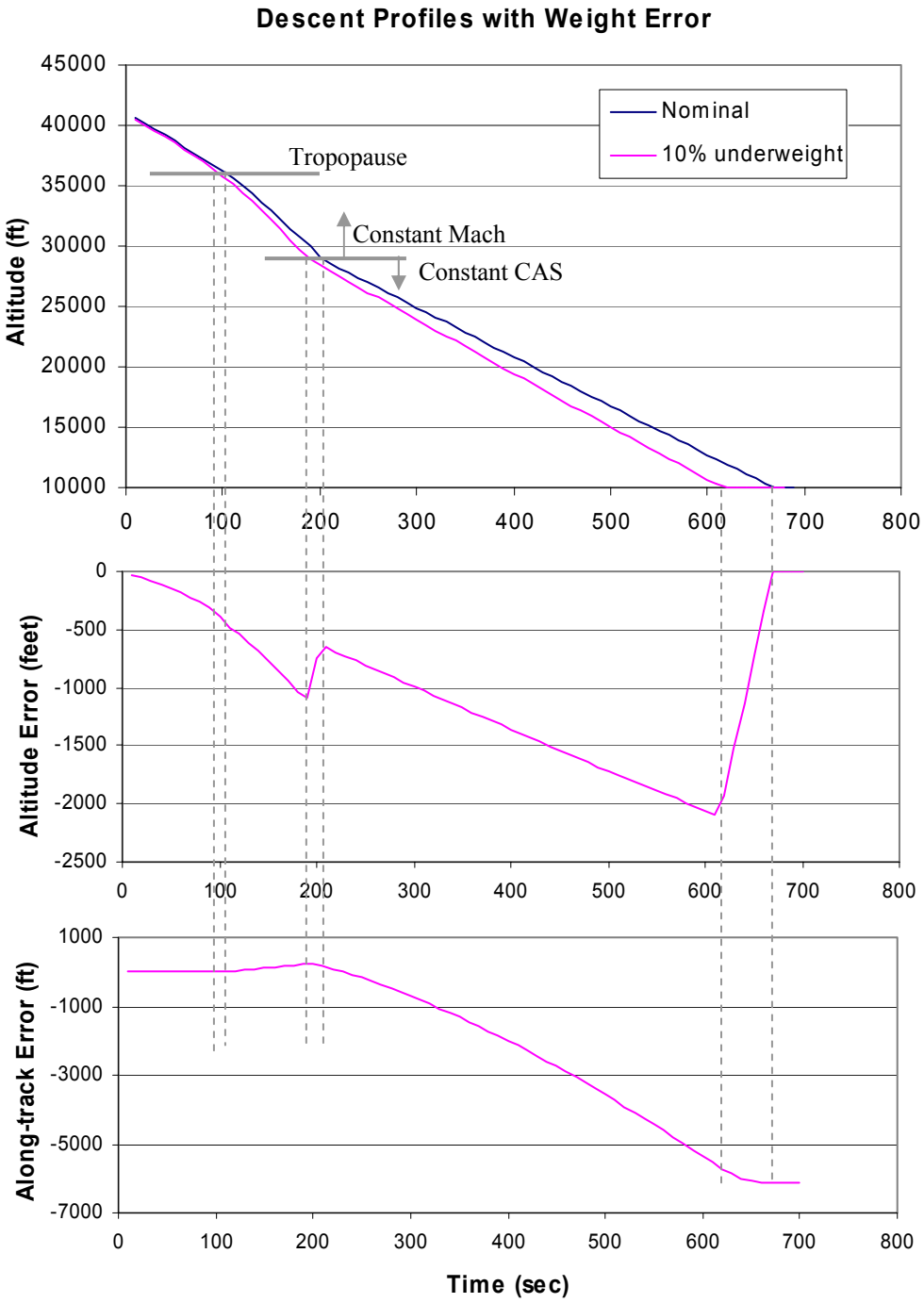

Figure 5-60 Explanation of the effect of a weight estimation error during descent

Figure 5-60 summarizes the errors one would encounter on descent due to errors in estimation of the weight. At top-of-descent, an underestimation of the weight requires that the aircraft descend at a steeper rate in order to maintain a target Mach number. This is intuitive when we consider that a lighter flight at the same descent gradient would tend to be slowed down if the drag was identical. However, since the drag is a function of the weight, the initial gradient error may flip sign.

As the predicted trajectory descends faster than the nominal flight, the prediction will accumulate an altitude error below the nominal flight. When both the prediction and actual flight are in the tropopause, altitude errors do not result in a speed error when flying at constant Mach. Thus, the along-track error is constant. After both flights descend into the troposphere, the lower flight will enjoy a higher temperature and hence a faster speed at the same Mach number. This will exaggerate the altitude error (versus time) and will result in the lower weight flight *leading* the nominal.

This estimated flight with a weight below actual will reach the Mach/CAS transition point at an earlier time than the actual flight. As a result, the estimated flight will reduce its descent gradient at a time when the nominal flight continues descending at a faster, constant Mach, rate. This results in the actual flight reducing the altitude error until it also crosses the Mach/CAS transition point.

Once both the predicted and the nominal flights are in the constant CAS domain, the lightweight prediction will have a steeper descent than the nominal. Since the prediction is under the flight path, the predicted airspeed will also be below the actual speed. This integrates into an along-track error increasingly lagging the actual. Eventually both flights level at the bottom-of-descent and the altitude error is recovered. However, the along-track error remains.

Climb Errors

Altitude and along-track errors during climb are reported in Figure 5-62 to Figure 5-66 for various aircraft types. As for the descent, errors in weight estimation result in an initial error in the climb gradient. This causes altitude errors to accumulate (see Figure 5-61). Errors in altitude cause differences in speed, which integrate into along-track errors (e.g. a heavy flight will be lower, causing the heavy flight to be slower during the CAS segment). Altitude errors result in flights reaching transition points at times different than forecast. For example, a flight lighter than forecast will climb to the M/CAS transition point early. This will reduce the discrepancy in speed, and will increase the gradient error. When both the forecast and actual are in the constant Mach segment, the altitude error is constant and may decrease slightly. The lower trajectory has an opportunity to "catch-up" when it is below the tropopause. After both flights cross into the tropopause, the along-track error is fixed and the altitude error is approximately constant until reaching cruise.

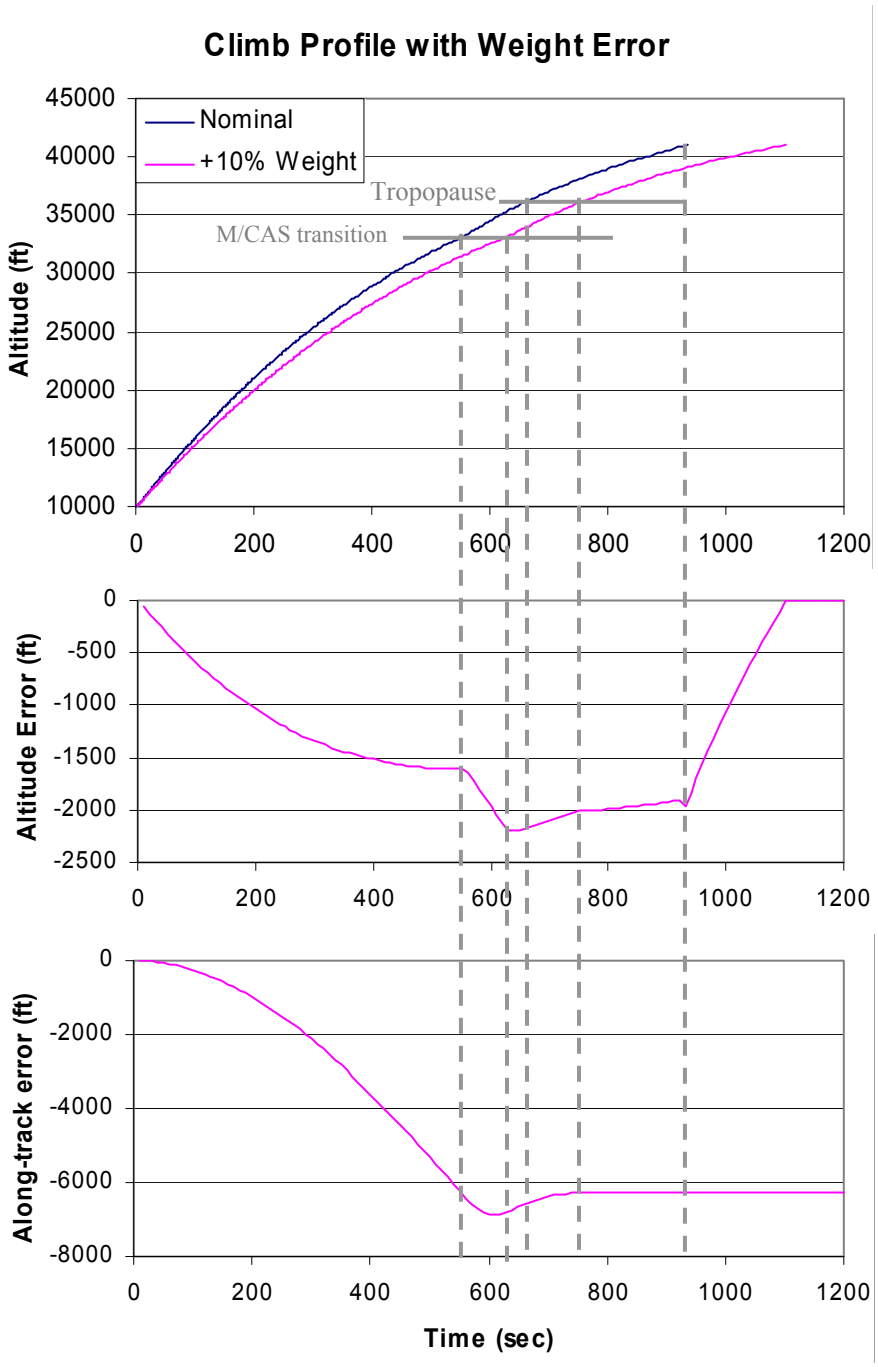

Figure 5-61 Explanation of the effect of a weight estimation error during climb

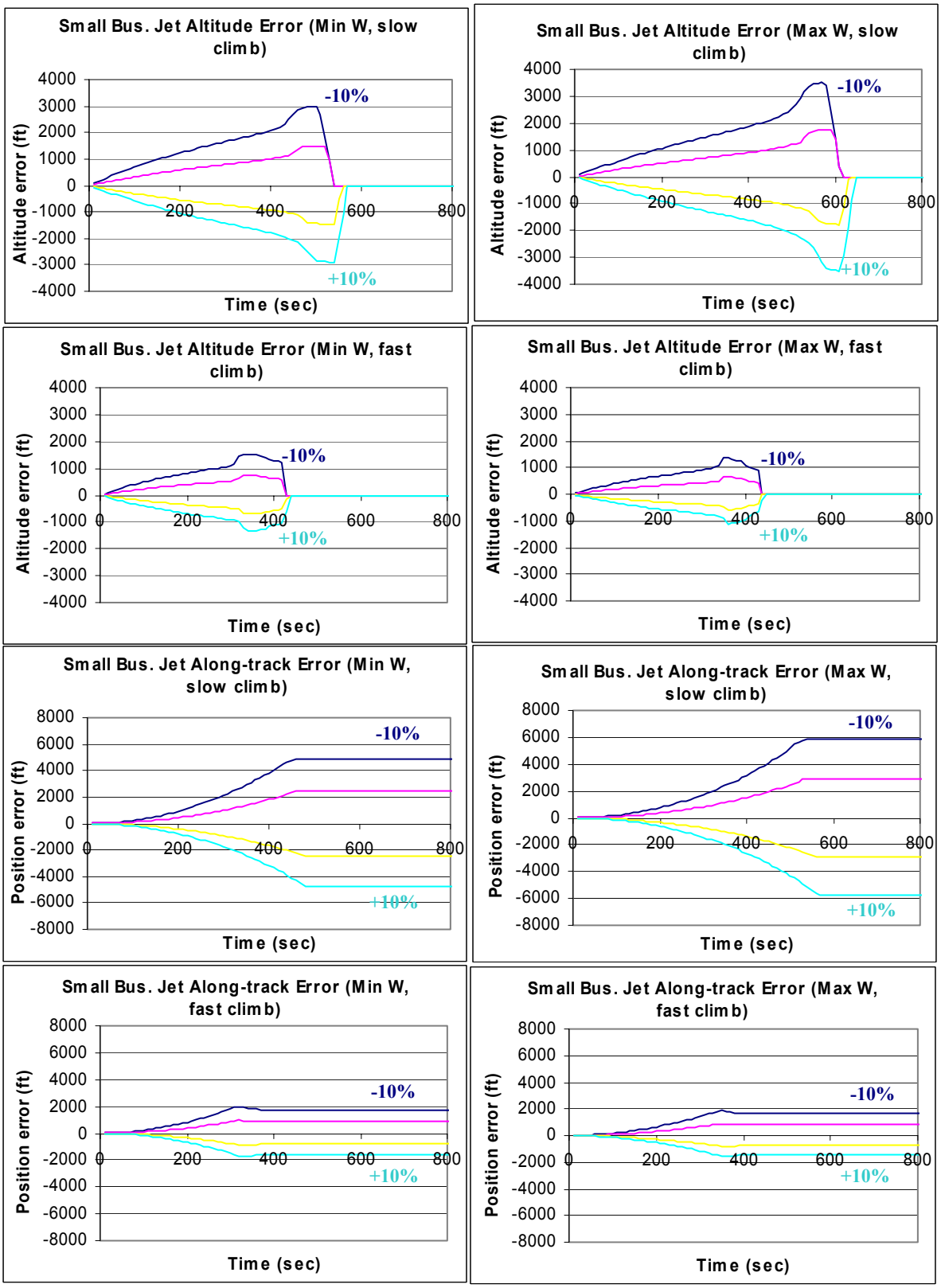

Figure 5-62 Small Business Jet - Errors due to weight estimation uncertainty during climb

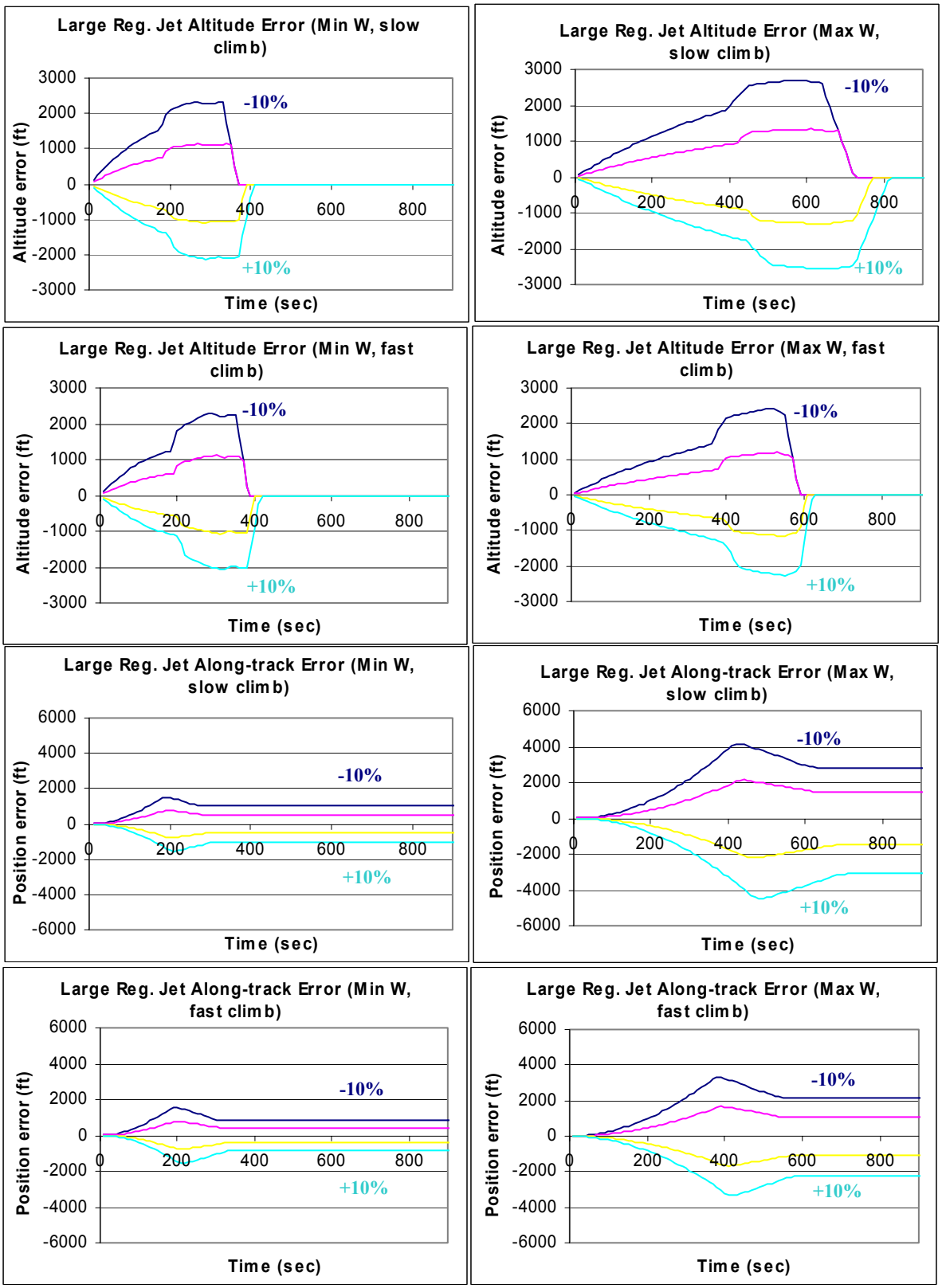

Figure 5-63 Large Regional Jet - Errors due to weight estimation uncertainty during climb

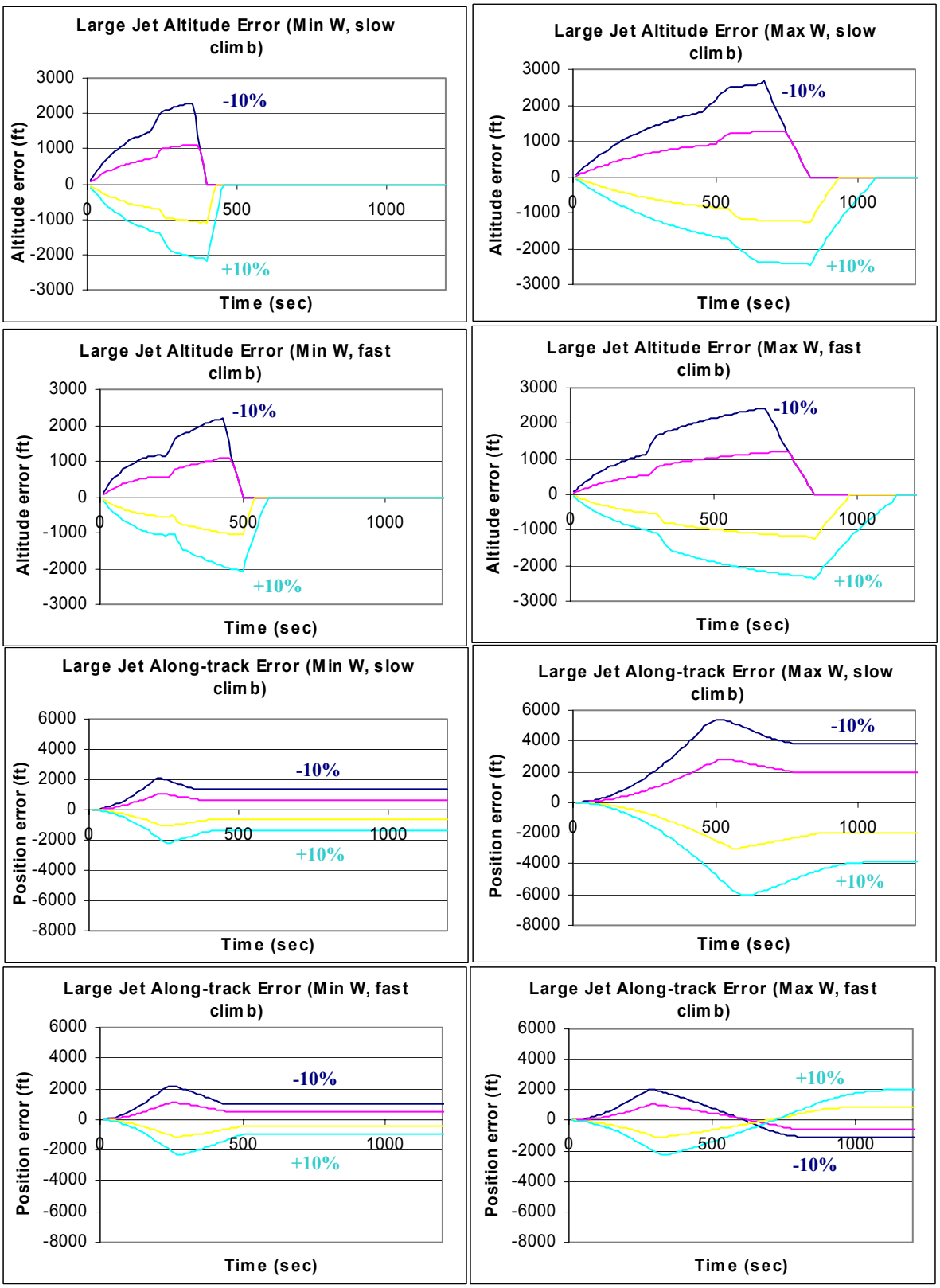

Figure 5-64 Large Jet - Errors due to weight estimation uncertainty during climb

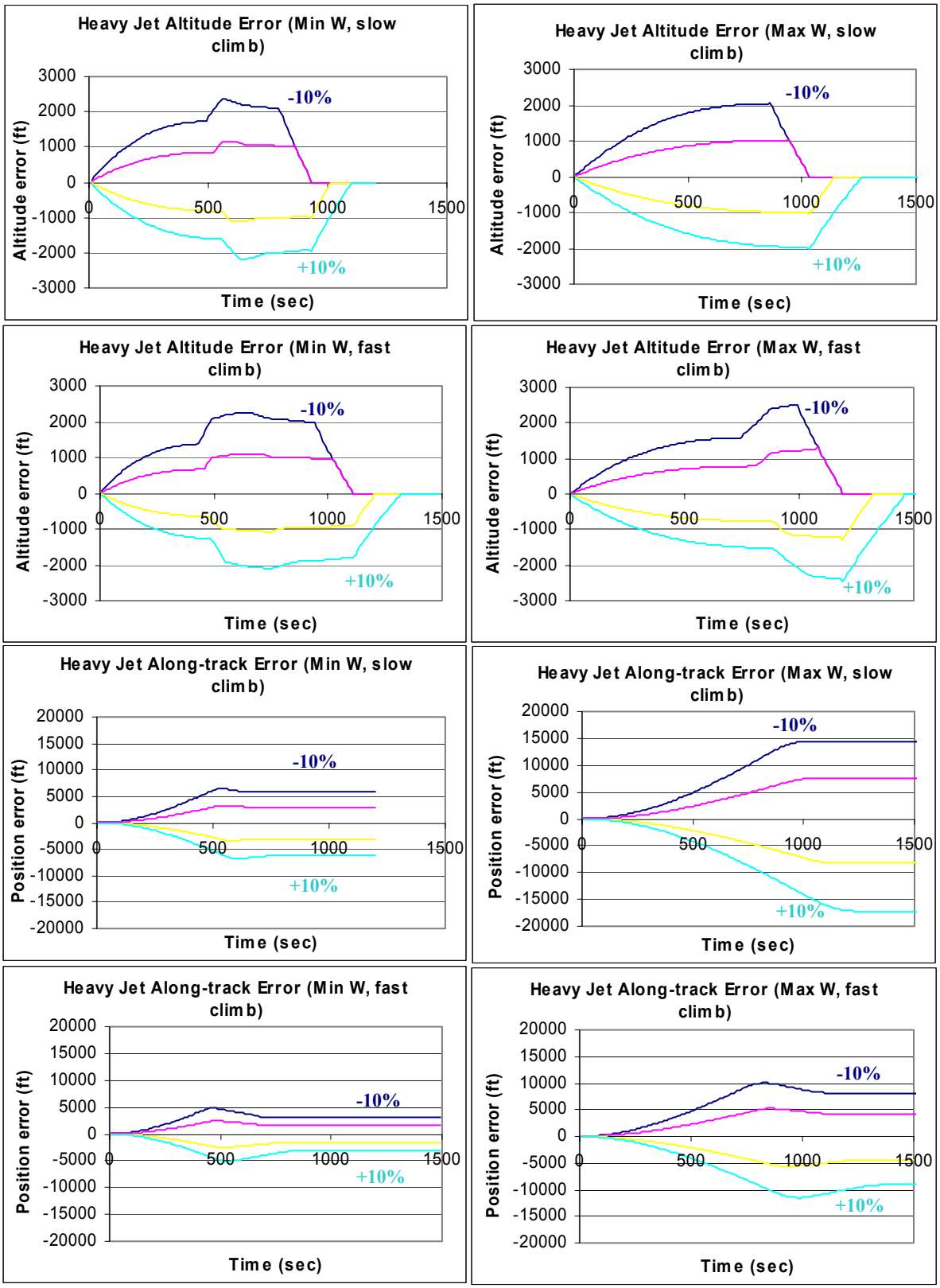

Figure 5-65 Heavy Jet - Errors due to weight estimation uncertainty during climb

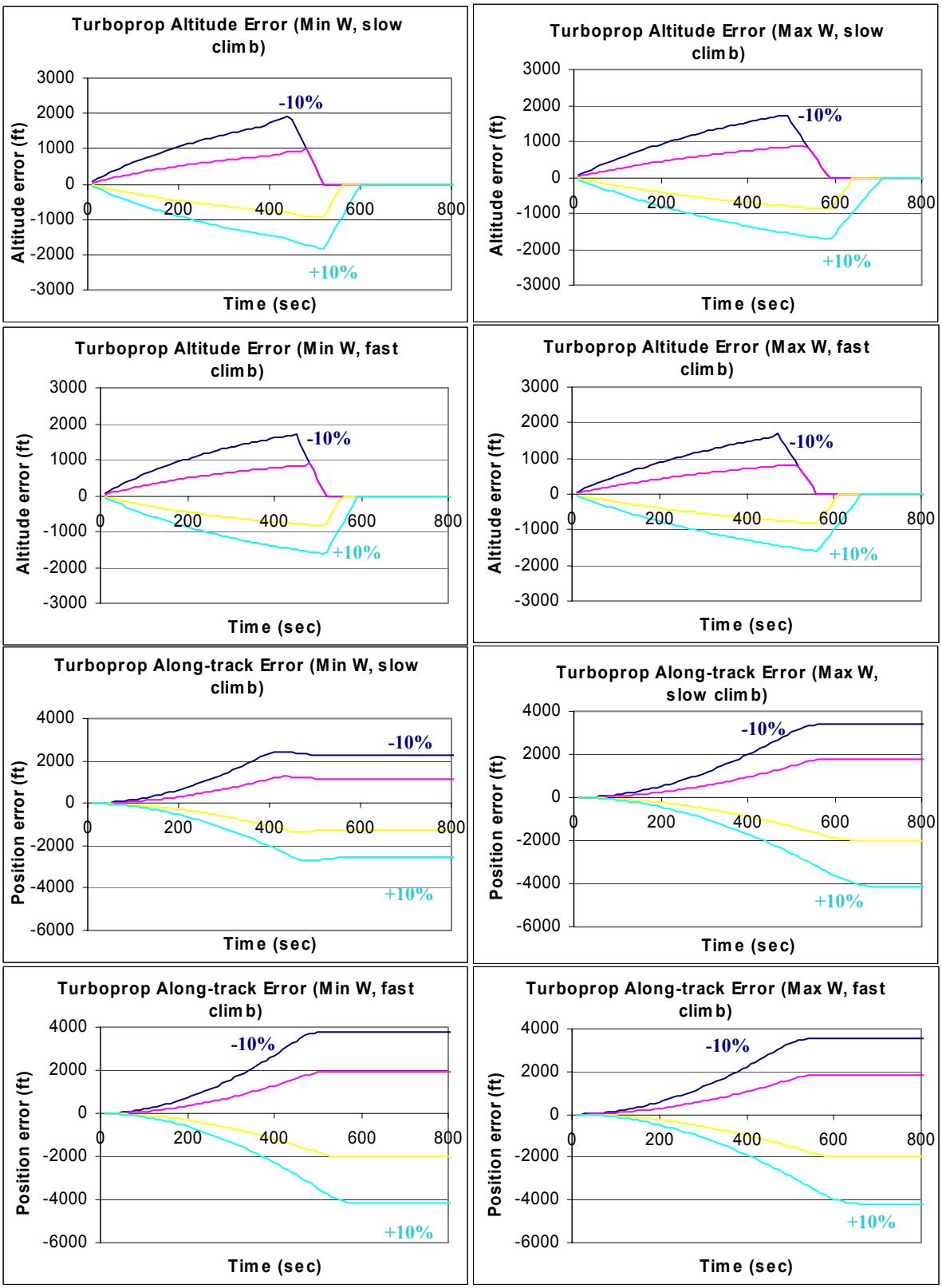

Figure 5-66 Turboprop - Errors due to weight estimation uncertainty during climb

Temperature Effects

As the ambient temperature changes from nominal, the climb trajectory is affected in several significant ways:

- The true airspeed is altered when following a specified CAS/Mach schedule. Higher temperatures result in a faster true airspeed for a constant CAS/Mach schedule.
- The CAS/Mach transition point is altered as a result of the different conversion above. As temperature increases, the transition altitude increases if the density is kept as ISA.
- The thrust of the aircraft is reduced as temperature is increased beyond the flat rating temperature.
- If the pressure is also altered with the temperature, the pressure altitude will be different than the absolute altitude.
- The aircraft flight envelope may be altered

Some authors have reported that temperature affects the coefficient of viscosity, and that this will impact the drag. While theoretically valid, a 20º K variation in temperature from ISO (at 250º K) will impact the viscosity of air by about 6%. This would impact the Reynolds number by the same relative magnitude. Looking at the skin friction on a turbulent plate, we can approximate the skin friction coefficient as:

$$C_f \approx \frac{0.455}{\ln^2(0.06\,\mathrm{Re}_x)}$$

With a typical Reynolds number of 10^7, a 6% error would yield less than a 0.9% error in the skin friction coefficient.

When operating at off-nominal temperatures, the temperature effects will alter the trajectory prediction errors due to uncertainty in weight. When imposing variations in weight, for the purposes of this parametric study, a constant offset is added to the entire ISO temperature curve. Density was assumed to remain with the standard atmosphere profile and the resulting pressure was computed. Aircraft were assumed to cruise to a specified pressure altitude.

Figure 5-67 to Figure 5-70 illustrate the effect of weight uncertainty during climb when the temperature is increased slightly (ISA + 10) and the engine is assumed to operate within the flat rated range. The effect of temperature in this case does not include the impact of climb thrust reduction. Note that the engines on the regional jets are likely to actually be flat rated to a lower temperature (ISA + 5, or ISA).

Figure 5-71 to Figure 5-74 illustrate the effect of weight uncertainty during climb when the temperature is increased beyond the engine flat rating (ISA + 20).

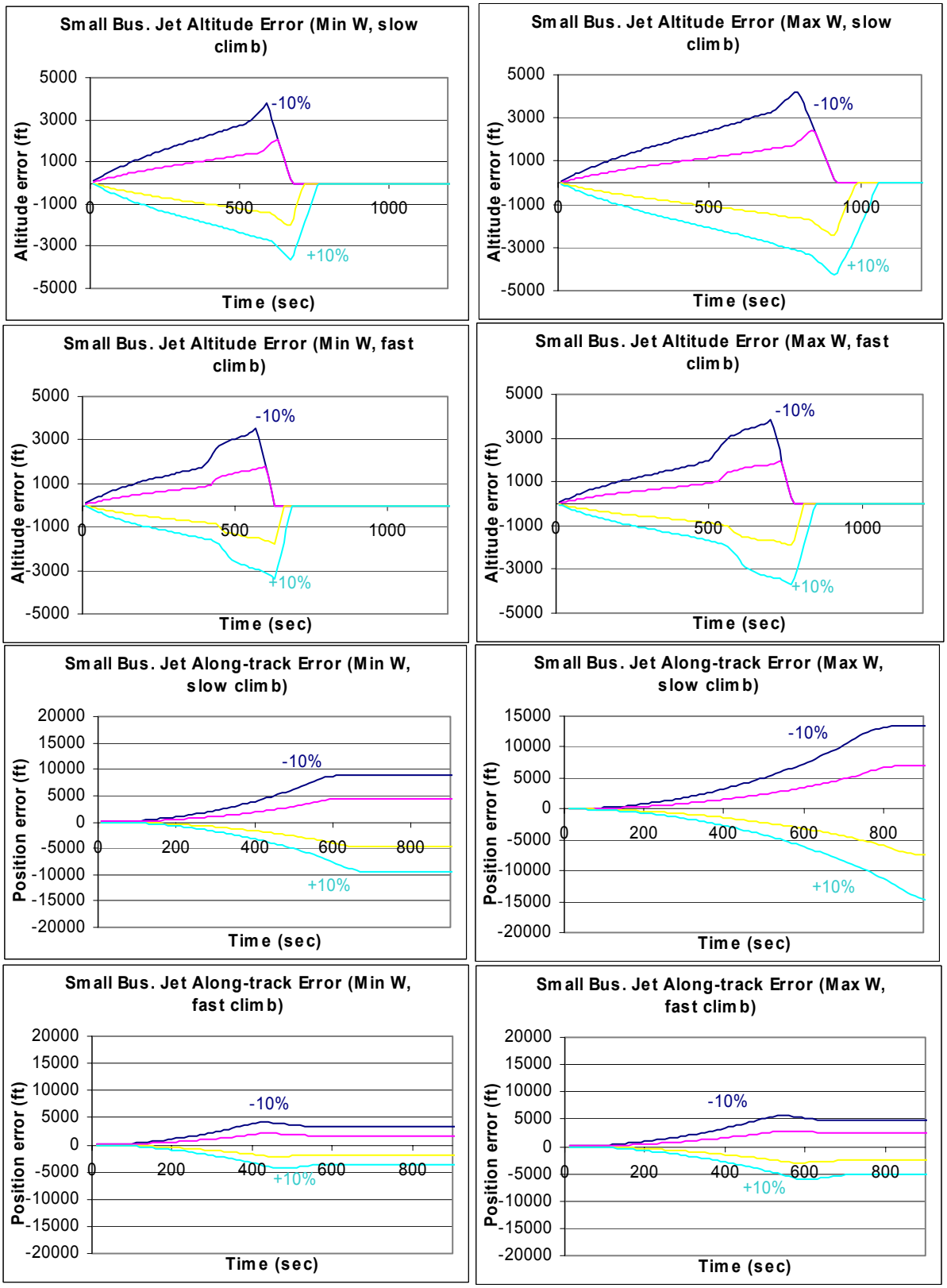

Figure 5-67 Small Business Jet - Errors due to weight estimation uncertainty during climb (ISA+10)

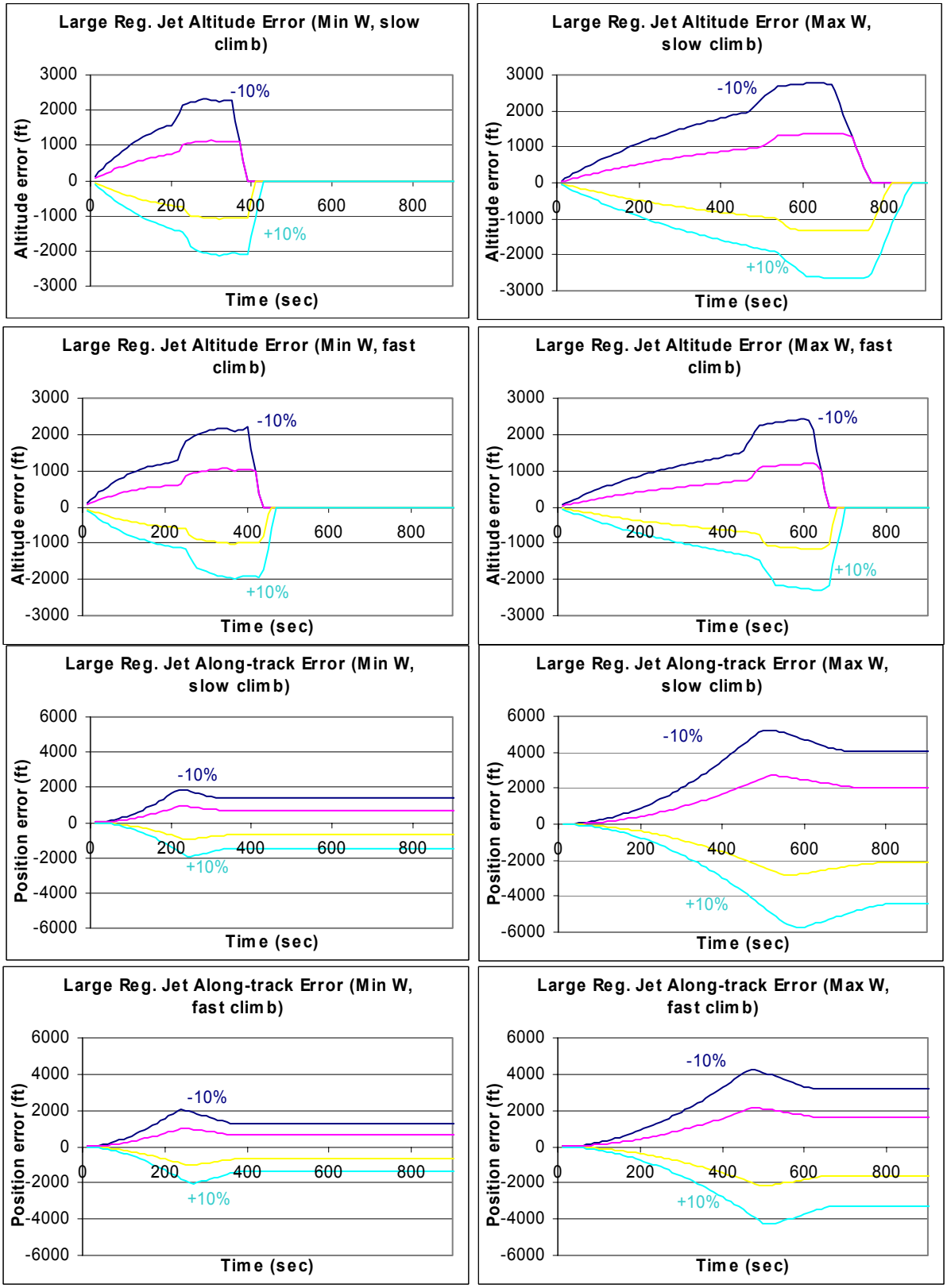

Figure 5-68 Large Regional Jet - Errors due to weight estimation uncertainty during climb (ISA +10)

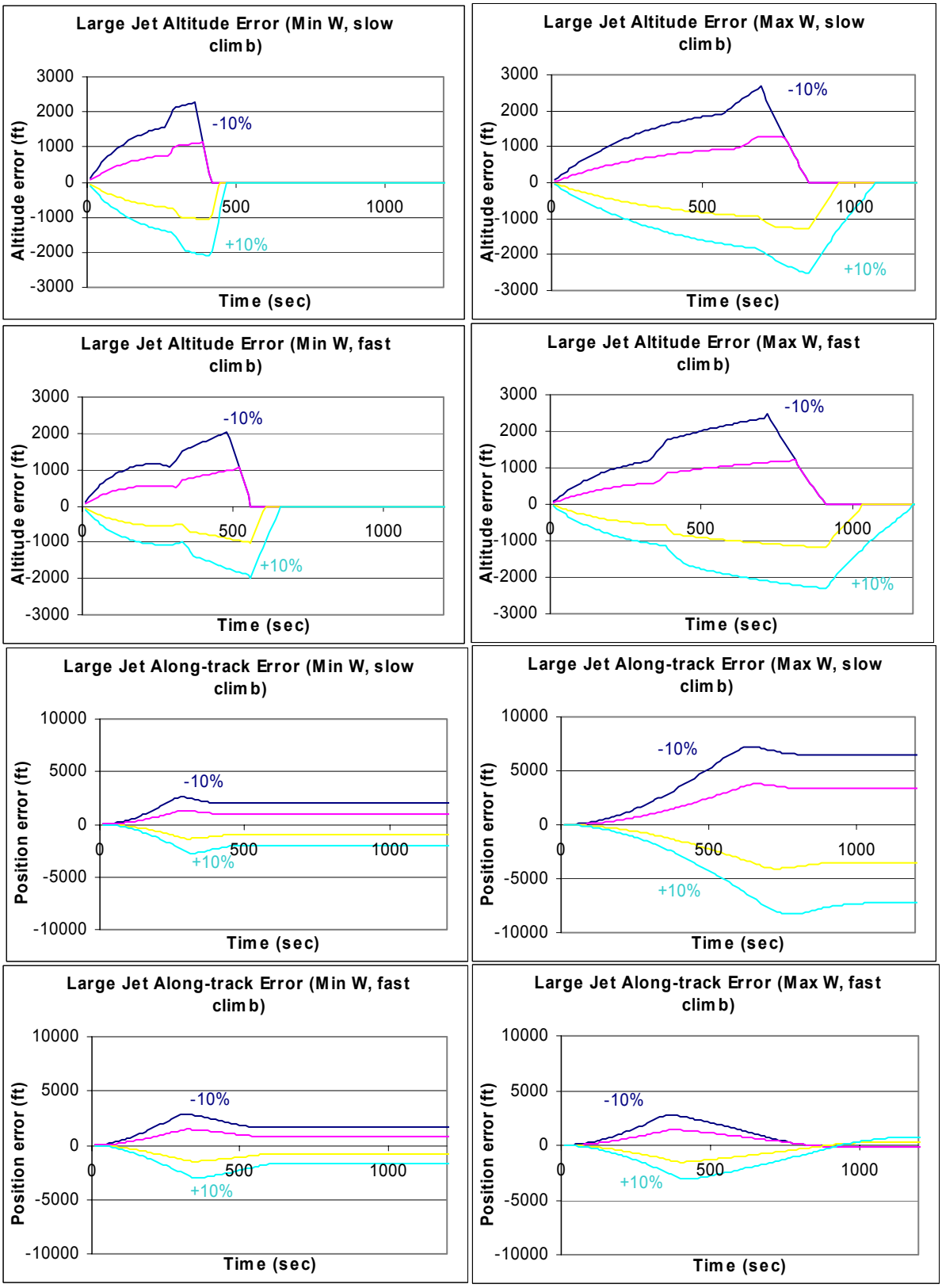

Figure 5-69 Large Jet - Errors due to weight estimation uncertainty during climb (ISA+10)

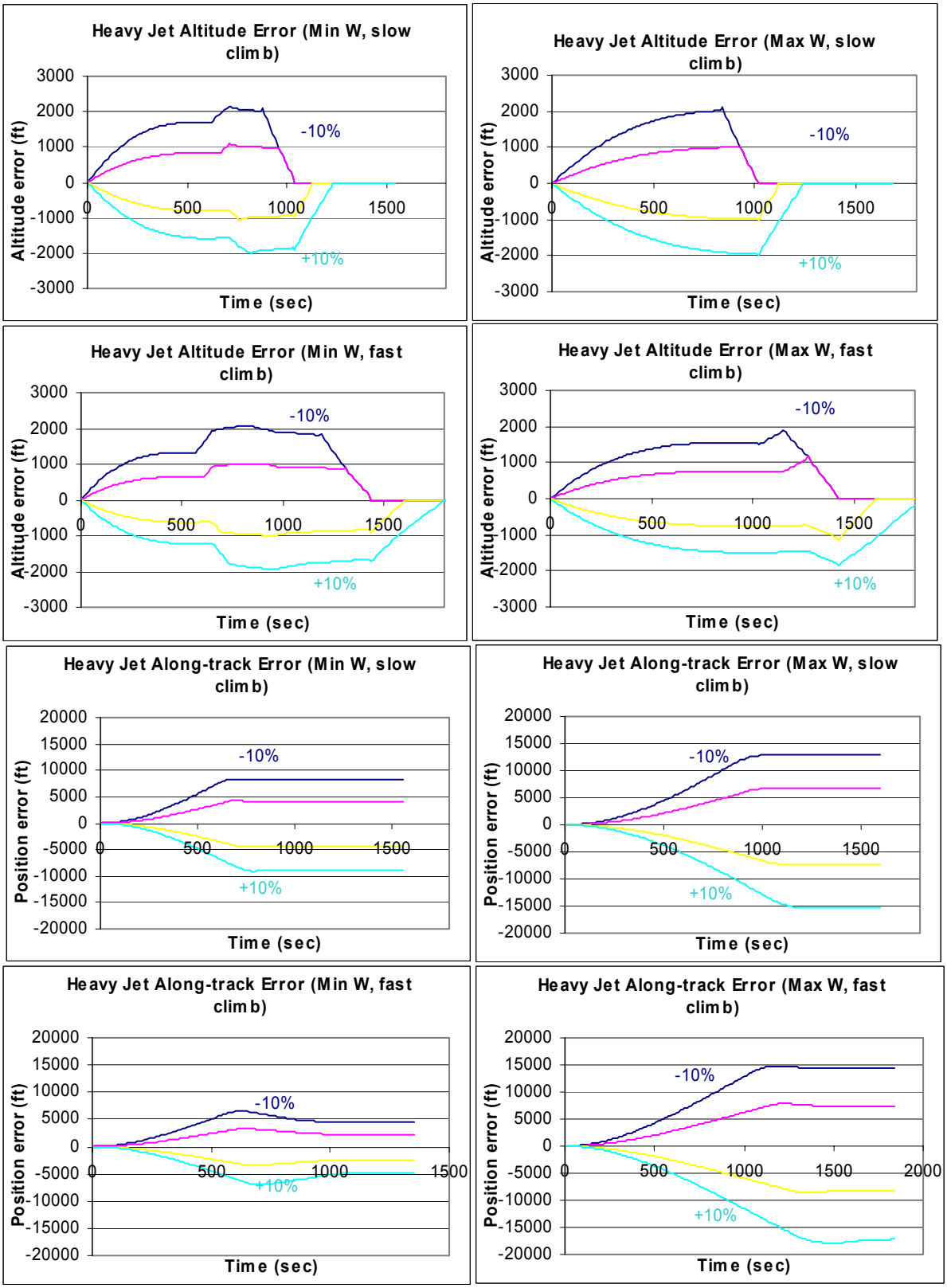

Figure 5-70 Heavy Jet - Errors due to weight estimation uncertainty during climb (ISA + 10)

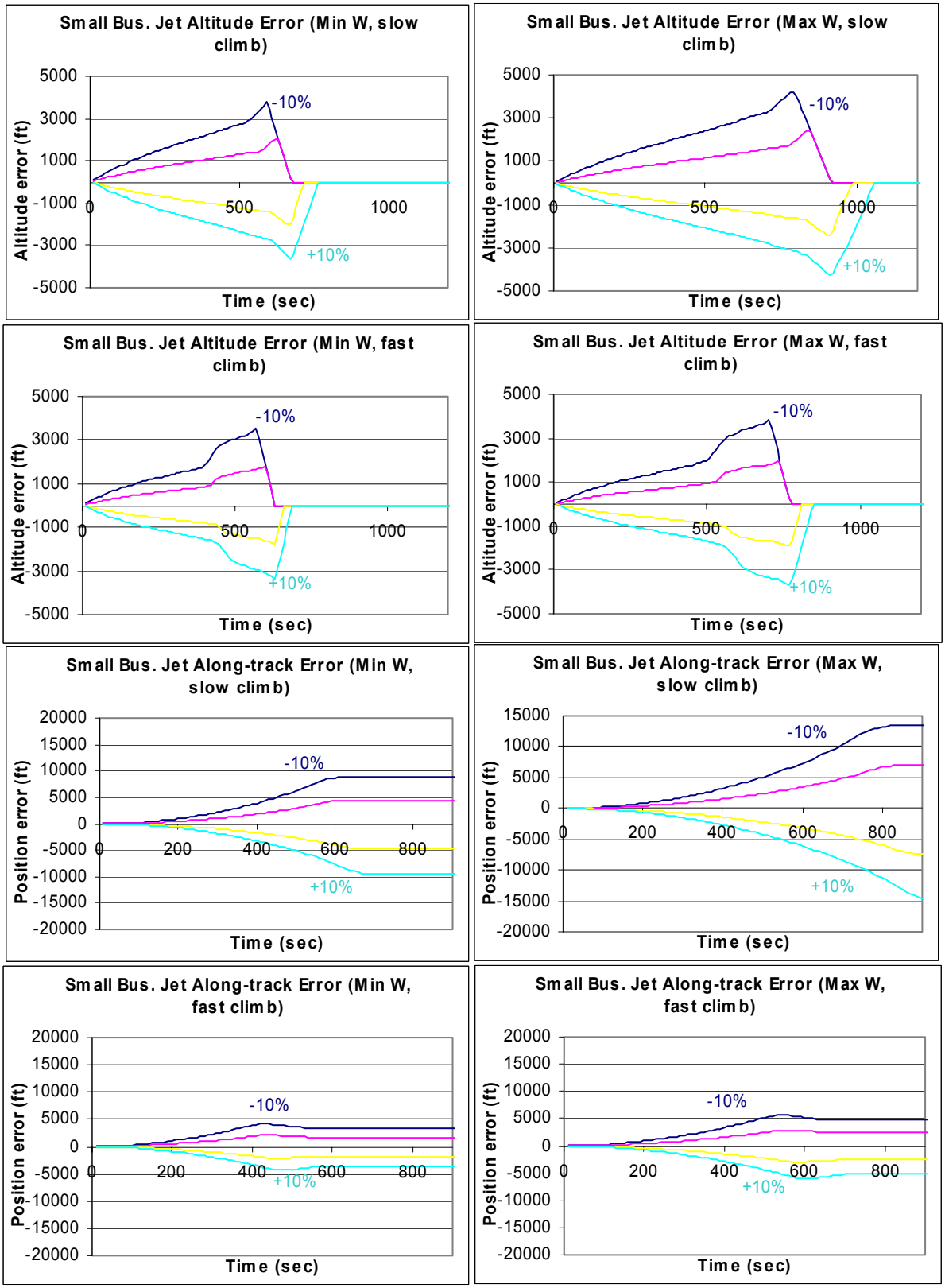

Figure 5-71 Small Business Jet - Errors due to weight estimation uncertainty during climb (ISA +20)

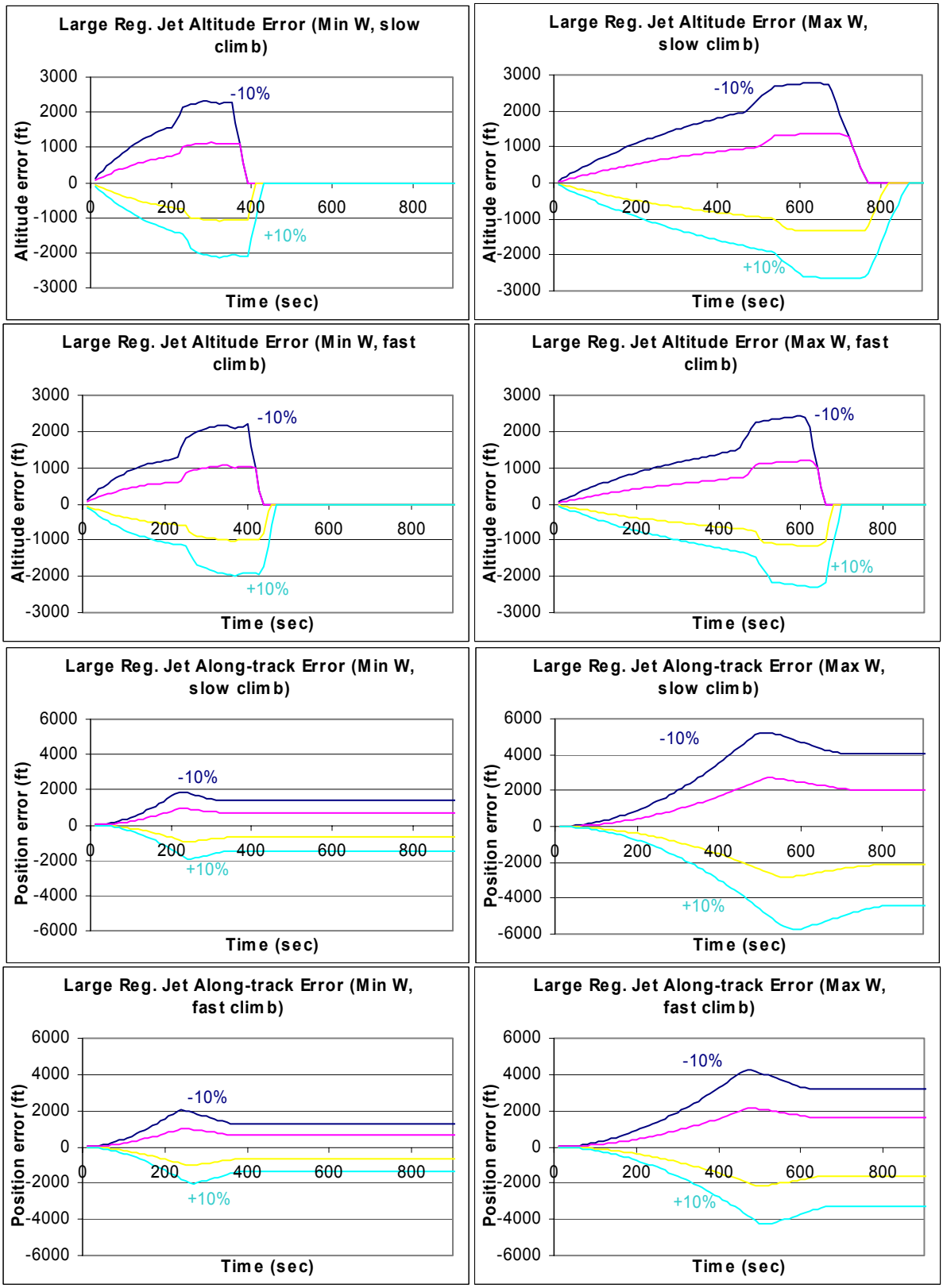

Figure 5-72 Large Regional Jet - Errors due to weight estimation uncertainty during climb (ISA +20)

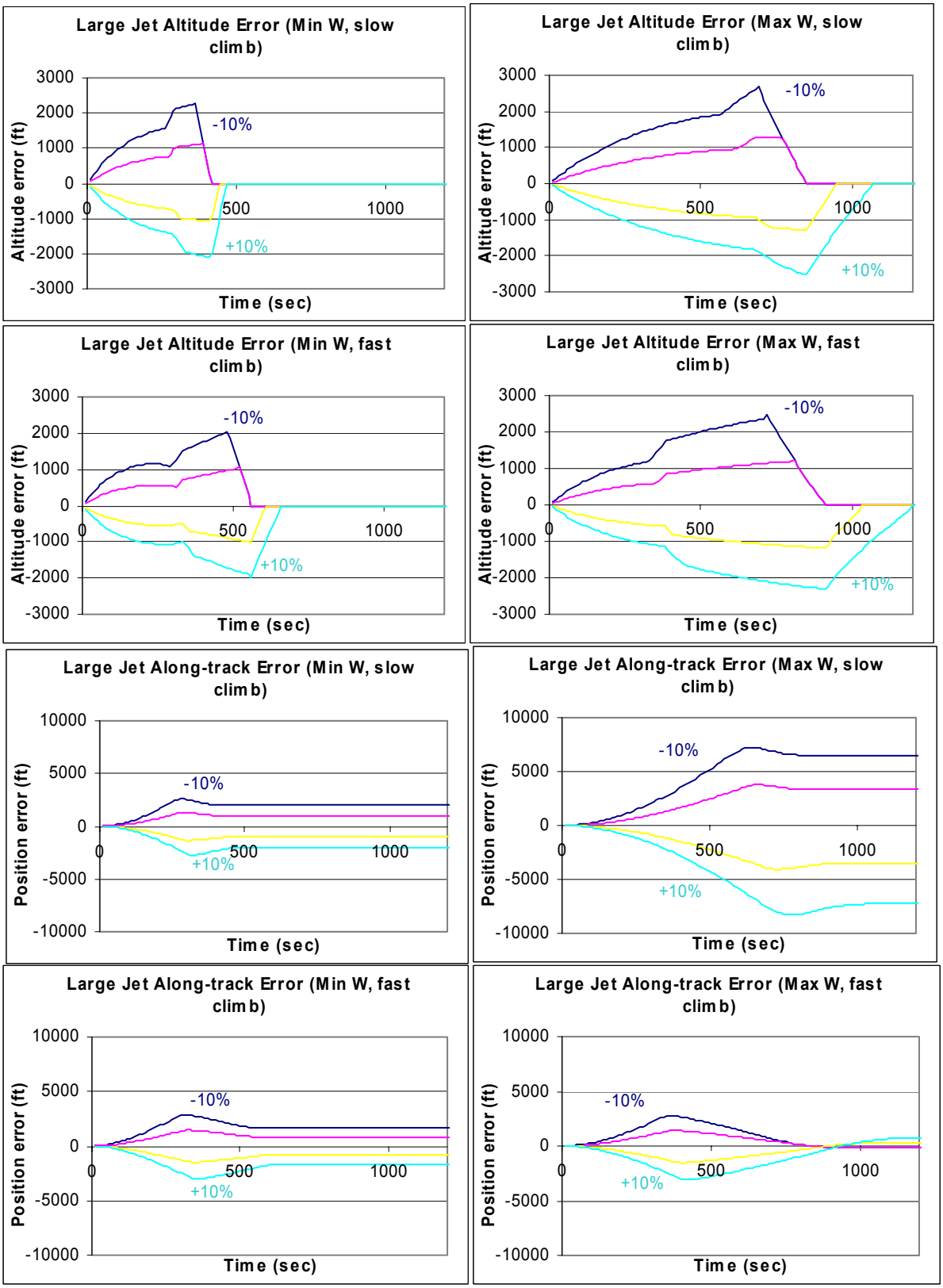

Figure 5-73 Large Jet - Errors due to weight estimation uncertainty during climb (ISA+20)

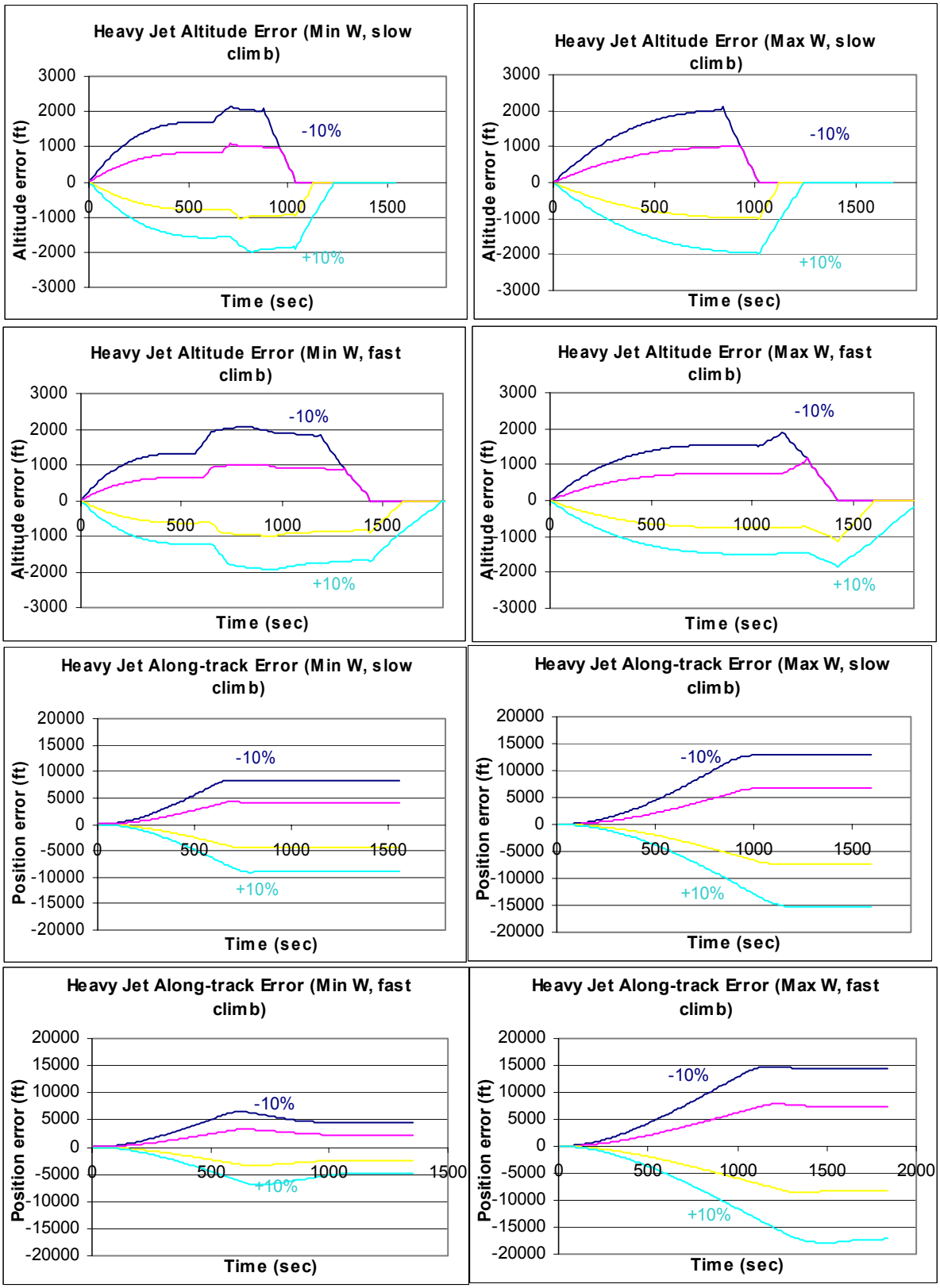

Figure 5-74 Heavy Jet - Errors due to weight estimation uncertainty during climb (ISA+20)

Effect of Fuel Consumption

A most basic description of aircraft fuel consumption known to all students is the Breguet range equation. This equation describes a relationship between final and initial weight for a flight traveling a specified range. The functional form of the equation is shown below:

$$\frac{W_{final}}{W_{initial}} = e^{-k(range)}$$

While seemingly simplistic, comparing the form of the equation to an airline operations manual yields good agreement as shown in the figure below. In terms of the impact on trajectory prediction, what is important to realize is that the *relative* error in weight will be approximately preserved as the flight cruises. Thus, a 5% error in weight during climb will roughly translate to a 5% error in descent.

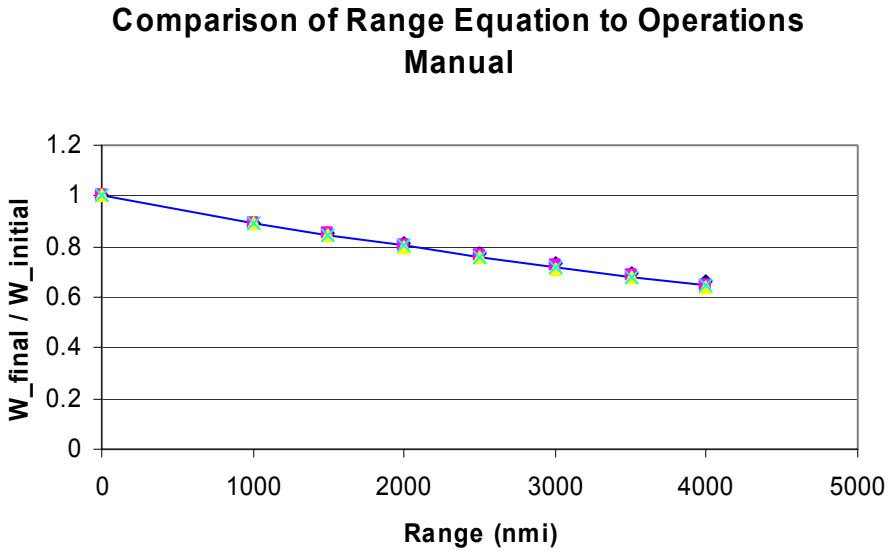

Figure 5-75 Comparison of Breguet range equation to data from an airline operator manual

Step Climb Errors

We can use the above range equation to approximate the error in the positioning of a step climb due to a relative weight error. Assuming that the optimal weight for a step climb is known, then an error in weight will result in the optimal weight being reached at the wrong location. This positional error can be approximated as follows:

$$\Delta x = \frac{\ln(\frac{W_i}{W_{step}})}{k} - \frac{\ln(\frac{W_i(1+\varepsilon)}{W_{step}})}{k}$$

$$= -\frac{\ln(1+\varepsilon)}{k}$$

In the above, a relative weight error has been assumed (ε). The weight at the step climb (W_{step}) is fixed according to an operator manual, but the initial weight (W_i) is subject to a relative error. Figure 5-76 illustrates the situation (notional figure only). A flight is modeled with an initial weight error. As fuel is consumed, the actual flight will reach the step climb weight at a different location as the modeled flight. The effect of the relative weight error on this positional error is shown in Figure 5-77.

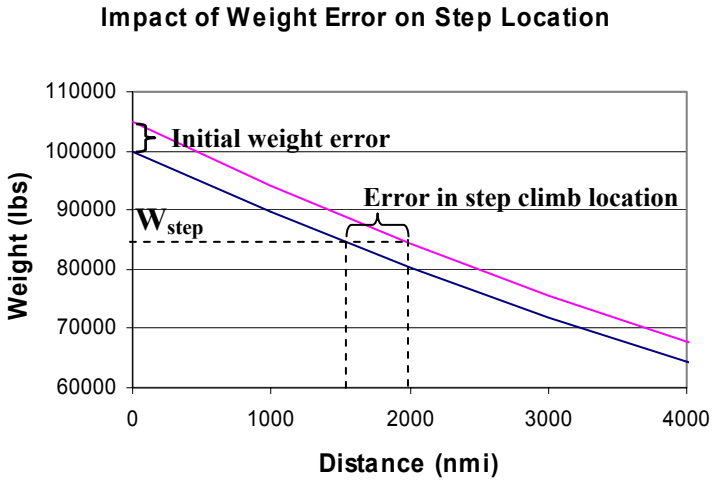

Figure 5-76 Impact of initial weight error on predicted step climb location

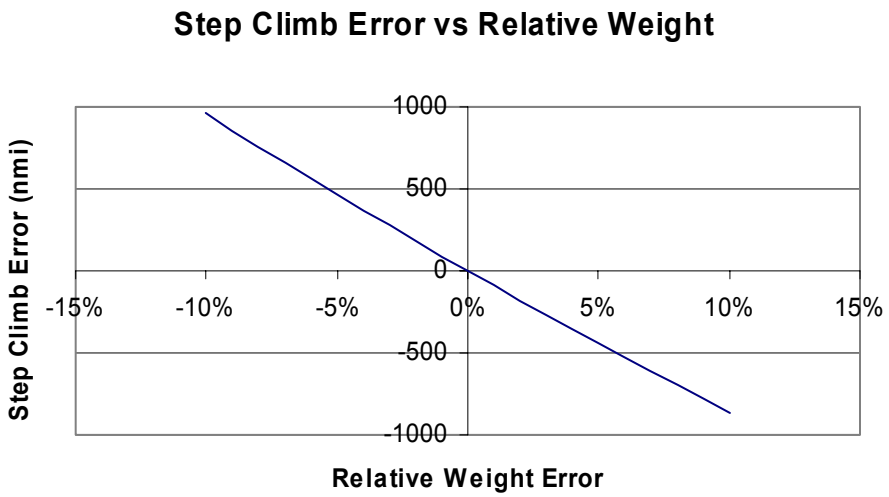

Figure 5-77 Effect of relative weight error on step climb location error for a typical transport aircraft

5.4 Wind Error

5.4.1 Description of Error

Accurate trajectory prediction depends on having an accurate representation of the environment within which the aircraft operates. In particular, errors in the predicted wind field have a direct influence on errors in the ground speed of the aircraft. Since trajectory predictors often operate under the assumption of constant airspeed segments, errors in wind speed and direction will translate into ground speed errors resulting in a growing along-track error.

While the *impact* of a specified wind error is simple to understand, the structure of the uncertainty due to wind is more complicated. In order to understand this uncertainty, it is worth developing a rudimentary understanding of the process used to forecast the wind and the resulting errors stemming from that process.

Wind Forecasting Process

One of the first steps in obtaining a future wind forecast is to obtain an assessment of the current wind field. This is accomplished through an *observation* phase during which data is collected through a variety of sensors with various accuracies. Information is gathered from multiple sources such as:

- Surface observations – A vast network of global observation stations are used to obtain measurements such as surface pressure, temperature, wind components and relative humidity. Models are used to correct for topography effects. Data is also obtained from ships along common shipping routes.
- Radiosondes and pilot balloons – Launching stations are located throughout the World with higher density near population centers. Weather ships also launch radiosondes at regular intervals. These sensors provide a vertical slice of information and errors tend to be vertically correlated.
- Aircraft Reports – Commercial aircraft report wind and temperature information in well-traveled areas. This data is reported asynchronously and provides point data at typical cruise altitudes.
- Vertical Temperature Soundings – Satellites obtain global temperature measurements with coarse vertical resolution. Errors are horizontally correlated and data tends to represent average areas rather than point estimates.
- Cloud Drift Winds – Observation of cloud drift is automatically computed from cloud photograph sequences obtained from satellite images.

While sensor technology will improve going forward, each approach described above is subject to errors in observation of atmospheric data elements. The magnitude and spatial autocorrelation properties of the errors will depend on the sensor type. We should also mention that certain atmospheric measurements, such as the wind, are a time sample of an unsteady process. If measurements are made during a period of high unsteadiness,

these measurements may appear as errors in the observation, but in fact represent a higher frequency phenomenon that is not typically modeled.
Once observations have been obtained, an *analysis* step follows to determine the proper initialization of models. While classically referred to as the analysis component, the term *data assimilation cycle* is used to represent the more elaborate process required to feed numerical models. This data assimilation cycle consists of four sub-components:

1. Quality control (data checking)
2. Objective Analysis
3. Initialization
4. Short forecasts to prepare the next background field

Figure 5-78 and Figure 5-79 illustrate the two types of data assimilation cycles. Both are based upon asynchronous receipt of observation data. However, the first conducts analysis in an intermittent fashion, whereas the second may continuously update its analysis as observation data is received.

The quality control sub-component removes gross errors and systematic biases from the observation data. Relationships between variables are compared against physical processes to ensure that consistent data is present. Error properties of various sensors are used to improve the observations.

Once a clean set of observation data is obtained, an analysis sub-component obtains the atmospheric variables throughout the modeling region. Since the observations may be irregular in both space and time, this sub-component takes this irregular set of data and obtains an estimate of the current field of atmospheric data across the entire modeling region (often on a uniform grid with interpolation functions). ***The resulting field from this analysis will not identically match the observation values***.

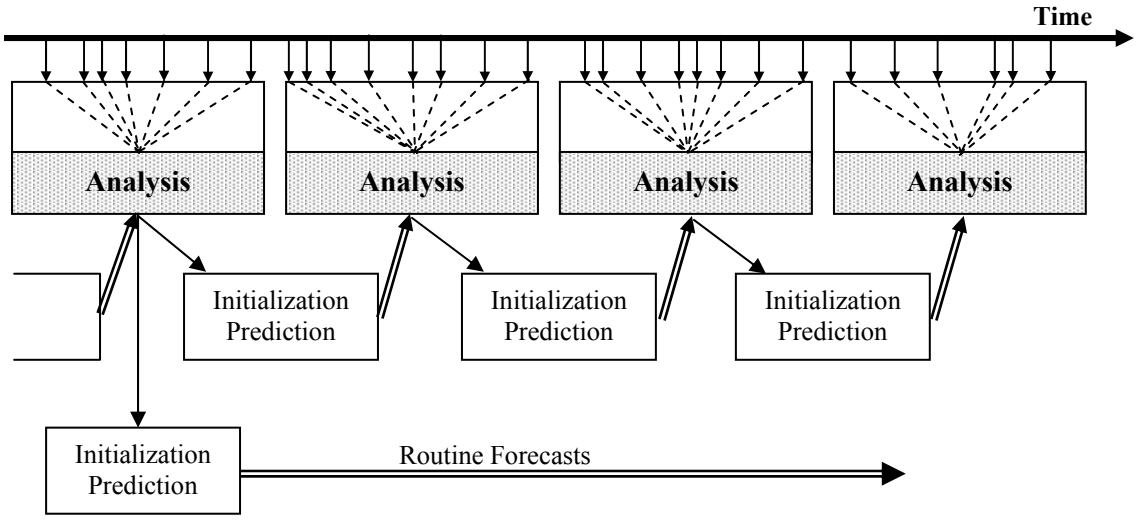

Figure 5-78 Intermittent data assimilation cycle (from [30])

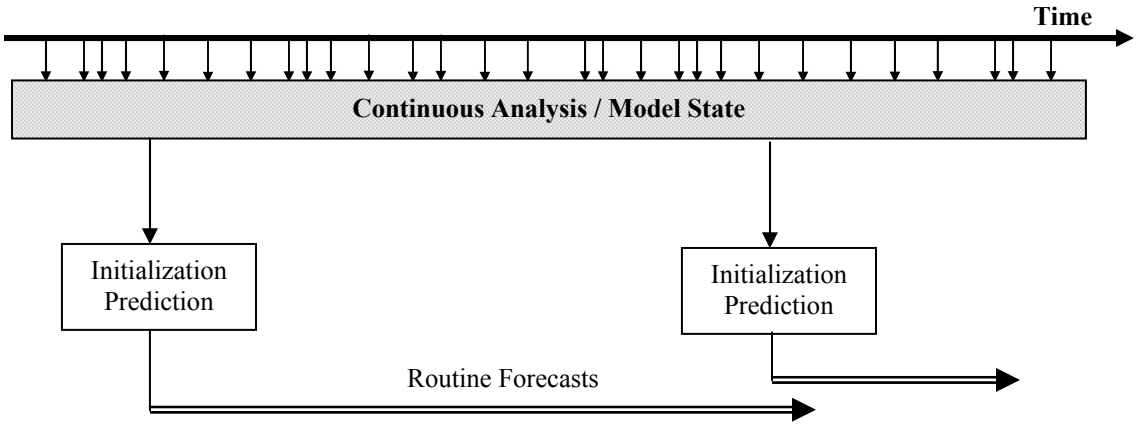

Figure 5-79 Continuous data assimilation cycle (from [30])

Results from the analysis sub-component are used to initialize the computational models, which provide both long-term forecasts and short-term forecasts. During the initialization phase, the data is prepared to ensure that high-frequency instabilities are not excited in the numerical computations used to provide forecasts. The short-term forecasts are used to prepare background fields necessary for the analysis sub-component.

Impact of Physical Phenomena Scales

Figure 5-80 below illustrates the spatial and temporal scales of various physical phenomena that affect the earth's climate system. When developing computational models to provide aviation forecasts, certain physical phenomena are modeled down to a specified scale. Often, the scale is limited due to computational resources or required time to obtain results.

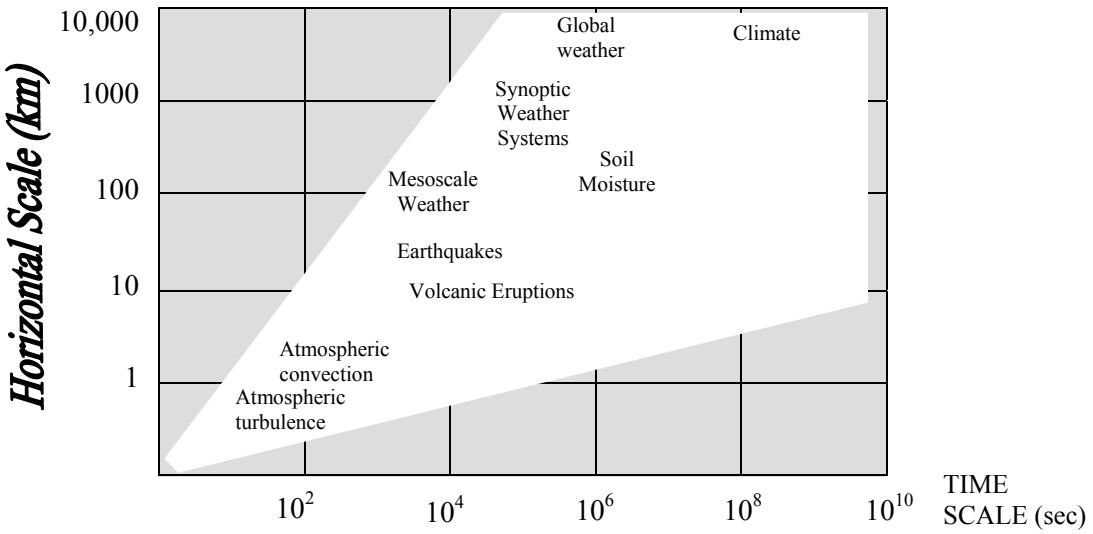

Figure 5-80 Temporal and spatial scales of select physical phenomena affecting the earth climate system (modified from [30])

The prior figure does not detail every single physical phenomena affecting weather, but illustrates the range of temporal and spatial scales that exist in the atmospheric forecasting problem. It is important to grasp this concept, as computational models do not currently model processes of every length and time scale occurring in nature. In order to be able to model smaller and smaller length (time) scales, more and more data would have to be gathered with increased spatial (and temporal) resolution just to be able to obtain the current state to serve as initial condition for the model.

The impact of this problem can be illustrated by investigating error correlations. If we compare a background (computed) field to observations at multiple observation stations, we will find errors between the background and the observation. The correlation in the error can be plotted as a function of distance between observation stations (and curve fit) to yield a figure as shown below (Figure 5-81). In the limit as the distance between stations approaches zero, we note that the correlation does not approach unity. However, by definition, the correlation in the error should be unity, at zero distance. The reason for the discrepancy is that there are some small-scale effects at the lower length scales that are not being captured in the observation network and forecast model. (More explanation can be found in Box 1).

As a simple example, consider an error that consists of the summation of a small-scale effect and a large-scale effect. Attempts to measure spatial correlation on a grid with spacing greater than the small-scale effects will miss the details of the small-scale errors. The form of the error will be identical to that shown for this case.

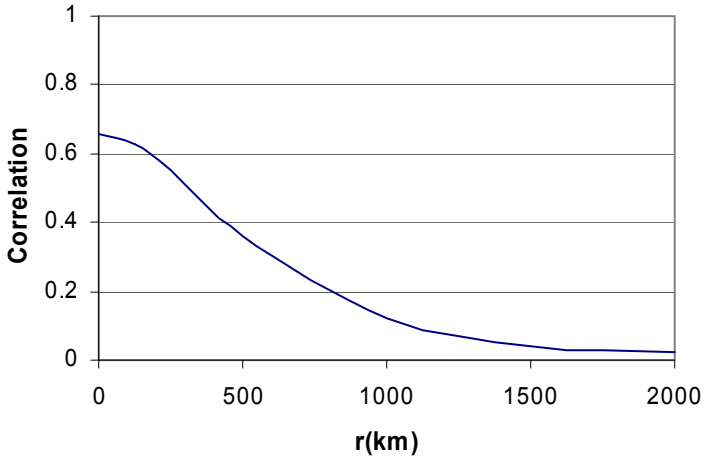

Figure 5-81 Observed minus background correlation for the 500mb geopotential as a function of distance between stations. The background is a forecast background (from [30])

Box 1. Effect of small-scales on correlations

A network of *K* stations, with multiple observations at each station (O_k) and a background value at each station (B_k) will have the following correlation:

$$R_{lk} = \frac{\overline{(O_k - B_k)(O_l - B_l)}}{\sqrt{\overline{(O_k - B_k)^2}\,\overline{(O_l - B_l)^2}}}$$

The observation value represents the measurement that is obtained at a station and includes measurement errors. The background value is the result of a prior analysis process. We can introduce a third variable (T_k), representing the "true" value at the observation station k. However, this "true" value consists only of those components of the spectrum that can be represented by the observation network. In this manner, we introduce the observation and background error terms as follows:

$$E_O{}^2 = \frac{1}{K}\sum_{k=1}^{K}\overline{(O_k - T_k)^2}$$

$$E_B{}^2 = \frac{1}{K}\sum_{k=1}^{K}\overline{(B_k - T_k)^2}$$

Note that the observation error includes errors of "representativeness" (the inability to represent smaller scales) together with measurement errors. The background error includes other analysis / modeling errors. The correlation function can be expanded as follows:

$$R_{lk} = \frac{\overline{\left[(O_k - T_k) - (B_k - T_k)\right]\left[(O_l - T_l) - (B_l - T_l)\right]}}{\sqrt{\overline{\left[(O_k - T_k) - (B_k - T_k)\right]^2}\,\overline{\left[(O_l - T_l) - (B_l - T_l)\right]^2}}}$$

We can expand the above expression and consider that background errors will not be correlated with observation errors.

$$R_{lk} = \frac{\overline{(O_k - T_k)(O_l - T_l)} + \overline{(B_k - T_k)(B_l - T_l)}}{E_o{}^2 + E_B{}^2}$$

If the errors are homogenous, and the observation errors are horizontally uncorrelated, in the limit as the distance between stations is reduced, the above reduces to:

$$\lim_{r \to 0} R(r) = \frac{E_B{}^2}{E_B{}^2 + E_O{}^2}$$

We note that the observation error term includes the effects of both the measurement errors and the errors due to the neglect of the small-scales in our observation network (errors of representativeness). This result illustrates how neglecting smaller scales leads to the paradox that the correlation does not approach unity as observation stations approach each other.

Wind Forecasting Errors

The preceding description of the weather prediction process indicates a few types of errors that can be present in the wind forecasts used for trajectory prediction. We are not attempting to categorize all wind prediction errors, but to understand some of the properties of the errors. Depending on the source of error, the properties of the error can be significantly different and will affect trajectory prediction uncertainty in different manners. For example, a point error in wind will not have as much of an impact on

prediction as a systematic bias. Some of the errors previously described are summarized below.

- Sensor errors during the observation phase, including errors introduced through averaging over larger volumes. These lead to point errors in an observed value. Depending on the sensor used, these may be uncorrelated or correlated with neighboring observations.
- The density of the observation grid will lead to errors on length scales smaller than the observation network. Forecasts based upon this observation network will cause this error to grow and "cascade" to longer length scales [31].
- Forecasts using intermittent data assimilation cycles and aircraft-based observations are subject to a tradeoff between temporal and spatial observation density. As the time window between observations is decreased, the number of observations decreases; yet the time difference between observation and analysis will also decrease. This effect is discussed in [32].
- Forecasting errors will grow with the forecast time horizon. In addition to growth of initial condition errors, models are subject to discretization errors and modeling errors. For example, the numerical model may neglect certain smaller-scale effects, independent of the data resolution.

An example of the properties of wind uncertainty is illustrated from [32] in Figure 5-82. This figure shows the rms vector difference in wind speed between observations and the analysis (0 hr), and forecasts of different time horizons. The root-mean-squared error grows as a function of forecast time and is a function of altitude. Further, the error between analysis and observation (0-hr) incorporates both the observation errors associated with the rawinsonde observation network and the additional analysis error.

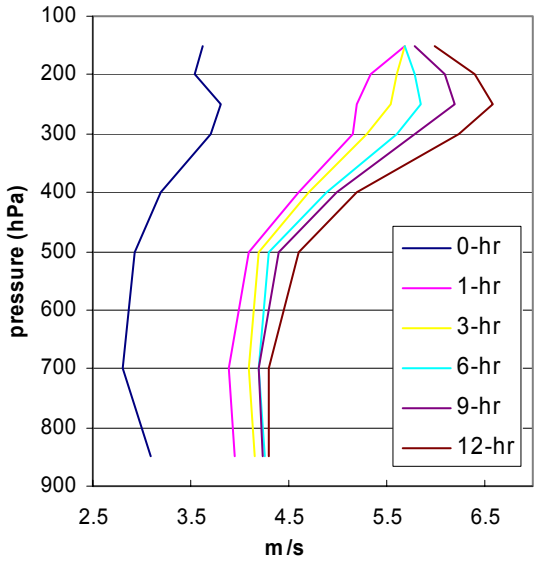

Figure 5-82 Verification of RUC forecasts against rawinsonde observation. RMS vector difference between observation and forecast is given for 1, 3, 6,9 and 12 hour forecast. Also shown is the difference between observation and analysis. Data from [32]

The above errors indicate a sense of the averaged magnitude of the errors *for this specific forecasting product*. However, as reported in [33], the rms statistics do not provide a complete picture of the wind uncertainty. In particular, vector errors are describable through a distribution function leading to large errors being encountered some percentage of the time. This distribution function is replicated below (see Figure 5-83) for the RUC-1 forecast, and can be approximated by a lognormal distribution as shown. However, this description of the error does not capture the geographical and temporal correlation that can occur in the wind uncertainty. Additional metrics were described in [33] to indicate the frequency of time periods during which errors were large. This correlation is seen more clearly in Figure 5-84 showing the geographical distribution of errors as reported in [32]. In this example, one can clearly see the impact of both geographical and temporal correlation of errors.

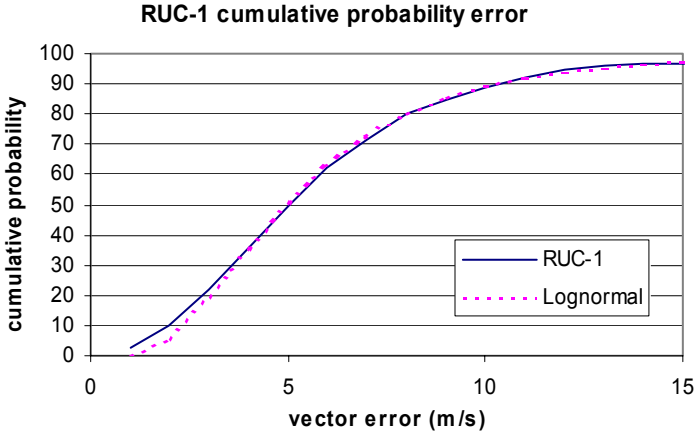

Figure 5-83 Cumulative distribution of errors for RUC-1 (from [33]) - Also shown is the fitted lognormal cumulative distribution

The spatial and temporal correlation of wind uncertainty will have a substantial impact on trajectory prediction. Since certain TP clients will be using the wind information to produce predictions for many flights in a given airspace, spatially and temporally correlated errors will impact all flights simultaneously. This implies that there are periods during which all predictions will be substantially affected by wind uncertainty.

Another important consideration for trajectory prediction is that the covariance structure of the wind errors will determine the ultimate impact of wind uncertainty on the aircraft. This can be illustrated by considering the extremes of white noise and a bias. If wind error appears as white noise, the impact on trajectory prediction will not be significant as the uncertainty will average out. Conversely, a wind bias will have the most significant direct effect (although, if it could be detected, it could be compensated for). For this reason, we discuss the covariance structure of wind uncertainty.

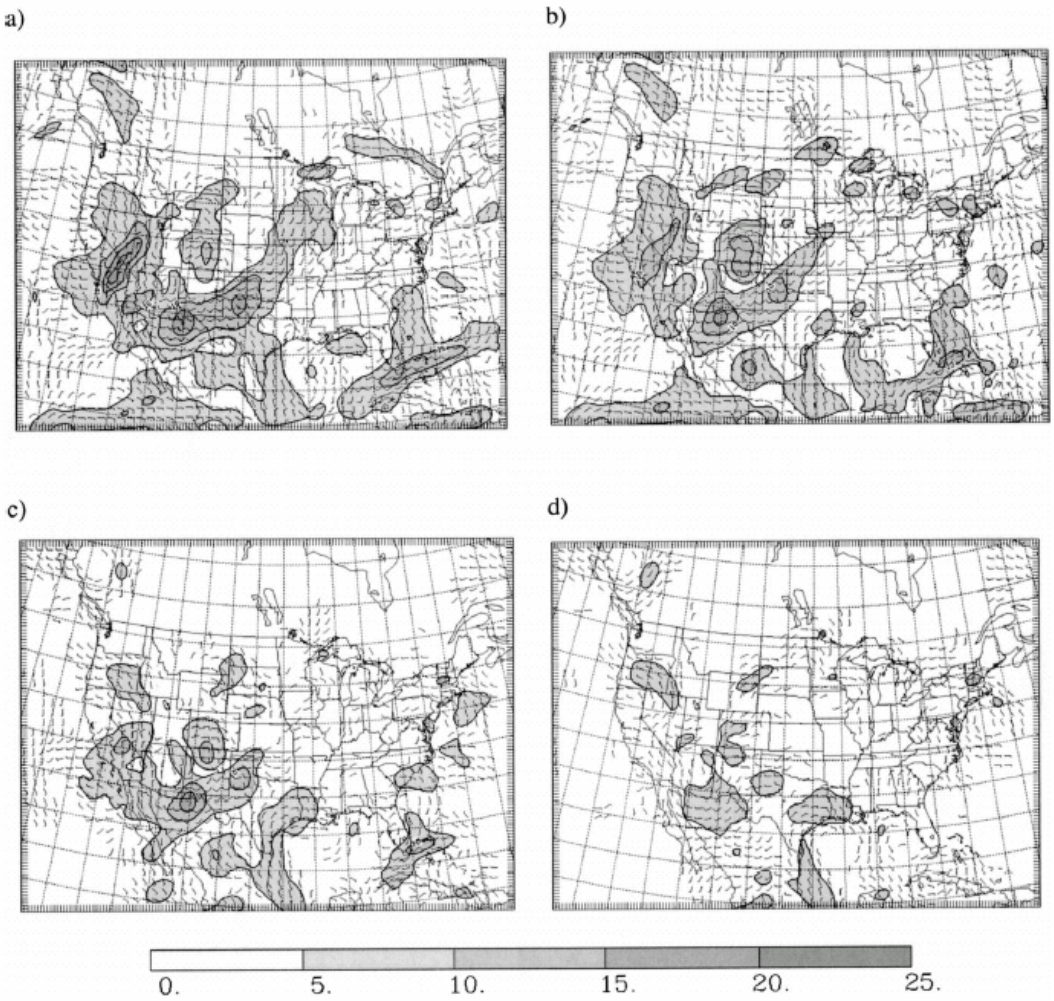

Figure 5-84 RUC-20 forecast vector difference from verifying analysis (forecast minus analysis) for 250 hPa wind forecast valid 1200 UTC 8 Feb 2001; (a) 12-h forecast initialized at 0000 UTC 8 Feb, (b) 9-h forecast initialized at 0300 UTC, (c) 6-h forecast initialized at 0600 UTC, and (d) 3-h forecast initialized at 0900 UTC. Units are in m/s.

Hollingsworth and Lönnberg [34] describe the covariance structure of the wind uncertainty assuming that errors are locally homogenous. The approach fits an uncertainty model (a series solution) to the error between forecast and observation data. A truncation distance of 3000 km is applied to the wind-wind correlation, thereby assuring that wind-wind correlations are zero at a distance greater than 3000km. The component of the wind error that is constant over this domain is treated as such and labeled the "large-scale" component of the error. Observation errors are treated as uncorrelated in space. Figure 5-85 illustrates the longitudinal speed correlation as obtained by this model. Also shown is a curve of the following form (from [30]). Where, L is a length scale characterizing the curve. The curve has been scaled to deal with the observation and "errors of representativeness" effects.

$$\left(1+\frac{r}{L}\right)e^{-r/L}$$

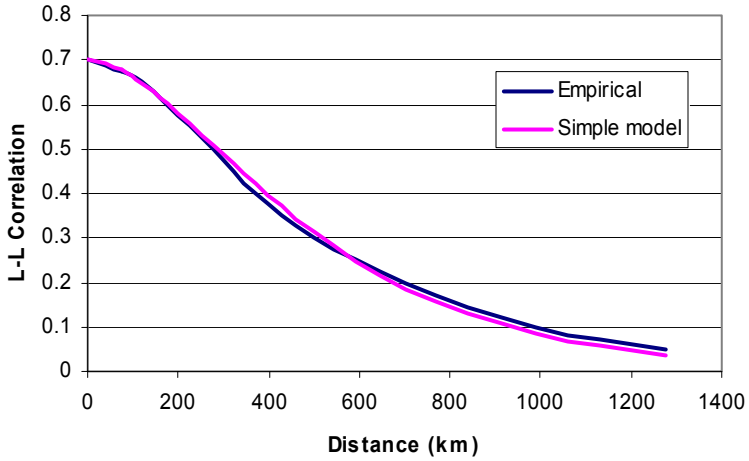

Figure 5-85 Variation at 200mB of the <l,l> longitudinal correlation of the error in wind forecast from observation as a function of station separation, from [34], compared to a simple theoretical model

When referring to longitudinal (l) and transverse (t) speed correlations at a distance r, Figure 5-86 illustrates the difference. While Hollingsworth also expresses results for the transverse correlation, these are not of great significance to trajectory prediction. For these applications, the longitudinal correlations are the most important component of the error for flights not subject to large turns. As one follows a straight flight path, the longitudinal component represents the along-track component of the wind error.

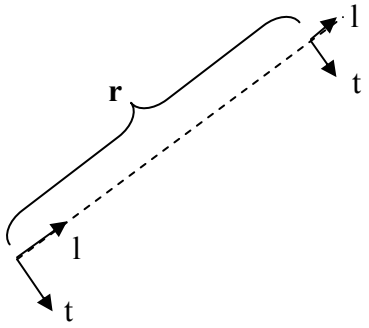

Figure 5-86 Illustration of longitudinal (l) and transverse (t) components of wind errors, the <l,l> and <t,t> correlations are a function of the distance (r) between the points of interest.

As explained previously, Figure 5-85 does not show a correlation of one at a distance of zero for two reasons: measurement errors and errors of representation. Since the measurement errors represent errors for the radiosonde data, these are simple to understand. This error also has the property of being uncorrelated in space. One may represent its correlation function as a Dirac delta at distance zero. From an impact on trajectory prediction, this term does not contribute to trajectory prediction uncertainty.

Errors of representativeness are those errors associated with not modeling the smaller, higher frequency scales. The correlation function for this term is *unknown*, but bounded. At one extreme, the correlation could be spatially uncorrelated, just like the observation error and represents missing ultra-high frequency effects. At the other extreme, the error

could be perfectly correlated within some cutoff distance representing the minimum resolved scales in the model. In this case, the error would be a highly localized bias in the wind prediction. Intuitively, one would expect this to be the worst-case impact on trajectory prediction. Unlike the measurement error, this term *will* contribute to trajectory prediction errors.

Figure 5-87 illustrates the possible impacts of these terms on the autocorrelation function. Note that the relative magnitude of the two terms has not been specified or drawn to scale on this figure. Measurement errors for radiosonde wind data are reported to be between 1.4 to 3.4 m/s [35]. However, this accuracy has improved since then. The observation error (measurement plus representativeness) at 200 mB is approximately 3.3 m/s [34] in the same data used to obtain the figure. Using the radiosonde measurement errors, this implies an error of representativeness between 0 and 3.0 m/s. In addition to these errors not captured in the correlation function, the large-scale error (assumed constant over a 3000 km range) has an r.m.s. between 1.5 to 2.5 m/s.

The above information is combined into a model of wind uncertainty that describes the error in wind forecast that will be encountered by an aircraft in flight. This model has been developed to provide an estimate, through parametric analysis, of the impact of various wind uncertainty on the flight in cruising flight.

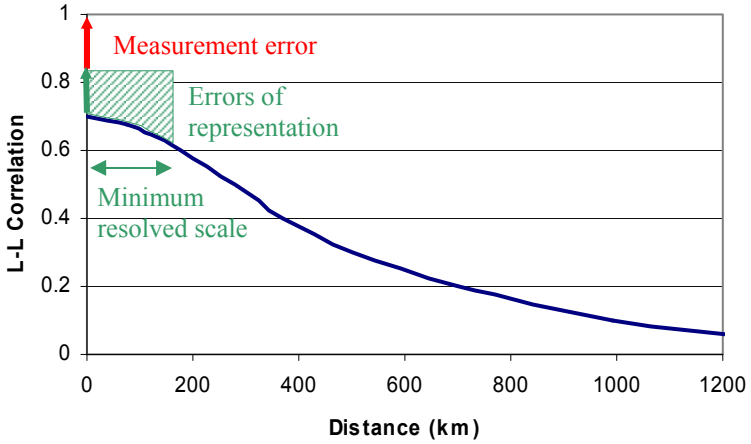

Figure 5-87 Impact of measurement error and errors of representation on the longitudinal correlation function (minimum resolved scale is notional, not to scale)

An Approximate Wind Uncertainty Model

The information from the above suggests an approximate wind uncertainty model comprised of three terms that will affect the aircraft trajectory prediction. The along-track wind uncertainty can be modeled as the sum of three terms:

- An error of representativeness (ε_R) effect previously described
- The prediction error (ε_S) describing the error in prediction occurring at the modeled scales
- A large-scale error (ε_L) which is assumed to be a constant bias over a range of 3000 km

The wind error affecting the flight is described as the sum of these three random components. (A measured wind error would additionally include a term for measurement error.)

$$w_{error} = \varepsilon_R + \varepsilon_S + \varepsilon_L$$

The total variance (σ_T) of the wind uncertainty that impacts the flight can be expressed as follows:

$$\sigma_T{}^2 = \sigma_R{}^2 + \sigma_S{}^2 + \sigma_L{}^2$$

We combine data from [34] with [35] to remove the effects of measurement error between the pressure altitudes of 1000 to 200 mB (a reasonable range for TP applications). This process provides the following range of values:

$$\sigma_L = (1.3, 2.4)$$
$$\sigma_S = (2.6, 6.5) \text{ in m/s}$$
$$\sigma_R = (1.3, 4.0)$$

For example, in the above reports at 200 mB, the rms values in the large scale, prediction and representation errors are: 2.4, 4.7 and 1.3 m/s respectively. This provides a total rms error of 5.4 m/s.

We model the error in representativeness (ε_R) as a random process with zero mean, a known rms (1.3 m/s from the previous example) and a correlation function with a length scale (L) commensurate with the observation network resolution. We use a correlation function as shown below.

$$E\left[\varepsilon_R(t)\varepsilon_R(t+\tau)\right] = \sigma_R{}^2 e^{-\left(U\tau/L\right)^2}$$

The distance-based correlation function has been transformed to a time-based one assuming a known aircraft ground speed (U). The above can be approximated using the following power spectral density function.

$$S_{\varepsilon_R}(s) = \frac{\sqrt{\pi}\sigma_R{}^2 (32)\left(U/L\right)^3}{s^4 - 8\left(U/L\right)^2 s^2 + 32\left(U/L\right)^4}$$

The prediction error occurring at the modeled scales (ε_S) is represented through a correlation function as shown below.

$$E\left[\varepsilon_S(t)\varepsilon_S(t+\tau)\right] = \sigma_S{}^2\left(1 + \frac{U\tau}{L}\right)e^{-(U\tau)/L}$$

The above correlation function can also be represented by its power spectral density function as follows:

$$S_{\varepsilon_s}(s) = \frac{4\sigma_s{}^2 \left(\frac{U}{L}\right)^3}{\left(\left(\frac{U}{L}\right)^2 - s^2\right)^2}$$

The large-scale error is represented as a constant sampled from a normal distribution with variance (σ_L).

With the above model of the wind uncertainty, one can generate a signal approximating the wind uncertainty encountered by an aircraft in level flight. Using the power spectral density functions, spectral decomposition is applied to obtain a second-order continuous shaping filter of the form:

$$\begin{pmatrix} \dot{x}_1 \\ \dot{x}_2 \end{pmatrix} = \begin{bmatrix} 0 & 1 \\ -a_1 & -a_2 \end{bmatrix} \begin{pmatrix} x_1 \\ x_2 \end{pmatrix} + \begin{pmatrix} 0 \\ w \end{pmatrix}$$

$$y = (\sigma\sqrt{2a_1a_2} \quad 0) \begin{pmatrix} x_1 \\ x_2 \end{pmatrix}$$

The output (y) represents the desired wind uncertainty. In matrix form, we have:

$$\dot{\underline{x}} = A\underline{x} + \underline{w}$$

The w term represents unity white noise. For numerical calculations, we integrate over a time step (Δt) to obtain the discrete equivalent as follows:

$$\underline{x}_{k+1} = \Phi_k \underline{x}_k + \beta_k \underline{w}_k$$

Where the state transition matrix can be evaluated through the exponential matrix:

$$\Phi_k = e^{A\Delta t}$$

The β matrix represents the effects of the white noise term integrated over one time step. It is obtained as the Cholesky decomposition ($\beta\ \beta^T$) of the covariance matrix of the response to white noise over one time step interval.

For the errors of representation, parameters can be represented as shown below with a length scale of 80 kilometers.

$$a_1 = 4\sqrt{2}\left(\frac{U}{L}\right)^2$$

$$a_2 = 4.395\left(\frac{U}{L}\right)$$

Errors in prediction at the modeled scales can be represented as follows using a length scale of 280 km.

$$a_1 = \left(\frac{U}{L}\right)^2$$

$$a_2 = 2\left(\frac{U}{L}\right)$$

When the above model is applied to a Monte-Carlo simulation of approximately 83,000 hours, the rms values of each contributor to uncertainty (unrepresented, modeled and large scales) approaches the specified value. Autocorrelations are well represented when correlation is high, but correlations do not fall off to zero in the simulated environment. This may be a result of the random number generation or approximations in generating the spectral densities.

The cumulative distribution function of the wind uncertainty is consistent with the results observed in [33] as shown in Figure 5-88. We note that this model duplicates the prevalence of a significant percentage of data points with large errors. For example, the 90th percentile wind errors are 9.77 m/s in this example.

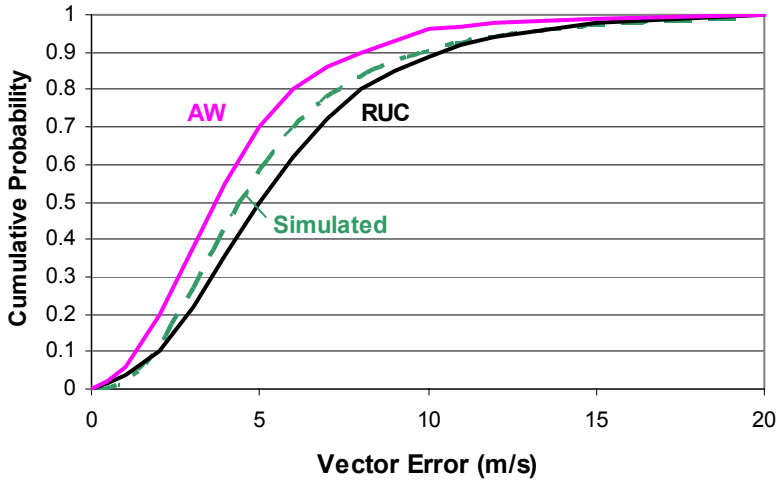

Figure 5-88 Cumulative probability of wind error for simulated versus RUC and Augmented Winds data (AW and RUC data from[33])

Regarding the persistence of errors, the model also accords with measures of the number of hours for which the Nth percentile exceeds a threshold. Table 5-3 shows the results for the model of uncertainty compared to the RUC and augmented winds case from [33]. Thus, for the modeled case, 33% of all hours had a 75th percentile wind vector error that exceeded 7 m/s. While the agreement in numerical values is not exact, the modeled error possesses values within the range of the RUC and AW forecasts. Furthermore, the model preserves the important property that substantial errors persist for a certain fraction of the time.

Table 5-3 Percentage of hours for which hourly 25th, 50th, and 75th percentile vector errors exceed a specified threshold (7 and 10 m/s)

	Exceeds 7 m/s			Exceeds 10 m/s		
	25th	50th	75th	25th	50th	75th
Model	4%	11%	33%	0%	1%	11%
RUC	1%	12%	59%	0%	2%	27%
AW	0%	1%	12%	0%	0%	3%

Figure 5-89 illustrates an example of the along-track error encountered by a hypothetical flight during 10 hours. Note the existence of various error scales.

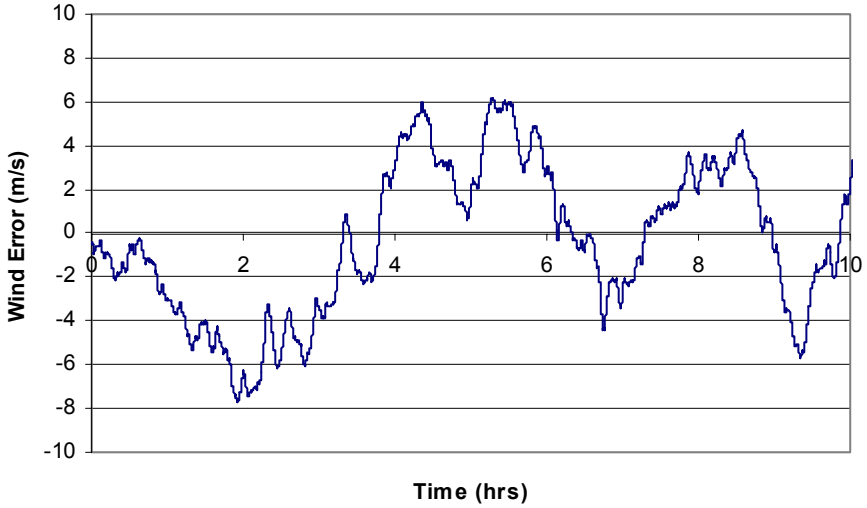

Figure 5-89 Illustration of along-track wind error encountered by an individual flight according to the proposed model

The described wind uncertainty model contains several parameters which are likely to not remain constant according to the forecasting techniques applied and to the age of the forecast being used. For example, the length scales (L) used for the unrepresented scales and the modeled scales errors were obtained by fitting existing data. However, improvements in the modeling of smaller-scale effects would decrease the length scale for the unrepresented scales. Seasonal effects are likely to impact both the length scales and the rms values of each component of the error. Usage of 1 hour forecasts, compared to 6 hour forecasts will affect the rms value of the error in the large-scale and modeled-scale terms.

The specific example shown above was derived for values observed at a pressure altitude of 200mB. The specific rms values for each error term are a strong function of altitude as shown in Figure 5-90. The value for the unrepresented scales was obtained by removing the effect of the measurement error (obtained as a function of altitude from [35]) from the observation error reported in [34]. Note that the effect of unrepresented scales is greater for all altitudes compared to the 200mB example used in the prior example.

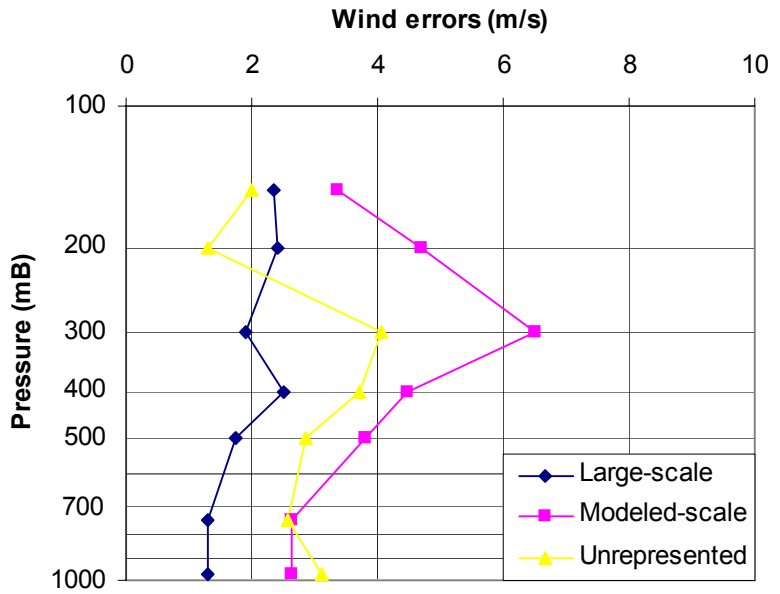

Figure 5-90 Effect of pressure altitude on the rms values of each term in the wind uncertainty model

The above illustrates that the magnitude of the wind uncertainty encountered is a function of altitude. However, our simple model of wind uncertainty must also account for the correlation of errors between altitudes. It is reasonable to assume that large errors at one altitude will lead to large errors at neighboring altitudes. Figure 5-91 shows data, again from [34], showing the vertical correlation in both the divergent and non-divergent wind prediction components. For the non-divergent component, the following approximation of the correlation can be made:

$$C = e^{-\left(\frac{|\Delta \ln p|}{a_\psi}\right)^{b_\psi}}$$

The above is expressed in terms of the difference of the log of pressure. For our simplified uncertainty model, we recast the above into a correlation as a function of altitude using the standard (ISO) atmosphere and obtain the following.

$$C = e^{-[a|\Delta h|]^b}$$

Some agreement in correlation can be had when the above parameters are set to:

$$a = .00009$$

$$b = 1.9$$

In this expression, the altitude (h) is expressed in feet. Figure 5-92 compares the modeled correlation at an altitude corresponding to 300mb to the same data found in Figure 5-91.

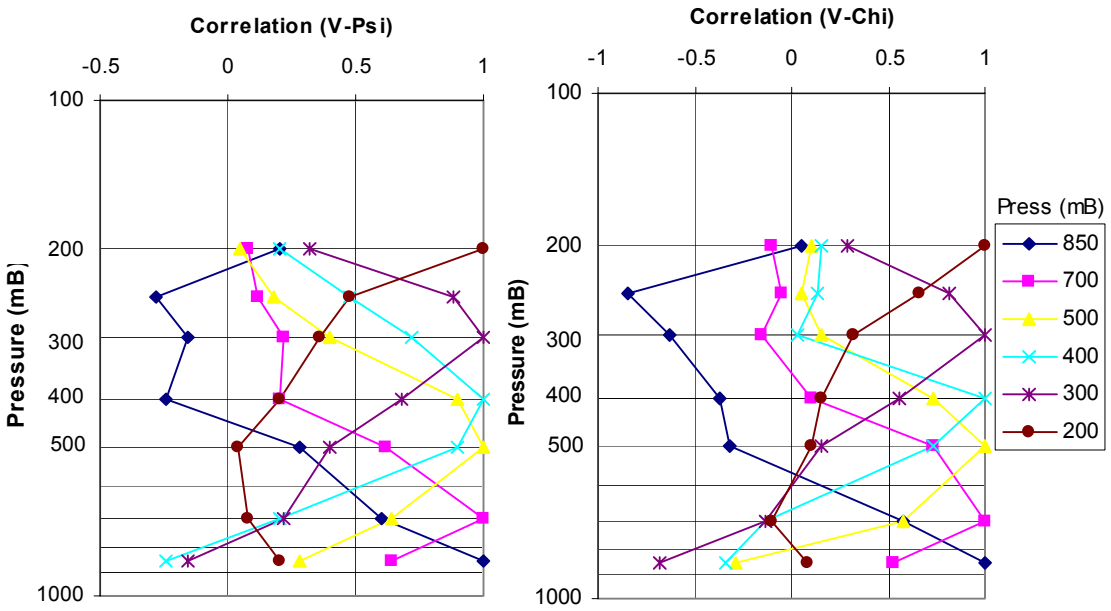

Figure 5-91 Vertical correlation of wind prediction errors for non-divergent (V-Psi) and divergent (V-Chi) terms

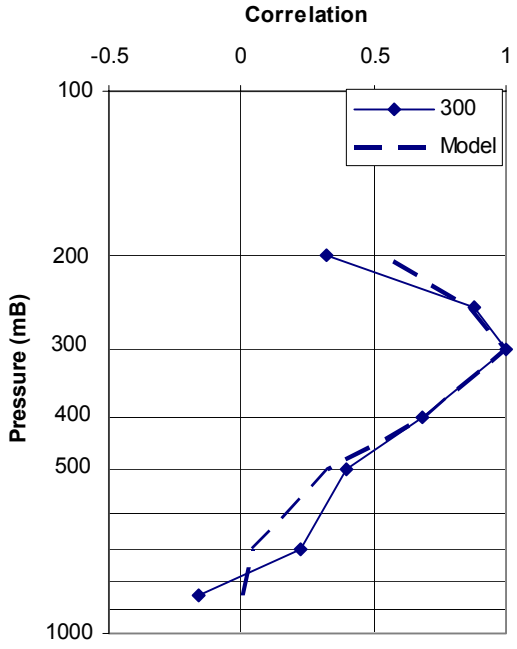

Figure 5-92 Comparison of modeled to non-divergent correlation at 300mB

For the altitude model, we applied the above correlation function between altitude levels to generate a series of correlated wind prediction errors at each altitude. We applied the above model (using the non-divergent correlation) because the altitude correlations of the non-divergent term agreed well with the total wind correlations. In the model, the correlation was obtained by ensuring that the white noise used to drive the shaping filter was correlated between altitudes. The above approximation of the correlation was applied for the prediction error component. This model leads to RMS errors in the wind

shear as shown in Figure 5-93 for the prediction component. We also assume that the large scale errors are perfectly correlated, but scale with different variances obtained from Figure 5-90.

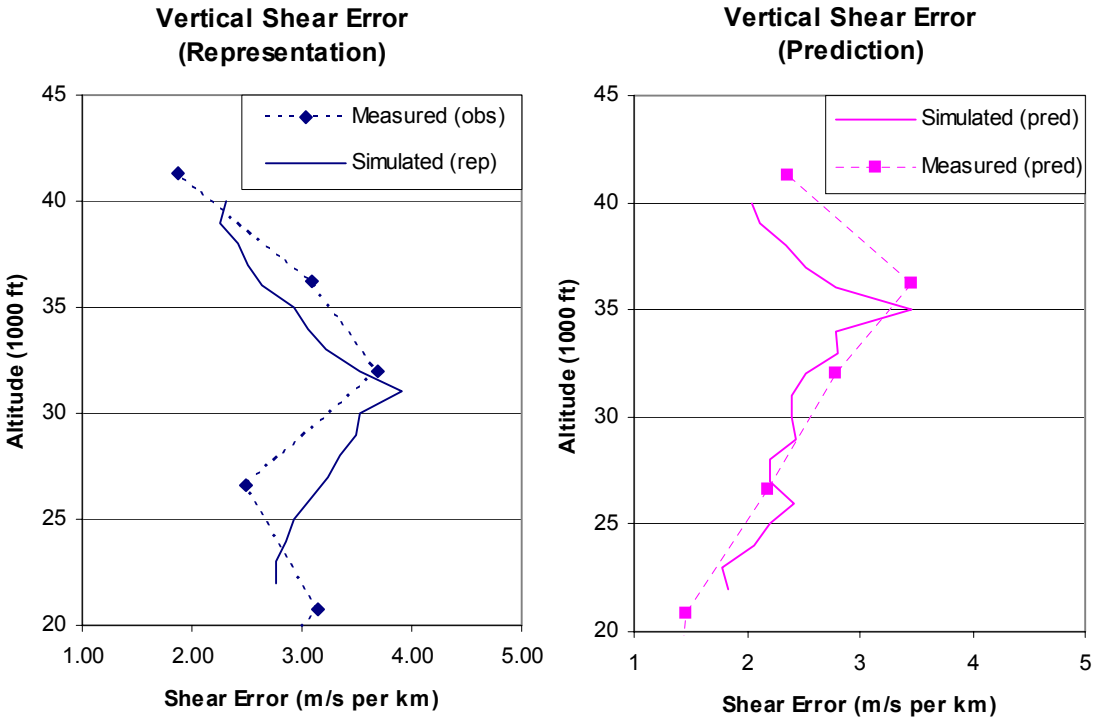

Figure 5-93 Vertical profile of the RMS error in vertical wind shear (in m/s per km) comparing modeled to measured for both the error of representation and the prediction error

For the error of representation, we inferred the correlation based upon the measured shear error component as a function of altitude (See Figure 5-93). Using a similar correlation function form, we assume a correlation between altitudes as follows:

$$C = e^{-\left[(a+bh)|\Delta h|\right]^c}$$

When this is applied to errors of representation, we obtain the following coefficients:

$$\left.\begin{array}{l} a = 0.00017 \\ b = 0 \\ c = 1.9 \end{array}\right\} h < 30{,}000$$

$$\left.\begin{array}{l} a = -0.00617 \\ b = 2.65e-8 \\ c = 1.9 \end{array}\right\} h \geq 30{,}000$$

We have presented a statistical model of wind uncertainty that captures several characteristics relevant to trajectory prediction. These properties are as follows.

1. Wind uncertainty is temporally correlated as an aircraft flies through a wind field. This temporal correlation has been shown to match the properties of measured data.
2. Wind uncertainty contains multiple scales consistent with various physical phenomena.
3. Large errors are shown to persist over large geographical areas for some percentage of the time commensurate with observation.
4. The distribution of errors is consistent with observations.
5. Correlation in wind uncertainty between altitude levels allows for proper RMS values of wind shear error which have a substantial impact on vertical trajectory prediction.

However, the model presented does have some limitations. In particular, the model attempts to capture some important statistics of the wind uncertainty to model the effect of wind uncertainty on a collection of flights. Yet, as presented, the uncertainty is not correlated to physical phenomenon. For example, large along-track errors would be observed for an aircraft flying parallel to a gust front if the location of the gust front were not properly forecast. While this event is represented statistically, the representation of the error described in this section does not correlate a large along-track uncertainty with the presence of a gust front.

5.4.2 Parametric Analysis

As the prior section has illustrated, uncertainty in wind prediction yields a time-varying wind field. Unlike other steady-state errors, this time variation will involve a dynamic response of the aircraft. As the aircraft is subject to a variable wind field, the aircraft will encounter a variable airspeed. The airspeed can change almost instantaneously, yet groundspeed changes must result from an acceleration of the airframe. As the airspeed changes, aerodynamic forces and moments are no longer in balance. The aircraft longitudinal modes are excited and the ground speed is eventually altered.

During cruising flight, the aircraft attempts to ensure constant altitude flight. One simple formulation of this flight mode uses elevator control to exactly ensure that the flight remains horizontal. This particular mode of motion leads to airspeed responses that can be described through a decaying exponential:

$$u(t) = u_0 e^{-t/T}$$

Where an initial speed disturbance (u_0) results in a response with some time constant that can be approximated as follows:

$$\frac{1}{T} = \frac{\rho S U}{m}\left(C_{D_0} - \frac{C_{D_\alpha}}{C_{L_\alpha}} C_{L_0} \right)$$

We use the above formulation, together with the wind uncertainty model from the prior section, to illustrate (Figure 5-94) the impact of the wind uncertainty on the aircraft airspeed (wind), groundspeed and eventually along-track error (Figure 5-95). Note that the ground speed uncertainty lags the wind speed uncertainty due to the dynamics described above. Since the along-track error is an integral of the ground speed error, a further lag is introduced in this error.

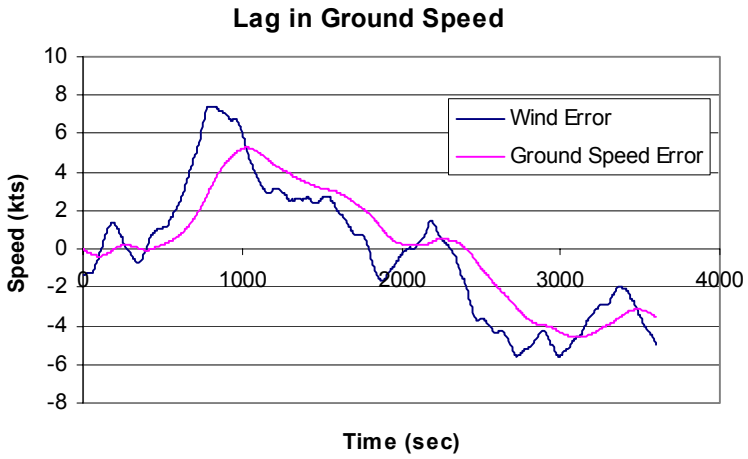

Figure 5-94 Illustration of lag in ground speed response to wind uncertainty during cruise

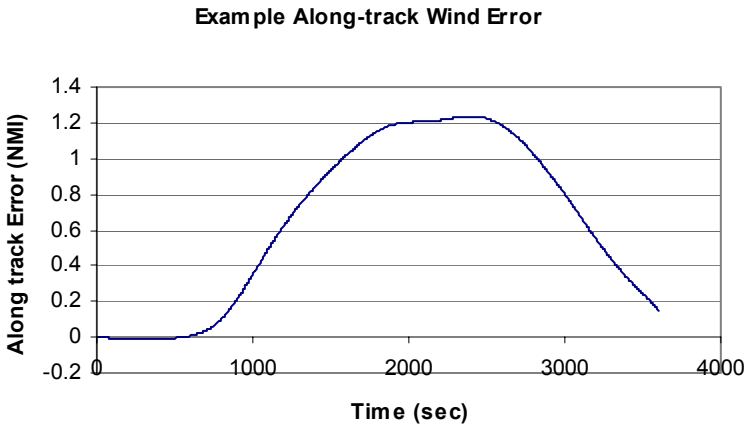

Figure 5-95 Integration of previous example ground speed yields along-track error

The impact of wind uncertainty on the trajectory error will depend on the manner in which the trajectory is projected. One approximation assumes that the target airspeed is known and a forecast wind is added to it to obtain the ground speed. The initial position is known precisely. In this example, the actual wind at a point will be the sum of the forecast plus the error term:

$$w = w_f + \hat{w}$$

The forecast ground speed is the target airspeed plus the forecast wind. The actual ground speed will also include an error due to wind in ground speed (the integral of the impact of all prior wind errors).

$$V_g = V_{air}\big|_{target} + w_f + \hat{w}_g$$

The actual airspeed must therefore be:

$$V_{air} = V_{air}\big|_{target} + \hat{w}_g - \hat{w}$$

In the analysis that follows, we assume that the *forecast* wind can be considered quasi-steady with regards to its impact on aircraft dynamics.

The error in along track position will be the integral of the ground speed error. If we assume that a trajectory predictor will compute the along-track position using a ground speed equal to the target airspeed plus the forecast wind speed, the target airspeed is known, but the initial ground speed is not known accurately. The total RMS along-track error is illustrated as a function of look-ahead time in Figure 5-96. The contribution to the total error due to each component term is also illustrated. The growth in the rms is not exactly linear in look-ahead time, primarily due to the effect of the high-frequency components found in the errors of representation and at the modeled scales. The initial growth in the errors (shorter times) can be approximated as a linear growth at the resulting ground speed rms error. The ground speed rms for each component depends on the impact of a low pass filter on the wind uncertainty rms since the aircraft ground speed response to wind uncertainty acts like a low pass filter. Figure 5-97 illustrates the same errors at an altitude of 40,000 feet.

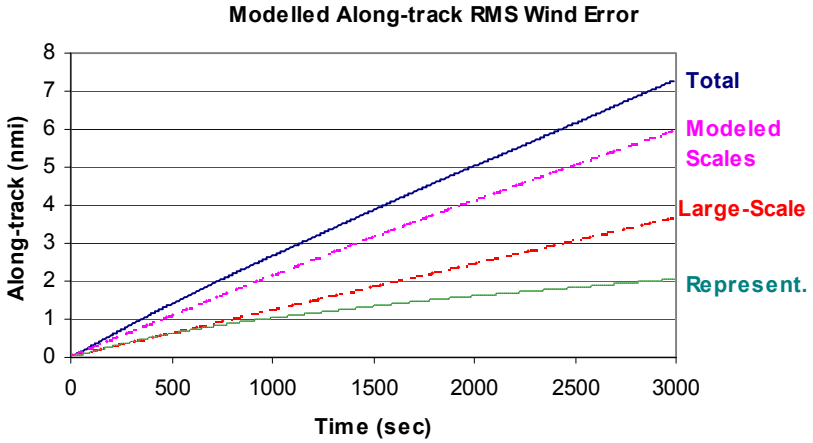

Figure 5-96 Along-track RMS error assuming known airspeed target (h=30,000')

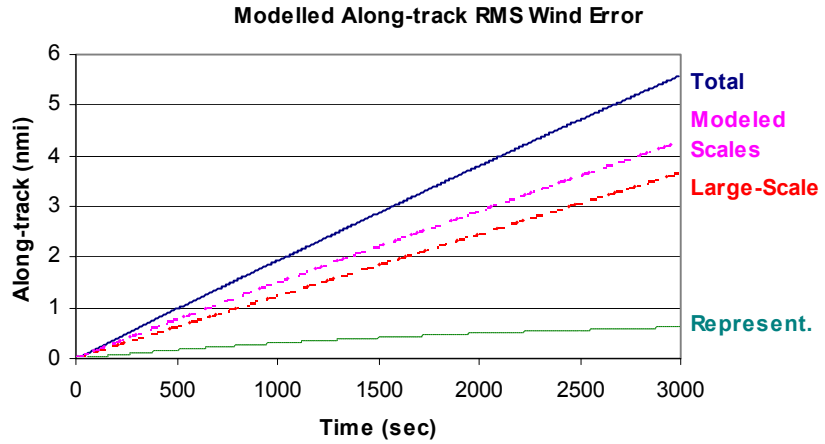

Figure 5-97 Along-track RMS error assuming known airspeed target (h = 40,000')

Each component of the error will scale in accordance with the rms of the individual component. Figure 5-98 and Figure 5-99 show the growth in the along-track error due to the representation and the modeled scales errors for various rms values. (The large-scale errors are not plotted as these are just a linear growth term at the average along-track speed error.) Note that at any given time doubling the rms will double the along-track errors. Thus, as improvements in wind forecasting allow reductions in these terms, the contribution to total uncertainty can be scaled accordingly. Errors of representation, due to their shorter time scales, do not grow linearly with look-ahead time; however, as the time scale of these errors are reduced, the "knee" in the curve will occur at a shorter look-ahead time, thereby decreasing the contribution of this term. Errors in the modeled scales appear to grow almost linearly with look-ahead time.

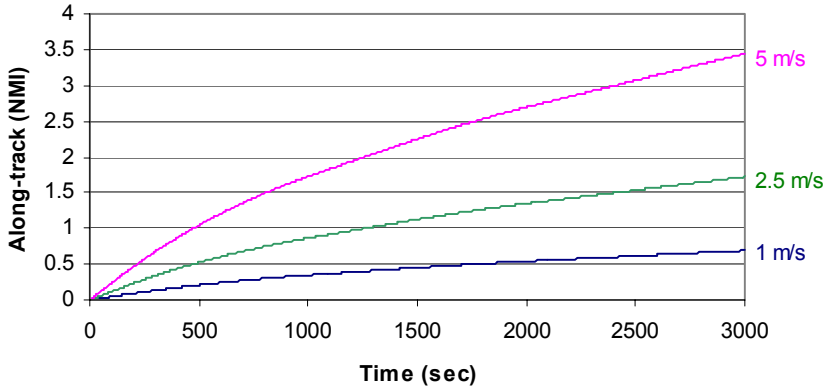

Figure 5-98 Growth in along-track RMS error due to errors of representation with various RMS values (1, 2.5 and 5 m/s)

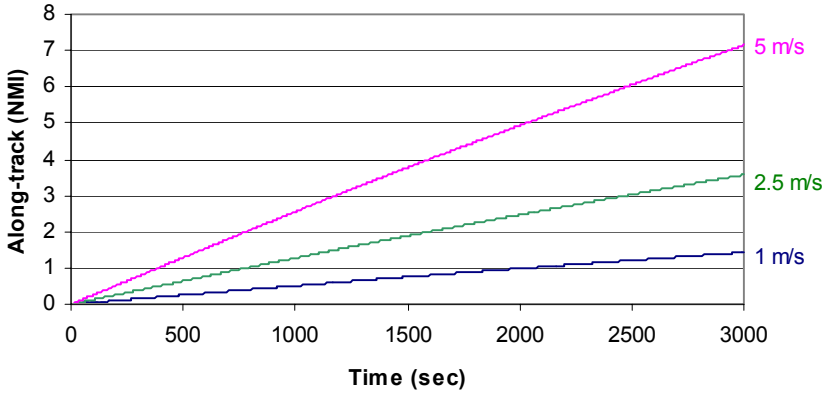

Figure 5-99 Growth in along-track RMS error due to errors at modeled scales with various RMS (1, 2.5, 5 m/s)

To further illustrate why the errors of representation do not grow linearly, Figure 5-100 shows a sample of the speed errors of representations obtained from the model described in the prior Section. Due to the predominance of higher frequencies, as look-ahead time is increased, later errors tend to cancel prior errors since the along-track error is obtained through an integration of the ground speed. In contrast Figure 5-101 shows a sample of the speed errors at modeled scales, the lower frequencies make the growth in along-track error closer to linear for longer look-ahead times. We note that since the modeled errors

have a crossover frequency that is one-fifth of the errors of representation, the linear regime will extend roughly five times the look-ahead. This is observed in the modeled data.

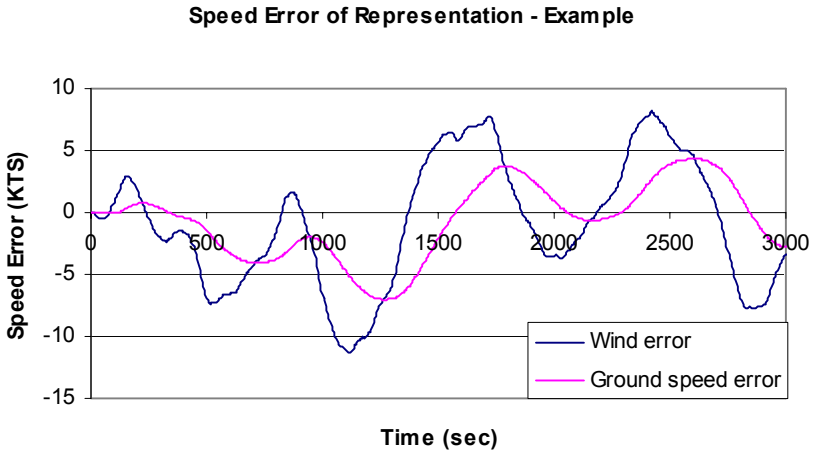

Figure 5-100 Sample of speed error of representation

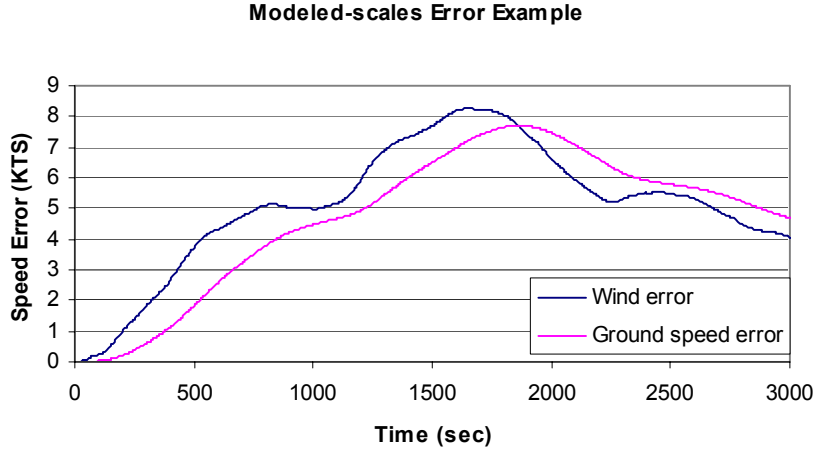

Figure 5-101 Sample of speed errors at modeled scales

An alternative to the above approach assumes that accurate measurements of the ground speed and actual airspeed are known. As before, the forecast wind and the target airspeed would be known as well. This additional knowledge allows one to obtain both the initial error in the predicted ground speed and the local wind error. The initial ground speed error can be removed in order to ensure a better short-term forecast. Figure 5-102 illustrates the resulting along-track error under this approach for both altitudes reported previously. Decoupling into respective components does not yield additional information as one could not "zero out" a single wind uncertainty component with the assumed measurements.

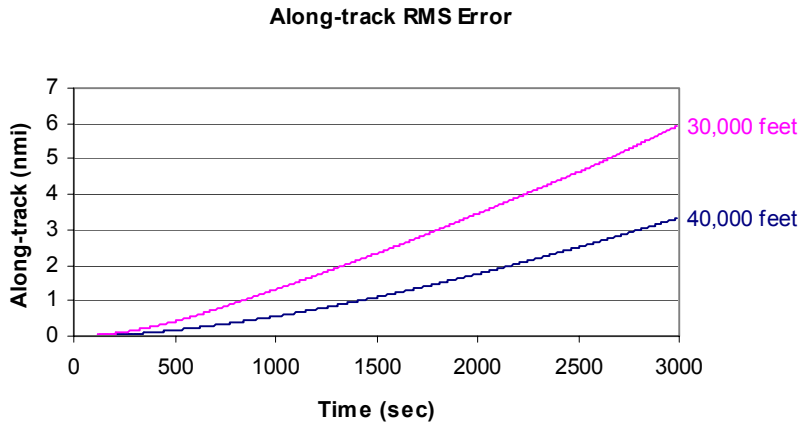

Figure 5-102 Along-track RMS error assuming known: airspeed target, initial airspeed and initial ground speed

What the above figures reveal is that a reduction in the along-track wind uncertainty can be obtained through precise knowledge of the initial conditions. For example, comparing the errors where only the target airspeed is known to the case with known initial conditions reveals that a significant reduction can be obtained in along-track error, particularly for shorter look-ahead times. Furthermore, a larger reduction can be obtained for circumstances with larger wind bias contributions from the large-scale error. This is intuitive, as the bias would be removed through knowledge of the initial condition wind error.

Despite the rather benign looking qualities of the RMS errors, individual trajectory projections can vary wildly, as Figure 5-103 seeks to illustrate. This shows the along-track error for a sub-sample of flights used to derive the previous RMS data shown in Figure 5-96. Excursions of individual flights can be significantly larger than the RMS, and geographically proximate flights will tend to have similar error properties. This later fact can lead to time periods during which forecasts will be poor for all flights within a geographic area.

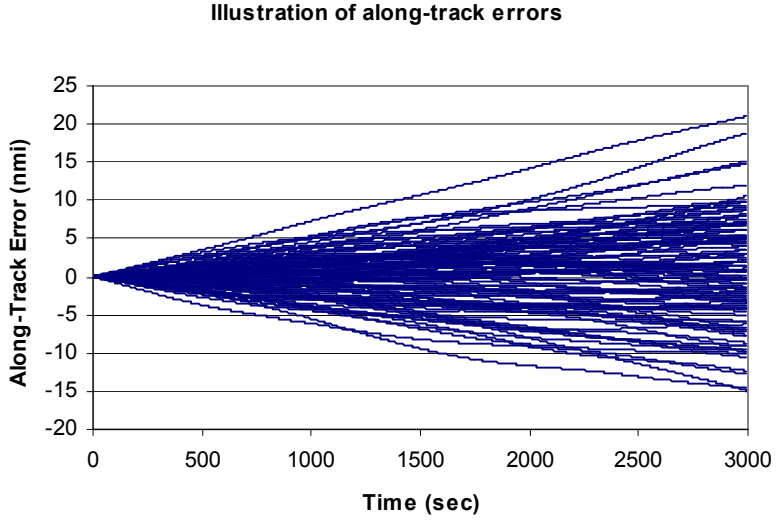

Figure 5-103 Illustration of along-track errors (30,000 feet) assuming known target airspeed and wind forecast

Cruising flights operating in an altitude-hold mode may have dynamics as described; however, climbing and descending flights will have different dynamics. Aircraft operating in VNAV PATH/SPD modes will be closing the loop on different variables, with gains and control laws that are not likely to be known to ground-based trajectory predictors. The resulting longitudinal dynamics will include excursions in altitude and speed contributing to the total trajectory prediction uncertainty. These altitude excursions can be large (e.g., 100 feet per 1 m/s speed change) in the case of an open-loop response without damping of the phugoid. Realistically, this mode of motion will be controlled and the altitude excursions will be much smaller. The resulting aircraft dynamical response will still result in the ground speed lagging any wind speed change. This lag will continue to act as a low-pass filter on the errors of representation, just as it did in the cruising case. The result of this lag is that the initial (t = 0+) growth rate in along-track (RMS) error for the error of representation is reduced from the RMS error in wind speed.

One of the reasons for incorporating the vertical correlation term is that errors in wind shear (gradient) can have a significant impact on the vertical profile. Through this vertical correlation, we seek to obtain a model of the wind uncertainty that can more appropriately capture the errors in wind shear. Prior data illustrated the RMS wind shear error that is encountered according to our wind error model. Figure 5-104 shows an aggregate of example wind shear error profiles that would be encountered by flights. As for the wind uncertainty, the impact of wind shear has large variation about the RMS values and flights are likely to encounter significant wind shear errors during climb and descent. This will lead to errors, as reported in the Chapter on wind gradient error, in climb and descent rates that integrate into altitude errors and additional along-track errors.

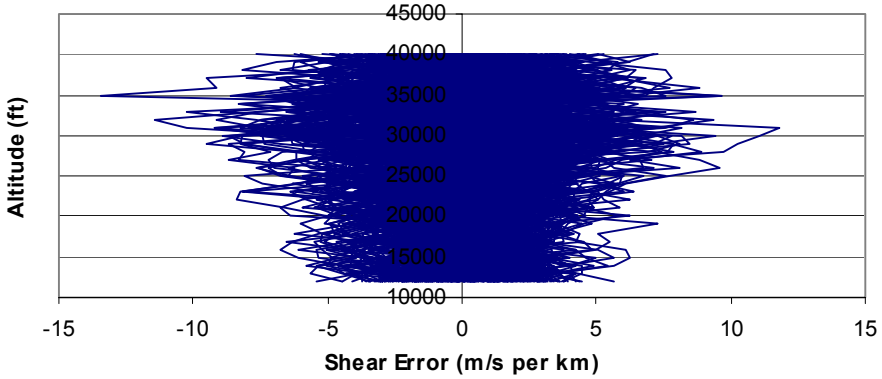

Figure 5-104 Illustration of range of wind shear errors encountered by transitioning aircraft

As an example of the impact of the total wind uncertainty on flights in transition, the RMS errors in altitude and along-track position are reported in Figure 5-105 for descending flights. A Monte Carlo simulation was run with the wind uncertainty model and compared to results without wind uncertainty. Errors in altitude and along-track position were time-synchronized and the RMS error was taken at each time slice. Note that we did not incorporate the effects of the short time-scale longitudinal dynamics (e.g., phugoid, short-period), here we assumed a quasi-steady aircraft response to wind uncertainty. This assumption is necessary as neither the dynamics, nor the gains applied for stability and control were known for these aircraft types. For the descending flights,

we assumed that the flight was in VNAV SPD mode. In VNAV PATH mode, as the altitude deviates a certain threshold (an unknown value) the flights would alter the speed (up to the maximum) to recapture the path. The effect of VNAV PATH mode is to tradeoff altitude error for along-track error.

Table 5-4 Legend for wind error curves

Weight	Speed	Color
Minimum	Slow	
Maximum	Slow	
Minimum	Fast	
Maximum	Fast	

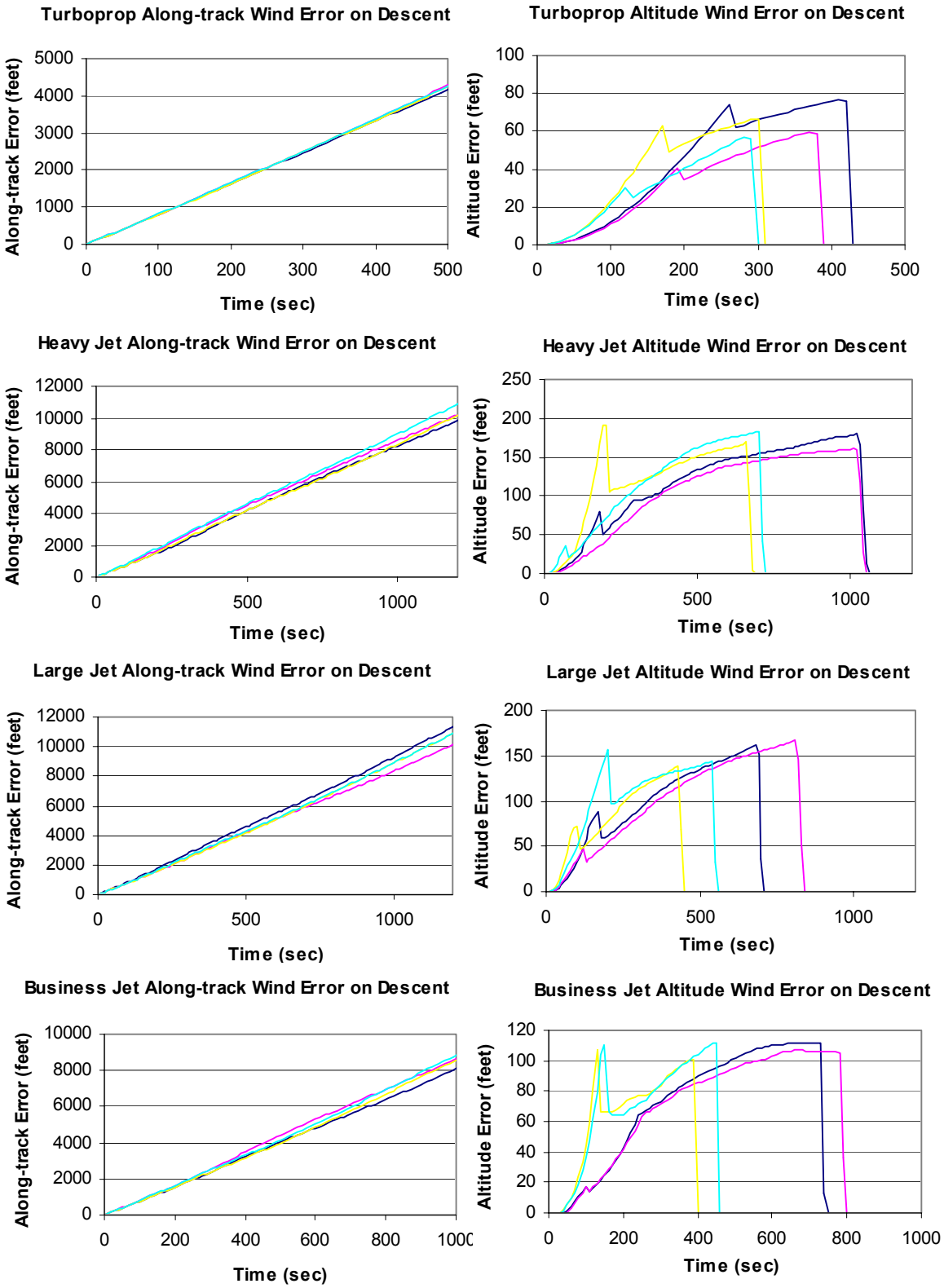

Figure 5-105 Effect of wind prediction uncertainty on trajectory prediction error for various weight, speed and aircraft types during descent (legend precedes)

The along-track error grows almost linearly for this error, regardless of the operating conditions (heavy/light, fast/slow, aircraft type). Furthermore, the growth rate is mostly independent of aircraft type. These observations are consistent with the dominance of the large-scale wind errors. Note that during descent, winds and their corresponding uncertainty decrease slowly as the aircraft descends after 30,000 feet. For this reason, since not all flights descend from the same cruising altitude (heavier aircraft are lower), the average speed uncertainty during descent is a slight function of aircraft weight.

Errors in wind prediction during descent lead to an error in prediction of the wind gradient. For this reason, the altitude uncertainty has similar properties to the altitude error due to errors or neglect of the wind gradient (see *Vertical Wind Gradient Omission*). However, the altitude error does not subsequently contribute a dominant effect to the along-track error due to the additional error of the wind itself. It is important to note that the resulting altitude error is quite small relative to other altitude error contributions and that following VNAV PATH mode combined with aircraft stability and control systems would likely decrease these variations further.

When applied to climb scenarios, altitude and along-track errors are illustrated in Figure 5-106 using the conditions shown in Table 5-4. Some noise is present in the data as the data is obtained from a Monte Carlo simulation. As for the descent, the along-track error grows almost linearly. Nonlinearities are a result of wind error being a function of altitude. Since flights of various weights are not targeting the same cruise flight level, the wind uncertainty rms is slightly different at the cruise altitudes. The along track error will continue to grow at the cruise flight level at different rates commensurate with the cruise flight level wind error.

The shape of the altitude error can best be explained through the same rational due to errors in the wind gradient term (see *Vertical Wind Gradient Omission*). Figure 5-107 illustrates the altitude error alongside the nominal altitude profile. The wind gradient error is not constant with altitude, but grows with altitude reaching a peak between 30 to 35,000 feet. The result is that the rms altitude error will grow faster at higher altitudes. Since the actual and error trajectory will not reach the Mach/CAS transition point at the same time, the altitude error will grow as the first one to reach the transition altitude will incur a faster climb rate. The tropopause has the opposite effect to the Mach/CAS transition point. Finally, the altitude error drops to zero as both the actual and error trajectory reach the cruise flight level.

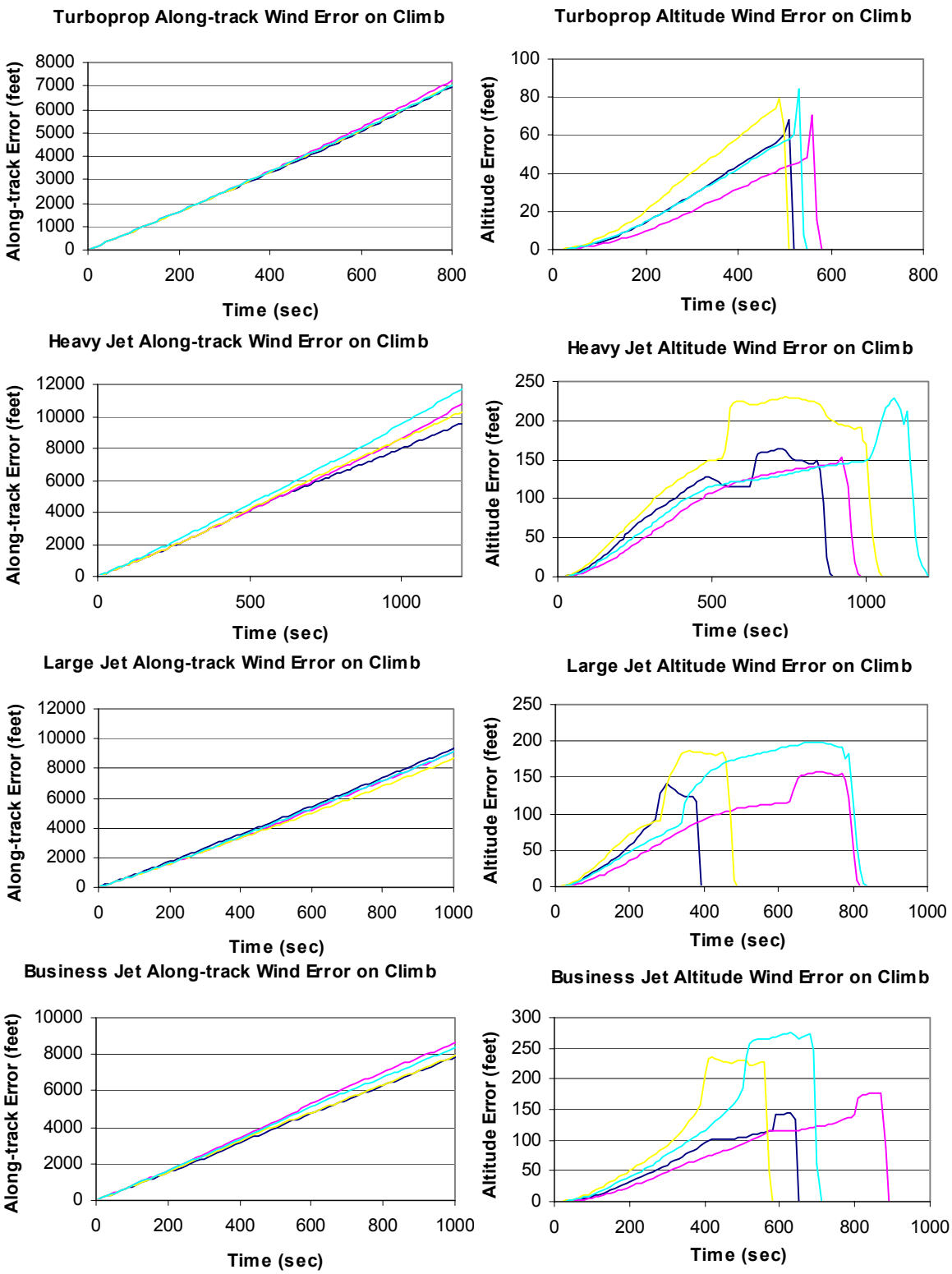

Figure 5-106 Effect of wind prediction uncertainty on trajectory prediction error for various weight, speed and aircraft types during climb (legend in preceding Table)

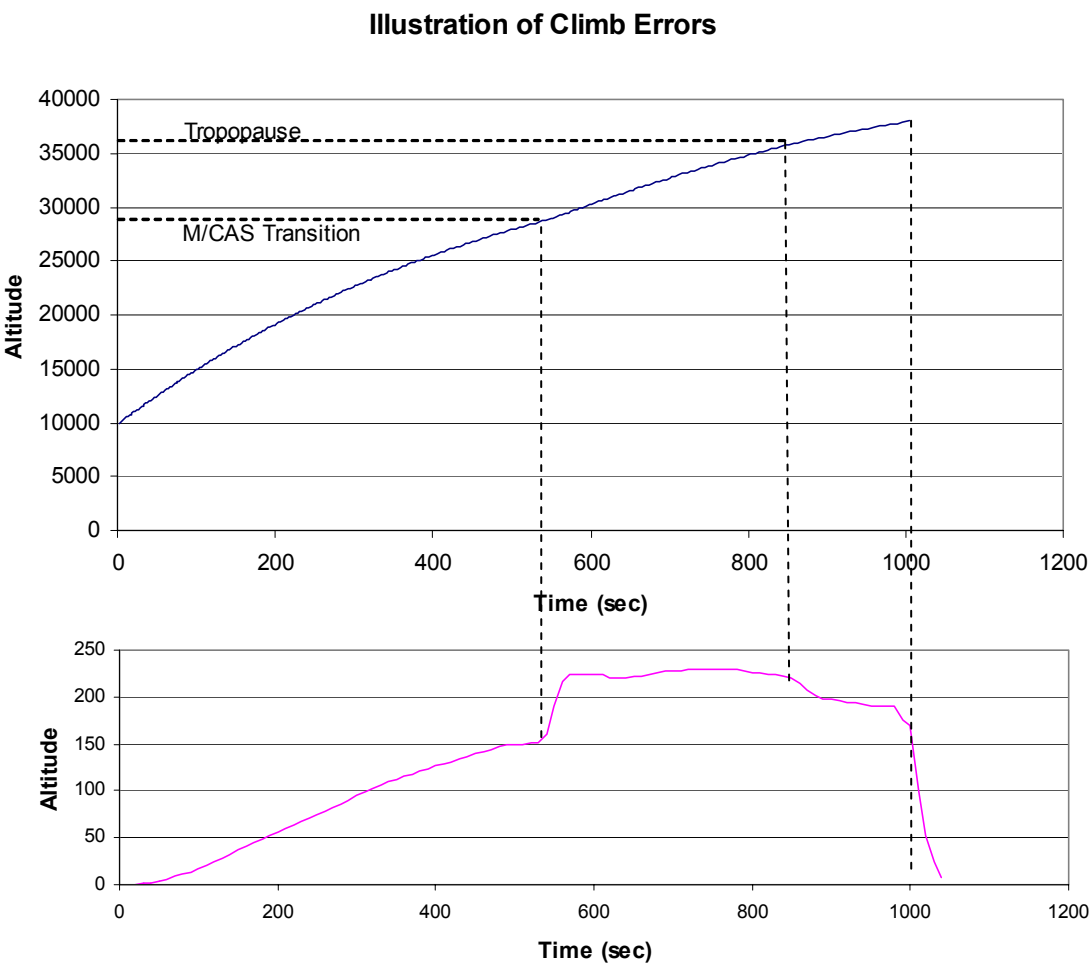

Figure 5-107 Illustration of climb errors at breakpoints

5.5 Top-of-Descent Uncertainty

5.5.1 Description of Error

Inconsistency in the location of the top-of-descent between the actual trajectory and a predicted trajectory will lead to errors in both altitude and along-track. Under conventional operations, the top-of-descent is the result of a clearance provided to the flight deck, followed by execution, by the flight crew, of that clearance. A clearance to descend may be provided (e.g. "DESCEND TO FLIGHT LEVEL 240") that requires the flight crew to begin the descent "immediately", allowing for latencies associated with the execution of the maneuver. However, until that instruction is provided, automation tools are not aware of the precise location or time at which that clearance will be provided. Controller experience, or standard operating procedures within an individual sector may dictate that flows to a specific destination be descended upon reaching a specific point. Typically, these descent points would be selected in a conservative manner such that a wide variety of aircraft types would be able to reach a downstream desired crossing constraint. Furthermore, controller workload may impact the decision of when to execute the clearance. The result of this approach is that that actual top-of-descent point is not typically known to automation with any level of precision.

An alternative error (see Figure 5-108) can be introduced into the top-of-descent if a trajectory predictor anchors the descent to a downstream constraint instead of a known top-of-descent point. Note that in any case, a trajectory predictor would not necessarily be aware of the descent clearance point.

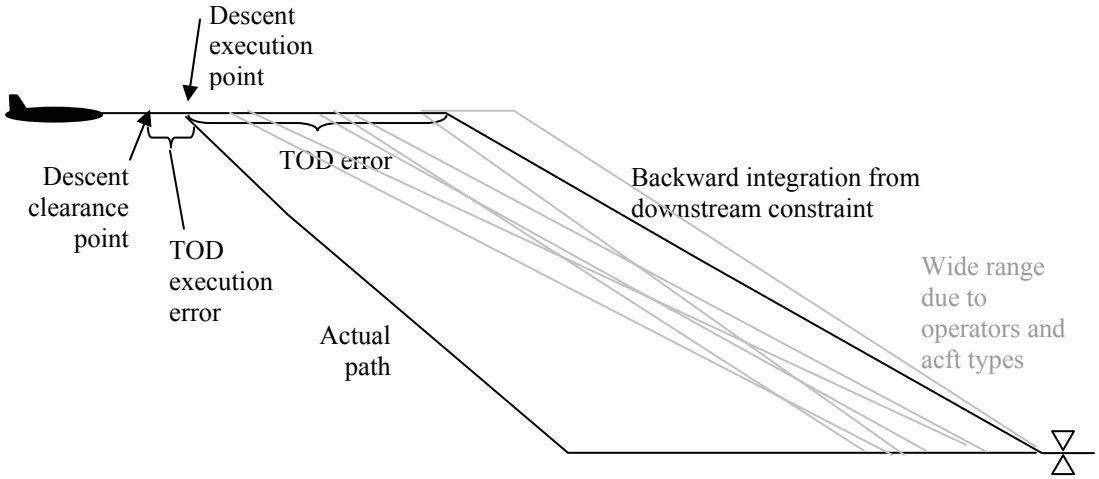

Figure 5-108 Illustration of top-of-descent error under specific procedure and backward integration prediction

An alternative clearance may leave more discretion to the pilot (e.g., "CROSS XYZ AT FL 240"). In this case, a predictor with knowledge of the constraint would be more capable of determining a performance path from the present position to the crossing constraint. The top-of-descent would be an outcome of backward integration. However,

the pilot may not elect to execute such a performance path, choosing to descend earlier instead.

When we refer to top-of-descent, we are describing a simplification, which is the location of the intercept of the descent path with the cruise segment. Flight crews may elect to descend first at a shallow fixed rate of descent in order to intercept a VNAV descent path (see Figure 5-109).

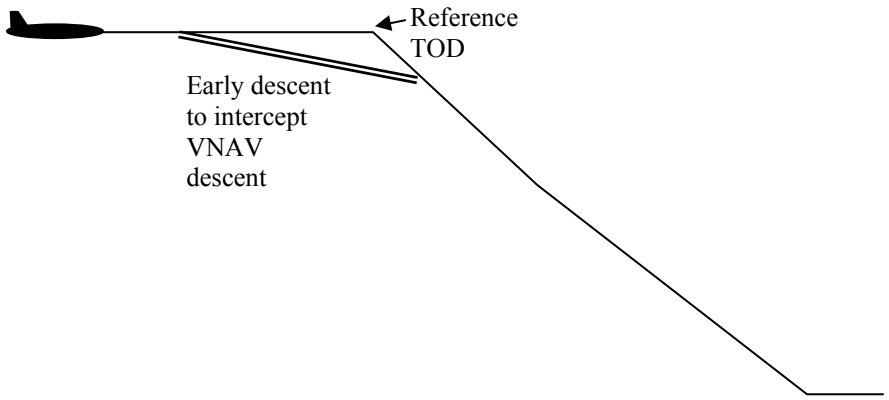

Figure 5-109 Illustration of early descent

Some investigations (e.g.,[10],[14]) have considered the specification of more precise top-of-descent locations to the flight deck and trajectory predictor with corresponding improvements in prediction during descent. In these cases, the predictor is aware of the desired TOD point and the flight deck is notified of a specified location for execution.

5.5.2 Parametric Analysis

As for the crossing restriction case, a simplified model of the top-of-descent error is developed to provide estimates of the along-track and altitude error as a result of this error for various aircraft models under differing conditions. The primary factors affecting this error will be the magnitude of the placement error (in time or distance), the cruise altitude of the flight and the cruise/descent speeds. A very simple model is illustrated in Figure 5-110.

When applied to a typical example, we can see the stages of error growth as shown in Figure 5-111. The relative difference in speed between actual and predicted altitude drives the along-track error. The altitude error is driven by the difference in vertical speed.

Figure 5-112 through Figure 5-115 show the impact of various duration top-of-descent placement errors. Various aircraft types under differing operational conditions are considered and illustrated.

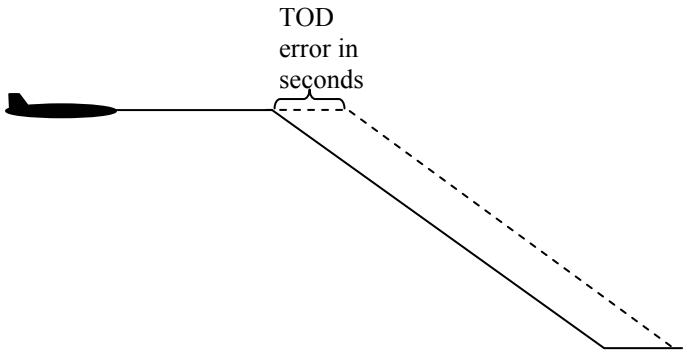

Figure 5-110 Simplified model of top-of-descent placement error

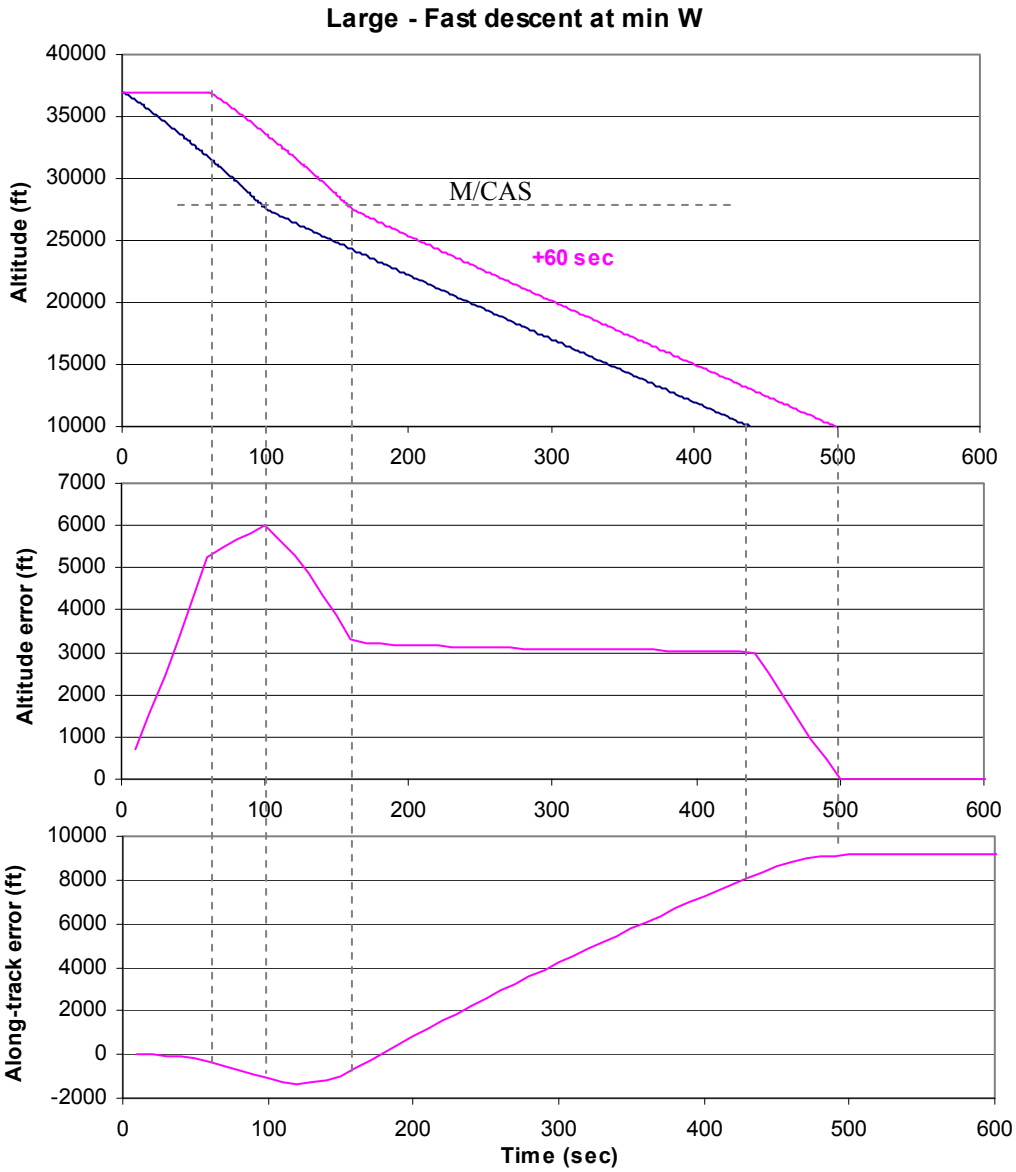

Figure 5-111 Illustration of along-track and altitude error profiles from TOD placement error

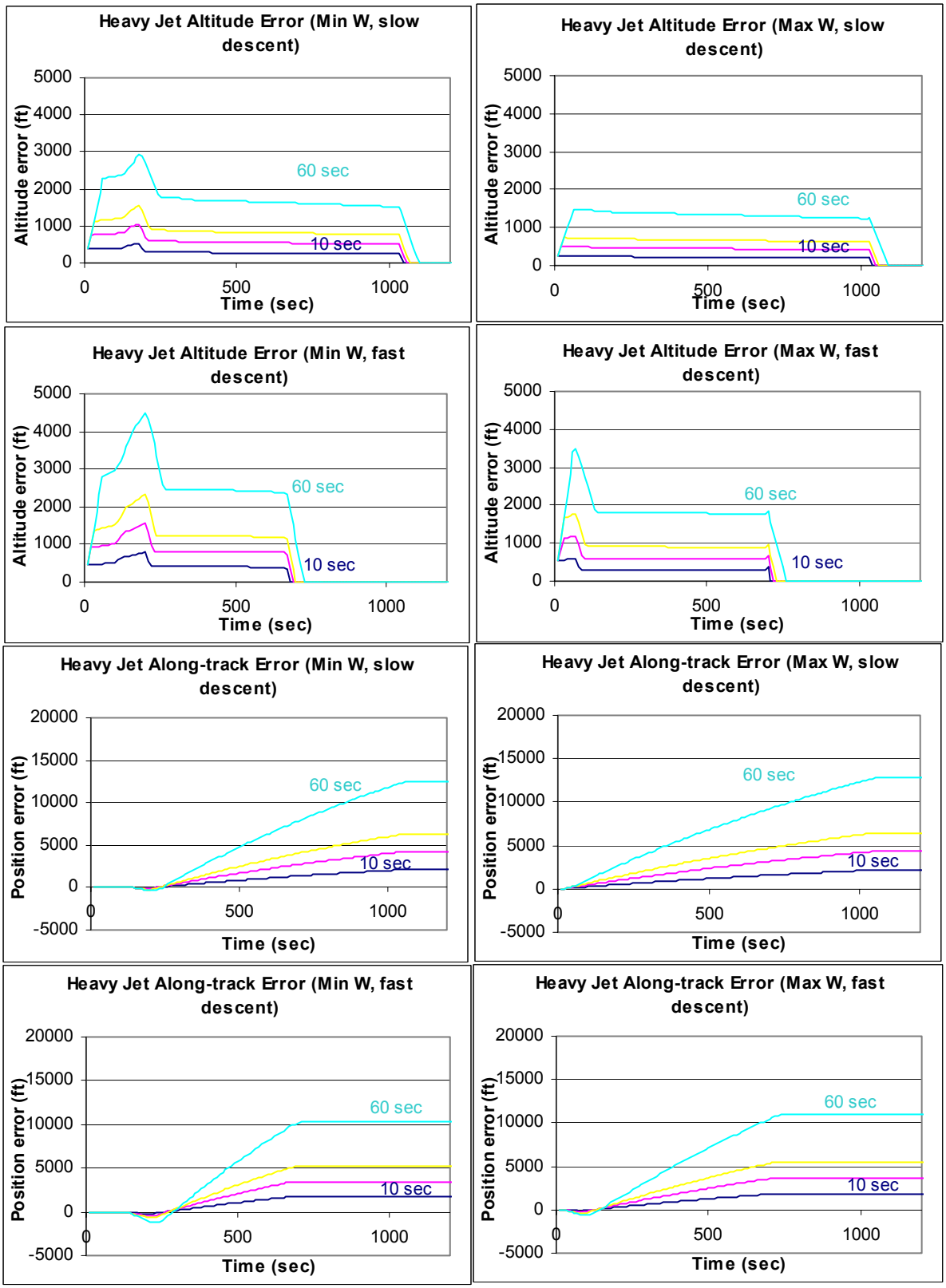

Figure 5-112 Impact of 10, 20, 30 and 60 second TOD placement errors on heavy jet along-track and altitude errors

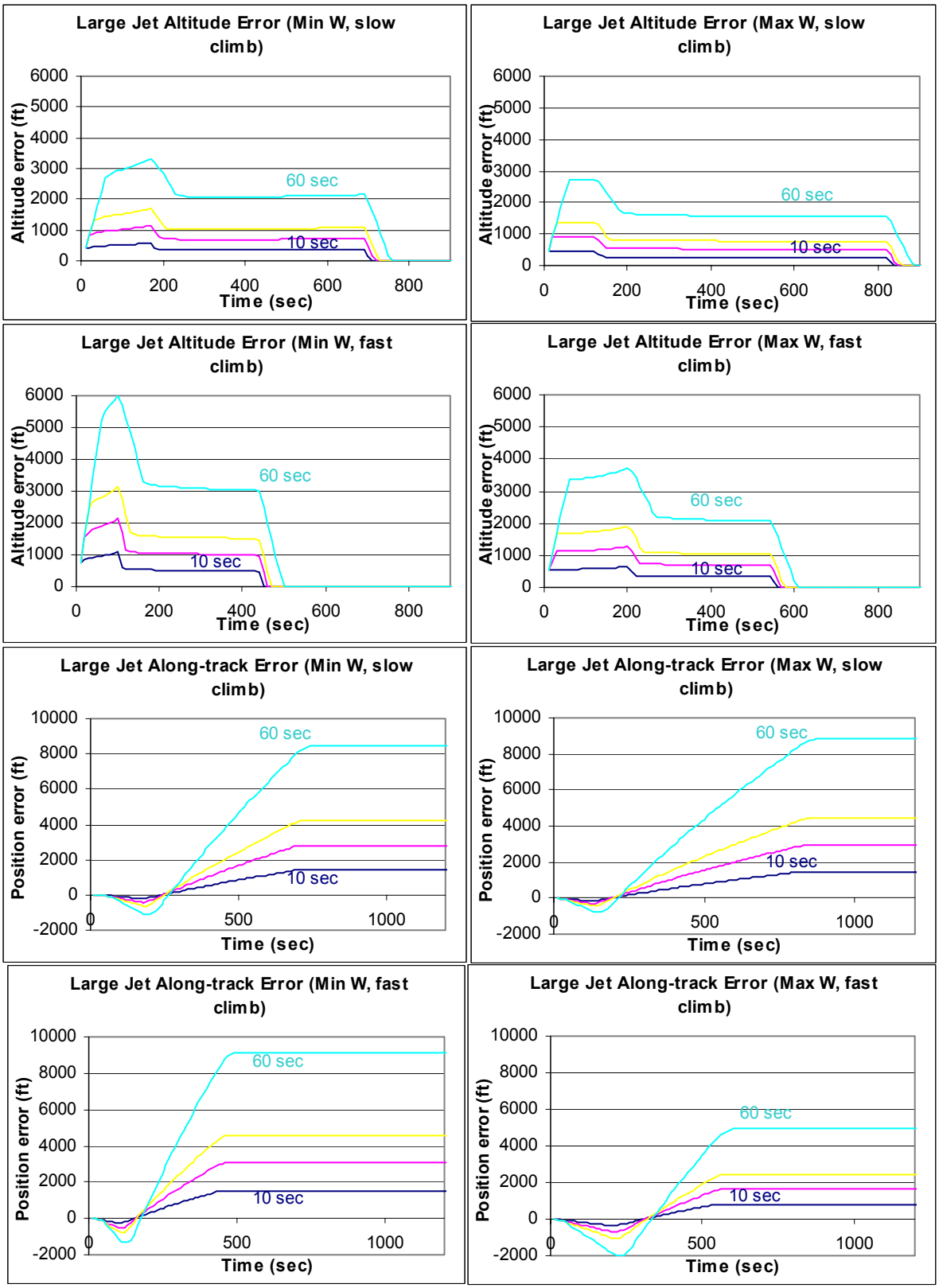

Figure 5-113 Impact of 10, 20, 30 and 60 second TOD placement errors on large jet along-track and altitude errors

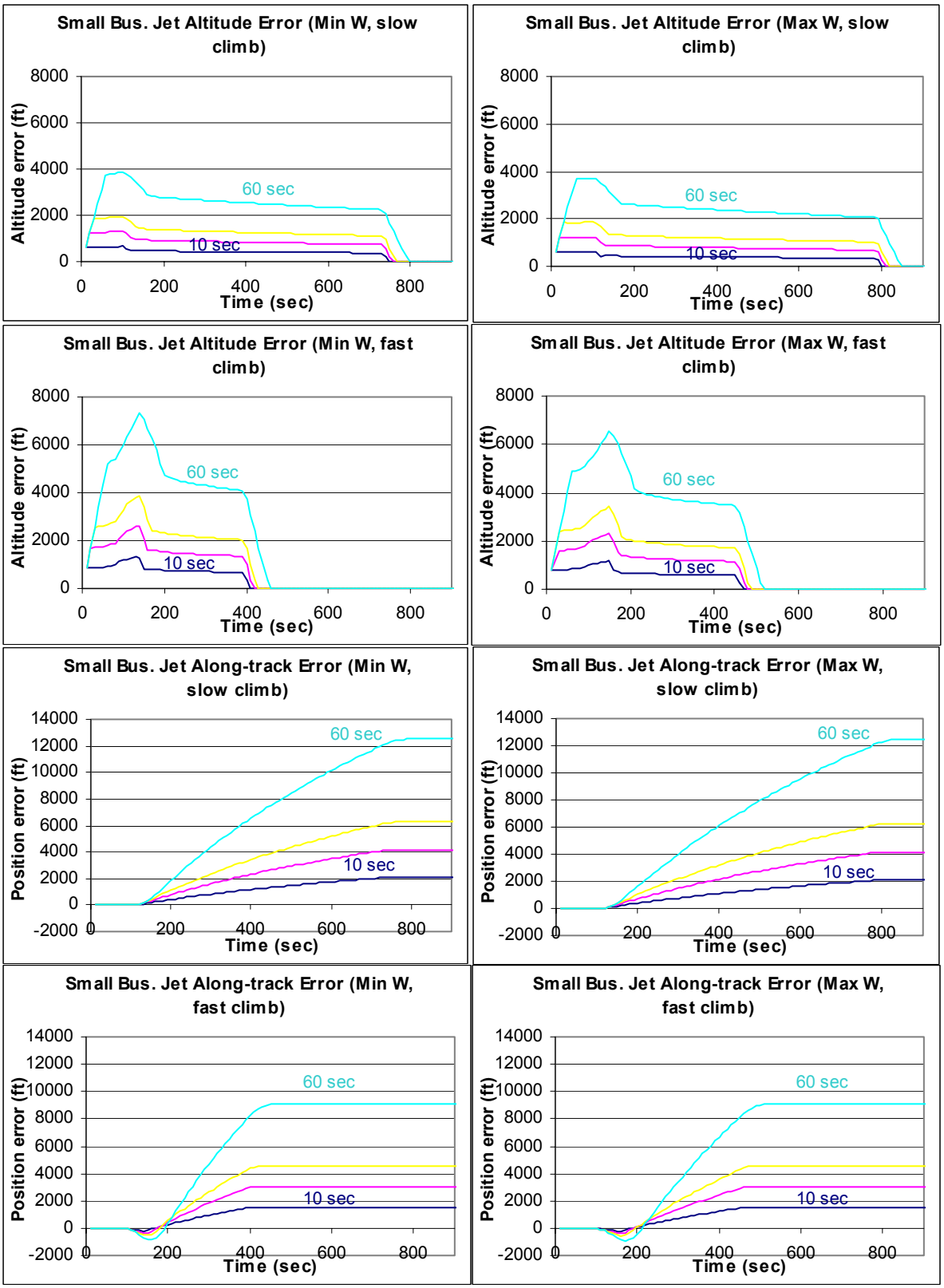

Figure 5-114 Impact of 10, 20, 30 and 60 second TOD placement errors on small business jet along-track and altitude errors

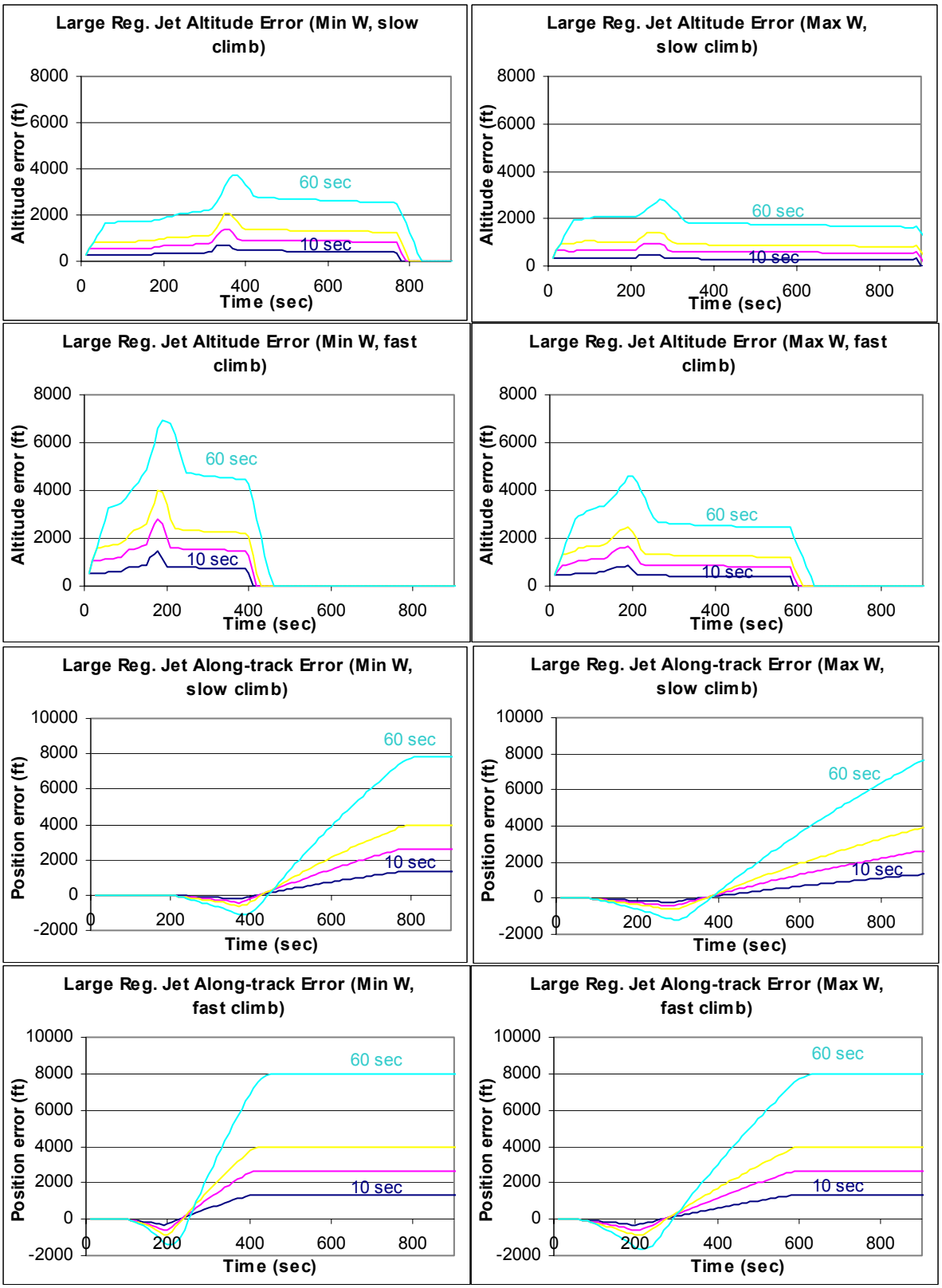

Figure 5-115 Impact of 10, 20, 30 and 60 second TOD placement errors on large regional jet along-track and altitude errors

5.6 Crossing Restrictions and Interim Altitudes

5.6.1 Description of Error

One source of uncertainty concerns the practice of aircraft flying for some duration at flight levels other than their filed cruise altitude. This can occur for a variety of reasons:

- Aircraft in transition may be held at an interim altitude by a controller in order to avoid a potential separation violation,
- An interim altitude is provided to a transitioning flight and the controller does not provide a continuing clearance until the aircraft has leveled off,
- A procedure is in place with a specified altitude restriction,
- A flight conducts a step climb to a new cruise level for improved fuel efficiency,
- A flight requests a new or different altitude to avoid turbulence.

Trajectory predictors attempting to predict the vertical profile of flights subject to interim altitudes will encounter some errors when a) the application of an interim altitude is not known a priori, and b) the duration of the level-off at the interim altitude is not known. In the case of known and consistently-applied procedures, interim altitudes may be known to a trajectory predictor at the time a prediction is made. However, in many cases, neither the altitude nor the duration will be known to a trajectory predictor. Various schemes for input of requisite information into automation may be considered to alleviate the various aspects of this error.

5.6.2 Parametric Analysis

Two fundamental parameters affect the impact of altitude level-off errors on a specific trajectory:

- The interim altitude(s)
- The duration at the interim altitude(s)

A very simple model of the impact of interim altitudes during climbs is illustrated in Figure 5-116. A climbing flight is subject to a level-off, unknown to the predictor. The actual flight is assumed to level-off (at the target climb speed) at the interim altitude for some duration. An altitude error will accumulate until the difference between the target cruise and interim altitude is reached. When the end of the level-off is reached, the altitude error will decay. However, an along-track error will accumulate due to the difference in speed at lower altitude compared to the speed at higher altitude. This error will remain even after return to the cruise level.

Certain situations may exist under which the interim flight level is known. An example includes the update of automation with an interim altitude, or the detection of a level-off situation. Under these circumstances (see Figure 5-117), the predicted trajectory profile would likely forecast a level-off using an expected duration for the level-off. Errors in

prediction (altitude and along-track) are then related to the difference between the actual and the expected level-off duration. The error is identical in form to the preceding case, except that the duration is replaced by the difference between duration and expected level-off duration. In the event that the actual level-off duration is less than expected, the sign of the errors are simply reversed.

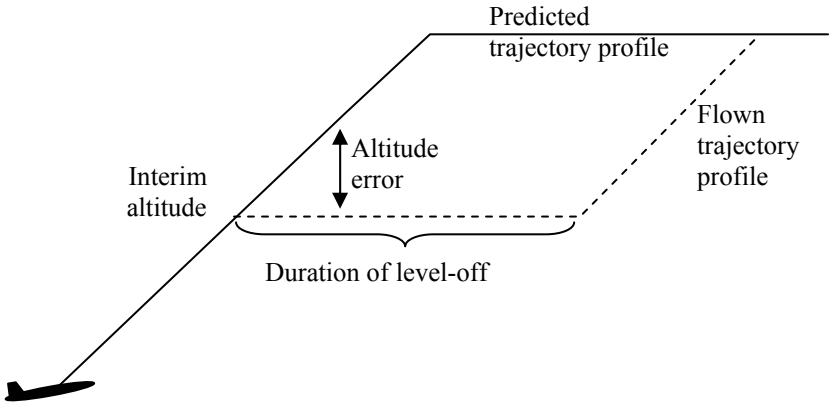

Figure 5-116 Simple description of level-off impact in climb

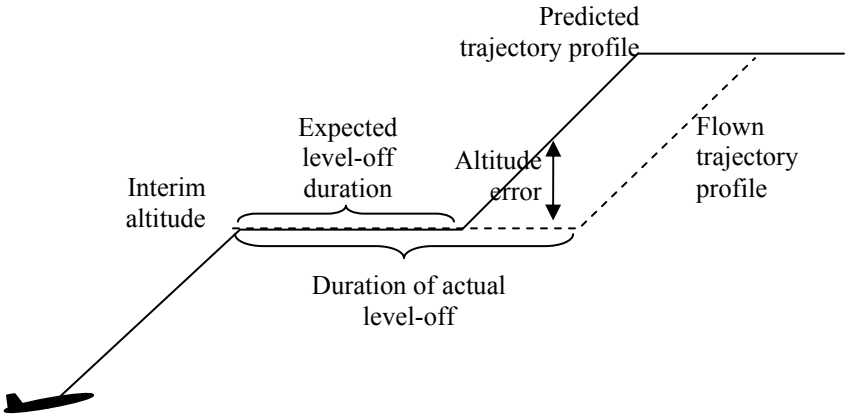

Figure 5-117 Description of level-off impact in climb with known interim level

The simple model presented does not consider multiple interim altitudes, yet this does occur in practice during both climb and descent. The model also assumes that a constant speed is maintained, consistent with the climb schedule, during the level-off. However, in practice, the flight could accelerate during the level-off segment. The speed schedule will have a significant impact on the along-track error as this determines the difference in speed between the level-off segment and the at-altitude error. In this analysis, we assumed a speed at cruise equal to the Mach climb speed; however, these will not be the same in general and will ultimately affect the along-track error.

Figure 5-118 through Figure 5-121 presents the altitude and along-track error for large aircraft in climb subject to unknown level-offs 18,000 feet, and flight levels 240 and 300. These are computed for a 30 second, 1 minute, 2 minute and 5 minute duration level-off.

Note that these are presented as examples of the behavior of the errors, but that the specific magnitude of the errors, in particular the along-track error, is highly sensitive to the specific problem.

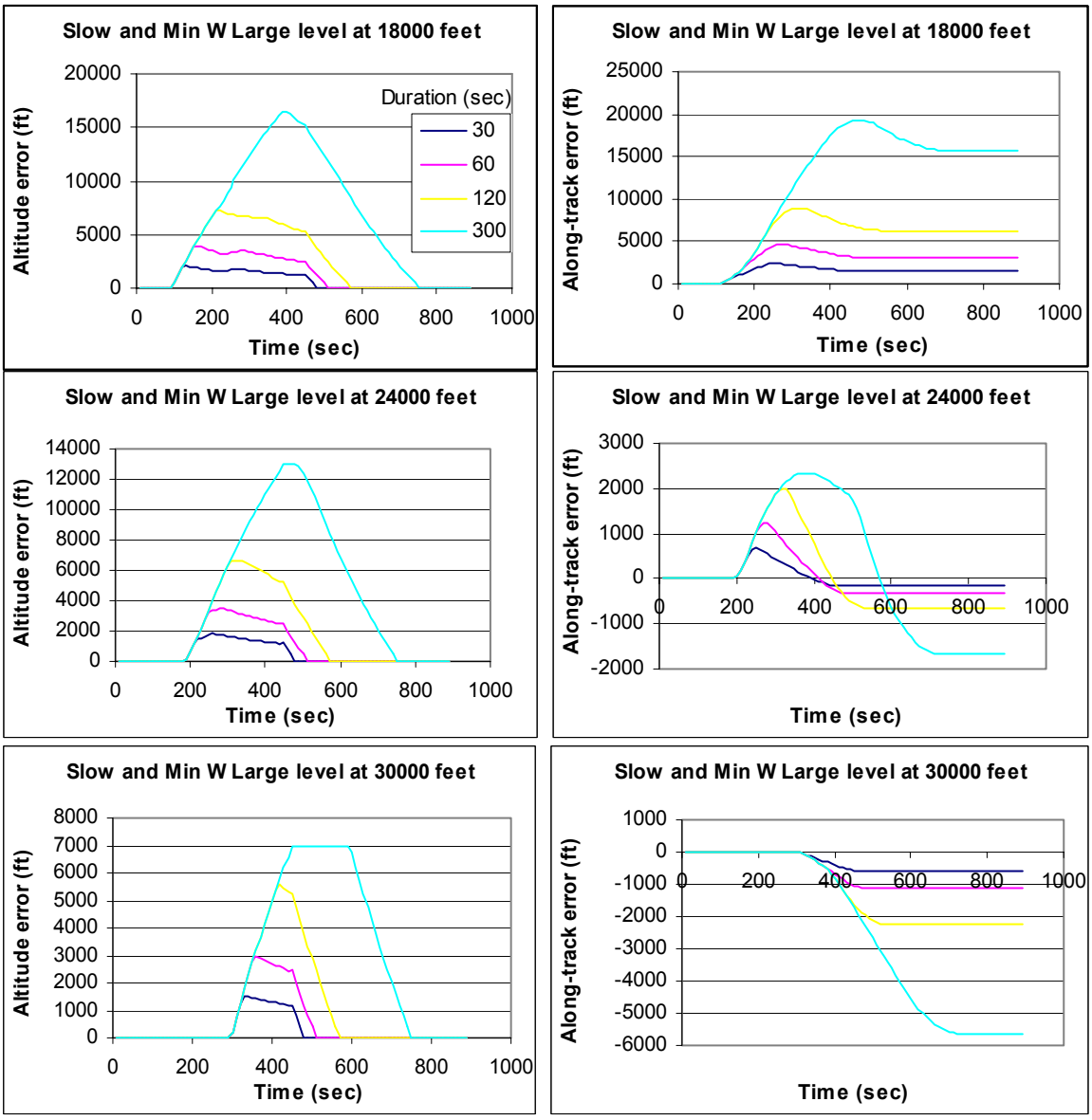

Figure 5-118 Impact of level-offs at various altitudes (FL180, 240 and 300) and of varying duration (30 to 300 seconds) on altitude and along-track error for a large jet in a slow climb at a light weight

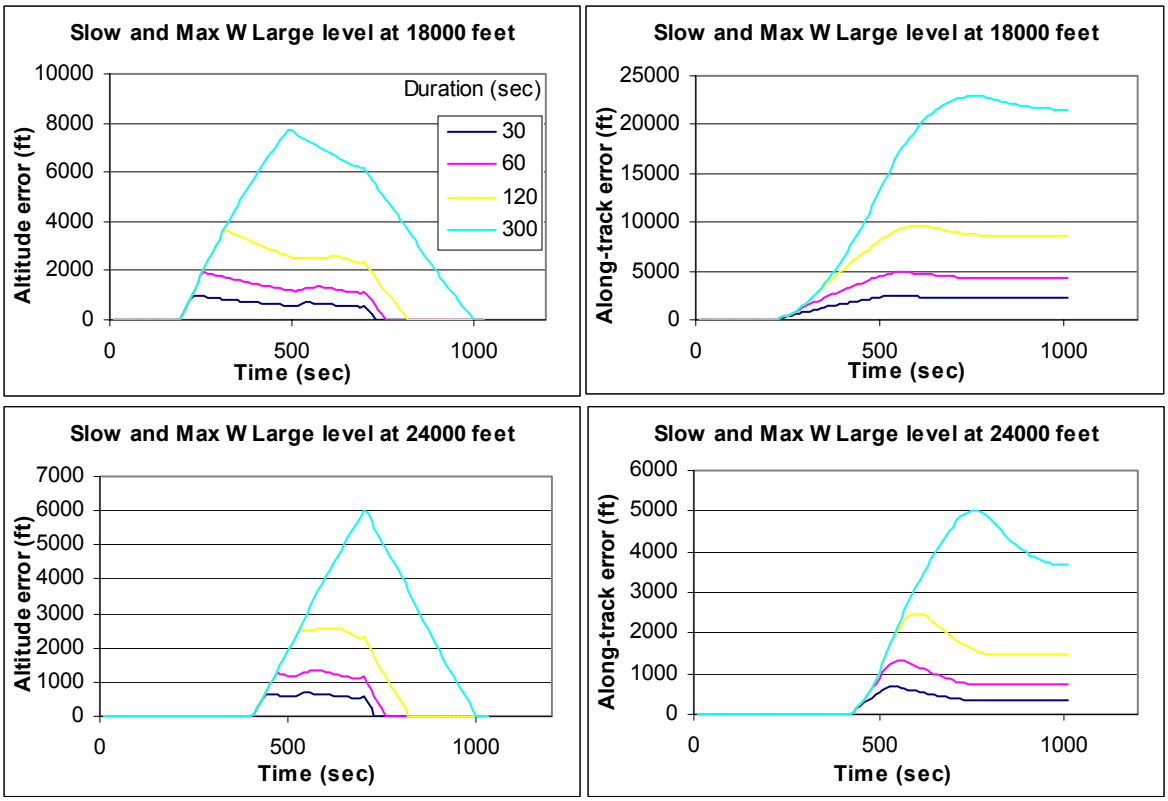

Figure 5-119 Impact of level-offs at various altitude (FL180 and 240) and of varying duration (30 to 300 seconds) on altitude and along track for a large jet in a slow climb at maximum weight

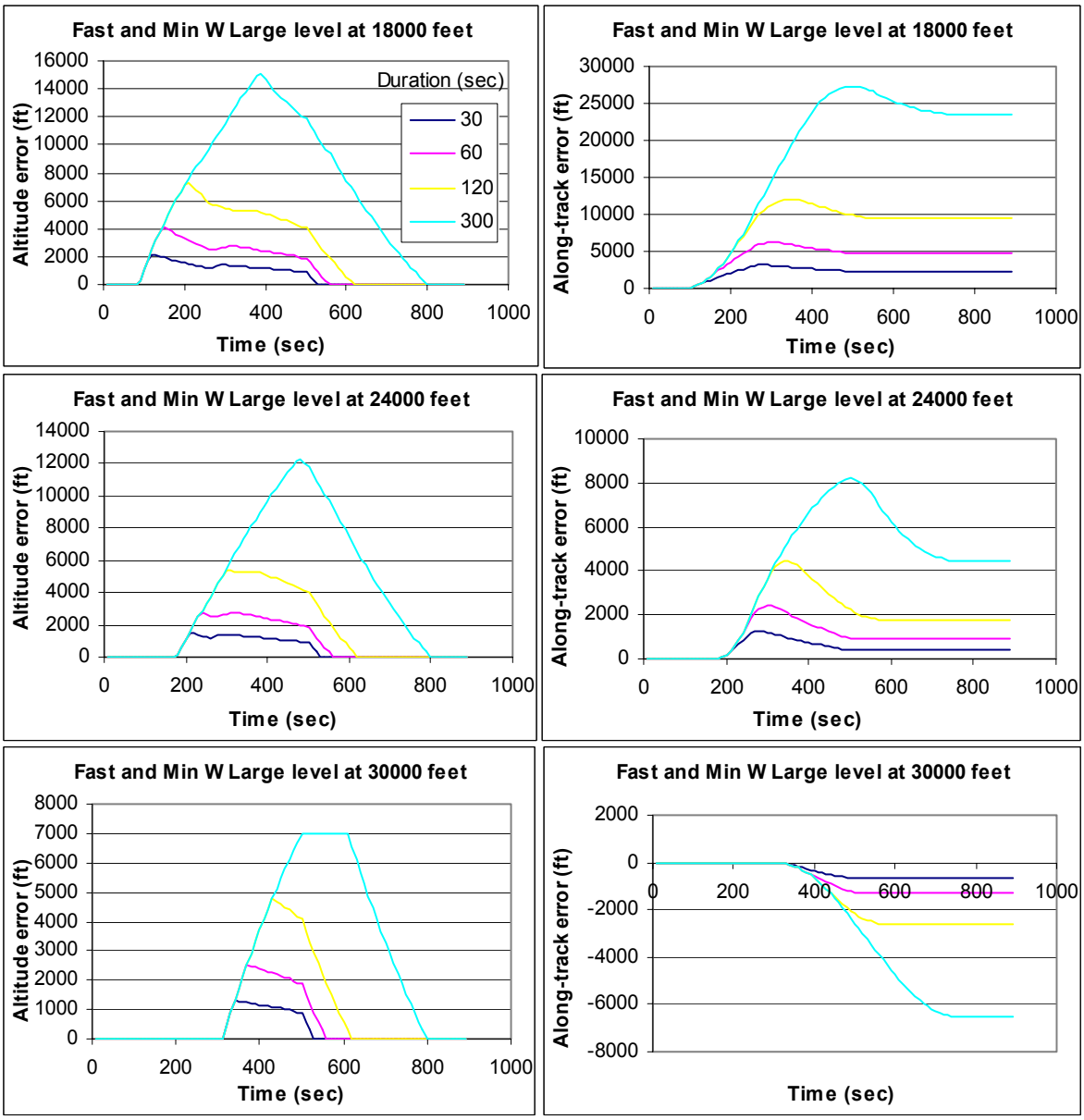

Figure 5-120 Impact of level-offs at various altitude (FL180, 240 and 300) and of varying duration (30 to 300 seconds) on altitude and along track for a large jet in a fast climb at low weight

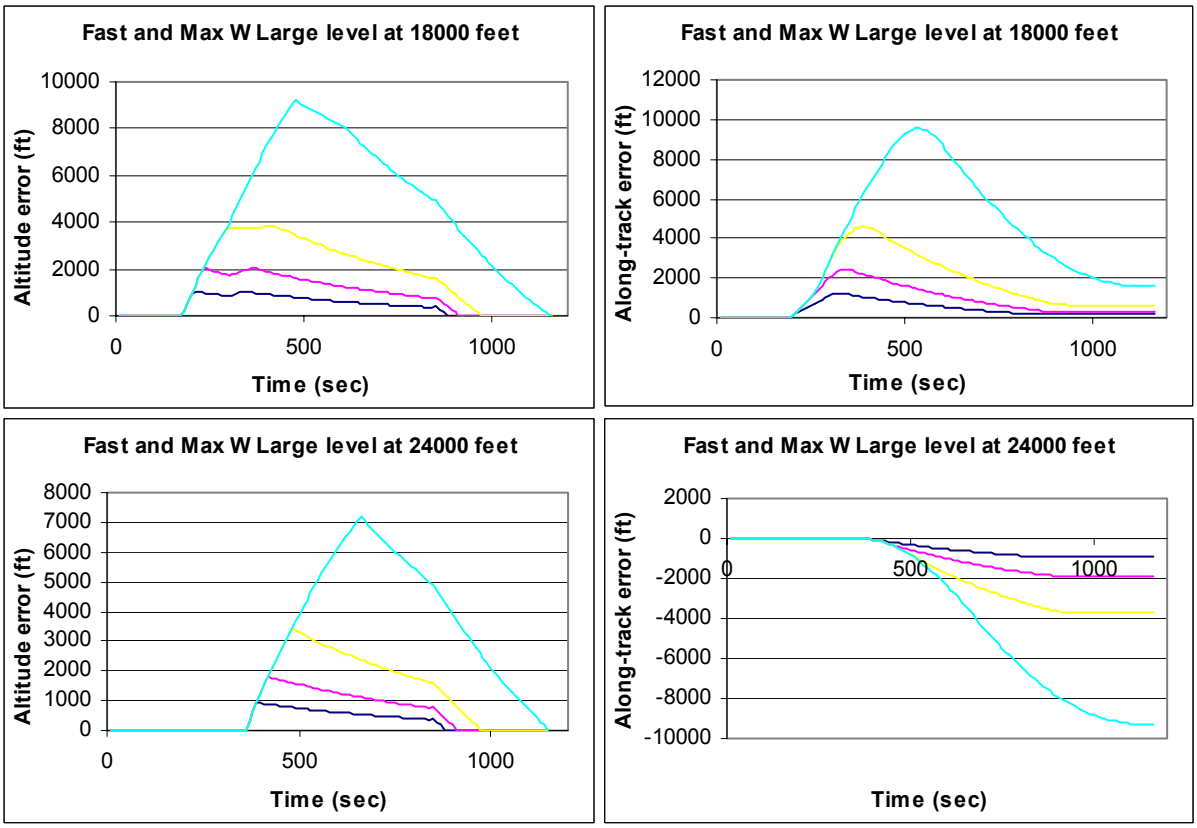

Figure 5-121 Impact of level-offs at various altitude (FL180 and 240) and of varying duration (30 to 300 seconds) on altitude and along track for a large jet in a fast climb at maximum weight

While the altitude error behavior is straightforward, the along-track error is sensitive to certain effects. Figure 5-122 and Figure 5-123 attempt to illustrate these. In the case of a level-off at lower altitude (below the M/CAS transition point), the initial level-off causes the altitude error to grow. The lower speed at the lower altitude may cause the along-track error to grow. However, *in practice a flight may take advantage of this level-off to accelerate to a faster speed*. The altitude error decays as the climb resumes due to the higher climb rate at lower altitude. Upon reaching the CAS/Mach transition point, the altitude error gets worse due to the higher climb rate (at fixed Mach) and subsequently recovers as the lower profile reaches the transition point. The along-path error recovers during the constant Mach segments as airspeed decreases with increasing altitude at a fixed Mach number (below the Tropopause). Note that the along-track error can become negative, depending on the circumstances.

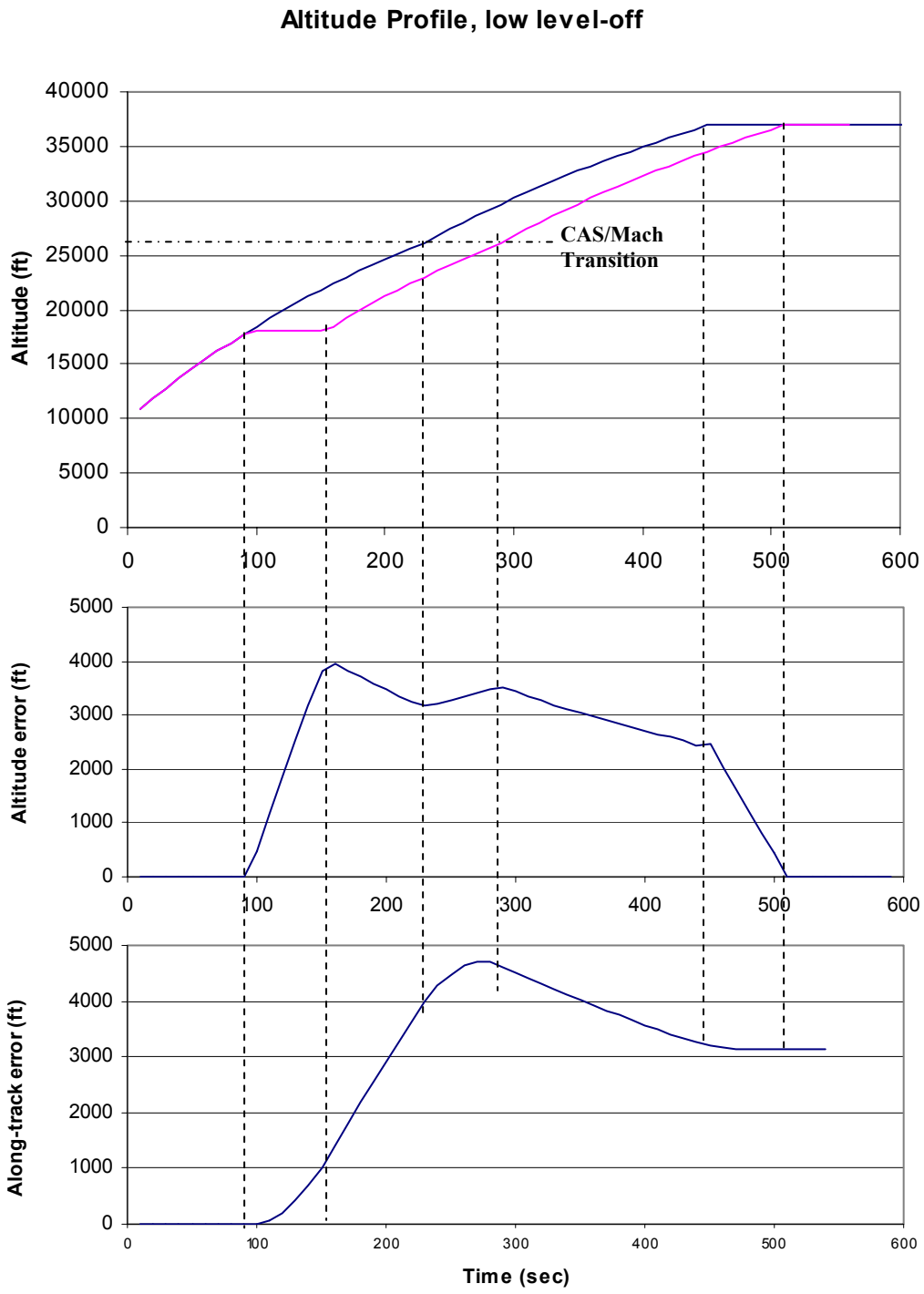

Figure 5-122 Explanation or errors on climb due to level-off

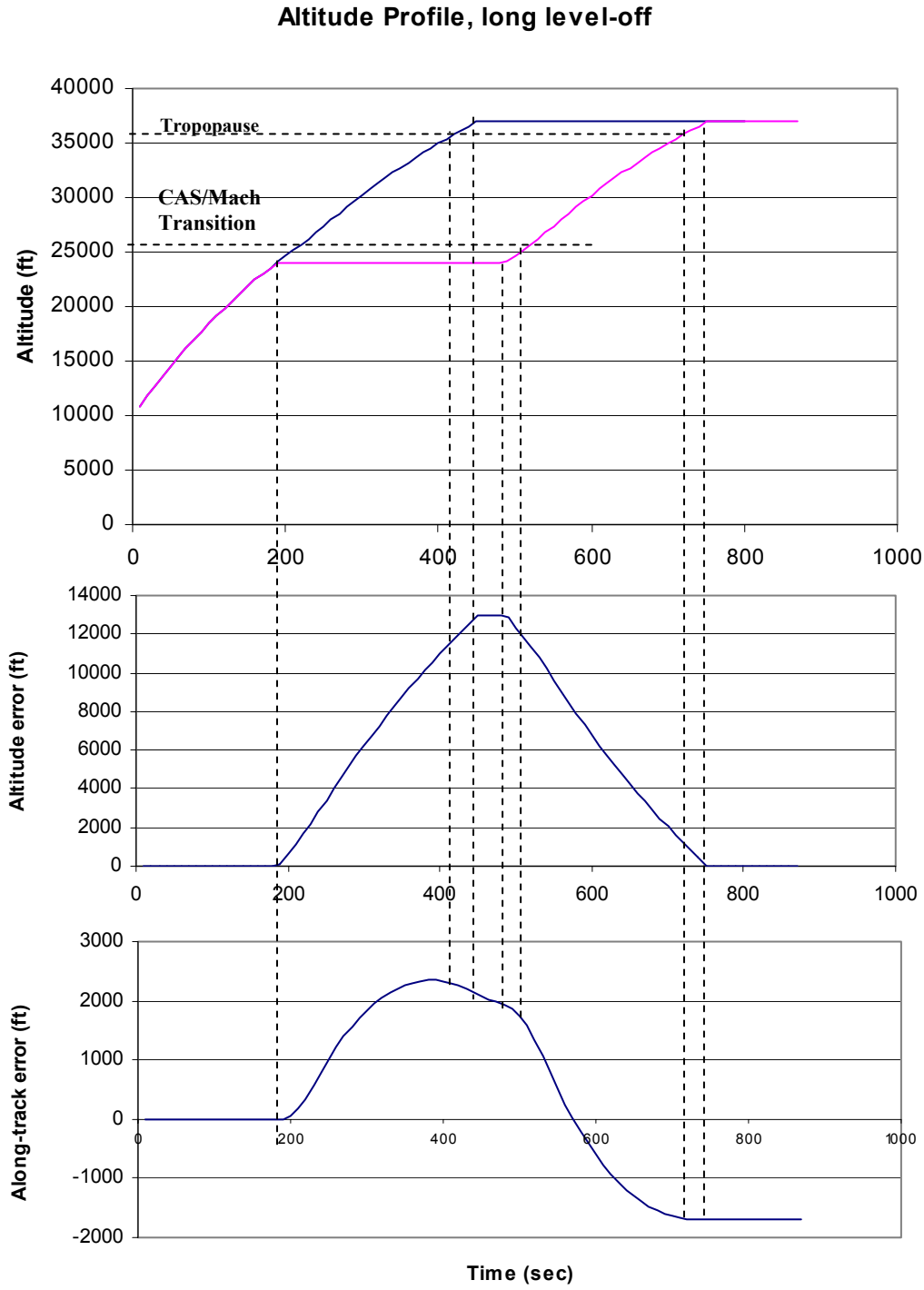

Figure 5-123 Explanation of errors on climb due to level-off of longer duration

During descent, as for all descent errors, the situation will depend on whether the top-of-descent is computed or specified. For the purposes herein, we assume the top-of-descent is specified and serves as the initial condition for evaluation of level-offs in descent. Figure 5-124 illustrates a simple model of this error used to generate error curves for various descent profiles. As for the errors in climb, readers are cautioned that the along-track errors will be a strong function of the speed profile, the level-off parameters, the wind profile and the speed at bottom of descent.

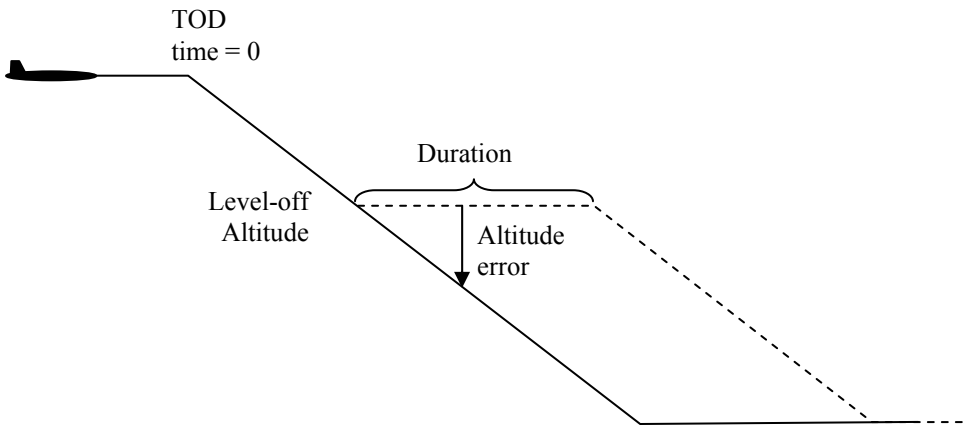

Figure 5-124 Illustration of simple level-off error model in descent

Figure 5-125 through Figure 5-132 shows the altitude error and along-track error stemming from neglect of level-offs of various duration (30, 60, 120 and 300 sec) during descent at both FL180 and 240 for various aircraft models under differing operating conditions. Peak altitude errors are determined by the average descent rate during the level-off period capped by the difference between the bottom-of-descent altitude (assumed here to be 10000 feet) and the level-off altitude. Figure 5-133 illustrates the typical errors on descent.

While this report focused on the sensitivity of trajectory errors to errors under various operational conditions, a preliminary look [36] at the frequency, altitudes and duration of level-offs in climb provides an indication of the range of parameters under current operational conditions (see Figure 5-134). Note that many of the high duration and high altitude level-offs likely stem from initial cruise levels that are lower than desired. We also note that [37] indicated that "almost all altitude clearances were correlated to a flight plan amendment, or interim altitude message". This indicates that while the clearances would not be know to automation prior to imposition by ATC, once the clearance is provided, in many cases only the duration would be unknown.

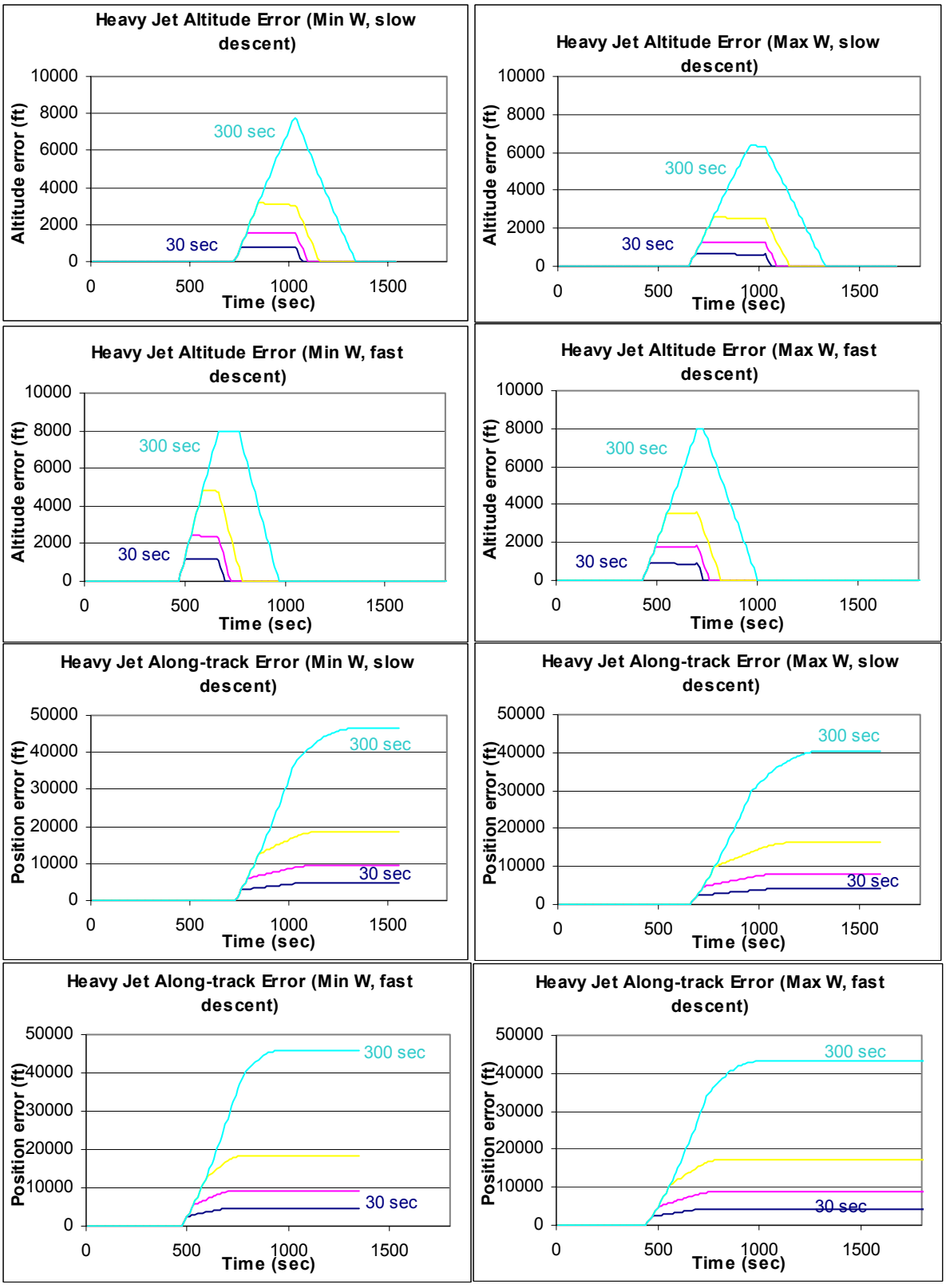

Figure 5-125 Errors due to level-offs (30, 60, 120 and 300 seconds) on descent at 18000 feet on a heavy jet

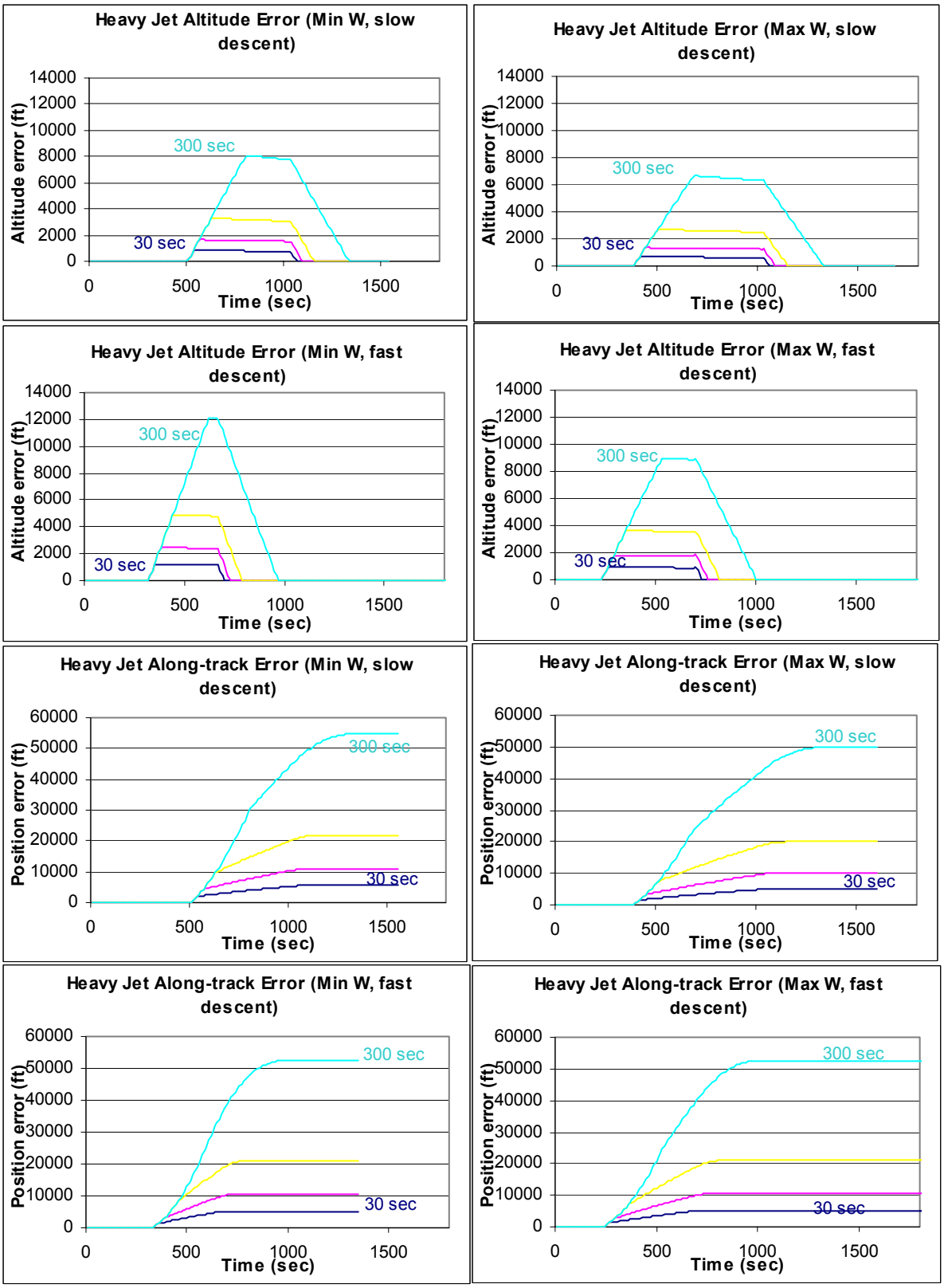

Figure 5-126 Errors due to level-offs (30, 60, 120 and 300 seconds) on descent at 24000 feet on a heavy jet

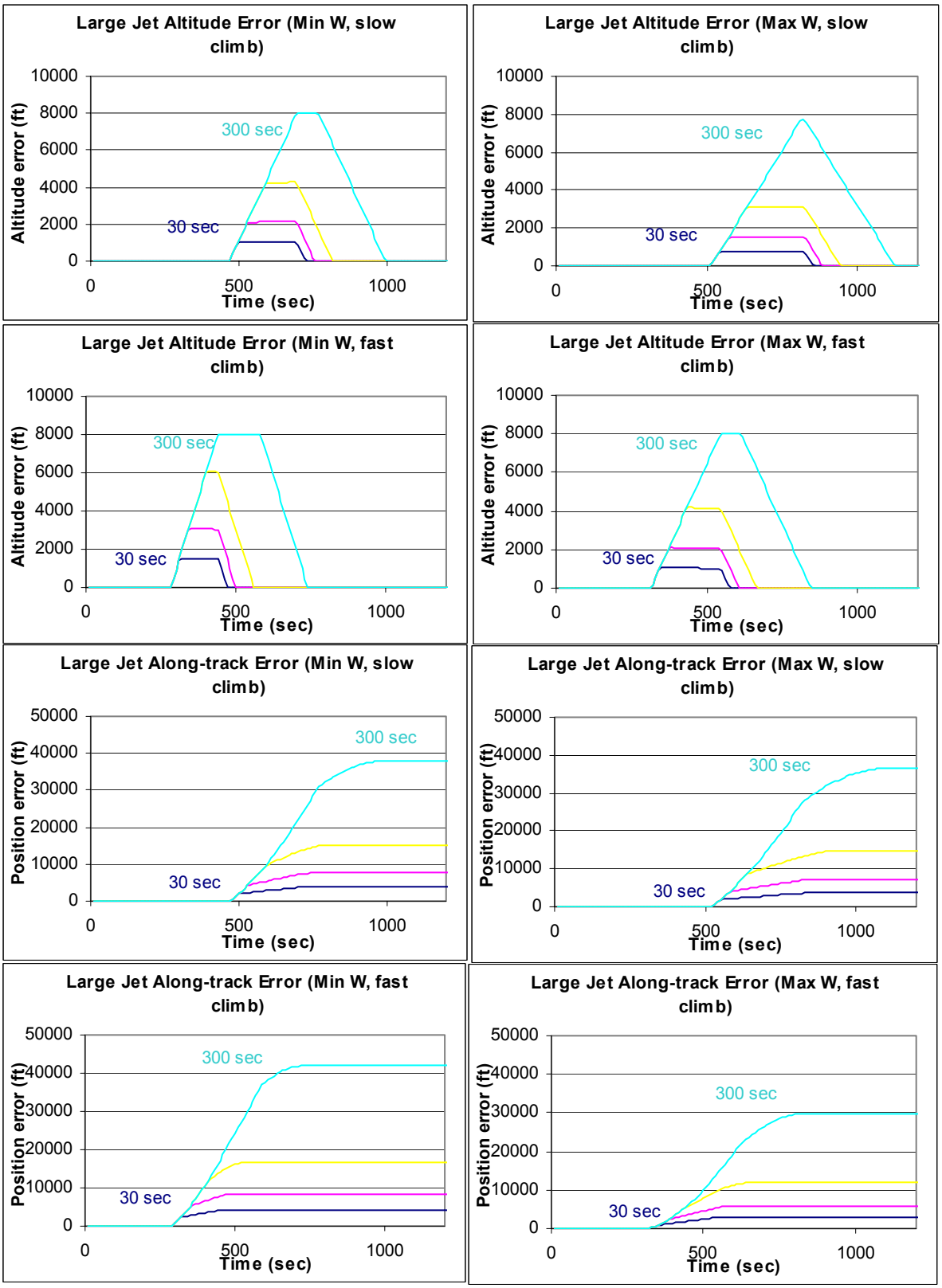

Figure 5-127 Errors due to level-offs (30, 60, 120 and 300 seconds) on descent at 18000 feet on a large jet

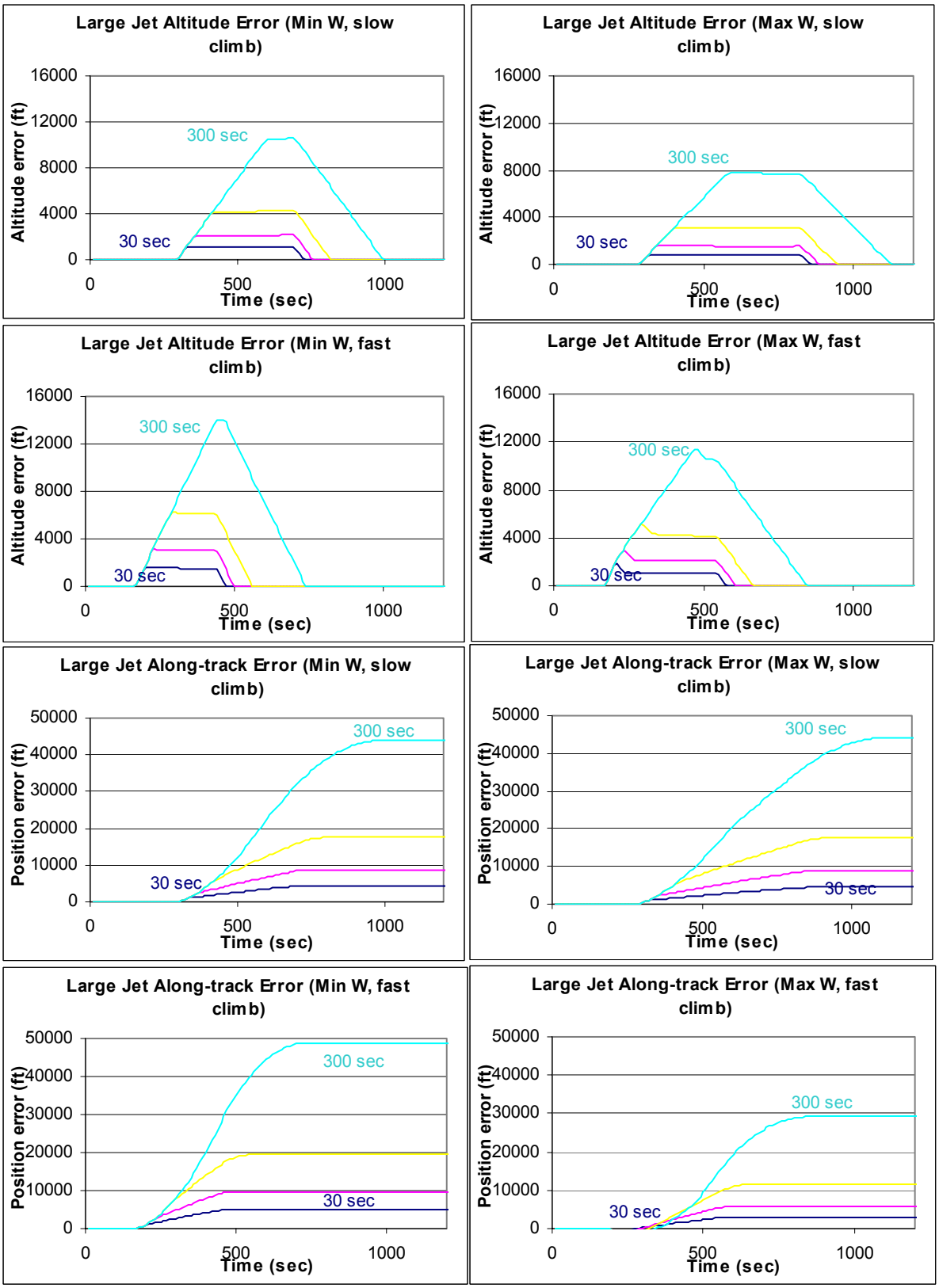

Figure 5-128 Errors due to level-offs (30, 60, 120 and 300 seconds) on descent at 24000 feet on a large jet

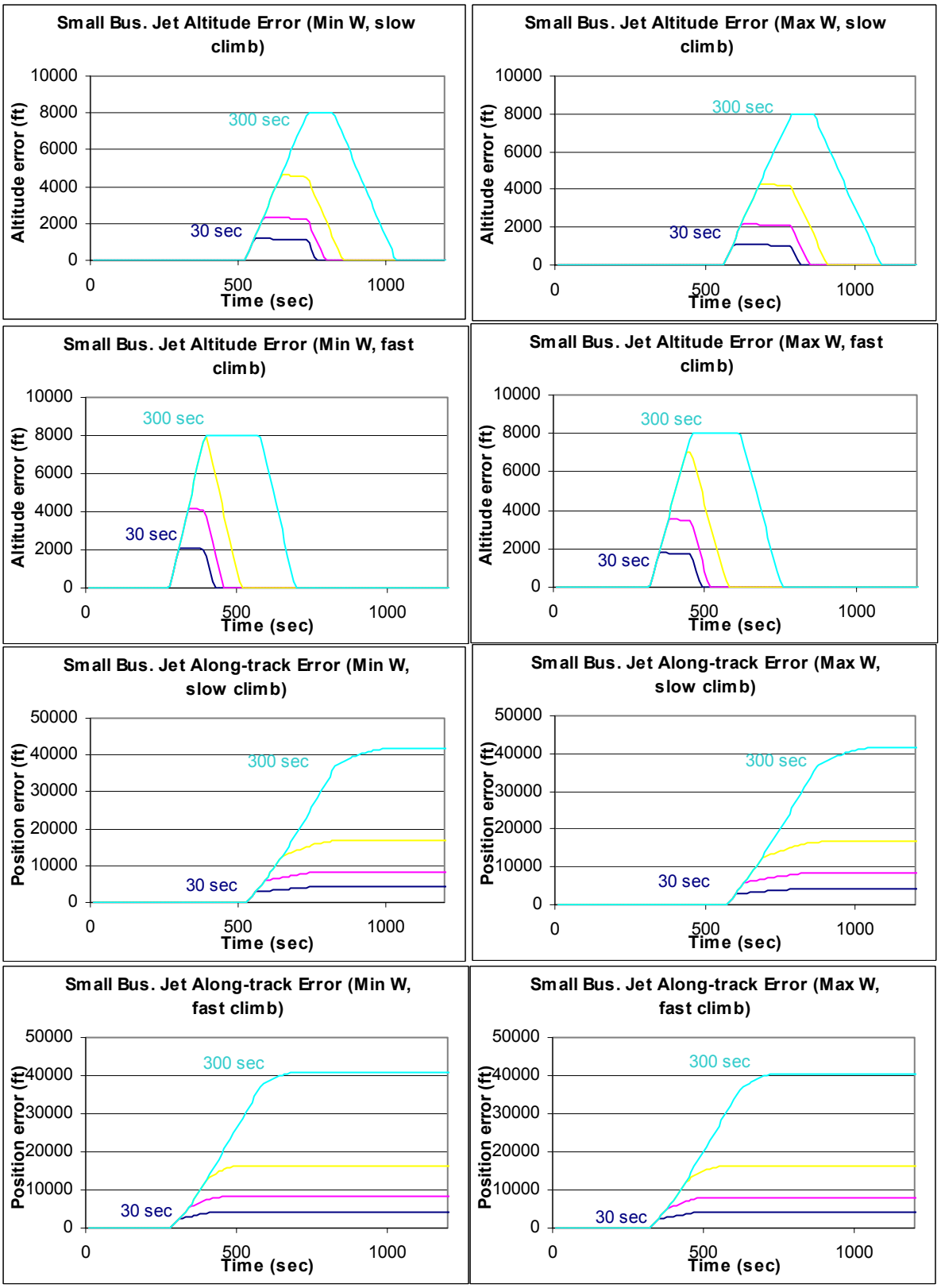

Figure 5-129 Errors due to level-offs (30, 60, 120 and 300 seconds) on descent at 18000 feet on a small business jet

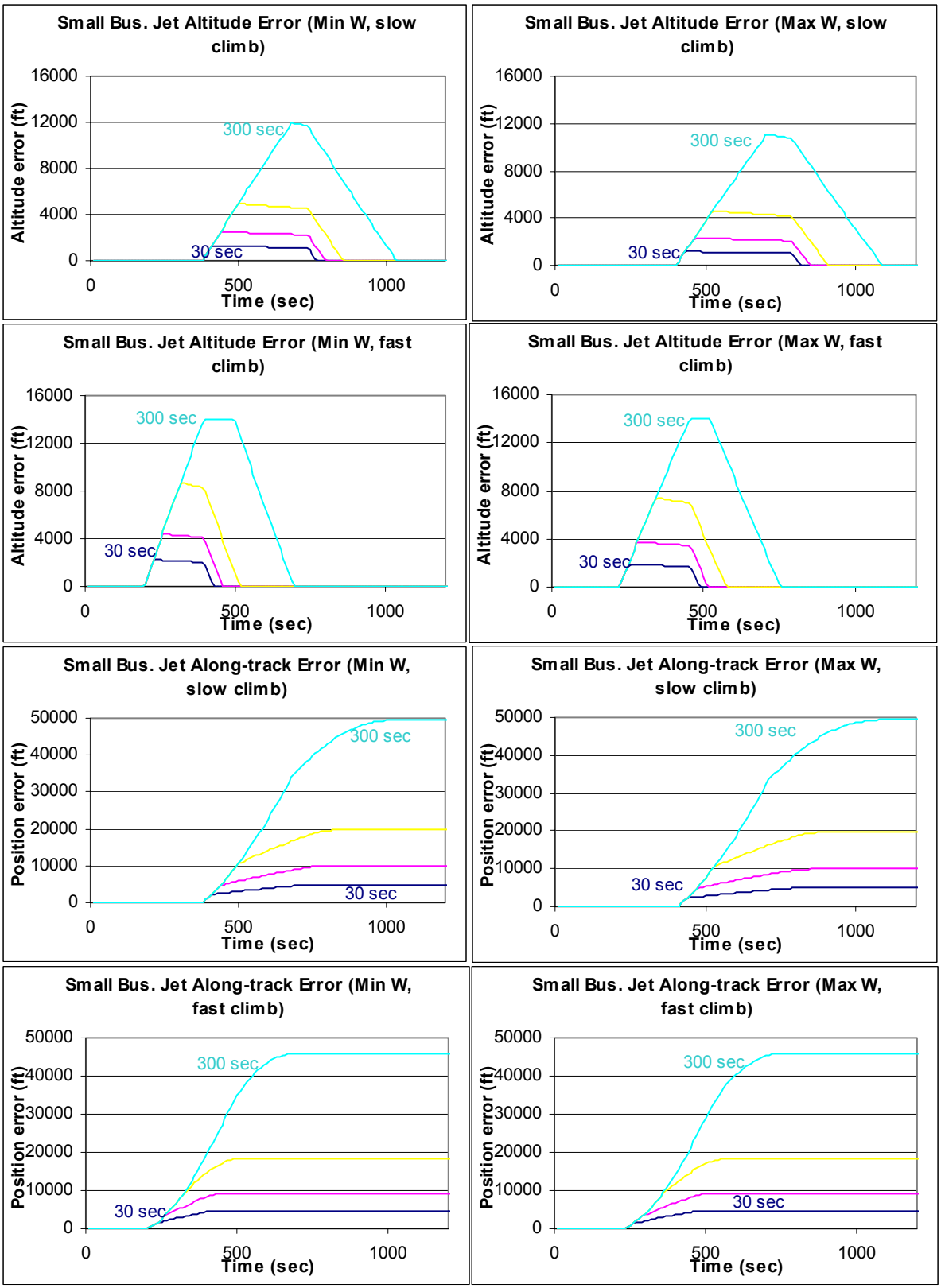

Figure 5-130 Errors due to level-offs (30, 60, 120 and 300 seconds) on descent at 24000 feet on a small business jet

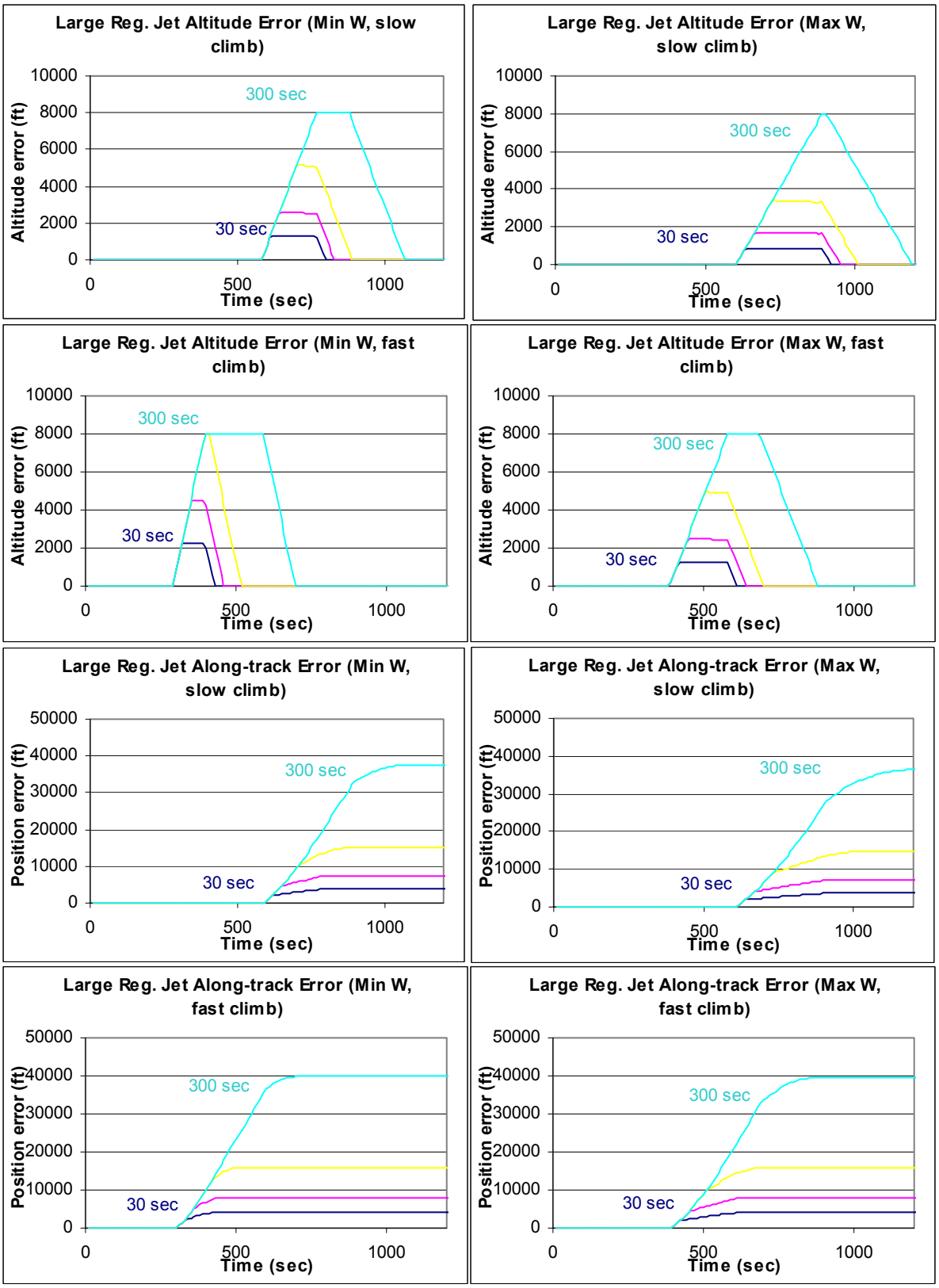

Figure 5-131 Errors due to level-offs (30, 60, 120 and 300 seconds) on descent at 18000 feet on a large regional jet

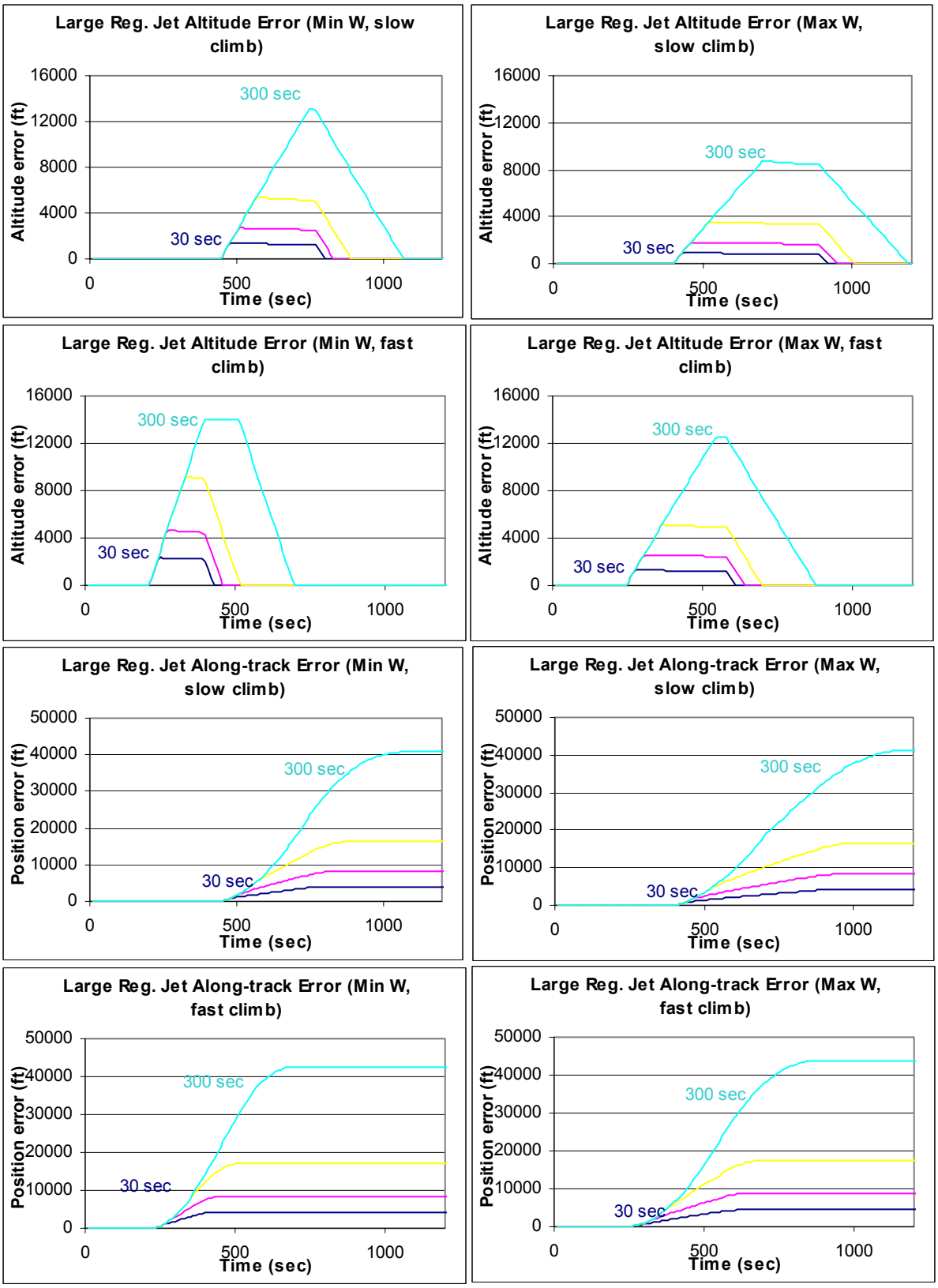

Figure 5-132 Errors due to level-offs (30, 60, 120 and 300 seconds) on descent at 24000 feet on a large regional jet

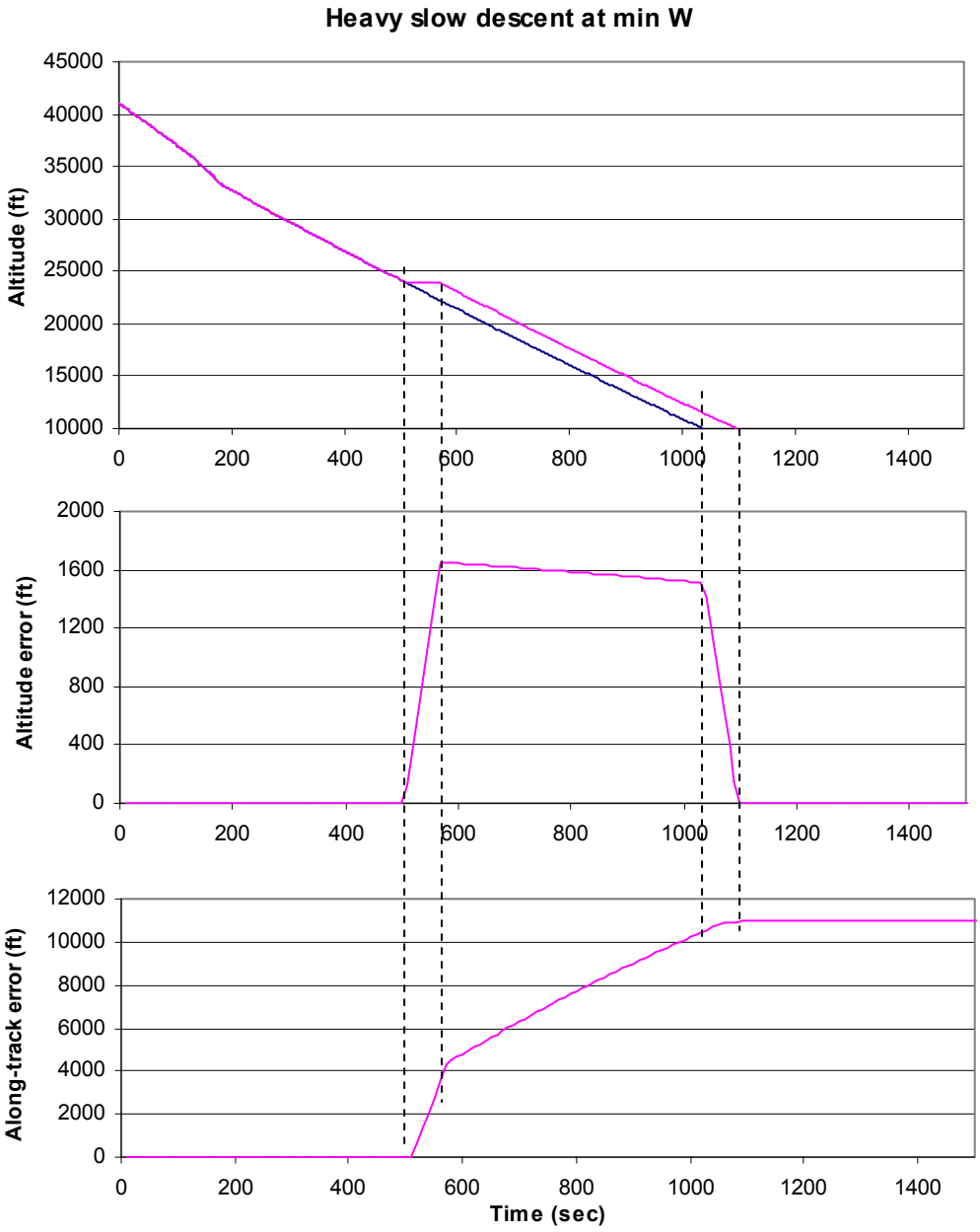

Figure 5-133 Illustration of altitude and along-track error due to level-off error

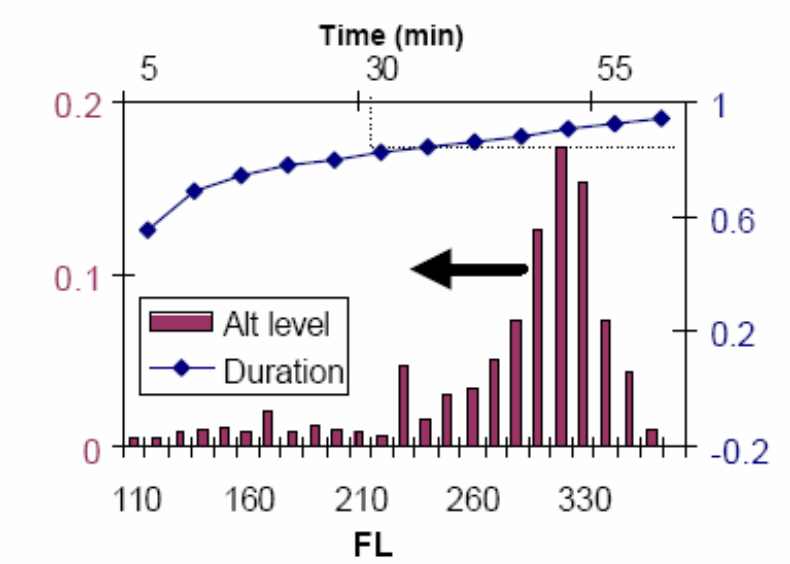

Figure 5-134 Level-off altitude histogram and cumulative duration distribution

5.7 Aircraft Speed Intent

5.7.1 Description of the Error

Trajectory predictors require knowledge of the intended speed of a flight in order to obtain a valid prediction of future position. This intended speed may be expressed as a true airspeed, calibrated airspeed, or Mach number. Ground speed is an outcome of the winds and intent is not expressed as ground speed. The trajectory predictor must rely on an atmospheric model, or atmospheric data to subsequently convert between the different types of speeds. The conversion between speeds is required since each type of speed is necessary for different portions of the calculation. The aerodynamic terms are expressed as a function of true airspeed and Mach number. Certain speed constraints are expressed in calibrated or indicated airspeed. Finally, ground speed is required to integrate the future forecast location of the flight.

While speed intent may be necessary to obtain a trajectory prediction, speed intent is often not known by a ground-based system performing trajectory prediction. The system may obtain the speed through a variety of error-prone mechanisms as detailed below. In general, estimates of ground speeds are obtained and converted to airspeeds using winds, or air-derived data can be obtained and converted to ground speeds using winds.

Obtained from Flight plan

Under current operations, aircraft filing flight plans are required to file their intended true airspeed at cruise (FAR §91.153, §91.169). Upon reaching their filed cruise level; flights are required to conform to their filed speed within the greater of 5% or 10 knots, or report the change (AIM 5-3-3e). When the controller has issued a speed instruction, "the pilot is expected to maintain a speed within plus or minus 10 knots or 0.02 Mach number of the specified speed" (AIM 4-4-11). Controller instructions are provided in terms of indicated airspeed or Mach number.

While a trajectory predictor may use the filed airspeed, this speed intent is strictly limited to the initial cruise segment and subject to the 5% or 10 knot conformance. Speeds in climb and descent cannot be obtained in this manner. Furthermore, the airspeed may be altered by the pilot and/or the controller and reported at a future point. When the controller has issued a speed instruction, the speed must be followed within tolerance; however, the speed instruction may not be known by automation.

Observed and Inferred

Speed intent can be assumed, at least in the near term, to continue following the current airspeed. During climb and descent, due to the variation of atmospheric parameters with altitude, one often assumes segments of constant Mach and calibrated airspeed. However, in order to apply this constant-airspeed assumption, the trajectory predictor

must first obtain an estimate of the current airspeed. In a radar environment, this is accomplished through a multiple step process, with each step subject to errors. The ground speed can be approximated from surveillance data, but is subject to the effects of surveillance errors and filtering effects. Once the ground speed is obtained, it must be translated into airspeed by removing the effects of wind. Since the wind is subject to errors described in the Section "Wind Error", obtaining the airspeed (from the ground speed) will be subject to these errors as well. Furthermore, variations in the wind speed will lead to a dynamical response of the aircraft with time scales on the order of a minute. Even if the wind and surveillance were known perfectly, the aircraft dynamics would have to be considered to obtain the intended airspeed. In practice the aircraft dynamics are not taken into account since the other errors are much larger. During the en route phase, a *constant* wind bias will lead to a corresponding error in airspeed; however, this will not lead to along-path errors as the ground speed is used for those calculations.

The current ground speed of a flight underway may be obtained through surveillance information. When radar surveillance is used, only positional information can be obtained. Ground speed can be obtained by processing the position information; however, filtering and smoothing is required due to measurement errors. Figure 5-135 illustrates the magnitude of the positional uncertainty associated with radar reports (see [38],[39]).

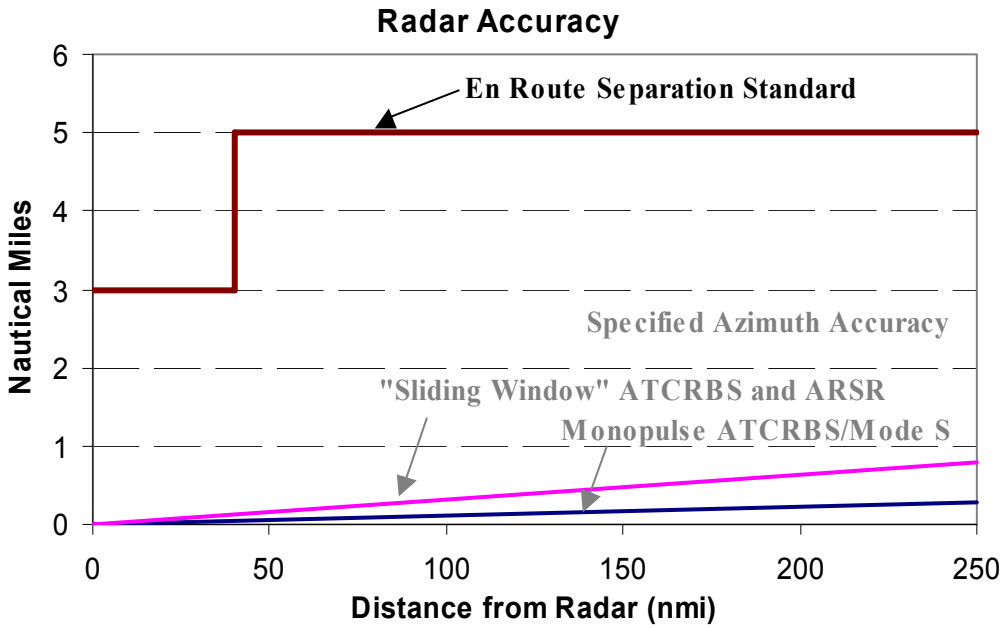

Figure 5-135 Radar accuracy versus distance from radar (reproduced from [38])

Given the above positional uncertainty, calculations of the speed through first-order numerical differentiation of the raw radar signal will yield a very noisy signal. To illustrate the magnitude of this error in speed, we have shown the results of numerical differentiation below.

We approximate the speed with a backward difference of position:

$$V_{n+1} = \frac{x_{n+1} - x_n}{t_{n+1} - t_n} = \frac{Vt_{n+1} + \tilde{x}_{n+1} - (Vt_n + \tilde{x}_n)}{t_{n+1} - t_n} = V + \frac{\tilde{x}_{n+1} - \tilde{x}_n}{\Delta t}$$

Where we have introduce the average speed (V) and a noise term ($\tilde{x}$) at each time step. We note that the speed estimate is just the average speed plus a noise term. If the noise terms between measurements are uncorrelated, the variance of the estimated speed can be expressed in terms of the variance in the surveillance error.

$$\sigma_V{}^2 = \frac{1}{N-1}\sum\left(\frac{\tilde{x}_{n+1} - \tilde{x}_n}{\Delta t}\right)\left(\frac{\tilde{x}_{n+1} - \tilde{x}_n}{\Delta t}\right)$$

$$= 2\frac{\sigma_x{}^2}{\Delta t^2}$$

With a 12 second update rate, a standard deviation of 0.4 nautical miles in positional uncertainty yields a 168 knot standard deviation in the speed measured using this approach. Figure 5-136 shows the speeds obtained using this approach from actual operational data with standard deviations of 157 and 105 knots.

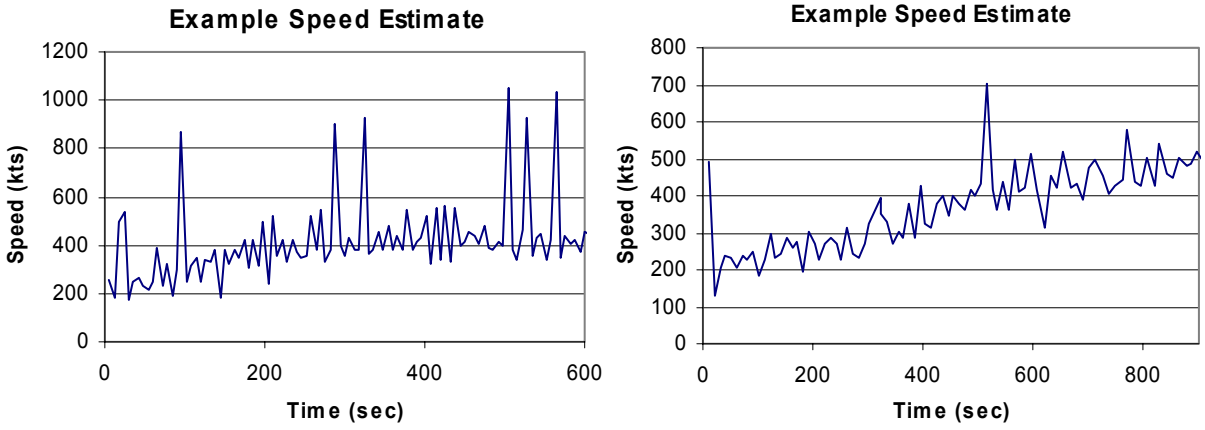

Figure 5-136 Illustration of noise in simple speed calculation

In practice, the ground speed used by a trajectory predictor is likely to be the output of a tracker seeking to remove the effects of sensor noise. Trackers smooth the data by combining information from prior data points to yield a better estimate of position and velocity. One of the drawbacks of this approach, however, is that trackers introduce lags into the estimate. Thus, changes in ground speed and heading will be detected with some time lag. Furthermore, errors in speed estimation will occur during turns. One of the trackers currently in use today is the α-β tracker, which will use the following equations (see NAS –MD-321) to obtain the smoothed velocity given position estimates.

$$\hat{x}_k(-) = \hat{x}_{k-1}(+) + \hat{v}_{k-1}(+)(t_k - t_{k-1})$$
$$\hat{v}_k(-) = \hat{v}_{k-1}(+)$$
$$\hat{x}_k(+) = \hat{x}_k(-) + \alpha(x_k - \hat{x}_k(-))$$
$$\hat{v}_k(+) = \hat{v}_k(-) + \frac{\beta}{(t_k - t_{k-1})}(x_k - \hat{x}_k(-))$$

Where the (-) refers to an initial prediction, while the (+) refers to a corrected prediction. Values are estimated at time t_k based upon values at time t_{k-1}. The above yields position (x) and velocity (v) estimates dependent upon the parameters $\alpha \in [0.2,0.32]$ and $\beta \in [0.015,0.05]$. The above equations apply when the new surveillance data falls within a "small search area" (SSA) of the predicted track position. Separate equations apply when the data falls within a "large search area" (LSA).

In terms of the impact on velocity prediction, we illustrate the impact of the filtering equations on a noiseless forty-five degree change in heading at constant speed (standard rate turn). We can see the effects of the lag on the position estimate, and the velocity estimate, even though the actual aircraft velocity was constant at 400 knots. While the LSA equations can improve the tracking of the turn, the peak speed error is of the same magnitude.

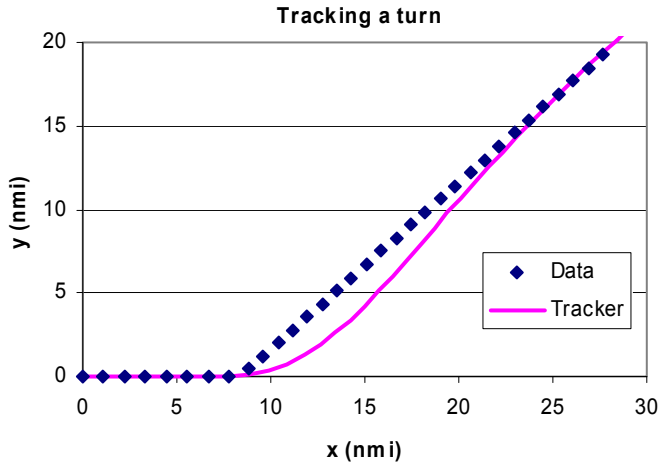

Figure 5-137 Impact of α-β tracker position estimate in turn (SSA)

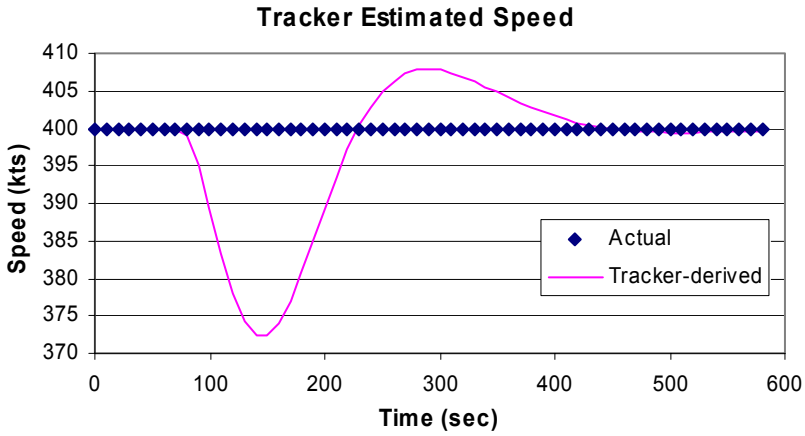

Figure 5-138 Impact of α-β tracker velocity estimate in turn (SSA)

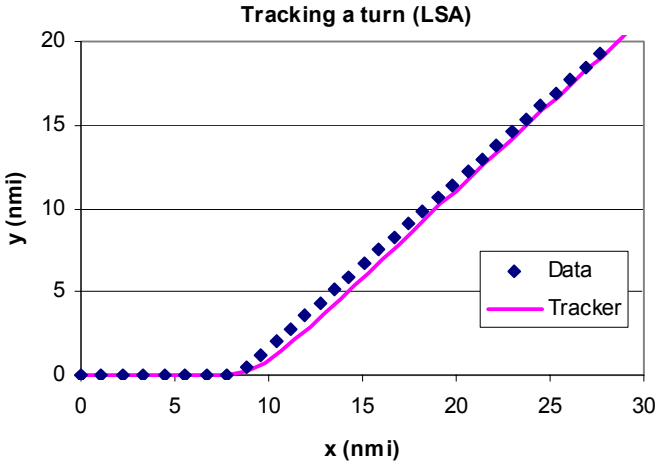

Figure 5-139 Impact of α-β tracker position estimate in turn (LSA)

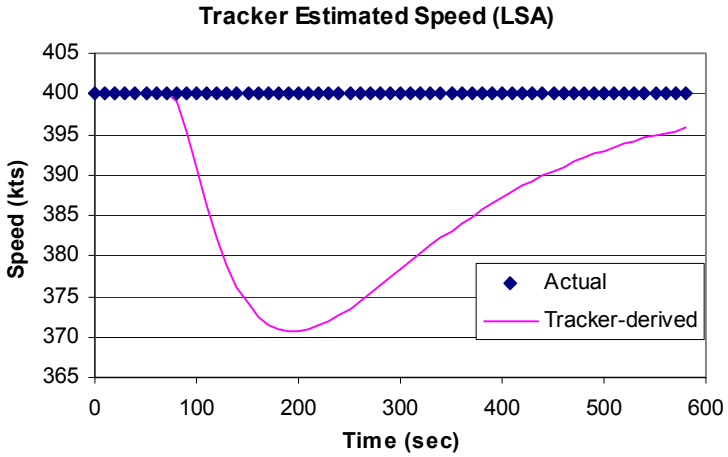

Figure 5-140 Impact of α-β tracker velocity estimate in a turn (LSA)

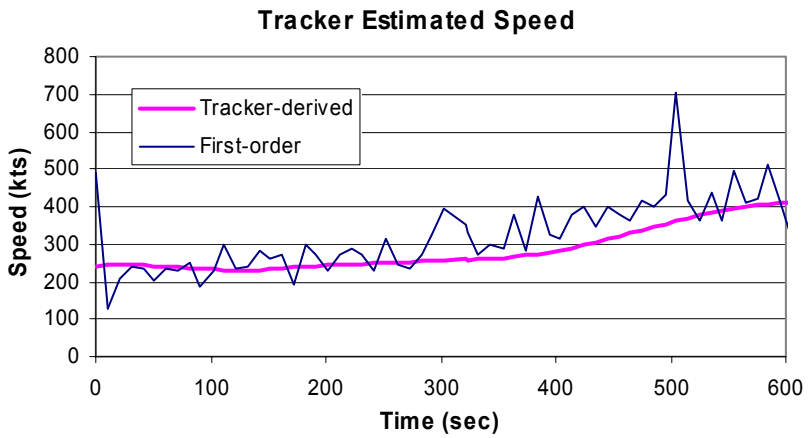

Figure 5-141 Velocity estimate obtained through α-β tracker equations

We can apply the α-β tracker equations to one of our data samples to illustrate the impact of the filter on the estimate of speed (see Figure 5-141). Clearly a lag is visible given speed changes. Different types of filters (e.g., Kalman filters) have been developed that improve on these lags and consider the statistics of the sensor errors [40],[41].

Once the ground speed is obtained, this ground speed must be converted to airspeed by incorporating the effects of wind. Given the errors in estimating ground speed, and the errors in obtaining wind speed, Figure 5-142 illustrates the resultant error in airspeed. Note that the errors are the summation of vector errors, not just scalars.

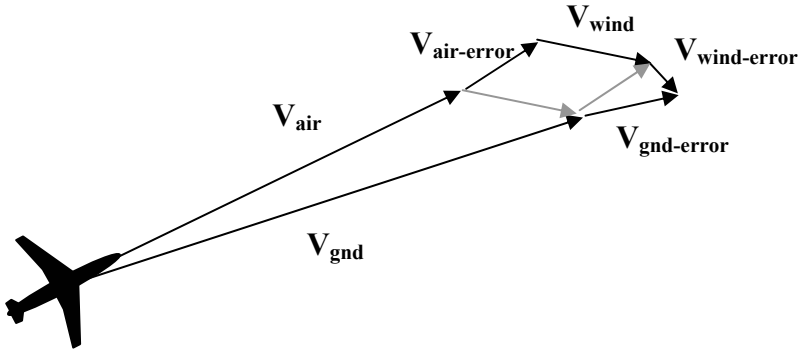

Figure 5-142 Error in airspeed derived from ground and wind errors

While the instantaneous airspeed, subject to uncertainty, can be obtained using the above approach, obtaining the airspeed intent has an additional problem: the interaction between aircraft dynamics and wind variations. As the flight progresses, the actual wind will continue to vary. This leads to changes in airspeed that result in a dynamical response of the aircraft. For example, a sudden increase in a headwind will lead to a sudden increase in airspeed. Drag will increase and the aircraft will eventually slow down to match the original trimmed airspeed. The result will be that ground speed will have decreased by the change in wind. However, that change will have occurred over a period of time commensurate with the dynamics of the aircraft. Without modeling the dynamics of the

aircraft, one can obtain the instantaneous airspeed, but one cannot obtain the target, or "intended" airspeed without some error.

Figure 5-143 illustrates the problem. An aircraft is subject to a variable wind field, even if the ground speed can be measured perfectly, the aircraft is constantly responding to the history of all wind fluctuations. As a result, the target airspeed, or speed intent (400 knots in this example) cannot easily be measured with a moving average. This error will be strongly coupled to the *variation* in the wind field. The more steady the wind, the smaller the aircraft response, and the easier it will be for the dynamics of the aircraft response to be neglected.

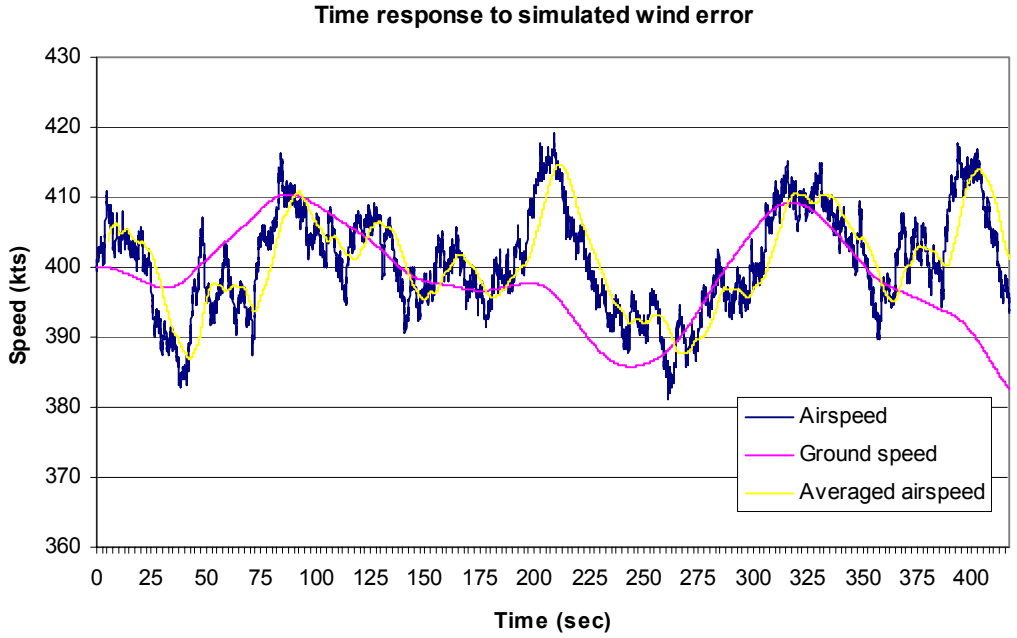

Figure 5-143 Illustration of dynamical response to fluctuating wind field (target airspeed = 400 kts)

Averages given an Aircraft Class

Another approach to obtaining the speed intent for the aircraft is to obtain average intended speeds for aircraft of a type. For example, a B767-200 would be considered to have a default climb and descent schedule. Aircraft types could further be subdivided according to operator to accommodate speed differences between operators. This type of averaged approach to obtaining the speed is likely to be used only for climb and descent speed profiles since the prior two methods would be more applicable to a flight in cruise.

The application of average speeds to infer speed intent leads to an error with distribution identical to the distribution of speeds occurring in reality. Thus, if all aircraft of a type climb with a 280/0.74 climb schedule, then no intent error occurs. As more aircraft deviate from this schedule, the speed intent error will also deviate. This type of approach to obtaining speed intent would neglect the variation due to user preferences and those differences between carriers and individual flights.

In order to *estimate* the magnitude of this error, we obtained a sample of clean climb data from ETMS segregated by aircraft type. For each climb data point, we obtained an estimate of the calibrated airspeed and Mach number using wind data for the specific day and computing the ground speed from the position data. Note that this approach contained radar uncertainty, tracker-induced lags and wind uncertainty. We obtained an estimate of the target climb CAS (above 10000 feet) and climb Mach by minimizing the sum of the variance over the climb trajectory segment.

For each climb trajectory segment, we obtained the variance in the CAS and Mach across data points as illustrated below. Each flight will have a different sample variance. However, since each flight is expected to be targeting a constant CAS and Mach, this sample variance will be sampled from a distribution that combines the effects of the wind error, tracker and positional uncertainty effects. The intent error will only be included when we look across different flights. From these samples, we obtain a 20 knot standard deviation in the calibrated airspeed and a standard deviation in Mach number of 0.05.

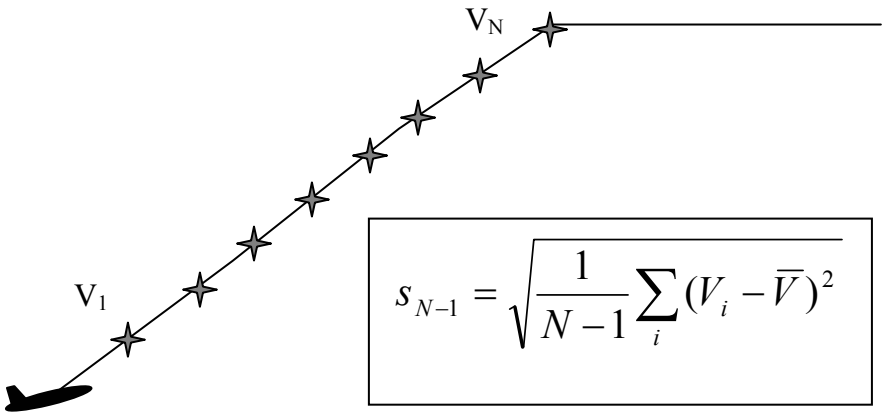

Figure 5-144 Sample climb speed variance illustrated for a single flight

We then obtained the standard deviation in climb speeds for all flights of a given aircraft type. This standard deviation will incorporate both the effects of variation in intent, and the errors discussed above.

$$V = V_{t\arg et} + \Delta V_{wind+radar+trac\ker}$$
$$= \bar{V}_{\text{int}\,ent} + \varepsilon_{\text{int}\,ent} + \Delta V_{wind+radar+trac\ker}$$

Assuming normal distributions to simplify the math, we can take the difference in the variances to obtain the standard deviation due to intent error only. These standard deviations are shown below for a selection of aircraft types to illustrate the range of variations in climb speed intent observed in the data.

Table 5-5 Climb speed standard deviation by aircraft type (from observations)

Aircraft Type	Climb CAS intent σ (kts)	Climb Mach Intent σ
A320	11	0.03
B727-200	6	0.03
B737-200	9	0.02
B737-300	13	0.03
B747-400	15	0.02
C550	18	0.05
CL60	34	0.05
MD88	11	0.04

The average aircraft type experiences a range in climb CAS (as measured through a standard deviation) of 15 knots. This range falls within the range of climb CAS schedules between the minimum cost index and the maximum cost index. Similarly, for the climb Mach, the average is a standard deviation of about 0.03, again consistent with the range from minimum to maximum cost index.

An interesting observation from the above data is that the variation due to intent, for any given aircraft type, tends to be lower than the combined effect of the wind and positional uncertainty. The implication is that using the average climb schedule for an aircraft type introduces less aggregate error than just inferring the speed from observations. However, through use of improved wind data and better positional information and tracking algorithms, this relationship will be reversed.

We can repeat the above analysis for flights in descent with similar results. (The sample size on descent was smaller than the sample size on climb since we were seeking uninterrupted descents. Given that current procedures will often have level-off segments during descent, this reduced the sample size.)

Table 5-6 Descent speed standard deviation by aircraft type (from observations)

Aircraft Type	Descent CAS intent σ (kts)	Descent Mach Intent σ
A320	16	0.03
B727-200	27	0.03
B737-200	30	---
B737-300	23	0.05
B747-400	18	---
C550	26	0.08
CL60	36	0.05
MD88	16	0.02

During descent, this provided an average standard deviation of 25 knots on calibrated airspeed and 0.04 on Mach number. The deviation on CAS is consistent with the range of CAS for transport aircraft operating between minimum and maximum cost index.

Obtained through the Flight Deck

Future concepts have been proposed that provide trajectory predictors using the explicit aircraft speed intent (e.g., [42]) from the flight deck. In such a case, the speed intent error will be identically zero. However, some intent error can occur due to a future unknown change in intent. These errors may be the result of controller instruction, or pilot action.

The degree to which the aircraft and pilot can meet the specified speed intent is the subject of other errors, namely the flight technical error (FTE).

5.7.2 Parametric Analysis

During climb and descent, the target climb (or descent) speed will impact the climb gradient. For example, slower climbs tend to have a higher gradient, both because the drag is lower and because of the slower horizontal speed at any given climb rate. We recall our simple expression for the gradient:

$$\gamma = \left(\frac{T-D}{mg}\right)\left[\frac{V}{g}\frac{dV}{dh} + \frac{V}{g}\frac{dw}{dh} + 1\right]^{-1}$$

Where terms are obtained from a force balance as shown in the Figure below.

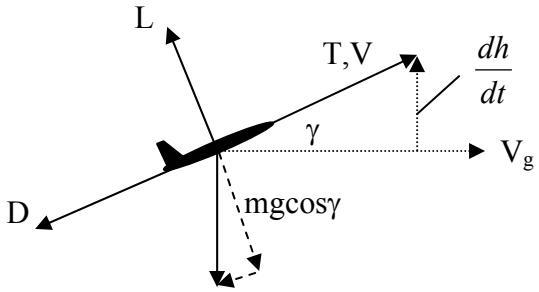

Figure 5-145 Force balance in climb

In order to estimate the impact of the speed on the climb and descent gradient, we express the drag coefficient using a quadratic drag polar. We note that the dependence of the drag coefficient on Mach number will be smaller than the dependence on speed at the Mach numbers under consideration.

$$\gamma = \left(\frac{T - qS\left[C_{D_0} + kC_L^2\right]}{mg}\right)\left[\frac{V}{g}\frac{dV}{dh} + \frac{V}{g}\frac{dw}{dh} + 1\right]^{-1}$$

$$= \left(\frac{T - qS\left[C_{D_0} + k\left(\frac{mg}{qS}\right)^2\right]}{mg}\right)\left[\frac{V}{g}\frac{dV}{dh} + \frac{V}{g}\frac{dw}{dh} + 1\right]^{-1}$$

We can obtain the derivative of the gradient with respect to the speed to give the following:

$$V\frac{d\gamma}{dV} = \frac{-2qS}{mg}\left[\frac{C_{D_0} - kC_L^{\ 2}}{\frac{V}{g}\frac{dV}{dh} + \frac{V}{g}\frac{dw}{dh} + 1}\right] - \frac{T-D}{mg}\left[\frac{\frac{V}{g}\frac{dV}{dh} + \frac{V}{g}\frac{dw}{dh}}{\left(\frac{V}{g}\frac{dV}{dh} + \frac{V}{g}\frac{dw}{dh} + 1\right)^2}\right]$$

The preceding expression is described in terms of several non-dimensional groupings with the following range of values:

$$\frac{qS}{mg} = \frac{1}{C_L} \in \left(\frac{1}{.05}, \frac{1}{.6}\right)$$

$$C_{D_0} \in (0.015, 0.025)$$

$$kC_L{}^2 \in (0.0002, 0.03)$$

$$\left.\frac{V}{g}\frac{dV}{dh}\right|_{CAS} \in (0.1, 0.4)$$

$$\left.\frac{V}{g}\frac{dV}{dh}\right|_{Mach} \in (-0.1, 0.)$$

$$\frac{V}{g}\frac{dw}{dh} \in (-.15, .15)$$

$$\left(\frac{T-D}{mg}\right)_{C\lim b} \in (0, 0.25)$$

$$\left(\frac{T-D}{mg}\right)_{Descent} \in (-.25, -0.04)$$

We have been unable to identify any dominant terms in the above equation. Furthermore, the above parameters are not all independent. We investigated the response of the gradient to a change in speed intent through numerical evaluation of the $\left(V\frac{d\gamma}{dV}\right)$ term for a large aircraft and for a heavy aircraft. Both of these aircraft exhibited similar behavior. We approximate the local change in gradient ($\Delta\gamma$) resulting from a relative change in speed ($\Delta V/V$) as follows.

$$\Delta\gamma = \left(V\frac{d\gamma}{dV}\right)\frac{\Delta V}{V}$$

During the constant CAS segment of climb, first term on the right $\left(V\frac{d\gamma}{dV}\right)$ ranges from 0 to -0.25. Thus a 5% change in speed can result in a 0.7 degree (0.0125 radians) change in climb gradient during a constant CAS segment. During a constant Mach segment, the magnitudes of the first term on the right are approximately the same (from 0.05 to -0.20).

The impact of a faster intent speed is to decrease the $\left(V\frac{d\gamma}{dV}\right)$ term. Since this term is often negative, an error in speed intent will usually lead to a greater error in climb gradient at faster speeds than it will at lower speeds. This can be reversed during

constant Mach segments at higher altitudes when the climb gradient increases as intent speed increases.

The impact of weight on the sensitivity of gradient to speed intent is significant. At lighter weights, the climb gradient is generally more sensitive to speed intent changes than at higher weights. This applies in all regimes except constant Mach at high altitudes when the sensitivity term changes sign.

The impact of the wind gradient term on the sensitivity is difficult to generalize, but it is not as large an effect as the weight and speed effects. Figure 5-146 to Figure 5-149 illustrate the sensitivity for various non-dimensional wind gradients $\left(\frac{V}{g}\frac{dw}{dh}\right)$, climb speeds, aircraft types, altitudes and weights.

During descent, the nominal gradient is negative. During the constant CAS segment, the $\left(V\frac{d\gamma}{dV}\right)$ term ranges from 0 to -0.25. This is the same range as during the climb segment, although the curves are slightly different (see Figure 5-150 to Figure 5-153). During a constant Mach descent segment, the term varies from -0.3 to 0.05.

The impact of a faster intent speed is to decrease the gradient sensitivity term (make it more negative). Thus, the descent gradient will suffer a greater error at faster speeds than at slower speeds. As for the climb, this can be reversed during a constant Mach descent segment at higher altitudes and slower speeds.

Heavier aircraft generally exhibit a decrease in the magnitude of the sensitivity term. Additionally a wind gradient term will affect the gradient sensitivity to speed slightly as shown in the various figures.

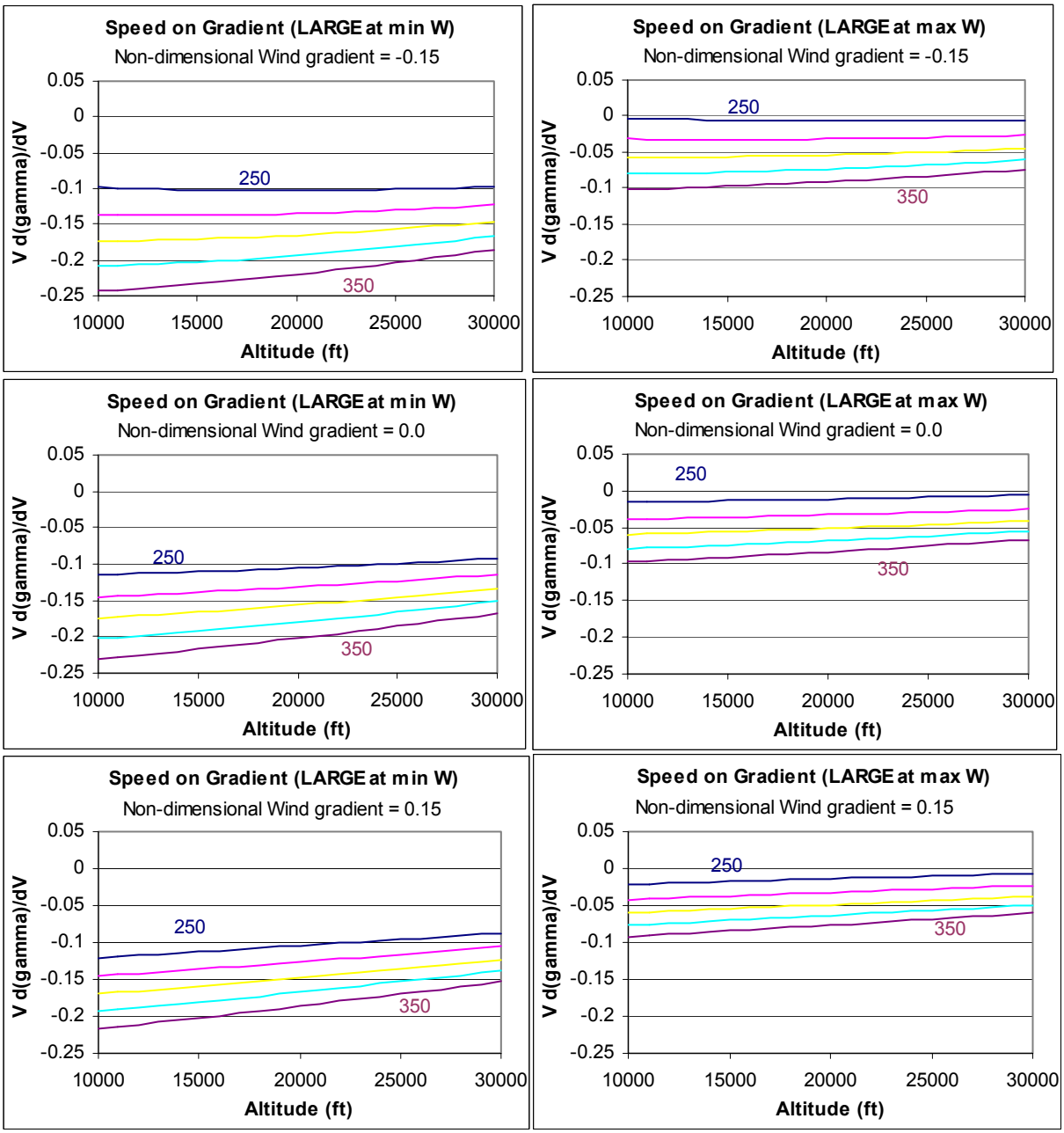

Figure 5-146 Impact of climb speed (CAS), weight, wind gradient and altitude on $\left(V\frac{d\gamma}{dV}\right)$ for a large jet

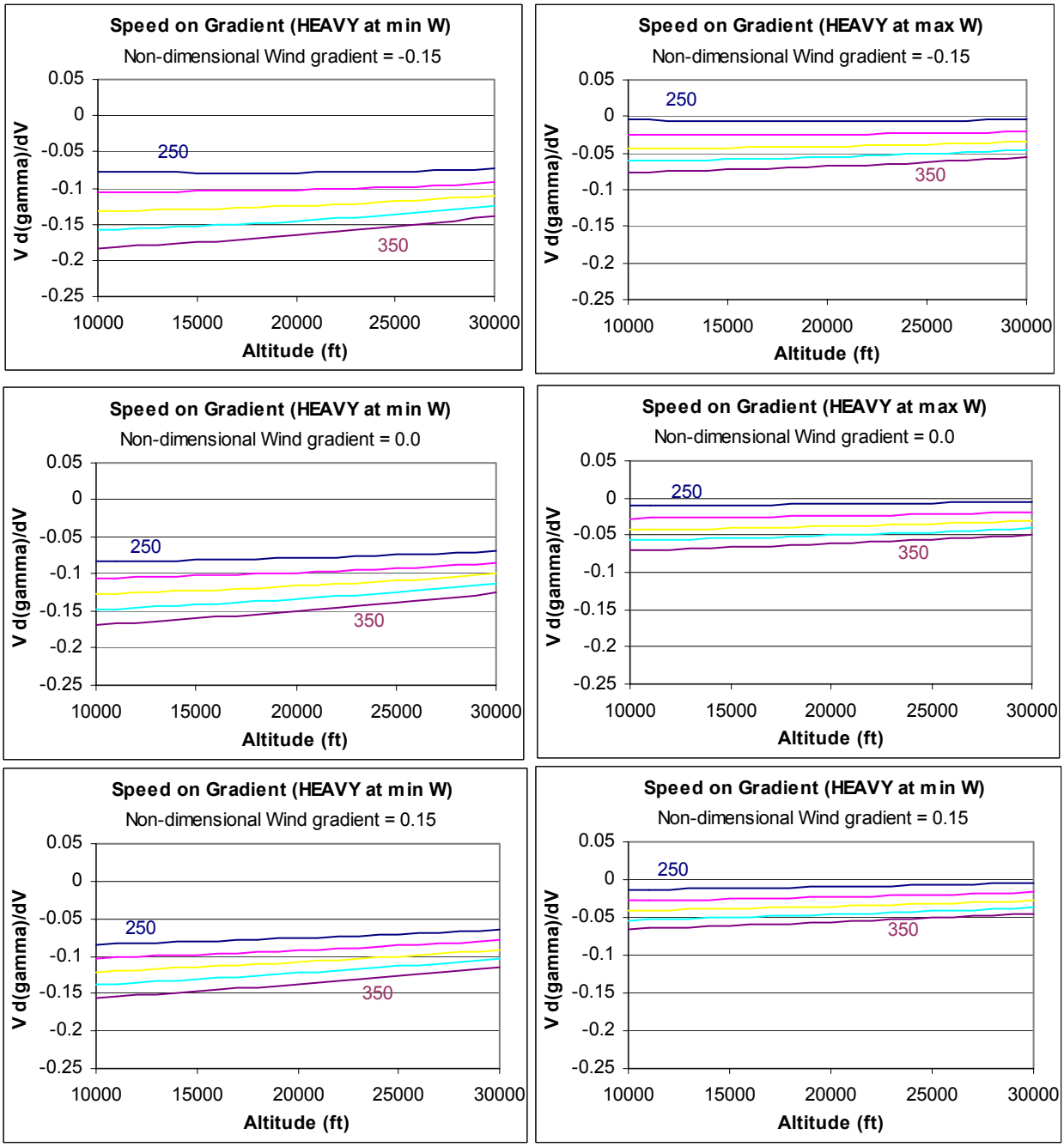

Figure 5-147 Impact of climb speed (CAS), weight, wind gradient and altitude on $\left(V\frac{d\gamma}{dV}\right)$ for a heavy jet

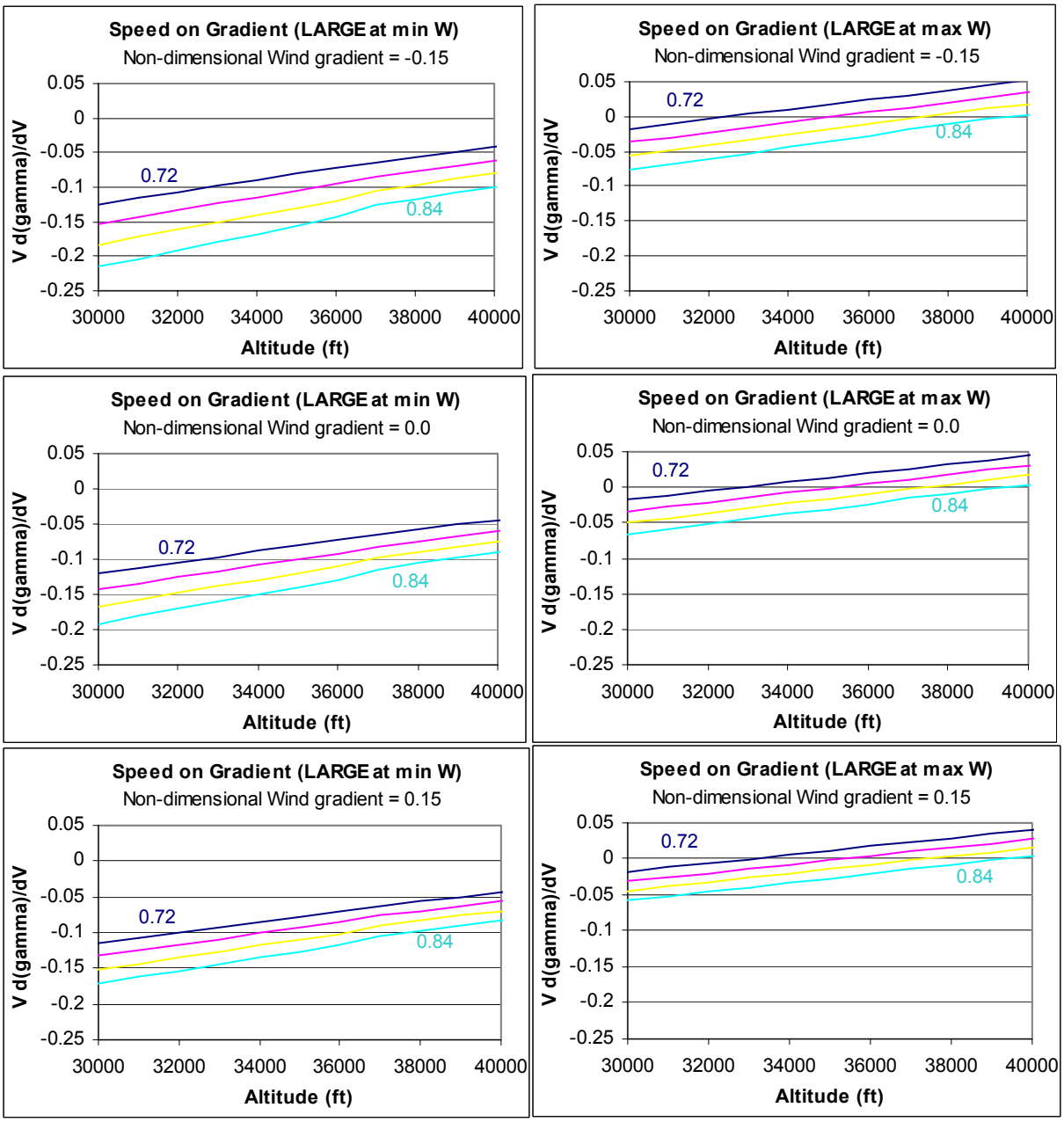

Figure 5-148 Impact of climb speed (Mach), weight, wind gradient and altitude on $\left(V\frac{d\gamma}{dV}\right)$ for a large jet

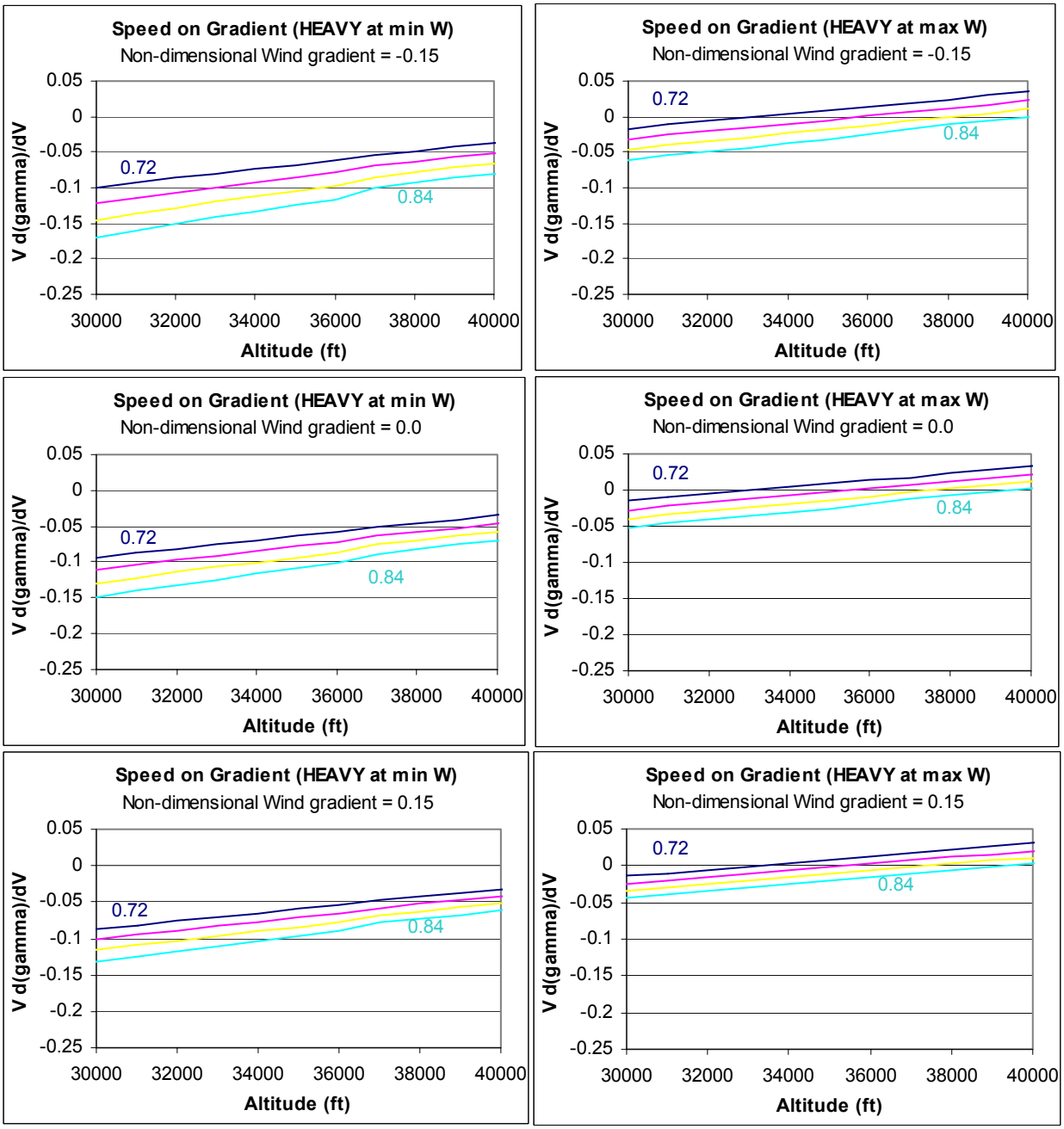

Figure 5-149 Impact of climb speed (Mach), weight, wind gradient and altitude on $\left(V\frac{d\gamma}{dV}\right)$ for a heavy jet

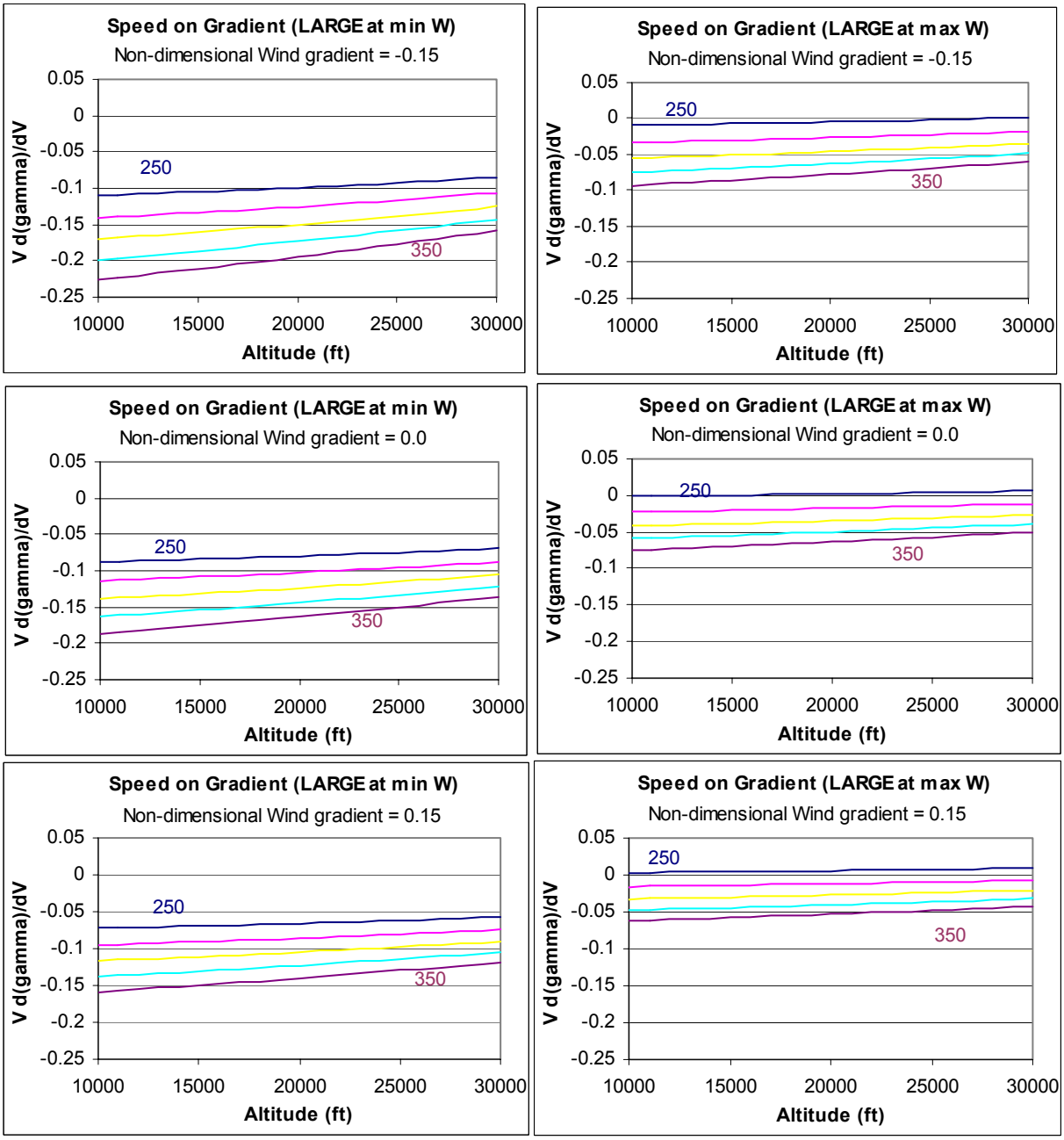

Figure 5-150 Impact of descent speed (CAS), weight, wind gradient and altitude on $\left(V\frac{d\gamma}{dV}\right)$ for a large jet

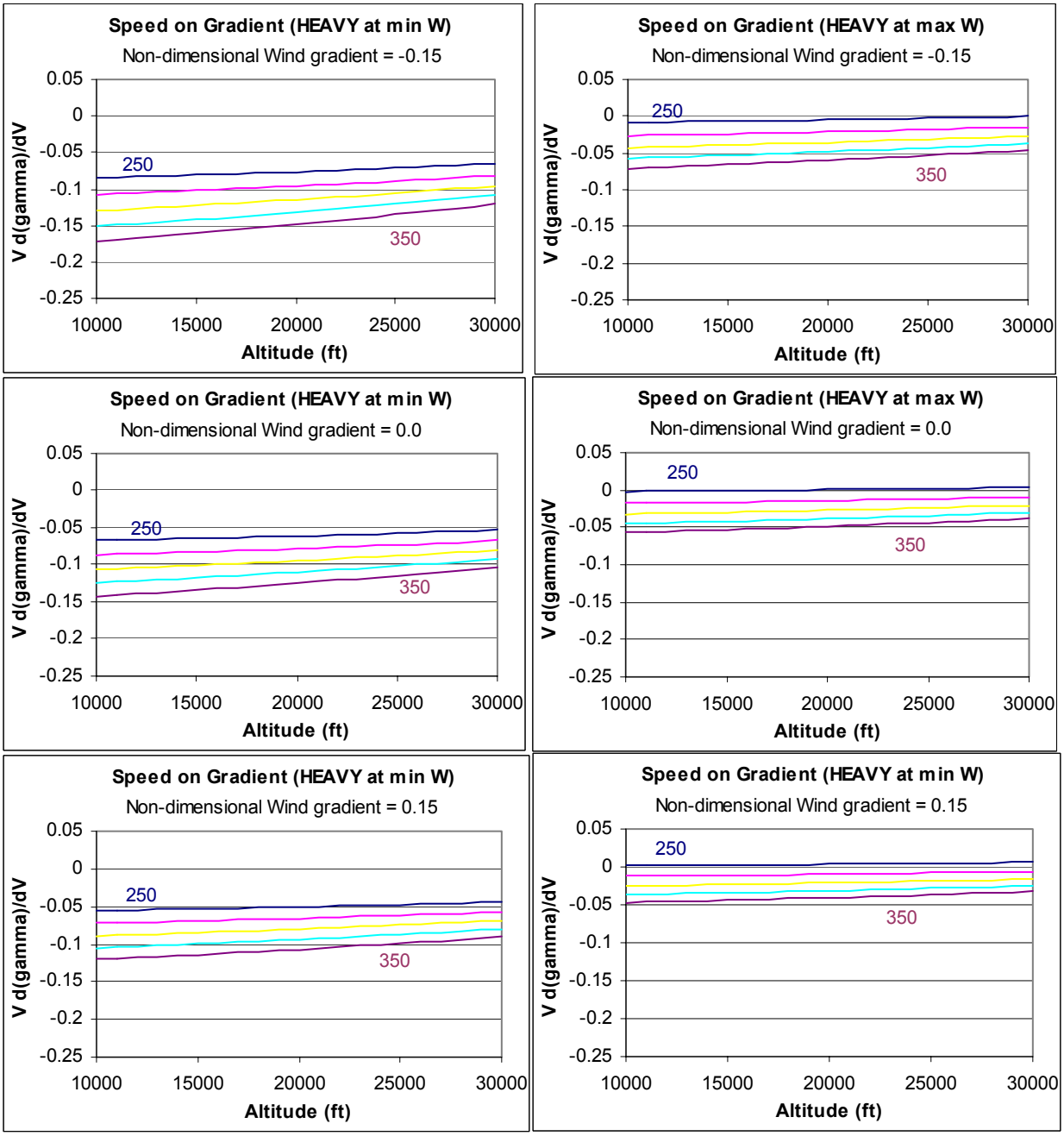

Figure 5-151 Impact of descent speed (CAS), weight, wind gradient and altitude on $\left(V\frac{d\gamma}{dV}\right)$ for a heavy jet

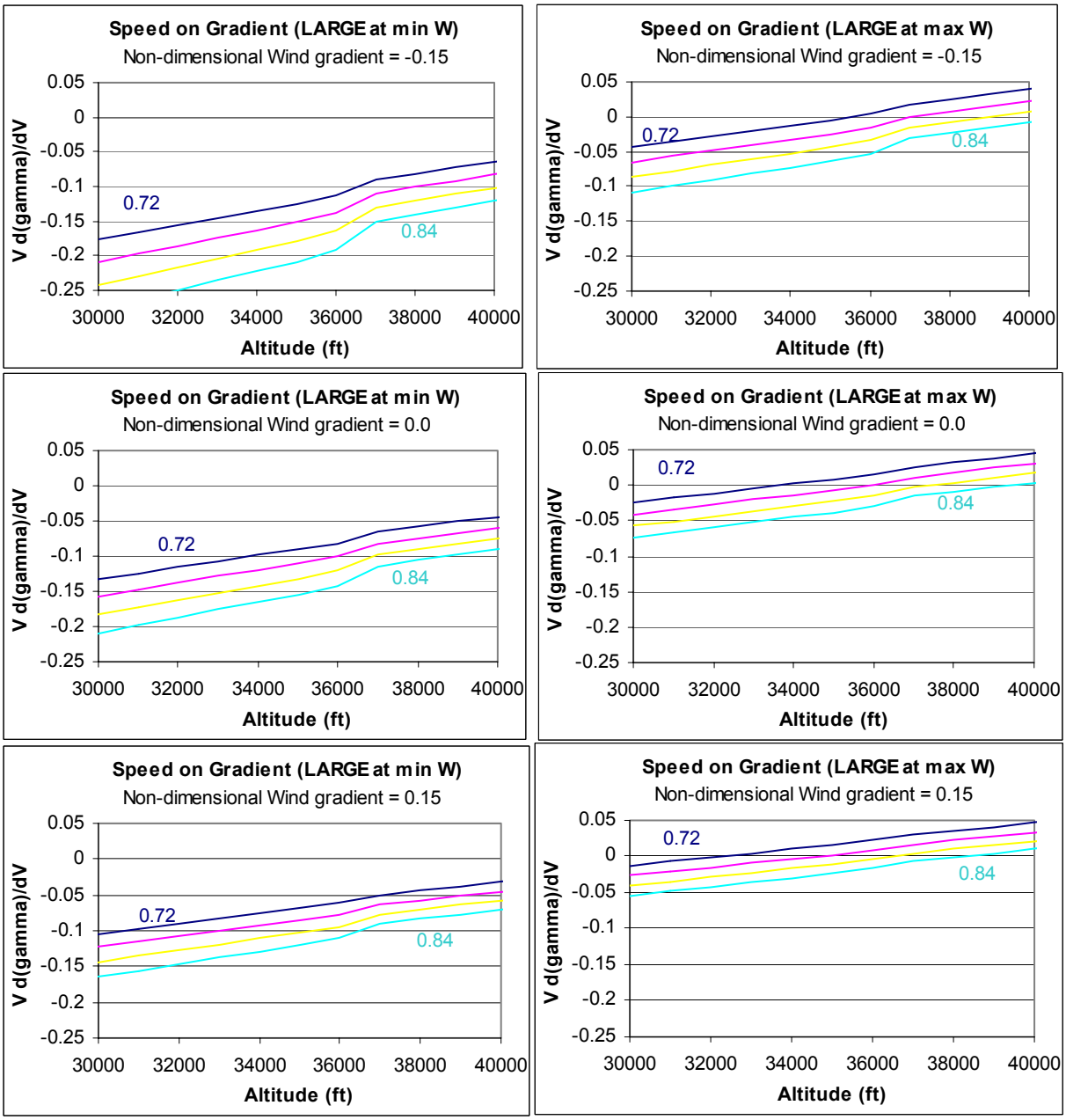

Figure 5-152 Impact of descent speed (Mach), weight, wind gradient and altitude on $\left(V\frac{d\gamma}{dV}\right)$ for a large jet

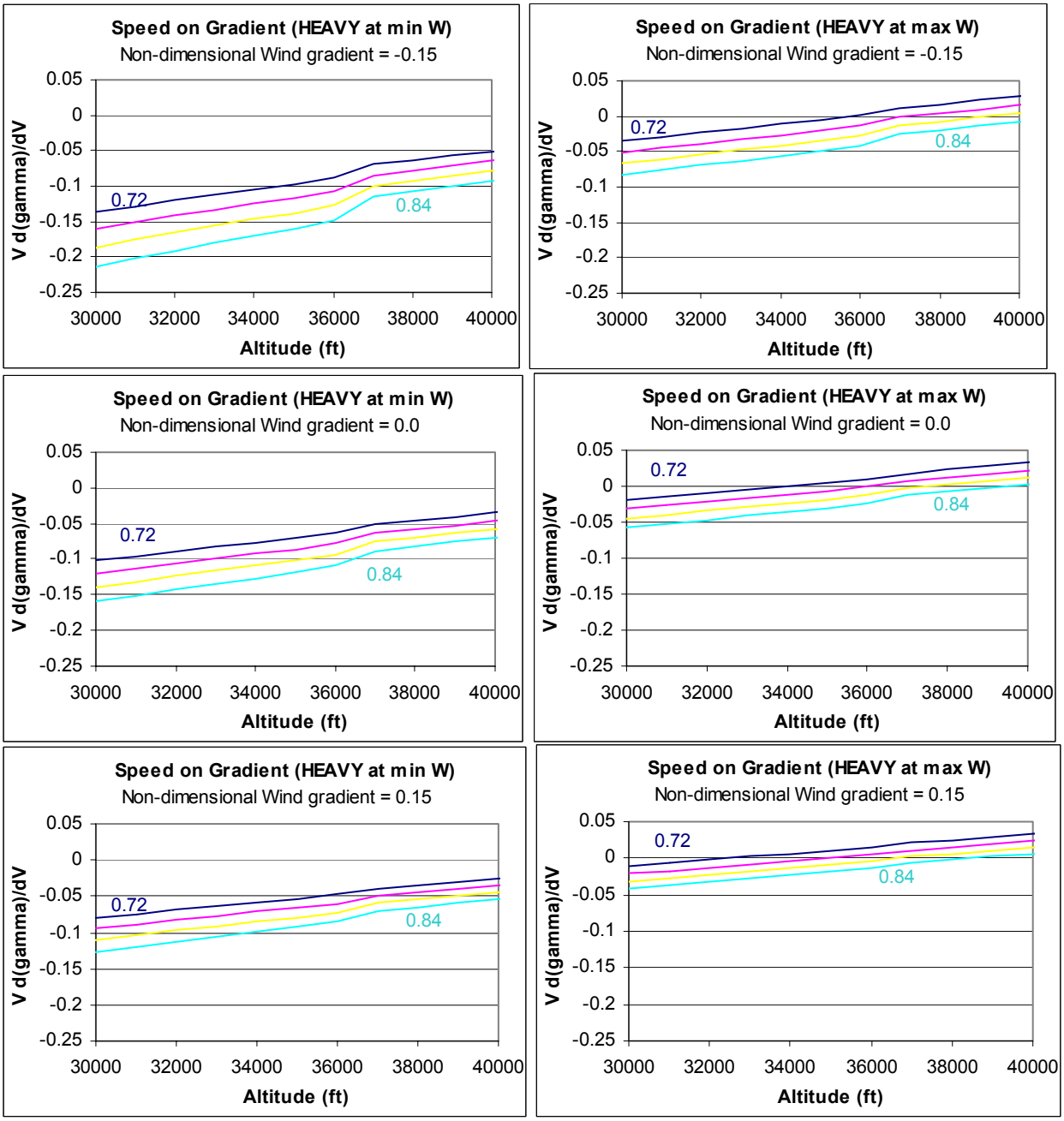

Figure 5-153 Impact of descent speed (Mach), weight, wind gradient and altitude on $\left(V\frac{d\gamma}{dV}\right)$ for a heavy jet

The altitude and along-track error during climb and descent has been reported in this document as a function of time. This type of error is useful for applications that require knowledge of the error at a fixed look-ahead horizon. However, because we are describing an error in speed, a difference exists between the errors as a function of time, and the errors as a function of distance. Consider Figure 5-154. Here we see the impact of an error in climb speed expressed both as a function of distance and as a function of time. We see that a higher speed results in a decrease in the climb gradient. When viewed as a function of time, the altitude error becomes small and reverses sign at higher altitudes.

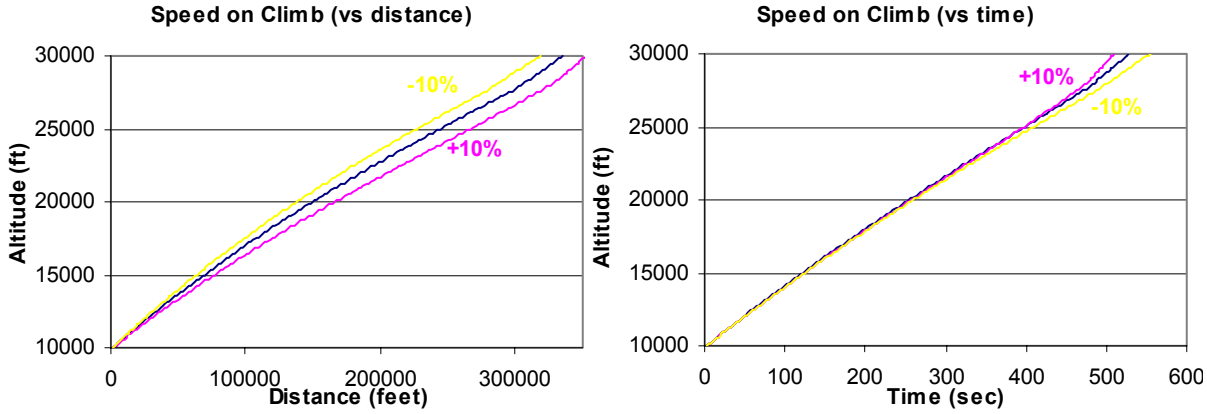

Figure 5-154 Comparison of impact of speed error (expressed as a percentage error) when expressed versus distance or time

When expressed as a function of time, the climb rate ($\dot{h}$) becomes a more important indicator of the behavior than the gradient. Recall that the climb rate can be expressed as a combination of speed and gradient as follows:

$$\dot{h} = V \sin\gamma \approx V\gamma$$

$$\frac{d(\dot{h})}{dV} \approx \gamma + \left(V \frac{d\gamma}{dV} \right)$$

The sensitivity of the climb rate to the speed can be expressed in terms of the lower expression. We recognize the climb gradient sensitivity term, but we now have an additional term. During the climb, the gradient (γ) is positive, but the second term is usually negative. The impact of speed on climb rate can therefore be ambiguous depending on the relationship between these two terms. This leads to a range of altitude errors as a function of time that is very sensitive to the parameters of the problem being considered.

During the climb phase, we applied a fixed percentage error to both the climb CAS and Mach. Since the range of climb CAS/Mach for many aircraft does not typically extend beyond 20%, we only report the impact of speed intent for a nominal initial speed (versus a fast and slow case). Readers interested in the impact on a fast case should take the case with a 10% increase in climb speed and switch the sign for the impact of an error that is 10% below the actual climb speed. It is assumed that trajectory predictors would not be

likely to consider errors in climb speed that exceed the climb speed schedules of the aircraft at either cost index extreme.

The figure below illustrates the errors obtained due to a speed error in climb for a heavy aircraft.

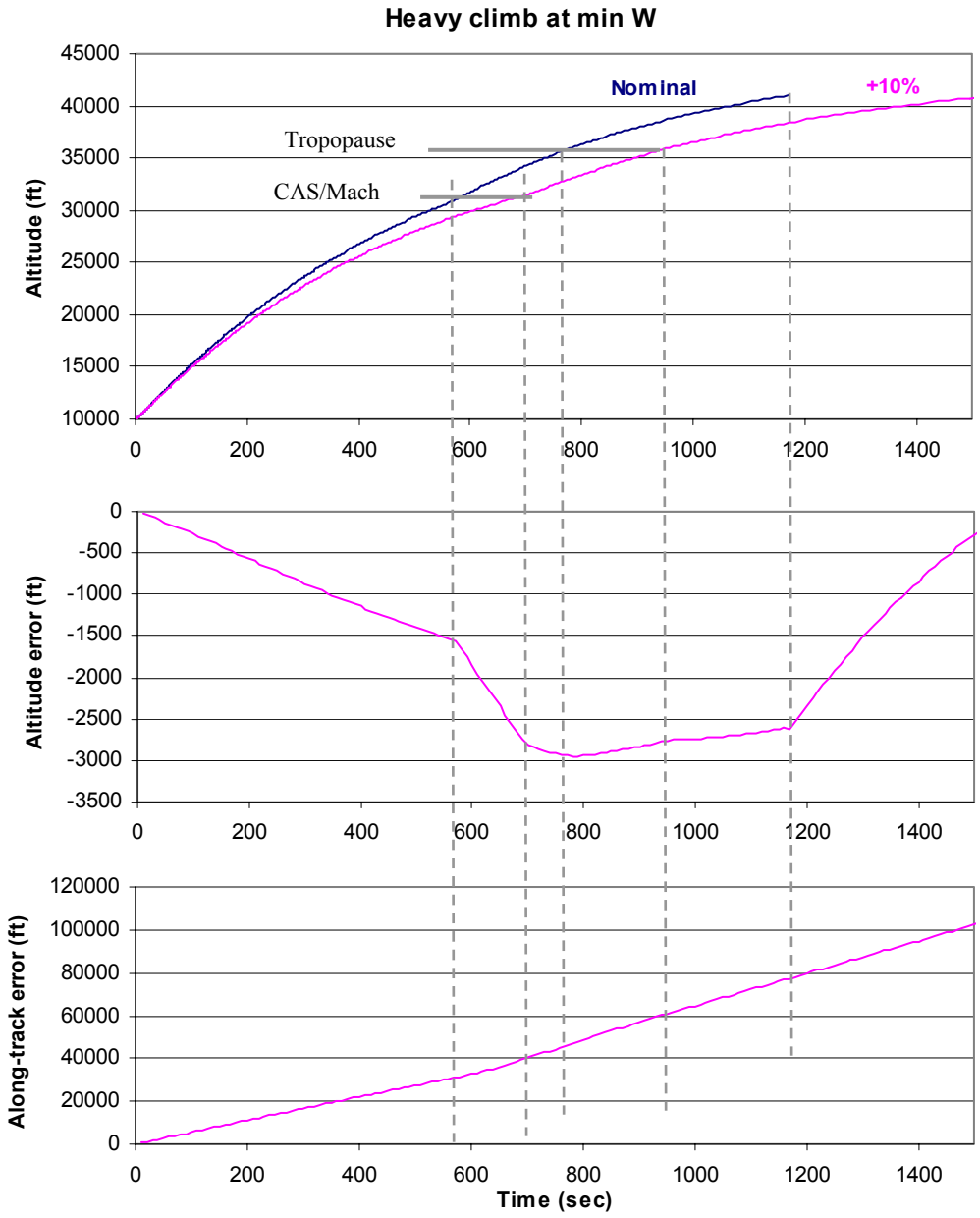

Figure 5-155 Illustration of impact of speed error in climb

In the case presented, the impact of overestimating the climb speed by 10% is to predict a flight that is below the nominal flight by up to 3000 feet. During the constant CAS segment, this leads to the lower flight having the faster CAS offset by the lower altitude. For this example, the CAS/Mach transition point is at approximately the same altitude for both flights, but this need not always be the case. Since the nominal flight transitions to a

constant Mach segment first, the altitude error grows as the climb rate increases during this segment (since the plane is now decelerating as it climbs). When the predicted flight reaches the constant Mach segment, the difference in climb rates moderates until the higher flight reaches the tropopause. At this point, the speed is constant with altitude so the climb rate is reduced. Since the lower flight has a higher climb rate, the altitude error diminishes. The altitude error flattens when both flights reach the tropopause. Eventually the error recovers to zero as both flights target the same cruise flight level. Since an error in speed intent is present, the along-track error continues to grow in accordance with the final speed error. Note that the growth in along-track error is higher during the constant Mach segment due to the lack of a moderating effect from the altitude error.

The figures below illustrate the impact of speed errors on a variety of aircraft types operating with a range of weights. Note the reversal of the altitude error and the large range in peak altitude errors. Unlike the example provided above, some aircraft will have their climb rate increased as a result of an increase in speed. This can occur when the initial gradient (γ) is greater in magnitude than the gradient sensitivity term $\left(V\frac{d\gamma}{dV}\right)$. Furthermore, during the constant Mach segment, the gradient sensitivity term can switch sign and become positive. This results in a substantial positive sensitivity of climb rate to speed error. On the curves below, this manifests itself as a sudden increase in the altitude error as the flight is near the top of climb.

The above model used to explain the behavior of altitude profiles due to errors in speed intent assumes a linear change in gradient or climb rate with speed changes. Clearly non-linear behavior is present as well, as evidenced by the behavior of the large jet operating at maximum weight. When the linear terms are close to zero, the behavior is driven by higher-order terms.

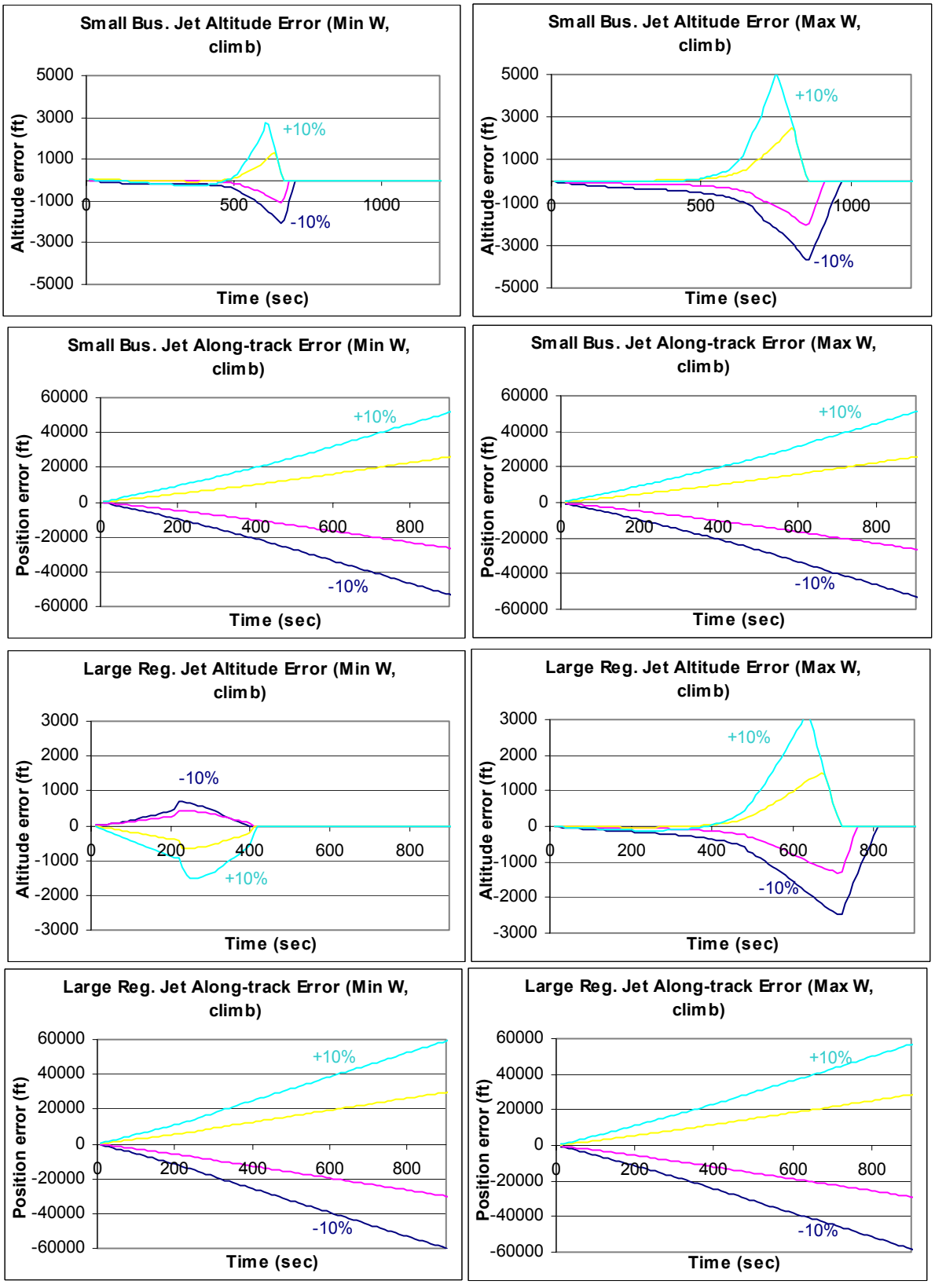

Figure 5-156 Small Business Jet & Large regional jet - Impact of climb speed intent errors (+10%, +5%, -5% and -10%) during climb

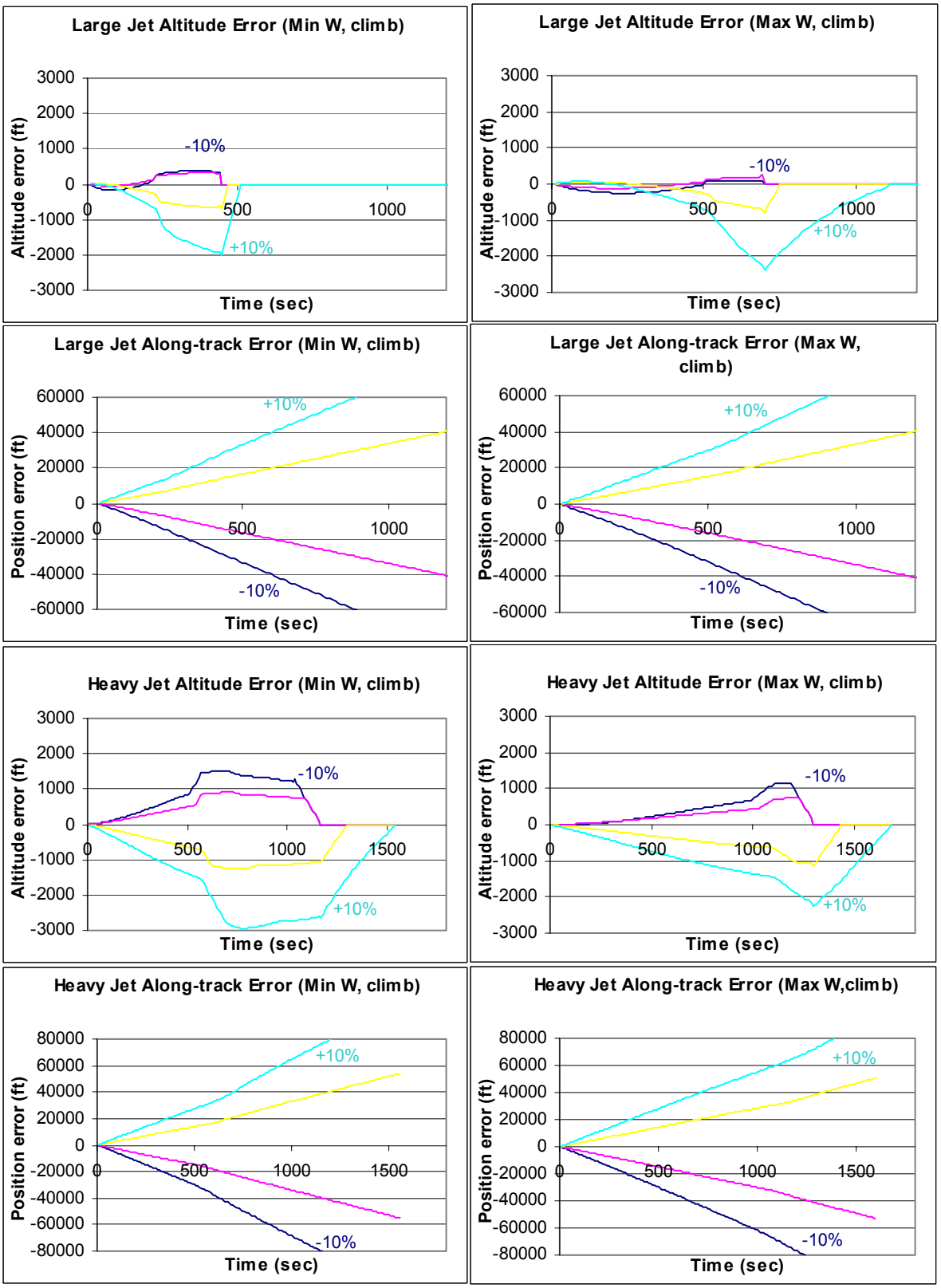

Figure 5-157 Large and heavy Jet - Impact of climb speed intent errors (+10%, +5%, -5% and -10%) during climb

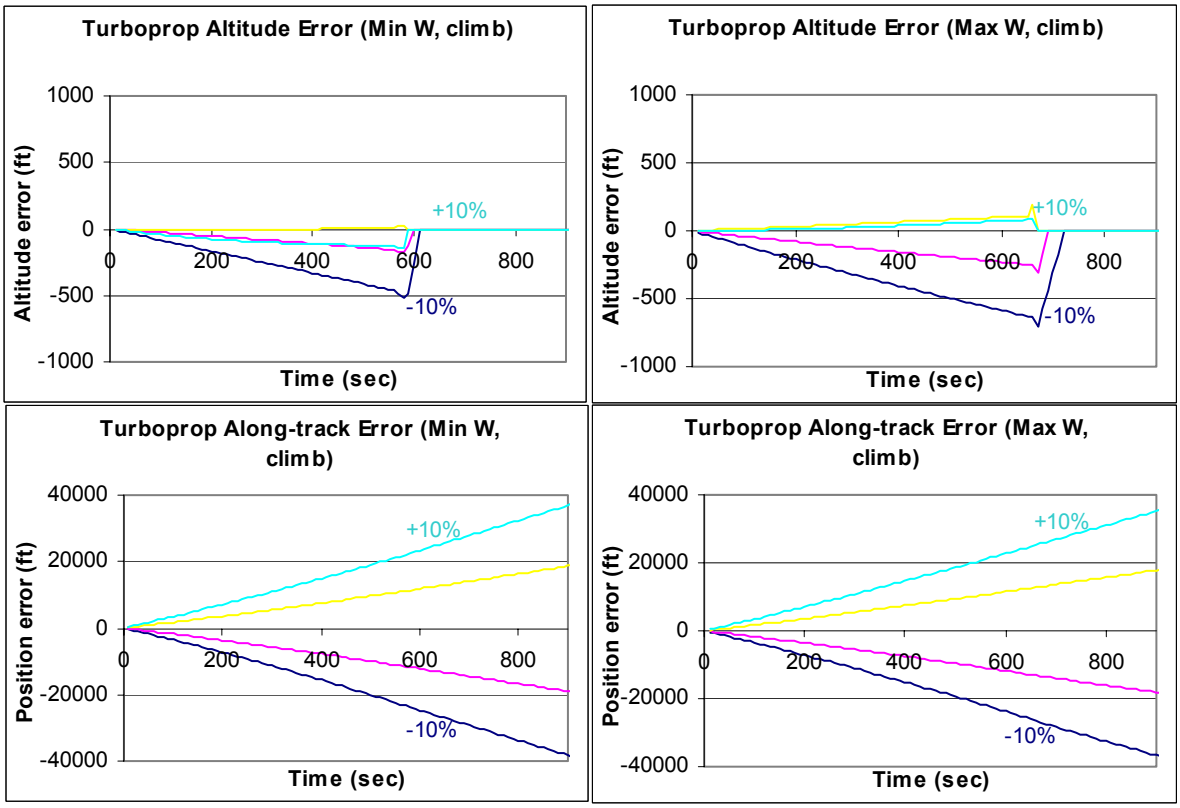

Figure 5-158 Turboprop - Impact of climb speed intent errors (+10%, +5%, -5%, -10%) during climb

Figure 5-159 illustrates the effect of a speed intent error during descent. A decrease in speed intent causes an increase in the $\dot{h}$ term since both the gradient and the $\left(V\frac{d\gamma}{dV}\right)$ terms are negative. This produces a positive altitude error. When the lower flight crosses the tropopause first, the error increases faster as the lower flight is now accelerating to maintain a constant Mach, and consequently descending at a faster rate than before. This is reversed when the lower flight crosses the Mach/CAS transition point first (now the lower flight must decelerate, and consequently descend at a slower rate). When the slower flight crosses the Mach/CAS transition point, the altitude error increases again as the slower flight descends at a slower rate than the faster flight. The error ultimately recovers when the flights reach a bottom-of-descent constraint. Since an error in speed intent exists, the along-track error continues to grow at a rate equal to the difference in speeds.

Figure 5-160 to Figure 5-164 illustrate the error on descent due to intent errors for various aircraft types at various weights and initial speeds. Since the range of descents speeds is larger than climb speeds, we illustrate the impact of slow and fast descents on the different aircraft types.

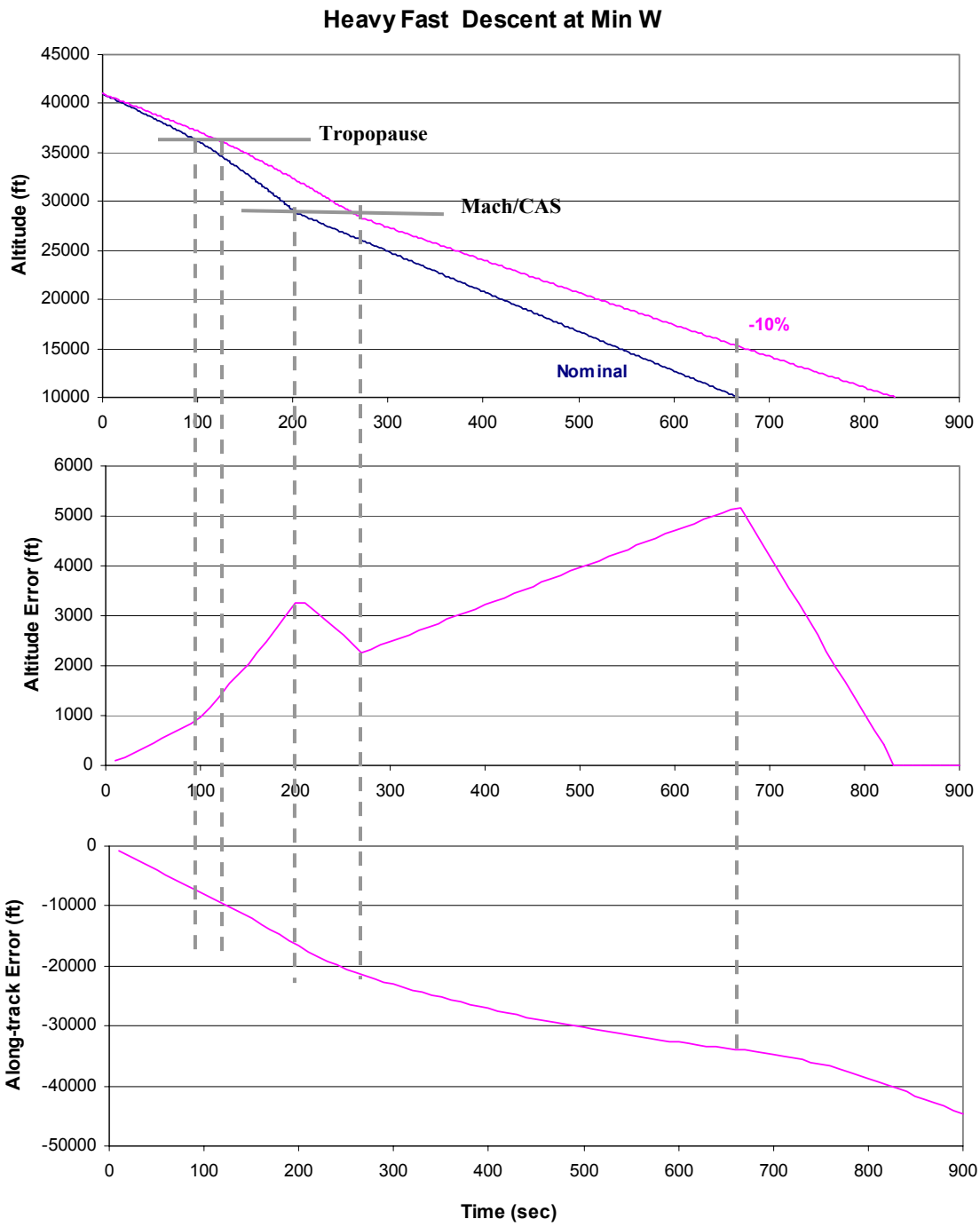

Figure 5-159 Illustration of error due to speed intent on descent

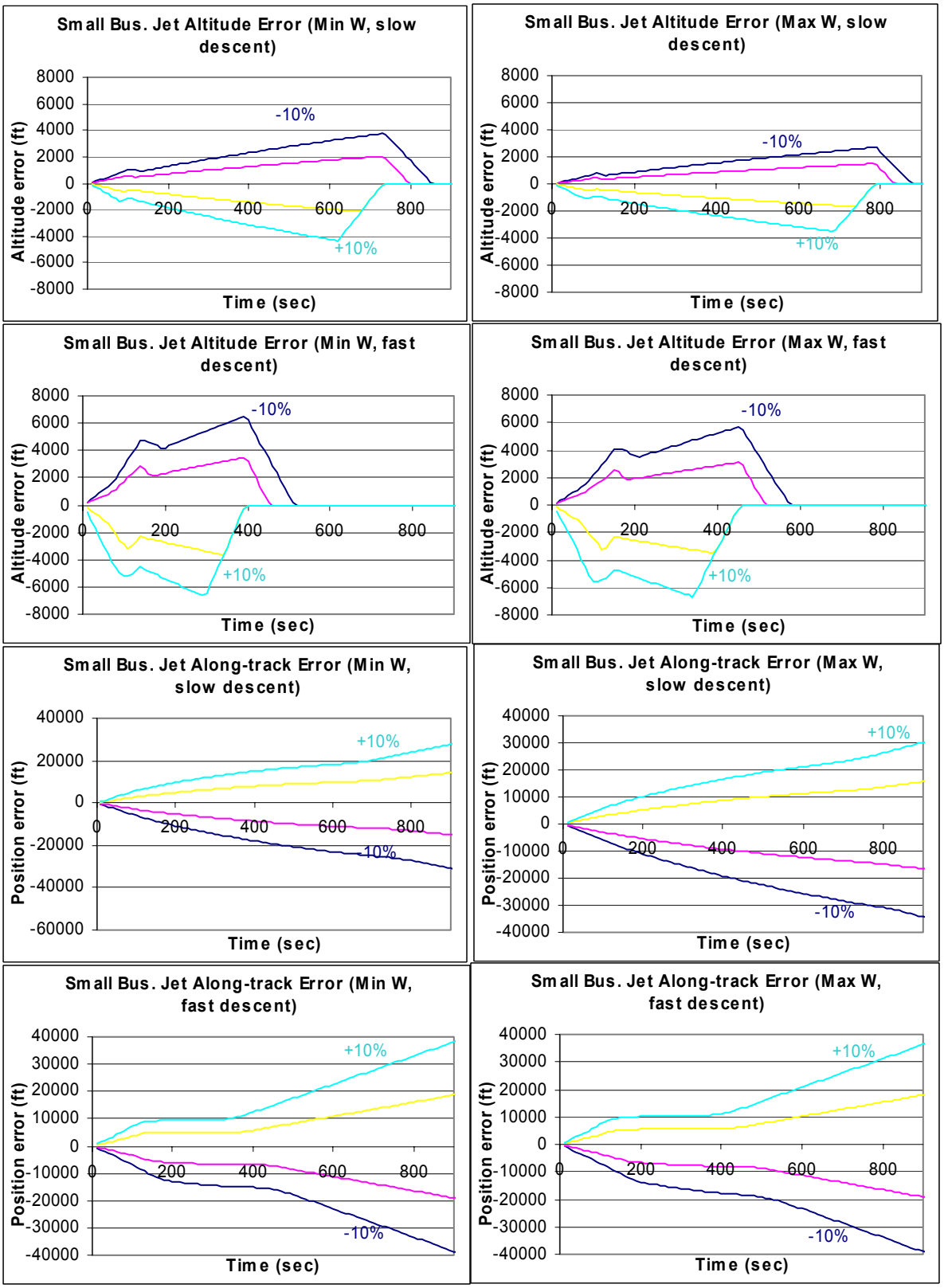

Figure 5-160 Small Business Jet - Impact of descent speed intent errors (+10%, +5%, -5%, -10%) during descent

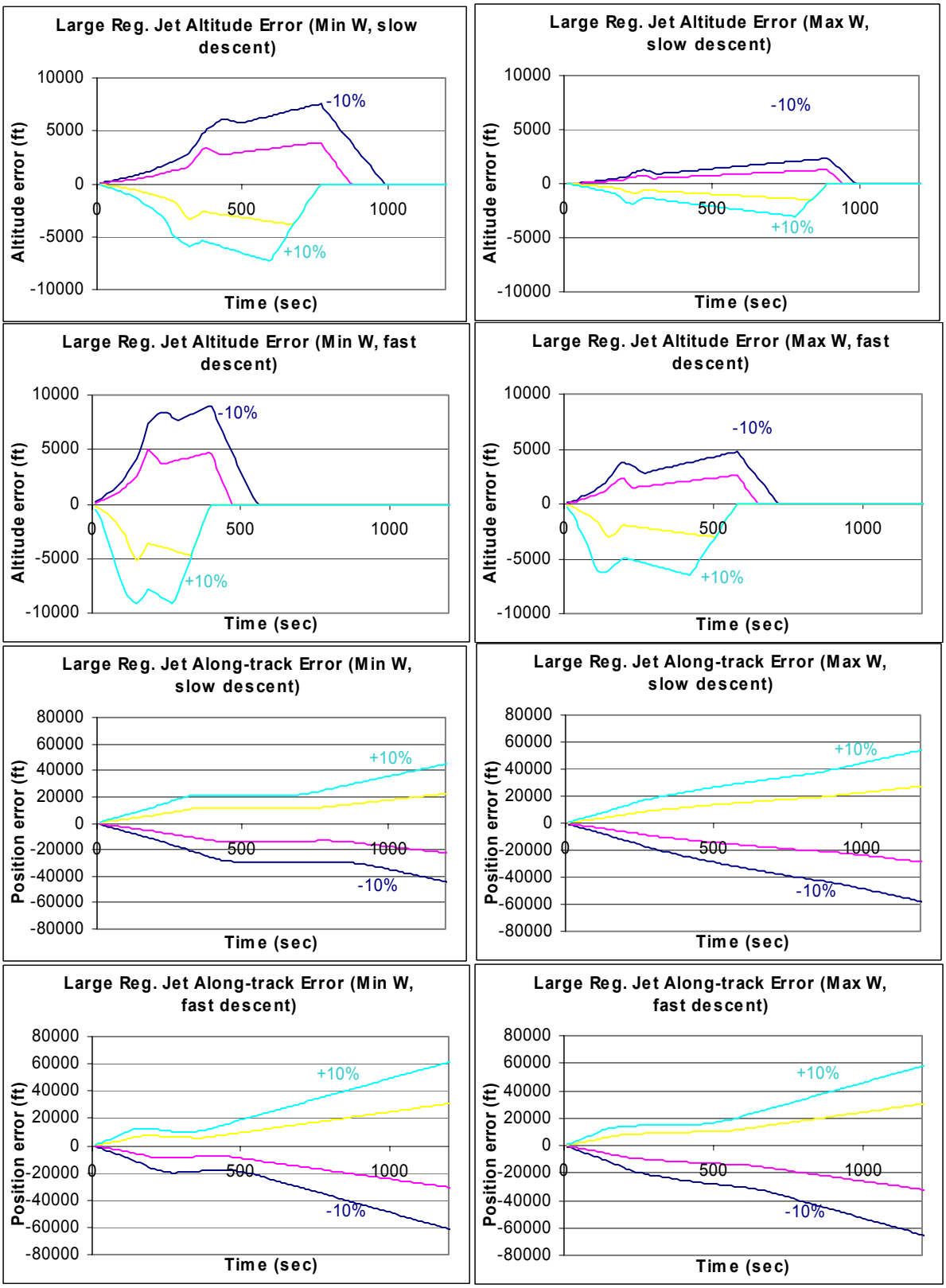

Figure 5-161 Large Regional Jet - Impact of descent speed intent errors (+10%, +5%, -5%, -10%) during descent

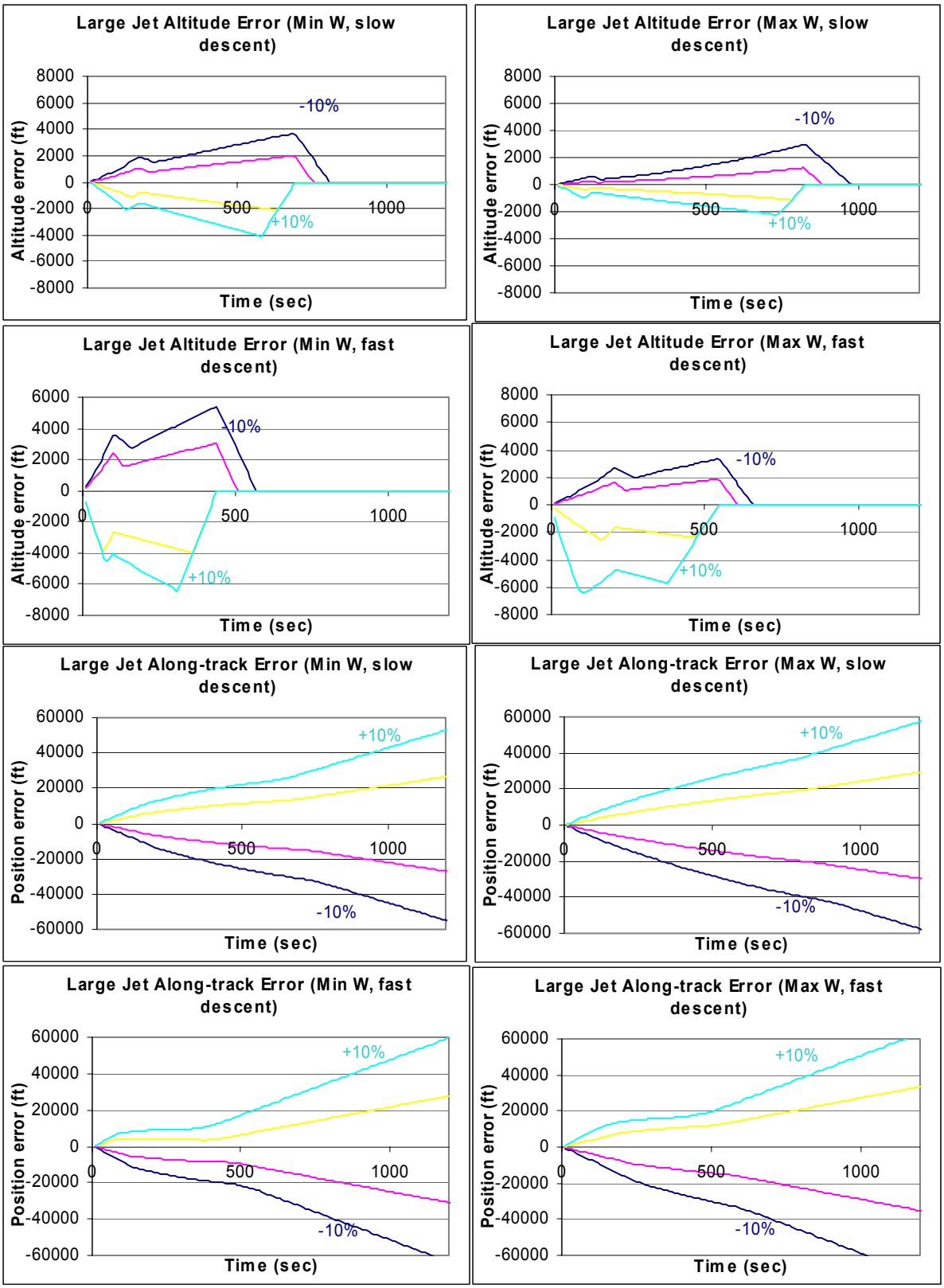

Figure 5-162 Large Jet - Impact of descent speed intent errors (+10%, +5%, -5%, -10%) during descent

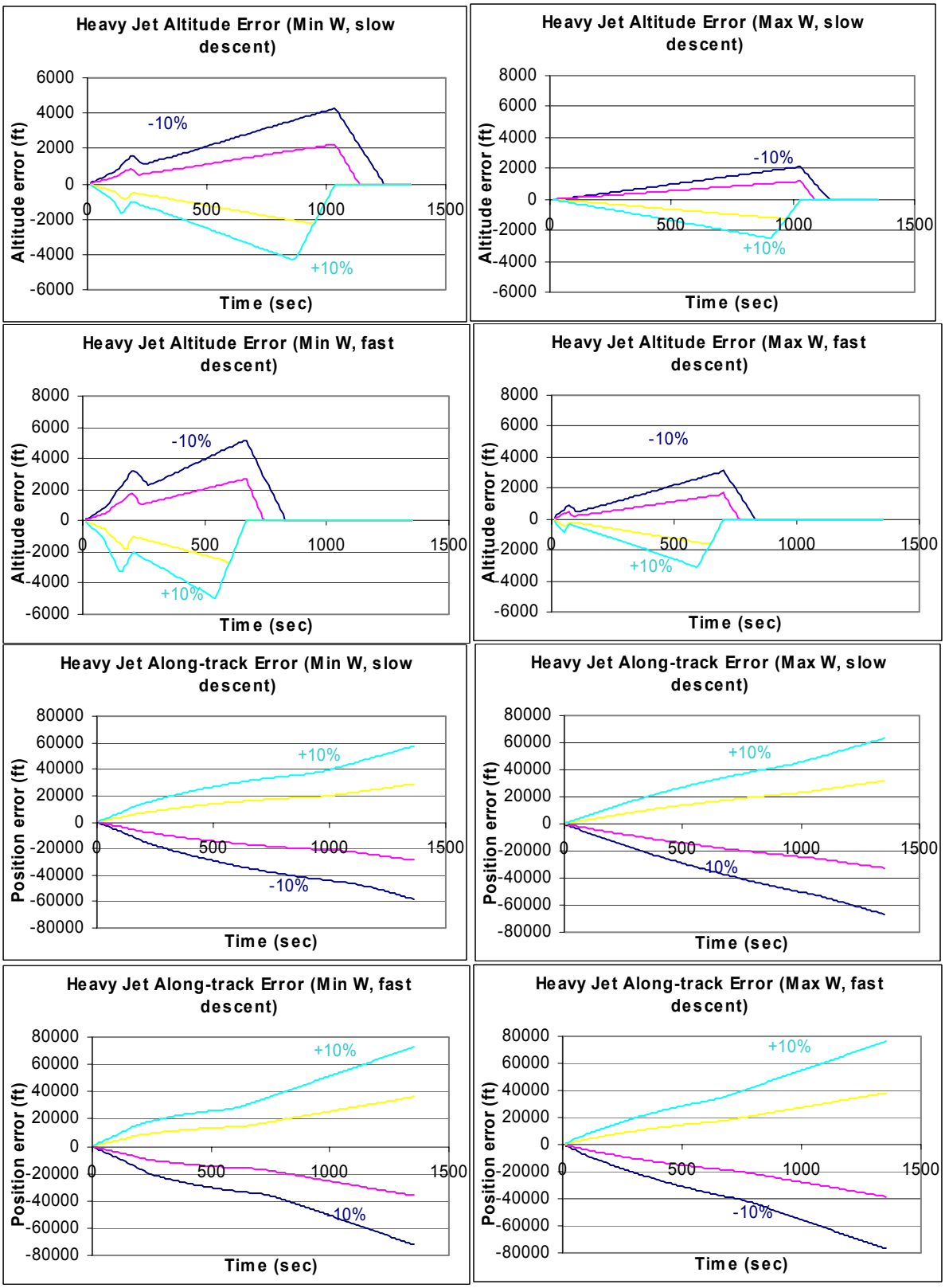

Figure 5-163 Heavy Jet - Impact of descent speed intent errors (+10%, +5%, -5%, -10%) during descent

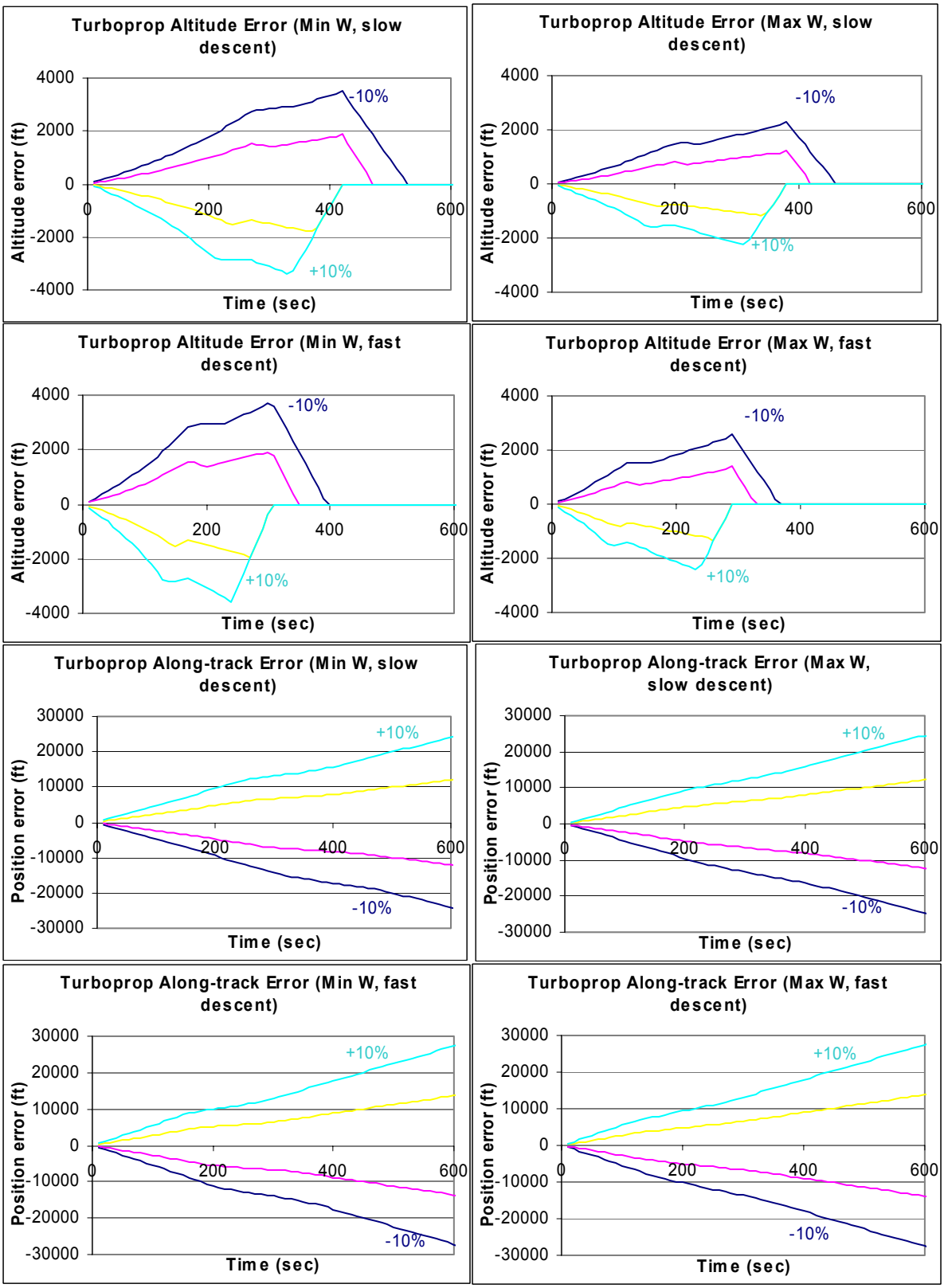

Figure 5-164 Turboprop - Impact of descent speed intent errors (+10%, +5%, -5%, -10%) during descent

5.8 Wind Gradient Error

5.8.1 Description of Error

We have investigated errors stemming from omission of the wind gradient term in the equations of motion (see Section 5.2), and those errors stemming from errors in the wind prediction (see Section 5.4). Errors in the wind gradient will occur as a consequence of errors in the wind prediction. Since errors in the wind gradient are simply a generalization of the wind gradient omission, the reader is referred to these prior Sections (Sections 5.2 and 5.4) for analytical tools to determine the impact of errors in the wind gradient.

5.9 Errors in co-ordinate System

TBD

5.10 Errors in Track Data

TBD

5.11 Departure Time Error

TBD

5.12 Flight Technical Error

TBD

5.13 Time Lags

TBD

5.14 Aircraft Performance Data Errors

5.14.1 Description of Error

Trajectory predictors require a model of aircraft performance in order to model climbing and descending flights. These models may be look-up tables expressing climb and descent rates as a function of operational conditions, or may express the thrust and drag curves as a function of various aerodynamic and atmospheric parameters. Naturally, the aircraft models will depend on the aircraft type, at a minimum. Some models will be very particular about the airframe/engine combination, while others will seek "generic" performance. Since we are dealing with physical systems, it is also reasonable to expect that even identical aircraft/engine models will not perform identically in the field over time.

Given that all aircraft performance models are a simplification of the real world they seek to represent; aircraft performance is subject to some modeling uncertainty. While we recognize that some models may be of higher accuracy than others, they are all subject to some level of inaccuracy. However, the description of this inaccuracy poses a

representational challenge. Given the wide range of operational conditions under which aircraft operate, modeling errors cannot be simply represented by a single number. If we assume a truth value for all operational conditions; modeling errors are represented by a curve in a high-dimensional space. How this error subsequently impacts trajectory prediction is then given by the result of applying that error under a specific set of circumstances.

Some [36],[43] have investigated the error on predictors relying on Thrust/Drag models of performance by imposing a fixed percentage error on the Thrust and Drag profiles. While this introduces some simplification in the error modeling, it does not represent the full scope of modeling errors. To illustrate the situation, Figure 5-165 shows a simplified drag polar for a theoretical aircraft. In this case, a very basic drag polar model is shown. This could be a model for an aircraft whose drag polar is actually one of many possible dotted lines. While this is a simple example showing the error in drag as a function of speed, it merely illustrates that for each possible aircraft performance parameter, errors can exist that are a function of many variables. Furthermore, these variables may be the same as used by the model, or external variables that are not being modeled.

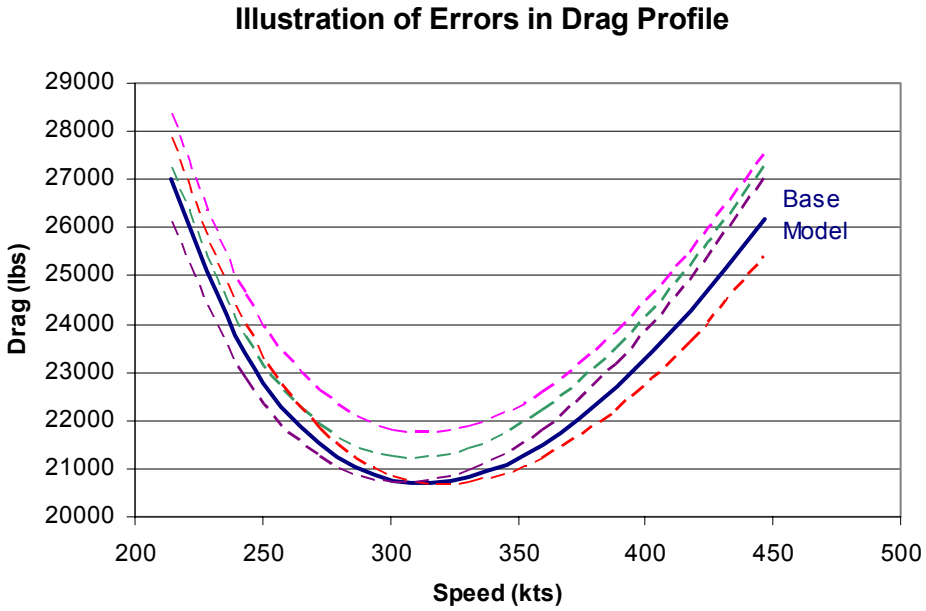

Figure 5-165 Illustration of potential drag profile errors

The impact of modeling uncertainty in a Thrust/Drag type model is to produce an error in the fuel-flow, climb or descent rate *at any given operational condition*. Since the fuel-flow has a small impact on trajectory prediction accuracy, we focus on the climb/descent rate impact. Aircraft performance models providing gradients as a function of specified operational condition can also have their errors expressed as an error in resultant gradient as a function of operational condition. References [27][44] show how the gradient errors can be expressed as a function of operational conditions as duplicated in Figure 5-166. However, these remain a function of the specific aircraft model being investigated.

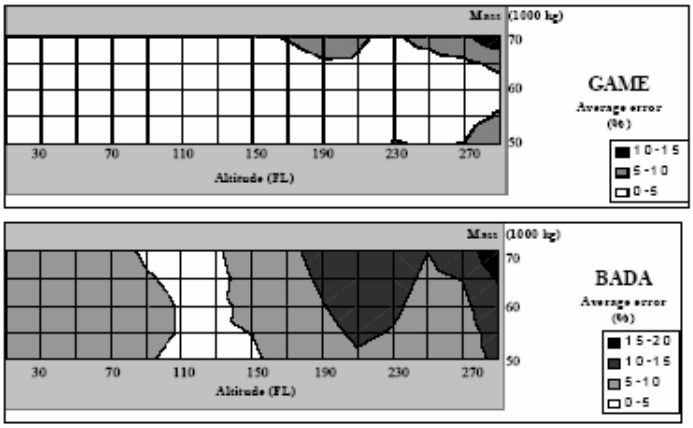

Figure 5-166 Example - Errors in vertical speed under averaged operational conditions

The errors are illustrated as a function of altitude and aircraft weight for a constant calibrated airspeed climb averaged across speeds and temperatures. In general, one would express the error as an error in vertical speed (or climb gradient) as a function of the altitude, weight, temperature, speed, density/pressure, and wind gradient. The error profile in any given scenario will be the result of the integral of the vertical error encountered during a climb or descent. The resulting along-track error will stem from the differences in speed at the computed versus actual altitude.

5.14.2 Parametric Analysis

The aircraft performance errors can be expressed as point-errors in climb or descent gradients. However, the functional form of these errors will determine the form of the output error profiles. For this reason, data presented as error profiles must rely on a specific assumption of the functional form of the error profile. At this point, the authors are not aware of a typical form for these errors.

As an example, mostly to provide an order of magnitude assessment, Figure 5-167 below illustrates the impact, during descent, of a ± 2.5 and 5% error on the drag term explicitly. Since the drag is the dominant term providing the climb gradient, this approximates a 2.5 and 5 percent error in the descent gradient uniformly for all conditions. ***The reader is cautioned that the impact of the error could be larger or smaller depending on the shape of the error as a function of speed***.

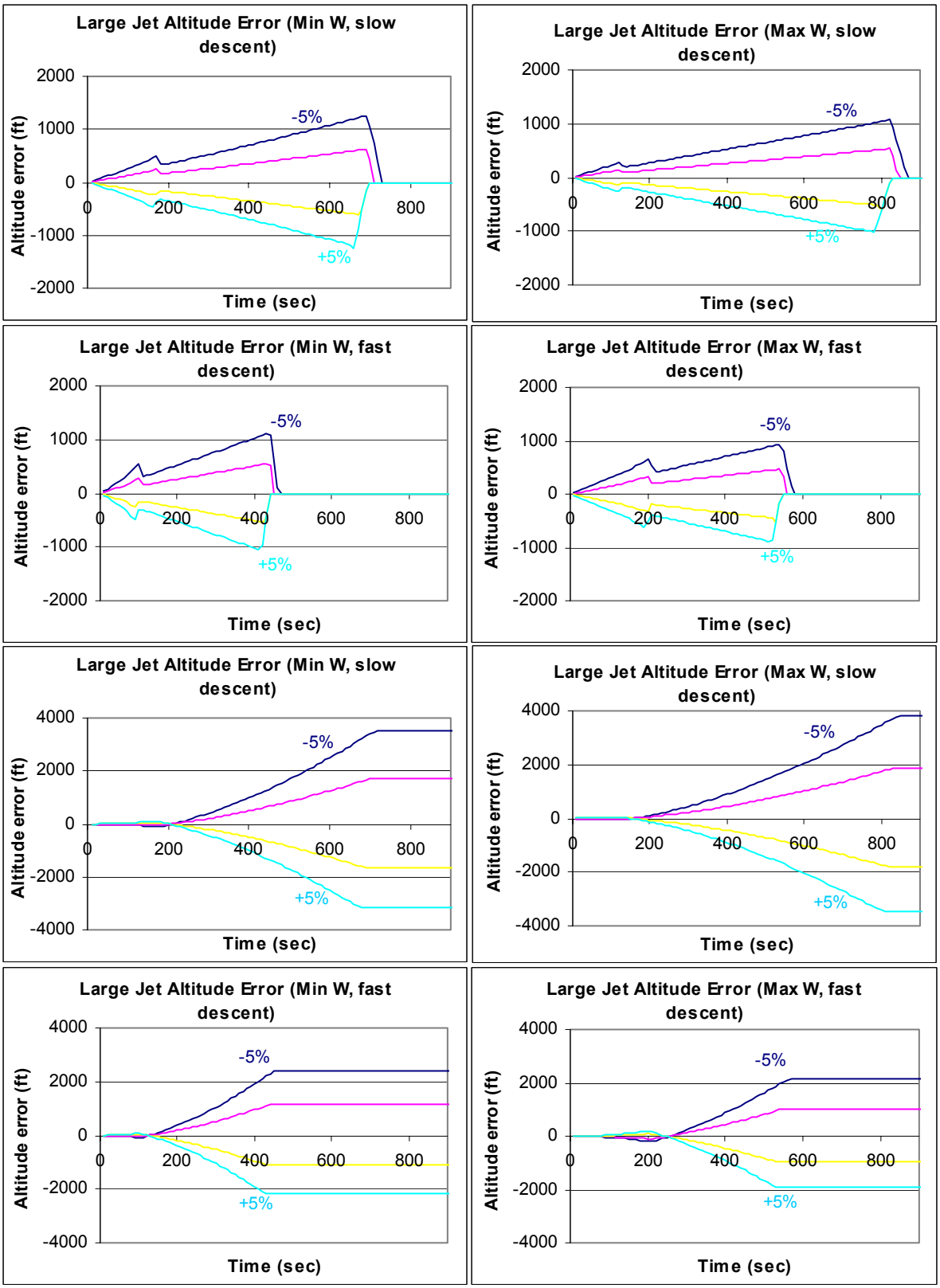

Figure 5-167 Effect of a fixed percentage error in drag coefficient on altitude and along-track error for a large jet

5.15 Pressure and Temperature Error
TBD

5.16 Unknown Lateral and Speed Changes
TBD

5.17 Exit Time from Hold Patterns
TBD

5.18 Pilot Deviations
TBD

5.19 Special Controller Instructions
TBD

5.20 Pilot Operating Procedure
TBD

References

[1] Lindsay, K.S., Green, S.M., Mondoloni, S., Paglione, M., *Common Trajectory Modeling for National Airspace System: Decision Support Tools*, Air Traffic Control Quarterly, Vol. 13, No. 1, pp. 55-82

[2] Warren, A., *Trajectory Prediction Concepts for Next Generation Air Traffic Management*, 3rd USA/Europe Air Traffic Management R&D Seminar, Napoli, IT, June 2000

[3] Jackson, M.R.C., Zhao, Y., Slattery, R., *Effects of Modeling Errors on Trajectory Predictions in Air Traffic Control Automation*, AIAA-96-3721, AIAA Guidance, Control and Navigation Conference, San Diego, CA, July 1996

[4] Waanders, T.C., *Propagation of Trajectory Prediction Uncertainties in the Vertical Plane*, Masters Thesis, Delft University of Technology, July 2005

[5] Mondoloni, S., Bayraktutar, I., *Impact of Factors, Conditions and Metrics on Trajectory Prediction Accuracy*, 6th USA/Europe Air Traffic Management Seminar, Baltimore, MD, 2005

[6] Jackson, M.R.C., *Sensitivity of Trajectory Prediction in Air Traffic Management and Flight Management Systems*, Doctoral Thesis, University of Minnesota, December 1997

[7] Gong, C., McNally, D., *A Methodology for Automated Trajectory Prediction Analysis*, AIAA 2004-4788, AIAA Guidance, Navigation and Control Conference, Providence, RI, August 2004

[8] Jung, Y.C., Isaacson, D.R., *Development of Conflict-Free, Unrestricted Climbs for a Terminal Area Departure Tool*, AIAA 2003-6794, 3rd Aviation Technology, Integration and Operations Conference, Denver, CO, 2003

[9] Hunter, G., *Toward a Standardized Reference Set of Trajectory Modeling Errors*, AIAA 2004-5037, AIAA Modeling and Simulation Technologies Conference and Exhibit, Providence, RI, August 2004

[10] Williams, D.H., Green, S.M., *Flight Evaluation of Center-TRACON Automation System Trajectory Prediction Process*, NASA/TP-1998-208439

[11] Arthur, W.C., McLaughlin, M.P., *User Request Evaluation Tool (URET) Interfacility Conflict Probe Performance Assessment*, 2nd USA/Europe Air Traffic Management R&D Seminar, Orlando, FL, December 1998

[12] Mondoloni, S., Ballin, M.G., *Evaluation of an Airborne Conflict Resolution Algorithm for Flow-Restricted Transition Airspace*, AIAA-2004-4991, AIAA Guidance, Navigation and Control Conference, Providence, RI, August 2004

[13] Green, S.M., Grace, M.P., Williams, D.H., *Flight Test Results: CTAS and FMS Cruise/Descent Trajectory Prediction Accuracy*, 3rd USA/Europe Air Traffic Management R&D Seminar, Napoli, IT, June 2000

[14] Green, S.M., Vivona, R.A., *Field Evaluation of Descent Advisor Trajectory Prediction Accuracy*, AIAA 96-3764, AIAA Guidance, Navigation and Control Conference, July, 1996

[15] Wanke, C., *Using Air-Ground Data link to Improve Air Traffic Management Decision Support System Performance*, 1st USA/Europe Air Traffic Management Seminar, Saclay, FR, 1997
[16] Erzberger, H., Paielli, R.A., Isaacson, D.R., Eshowl, M.M., *Conflict Detection and Resolution in the Presence of Prediction Error*, 1st USA/Europe Air Traffic Management R&D Seminar, Saclay, France, 1997
[17] Durand, N., Alliot, J., *Optimal Resolution of En Route Conflicts*, 1st USA/Europe Air Traffic Management R&D Seminar, Saclay, France, 1997
[18] Whysall, P., *Future Area Control Tools Support (FACTS)*, 2nd USA/Europe Air Traffic Management Seminar, Orlando, December 1998
[19] Swenson, H., N., et al, *Design and Operational Evaluation of the Traffic Management Advisor at the Forth Worth Air Route Traffic Control Center*, 1st USA/Europe Air Traffic Management Seminar, Saclay, FR, 1997
[20] Mueller, K.T., Sorensen, J.A., Couluris, G.J., *Strategic Aircraft Trajectory Prediction Uncertainty and Statistical Sector Traffic Load Modeling*, AIAA-2002-4765, AIAA Guidance, Navigation and Control Conference, Monterey, CA, August, 2002
[21] Blakelock, J. H., *Automatic Control of Aircraft and Missiles*, John Wiley, 2nd Edition, 1991.
[22] Etkin, B., *Dynamics of Flight – Stability and Control*, John Wiley, 2nd Edition, 1982.
[23] Slattery, R., Zhao, Y., *Trajectory Synthesis for Air Traffic Automation*, Journal of Guidance, Control and Dynamics, Vol. 20, No.2, March-April 1997.
[24] Zhao, Y., Slattery, R.A., Capture Conditions in Center Trajectory Synthesizer for Center-TRACON Automation System, AIAA-95-3365-CP, AIAA GN&C Conference, Baltimore, MD, August 1995.
[25] Green, S.M., Davis, T.J., Erzberger, H., *A Piloted Simulator Evaluation of a Ground-Based 4D Descent Advisor Algorithm*, AIAA-87-2522-CP, AIAA Guidance, Control and Navigation Conference, Monterey, CA, August 1987
[26] Calders, P., *G.A.M.E. Aircraft Performance Model Description*, Eurocontrol, DIS/ATD Unit, DOC. CoE-TP-02002, September, 2002.
[27] Swierstra, S., Green,S.M., *Common Trajectory Prediction Capability for Decision Support Tools*, 5th USA/Europe Air Traffic Management Seminar, Budapest, Hungary, June 2003
[28] Ryan, H.F., Paglione, M.M., Green, S.M., *Review of Trajectory Accuracy Methodology and Comparison or Error Measurement Metrics*, AIAA 2004-4787, AIAA Guidance, Navigation and Control Conference, Providence, RI, August 2004
[29] Eurocontrol, *Operational Requirements for Trajectory Prediction for EATCHIP Phase III*, OPR.E1.ST03.1000-ORD-02-00, October 1998.
[30] Daley, R., *Atmospheric Data Analysis*, Cambridge Atmospheric and Space Sciences Series, Cambridge University Press, 1996
[31] Hamill, T. M., Whitaker, J.S., *Model Errors in Ensemble Forecasts: The Structure of Errors from Unrepresented Scales*, 16th NWP/20th W&F Conference, American Meteorological Society, 2004
[32] Benjamin, S.G., et al, *An Hourly Assimilation Forecast Cycle: The RUC*, Mon. Wea. Rev., 132, pp. 495-518, February 2004

[33] Cole, R.E., Green, S.M., Jardin, M., Schwartz, B.E., Benjamin, S.G., *Wind Prediction Accuracy for Air Traffic Management Decision Support Tools*, 3rd USA/Europe Air Traffic Management R&D Seminar, Napoli, IT, June 2000
[34] Hollingsworth, A., Lonnberg, P., *The statistical structure of short-range forecast errors as determined from radiosonde data. Part I: The wind field*, Tellus (1986), 38A pp.111-136
[35] Parrish, D.F., Derber, J.C., *The National Meteorological Center's Spectral Statistical-Interpolation Analysis System*, Mon. Wea. Rev. 120, pp. 1747-1763, August 1992
[36] Mondoloni, S., Paglione, M, Green, S., *Trajectory Modeling Accuracy for Air Traffic Management Decision Support Tools*, ICAS Congress, Toronto, September, 2002
[37] Brudnicki, D.J., McFarland, A.L., *User Request Evaluation Tool (URET) Conflict Probe Performance and Benefits Assessment*, 1st USA/Europe Air Traffic Management R&D Seminar, Saclay, France, 1997
[38] LaFrey, R., *ATC Surveillance – A Retrospective Look*, presentation at the NASA GRC CNS Conference, April 2001
[39] Reynolds, T.G., Hansman, R.J., *Analysis of Separation Minima Using a Surveillance State Vector Approach*, 3rd USA/Europe Air Traffic Management R&D Seminar, Napoli, IT, June 2000
[40] Mondoloni, S., Liang, D., *Improving Trajectory Forecasting Through Adaptive Filtering Techniques*, 5th USA/Europe Air Traffic Management R&D Seminar, Budapest, Hungary, June 2003
[41] Chamlou, R., *Methods for Computing Navigation Accuracy Category(NAC) for Traffic Information Service – Broadcast (TIS-B)*, ICNS Conference, Fairfax, VA, 2004
[42] Coppenbarger, R.A., Kanning, G., Salcido, R., *Real-Time Data Link of Aircraft Parameters to the Center-TRACON Automation System (CTAS)*, submitted to 4th USA/Europe ATM R&D Seminar, Santa Fe, NM, December 2001
[43] Weidner, T.J., *Capacity-Related Benefits of Proposed CNS/ATM Technologies*, 2nd USA/Europe Air Traffic Management Seminar, Orlando, December 1998
[44] Suchkov, A., Swierstra, S., Nuic, A., *Aircraft Performance Modeling for Air Traffic Management Applications*, 5th USA/Europe Air Traffic Management Seminar, Budapest, Hungary, June 2003